

PROCEEDINGS OF INTERNATIONAL SYMPOSIUM ON A RECENT PROGRESS IN FOREST ECOLOGY AND MANAGEMENT 2021



INTERNATIONAL SYMPOSIUM ON A RECENT PROGRESS IN FOREST ECOLOGY AND MANAGEMENT 2021 & THE 9TH IC-GU12 ROUNDTABLE 2021

ORGANIZER:

INTERNATIONAL CONSORTIUM OF UNIVERSITIES IN SOUTH AND SOUTHEAST ASIA FOR THE
DOCTORAL EDUCATION IN AGRICULTURAL SCIENCE AND BIOTECHNOLOGY (ICGU12)

UGSAS-GU & BWEL JOINT POSTER SESSION ON AGRICULTURAL AND BASIN WATER ENVIRONMENTAL SCIENCES 2021

ORGANIZERS:

THE UNITED GRADUATE SCHOOL OF AGRICULTURAL SCIENCE, GIFU UNIVERSITY

GIFU UNIVERSITY REARING PROGRAM
FOR BASIN WATER ENVIRONMENTAL LEADERS



DATE: NOVEMBER 10-11, 2021

International Symposium
on a Recent Progress
in Forest Ecology and Management
2021
&
The 9th IC-GU12
Roundtable 2021





Greetings from the Roundtable and Symposium Chair

It is a great pleasure and an honor for me to welcome distinguished guests, colleagues, friends, and our alumnae/alumni of the UGSAS to the 9th IC-GU12 (International Consortium of Universities in South and Southeast Asia Region for the Doctoral Education on the Agricultural Science and Biotechnology; IC of Great Universities established in 2012) Roundtable and Symposium 2021. Though meeting face to face is a shortcut to exchange knowledge and promote friendship, the roundtable and symposium of this year are carried on a video conference unfortunately like last year. I am sorry for the inconvenience. We, however, have succeeded to invite many excellent researchers to the symposium on forest management and ecology, which must contribute to the progress of our consortium.

The symposium of this year is a first case to discuss forestry at IC-GU12. Forestry is, however, one of most important fields of expertise for Gifu University, because Gifu prefecture has the second largest ratio of forest area/total area among all the prefectures in Japan and therefore its forest industry is active. Therefore, we have been hoping to have this symposium for long years. And not a few member Universities considers the importance of forestry and agrees our proposal. I would like to appreciate the cooperation. In addition, I believe expansion of the fields of expertise to collaborate would strengthen the connection of each University in IC-GU12 like a line to a network.

I hope it will bring fruitful achievements and be a priming of research promotion of forestry and ecology.

The following events are scheduled for the period:

- 1) Roundtable for "IC-GU12" at 18:00 JST(Japanese Standard Time) on 10th November
- 2) Symposium on forest management and ecology at 12:00 JST on 10-11th November
- 3) Joint Poster Session on Agriculture and Basin Water Environmental Science 2021
co-organized by BWEL at 15:00 JST on 11th November.

In this roundtable meeting, we will discuss about the sharing of international lectures using a video conference system. It would give students a great chance to touch international education and encourage them to fly to the international society.

In the symposium of this year, "Forestry management and ecology" is the main theme as above mentioned and it is expected to have interesting academic reports and intensive discussions.

We also have the research activity reports by UGSAS (United Graduate School of Agricultural Science) students and BWEL (Rearing Program for Basin Water Environmental Leaders) students as we do every year. I eagerly ask you to join the session actively, encourage the students and share their research results and accomplishments.

We would like to express our deep gratitude for your participation to our Roundtable and Symposium of IC-GU12 in November 2021.



Ken HIRAMATSU, Dr. Agr.
Dean of the United Graduate School of
Agricultural Science, Gifu University

Message from the Editor in Chief of REVIEWS IN AGRICULTURAL SCIENCE (RAS) e-journal



Greetings to all the participants of the UGSAS-GU International Symposium of 2021.

I would like to introduce myself. My name is Masateru Senge, chief-editor of the international journal "Reviews in Agricultural Science (RAS)" from April, 2020. And emeritus professor Fumiaki Suzuki has also been kindly supporting to edit the submitted papers of the fields related to the chemical and biotechnology as an associate editor.

There are 74 review papers published in this journal from the 1st (2014) volume to the 8th volumes (2020), and which had been cited 817 times by scientific journal listed in "Google Scholar" as of June 15th, 2021. The average citations per document during 2014 to 2020 exceeded 11times. Furthermore, SCOPUS estimated the rank of RAS as Q3 in the field of "Agricultural and biological sciences".

This year, there has been 44 papers submitted to our journal from the academia of 9 countries including of 6 papers from UGSAS-GU until August 15th, 2021, and now 11 papers were accepted for publication and 8 papers are under review.

We welcome your review contributions to RAS, on any aspects that relate to agricultural themes. Your submissions will certainly receive utmost attention and refinement by our editorial board before acceptance.

Please have a look at our website <https://www.jstage.jst.go.jp/browse/ras/-char/en> in the J-Stage platform.



A handwritten signature in black ink, appearing to read "Masateru Senge".

Masateru Senge, Ph.D.

Editor in Chief, *Reviews in Agricultural Science*

August 15, 2021

International Symposium on a Recent Progress in Forest Ecology and Management 2021

10th November, 2021

12:00-12:05	OPENING REMARKS
12:00-12:05	Toshiyuki Ohtsuka, Professor Head Organizer of the Symposium Gifu University
12:05-13:25	KEYNOTE SPEECH 1
12:05-12:45	Michiko Nakagawa, Associate Professor Nagoya University Long-term Field Data Unveil Characteristics of Phenology and Forest Dynamics in a Bornean Tropical Rain Forest
12:45-13:25	Sasitorn Pongparn, Associate Professor Chulalongkorn University Unfolding a Mystery of Tropical Mangroves from a Two-decade Journey in Mangrove Study
13:25-13:45	Break
13:45-15:00	FOREST CARBON CYCLE AND CLIMATE CHANGE (Session 1) Chair: Professor Toshiyuki Ohtsuka (Gifu University)
13:45-14:00	Suthathip Umnouysin, PhD (Silpakorn University) Net Primary Productivity Estimation in the Chronosequence Coastal-mangrove Plantations in Central Thailand
14:00-14:15	Christine Wulandari, PhD (The University of Lampung) Relationships Between Carbon Stocks and Trees Biodiversity in Production Forest of Register 24, Lampung Province
14:15-14:30	Komariah, PhD (Sebelas Maret University) The Effects of Climate Change on Indonesian Forests
14:30-14:45	Sutheera Hermhuk, PhD (Maejo University) Tropical Montane Forest Ecotone Dynamics in the Context of Climate Change: Case Study in the Doi Suthep-Pui National Park, Thailand

14:45-15:00 Wongsatorn Phumphuang, Master (Kasetsart University)
Effect of Climate Changes on Dry Evergreen Forest Dynamics in Sakaerat
Biosphere Reserve, Northeastern Thailand

15:00-15:20 Break

15:20-16:05 ECOLOGY OF TROPICAL TO TEMPERATE FORESTS (Session 2)
Chair: Associate Professor Atsuhiko Iio (Shizuoka University)

15:20-15:35 Qingmin Han, PhD (Forestry and Forest Products Research
Institute (Japan))
Mast Seeding and Associated Resource Dynamics in *Fagus* Species

15:35-15:50 Nguyen Trong Minh, PhD (Vietnam National University of Forestry)
Anchorage and Stability Characteristic of Forest Tree Species in Tropical Region
and a Suitable Wind Damage Assessment Mode for Planted Forest in Vietnam

15:50-16:05 Momi Tsuruta, PhD (Forestry and Forest Products Research
Institute (Japan))
Hybrid Breakdown as a Result of Up-regulated Expression of Defense-related
Genes in the Hybrid Seedlings of Japanese Flowering Cherry

16:05-16:25 Break

16:25-17:10 AGROFORESTRY OF TROPICAL REGION (Session 3)
Chair: Assistant Professor Isao Hirota (Gifu University)

16:25-16:40 Maria Theresia Sri Budiastuti, PhD (Universitas Sebelas Maret)
Agroforestry System as the Best Vegetation Management to Face Forest
Degradation

16:40-16:55 Cahyo Wisnu Rubiyanto, Master (Gifu University)
Contribution of Forest Resources in Shifting Cultivation System to Livelihood
Diversification in Mountain Villages of Northern Laos

16:55-17:10 Zuhud Rozaki, PhD (Universitas Muhammadiyah Yogyakarta)
Agroforestry Practice in Volcano Prone Area: Findings from Mount Merapi
Indonesia

17:10-18:00 Break

18:00-19:00 The 9th IC-GU12 ROUNDTABLE 2021

11th November, 2021

12:00-13:20	KEYNOTE SPEECH 2
12:00-12:40	Atsuhiko Iio, Associate Professor Shizuoka University Masting Impact on Canopy Structure and Photosynthesis in Beech Forests Does Masting Perform as Gap?
12:40-13:20	So Hanaoka, Chief of Breeding Laboratory Forestry and Forest Products Research Institute (Japan) Forest Tree Breeding in Hokkaido Japan
13:20-13:40	Break
13:40-14:40	FOREST HYDROLOGY AND BIOGEOCHEMISTRY (Session 4) Chair: Associate Professor Takeo Onishi (Gifu University)
13:40-13:55	Siyu Chen, PhD (Nanning Normal University) Seasonal Variations of Dissolved Organic Carbon Concentrations and Fluxes in an Evergreen Broadleaved Subtropical Forest in Central Japan
13:55-14:10	Taketo Uemura (Gifu University) Differences of Water and Material Dynamics between Coniferous Plantation and Deciduous Secondary Forest Watershed -Focusing on Dissolved Organic and Inorganic Carbon
14:10-14:25	Dwi Priyo Ariyanto, PhD (Universitas Sebelas Maret) Estimating of Run off Using SCS-CM Model in Gunung Bromo Education Forest Discharging to Kalijirak River
14:25-14:40	Edwina Zainal, PhD (Bung Hatta University) The Runoff and Sediment Response Due to Land Use Change in the Lubuk Paraku Sub-Watershed
14:40-14:45	CLOSING REMARKS
14:40-14:45	Ken Hiramatsu, Professor Dean of the UGSAS-GU Gifu University
14:45-15:00	Break
15:00-17:15	UGSAS, GU & BWEL Joint Poster Session on Agricultural and Basin Water Environmental Sciences 2021 (Poster Session)

The 9th IC-GU12 Roundtable 2021

Date: 10th November

18:00~19:00JST

Web Conference

Participants: Liaison of member universities in IC-GU12

Bangladesh Agricultural University (Bangladesh)
University of Dhaka (Bangladesh)
Guangxi University (China)
Assam University (India)
Indian Institute of Technology Guwahati (India)
Andalas University (Indonesia)
Bandung Institute of Technology (Indonesia)
IPB University (Indonesia)
Gadjah Mada University (Indonesia)
Sebelas Maret University (Indonesia)
University of Lampung (Indonesia)
National University of Laos (Laos)
Mariano Marcos State University (Philippines)
Chulalongkorn University (Thailand)
Kasetsart University (Thailand)
King Mongkut's University of Technology Thonburi (Thailand)
Hanoi University of Science and Technology (Vietnam)
Thuyloi University (Vietnam)
Shizuoka University (Japan)
Gifu University (Japan)

Chair: Ken HIRAMATSU, Dean of UGSAS

Moderator: Tomio YABE, Vice Dean of UGSAS (International Affairs)

Topic: Building a Framework for Collaborative Education among Member Universities of IC-GU12 Using a Remote Lecture System

Contents

Discussion and information exchange

UGSAS-GU & BWEL Joint Poster Session on Agricultural and Basin Water Environmental Sciences 2021

11th November

15:00-17:15 JST

Organized by The United Graduate School of Agricultural Science, Gifu University (UGSAS-GU)
Gifu University Rearing Program for Basin Water Environmental Leaders (BWEL)

Online Poster Presentation

15:00-15:05 Opening remarks

Prof. Ken Hiramatsu (Dean of UGSAS-GU)

Poster Core Time

15:10-15:50 Odd numbered posters

15:50-16:30 Even numbered posters

16:30-16:45 Free discussion time

16:45-16:50 Announcement of the winners of the Best Presentation Award

17:00-17:10 Awarding ceremony

17:10-17:15 Closing remarks

Prof. Fusheng Li (Head of the Promotion Office of BWEL)

Presentations

P01: Effects of curcumin nanoemulsion on the water vapor permeability and antioxidant activities of chitosan-based films

Fakfan Luangapai (UGSAS-GU)

P02: LAMP-FLP for detection of thiophanate-methyl resistant strains of *Fusarium fujikuroi* in Japan

FangJing Li (UGSAS-GU; BWEL)

P03: Changes in chlorophyll and carotenoid profiles and gene expression during fruit regreening in Valencia orange

Nichapat Keawmanee (UGSAS-GU)

P04: Modified newmark approach for evaluation of earthquake-induced displacement of earthdams

Phuong Le-Hong (UGSAS-GU)

P05: Development of a HS-SPME/GC-MS method for the extraction and identification of the volatile compounds in coffee

Fawzan Sigma Aurum (UGSAS-GU)

P06: Development of a program for constructing ortholog data set using taxonomic information

Tomoaki Watanabe (UGSAS-GU)

- P07: Visualization of low molecule phenol (LMP) and copper naphthenate in oil palm veneer using X-ray microtomography
Ayuni Nur Apsari (UGSAS-GU)
- P08: Generalized pollination and floral scent chemistry in the invasive *Coreopsis lanceolata*
Muhammad Arifin (UGSAS-GU)
- P09: Inhibition effect of different sorbent materials on transfer of cesium and arsenic from contaminated soil to vegetation
Shiamita Kusuma Dewi (UGSAS-GU; BWEL)
- P10: Ensemble prediction of solar irradiance in tropical regions
Daiki Harada (Graduate School of Natural Science and Technology, Gifu University; BWEL)
- P11: Short-term prediction of cloud movements with meteorological satellite images processed in spectrum space
Yuto Hara (Graduate School of Natural Science and Technology, Gifu University; BWEL)
- P12: Application of Kalman filter to solar irradiance forecasting with a meteorological model in tropical region
Naoki Moriai (Graduate School of Natural Science and Technology, Gifu University; BWEL)
- P13: Bacterial activity and EPS affect the performance of household wastewater treatment facility
Haoning Su (Graduate School of Engineering, Gifu University; BWEL)
- P14: Steam gasification of woody biomass with renewable hydrogen
Sheng-Wen Xiao (Graduate School of Natural Science and Technology, Gifu University; BWEL)
- P15: Adsorbability of organic matter released from drinking water treatment sludge onto activated carbon
Sri Anggreini (Graduate School of Engineering, Gifu University; BWEL)
- P16: Coexisting and competing algal species with moldy odor-causing blue algae in Nagara River
Wenqing Li (Graduate School of Natural Science and Technology, Gifu University; BWEL)
- P17: Fate and effect of microplastic and heavy metal in agricultural soil added with biochar
Rahman Fariha (Graduate School of Natural Science and Technology, Gifu University; BWEL)
- P18: MODIS-based estimation of carbon sequestration of different vegetation in Qilian Mountains, China
Zhou Jieli (Graduate School of Natural Science and Technology, Gifu University; BWEL)
- P19: Association of bacterial community with heavy metals in soils of different coal mining areas
Yajie Wang (Graduate School of Engineering, Gifu University)
- P20: Changes of 16S rDNA and antibiotic resistance genes in the drinking water treatment process
Nadya Diva Sagita (Graduate School of Engineering, Gifu University)
- P21: Changes of dissolved organic matter from source to treated water in drinking water treatment plant:
Evaluation based on fluorescence excitation-emission matrix analysis
Maulana Yusup Rosadi (Graduate School of Engineering, Gifu University)

CONTENTS

KEYNOTE SPEECH 1

Long-term Field Data Unveil Characteristics of Phenology and Forest Dynamics in a Bornean Tropical Rain Forest

Michiko Nakagawa p. 2

Unfolding a Mystery of Tropical Mangroves from a Two-decade Journey in Mangrove Study

Sasitorn Pongparn p. 3

SESSION 1 -FOREST CARBON CYCLE AND CLIMATE CHANGE-

Net Primary Productivity Estimation in the Chronosequence Coastal-mangrove Plantations in Central Thailand

Suthathip Umnouysin, Sasitorn Pongparn, Vilanee Suchewaboripont, Chadtip Rodtassana and Tanapon Pongsuvarod p. 6

Relationships between Carbon Stocks and Trees Biodiversity in Production Forest of Register 24, Lampung Province

Christine Wulandari, Samsul Bakri, Yanfa Ghiyats Ghifari, Destia Novasari, Lia Mulyana, Azhary Taufiq, Nindya Tria Puspita and Imawan Abdul Qohar p. 11

The Effects of Climate Change on Indonesian Forests

Komariah and Umami Marfu'ah p. 20

Tropical Montane Forest Ecotone Dynamics in the Context of Climate Change: Case Study in the Doi Suthep-Pui National Park, Thailand

Sutheera Hermhuk and Dokrak Marod p. 25

Effect of Climate Changes on Dry Evergreen Forest Dynamics in Sakaerat Biosphere Reserve, Northeastern Thailand

Wongsatorn Phumphuag and Dokrak Marod p.29

SESSION 2 - ECOLOGY OF TROPICAL TO TEMPERATE FORESTS –

Mast Seeding and Associated Resource Dynamics in *Fagus* Species

Qingmin Han, Daisuke Kabeya, Yoshiyuki Inagaki, Akira Kagawa, Günter Hoch and Atsuhiko Iio p. 36

Anchorage and Stability Characteristic of Forest Tree Species in Tropical Region and a Suitable Wind Damage Assessment Mode for Planted Forest in Vietnam

Nguyen Trong Minh, Fukui Sho, Iwama Shintaro, Dang Thinh Trieu, Koyano Kaita and Hizomi Mizunaga p. 40

Hybrid Breakdown as a Result of Up-regulated Expression of Defense-related Genes in the Hybrid Seedlings of Japanese Flowering Cherry

Momi Tsuruta, Chunlan Lian and Yuzuru Mukai p.47

SESSION 3 - AGROFORESTRY OF TROPICAL REGION –

- Agroforestry System as the Best Vegetation Management to Face Forest Degradation**
Maria Theresia Sri Budiastuti, Djoko Purnomo and Desy Setyaningrum p.54
- Contribution of Forest Resources in Shifting Cultivation System to Livelihood Diversification in Mountain Villages of Northern Laos**
Cahyo Wisnu Rubiyanto and Isao Hirota p. 61
- Agroforestry Practice in Volcano Prone Area: Findings from Mount Merapi Indonesia**
Zuhud Rozaki, Nur Rahmawati, Oki Wijaya, Atikah Fajriyah Mubarak,
Masateru Senge and Mohd Fauzi Kamarudin p. 65

KEYNOTE SPEECH 2

- Masting Impact on Canopy Structure and Photosynthesis in Beech Forests**
Does Masting Perform as Gap?
Atsuhiko Iio p. 72
- Forest Tree Breeding in Hokkaido, Japan**
So Hanaoka p. 73

SESSION 4 - AGROFORESTRY OF TROPICAL REGION –

- Seasonal Variations of Dissolved Organic Carbon Concentrations and Fluxes in an Evergreen Broadleaved Subtropical Forest in Central Japan**
Siyu Chen, Ruoming Cao, Shinpei Yoshitake and Toshiyuki Ohtsuka p. 76
- Difference of Water and Material Dynamics between Coniferous Plantation and Deciduous Secondary Forest Watershed - Focusing on Dissolved Organic and Inorganic Carbon**
Taketo Uemura, Takeo Onishi, Toshiyuki Otsuka and Ken Hiramatsu p. 81
- Estimating of Run off Using SCS-CM Model in Gunung Bromo Education Forest Discharging to Kalijirak River**
Dwi Priyo Ariyanto, Tio Egar Nurhutomo, Mujiyo, Komariah p. 90
- The Runoff and Sediment Response Due to Land Use Change in the Lubuk Paraku Sub-Watershed**
Edwina Zainal, Zufrimar, Zahrul Umar and Irfan Andika S p. 94

UGSAS-GU & BWEL Joint Poster Session on Agricultural and Basin Water Environmental Sciences 2021

- P01: Effects of curcumin nanoemulsion on the water vapor permeability and antioxidant activities of chitosan-based films
Fakfan Luangapai 1, Methavee Peanparkdee and Satoshi Iwamoto p. 100
- P02: LAMP-FLP for detection of thiophanate-methyl resistant strains of *Fusarium fujikuroi* in Japan
FangJing Li, Ryoji Komura, Chiharu Nakashima, Masafumi Shimizu,
Koji Kageyama and Haruhisa Suga p. 102
- P03: Changes in chlorophyll and carotenoid profiles and gene expression during fruit regreening in Valencia orange
Nichapat Keawmanee, Gang Ma, Lancui Zhang, Masaki Yahata, Masaya Kato
. p. 104
- P04: Modified newmark approach for evaluation of earthquake-induced displacement of earthdams
Phuong Le-Hong, Shin-ichi Nishimura and Tatsuro Nishiyama p. 106
- P05: Development of a HS-SPME/GC-MS method for the extraction and identification of the volatile compounds in coffee
Fawzan Sigma Aurum, Teppei Imaizumi, Manasikan Thammawong, Kohei Nakano
. p. 108
- P06: Development of a program for constructing ortholog data set using taxonomic information
Tomoaki Watanabe and Tokumasa Horiike p. 110
- P07: Visualization of low molecule phenol (LMP) and copper naphthenate in oil palm veneer using X-ray microtomography
Ayuni Nur Apsari1, Eko Sudoyo, Eka Mulya Alamsyah, Kenji Kobayashi and
Takashi Tanaka p. 112
- P08: Generalized pollination and floral scent chemistry in the invasive *Coreopsis lanceolata*
Muhammad Arifin and Tomoko Okamoto p.114
- P09: Inhibition effect of different sorbent materials on transfer of cesium and arsenic from contaminated soil to vegetation
Shiamita Kusuma Dewi and Yongfen Wei p. 116
- P10: Ensemble prediction of solar irradiance in tropical regions
Daiki Harada, Naoki Moriai and Tomonao Kobayashi p. 118
- P11: Short-term prediction of cloud movements with meteorological satellite images processed in spectrum space
Yuto Hara, Rina Takada, Tomonao Kobayashi and Jun Yoshino p. 120

- P12: Application of Kalman filter to solar irradiance forecasting with a meteorological model in tropical region**
Naoki Moriai, Daiki Harada and Tomonao Kobayashi p. 122
- P13: Bacterial activity and EPS affect the performance of household wastewater treatment facility**
Haoning Su, Miya Ogata, Yuuki Okochi, Shinya Okumura, Yasushi Ishiguro and Fusheng Li p. 124
- P14: Steam gasification of woody biomass with renewable hydrogen**
Sheng-Wen Xiao and Kazuhiro Kumabe p. 126
- P15: Adsorbability of organic matter released from drinking water treatment sludge onto activated carbon**
Sri Anggreini, Maulana Yusup Rosadi, Miya Ogata and Fusheng Li p. 128
- P16: Coexisting and competing algal species with moldy odor-causing blue algae in Nagara River**
Wenqing Li, Haoning Su, Shoma Wakamiya and Fusheng Li p. 130
- P17: Fate and effect of microplastic and heavy metal in agricultural soil added with biochar**
Rahman Fariha, Shiamita Kasuma Dewi, Zaw Min Han and Wei Yongfen p. 132
- P18: MODIS-based estimation of carbon sequestration of different vegetation in Qilian Mountains, China**
Zhou Jieli, Zhang Fuping and Wei Yongfen p. 134
- P19: Association of bacterial community with heavy metals in soils of different coal mining areas**
Yajie Wang, Zāw Min Han, Yongfen Wei and Fusheng Li p. 136
- P20: Changes of 16S rDNA and antibiotic resistance genes in the drinking water treatment process**
Nadya Diva Sagita, Sutra Maysaroh, Maulana Yusup Rosadi and Fusheng Li p. 138
- P21: Changes of dissolved organic matter from source to treated water in drinking water treatment plant: Evaluation based on fluorescence excitation-emission matrix analysis**
Maulana Yusup Rosadi, Nadya Diva Sagita, Sutra Maysaroh and Li Fusheng p. 140

**INTERNATIONAL SYMPOSIUM ON A RECENT PROGRESS
IN FOREST ECOLOGY AND MANAGEMENT
2021**

KEYNOTE SPEECH 1

**Wednesday, 10th November 2021
12:05 - 13:25**

ORGANIZER:

THE UNITED GRADUATE SCHOOL OF AGRICULTURAL SCIENCE, GIFU UNIVERSITY

Long-term Field Data Unveil Characteristics of Phenology and Forest Dynamics in a Bornean Tropical Rain Forest

Michiko Nakagawa

Graduate School of Bioagricultural Sciences, Nagoya University

Corresponding Author: miko@agr.nagoya-u.ac.jp

SUMMARY

Tropical rainforests in Borneo, which are known to possess extremely species-rich tree communities, are characterized by abundant rainfall throughout the year, and are thought to be among the most humid biomes in the world. In such a forest, tree phenology and forest dynamics would be expected to be stable. Meteorological conditions, flowering and fruiting phenology, litterfall production, tree growth, and tree mortality/recruitment have been monitored for long term in Lambir Hills National Park, Sarawak, Malaysia, with the cooperation of a lot of researchers and local assistants. Contrary to our expectations, long-term field data indicate that temporal fluctuations in climatic conditions drive community-wide phenomena such as intermittent mass flowering and mass fruiting, dynamic changes in tree mortality, recruitment rate, and litterfall production.

Keywords: *General flowering and fruiting; Lambir Hills National Park; Tree mortality; Litterfall production; Drought*

Unfolding a Mystery of Tropical Mangroves from a Two-decade Journey in Mangrove Study

Sasitorn Pongparn

Department of Botany, Faculty of Science, Chulalongkorn University, Bangkok, Thailand

Corresponding Author: Sasitorn.P@chula.ac.th

SUMMARY

Mangrove study has been attracting scientists for several decades as a prominent global carbon sink ecosystem. Relating to this topic, I have been spending two decades studying a mangrove forest under a tropical monsoon climate in eastern Thailand. A long-term study plot was firstly established at this estuarine mangrove forest in Trat province in 2001, led by Prof. A. Komiyama of Gifu University. My journey in mangrove study began with root biomass study because I was astonished by the peculiar shapes and large accumulation of roots in the mangrove forest. However, the estimation of root biomass was a hard work at that moment. We took a big step closer in 2005 that we successfully established the common allometric relationships for biomass estimation in mangrove forests by using an ecological theory of tree form “Pipe Model”, which enables biomass estimation of major mangrove tree species.

By using the powerful tool “common allometry”, a study on net primary production (NPP) and CO₂ efflux from the soil respiration was consecutively conducted in this study plot. The results revealed the high NPP and low CO₂ efflux by heterotrophic respiration under submerged soils of the mangrove forest and consequently led to high net ecosystem production (NEP). The high NPP of this mangrove forest was partly contributed by fine roots that we uncovered the high production of fine roots by using the ingrowth core method. Moreover, we tackled a frequently-neglected problem “coarse woody debris” in the NPP estimation. A long-term NPP estimation of this forest (2008-2018) signified that the interannual variation of the rainfall and the maximum air temperature in the dry season caused increasing tree mortality leading to lower NPP.

However, another perplexing mystery of mangrove forests having high NPP and NEP will be profoundly related to adaptation of mangroves in fluctuated salinity environment of the estuary. Congruently, global climate change has intensified the extreme events which may alter the salinity environment in the coastal areas and affect several organisms in coastal ecosystems. Therefore, our most recent studies focus on how the mangroves can survive and provide high productivity in the fluctuating, both seasonally and daily, saline environment under a tropical monsoon climate. At our study site, we found the seasonal variation of soil-water salinity that negatively correlated with monthly rainfall showing the lower salinity during the wet season and vice versa in the dry season. The mysterious salinity fluctuation was clarified that the seasonal variation was induced by the daily inundation and the pattern of soil water movement across the soil profiles as we defined them as thin ‘tide-sensitive’ and ‘aquifer’ layers of the soils.

Interestingly, we disclosed that the *Avicennia alba* tree, a fast-growing species, has a seasonal trunk-growth pattern, which has a higher growth rate in the wet season under low salinity of soil water close to the freshwater. There was very small trunk growth during the dry season with high soil-water salinity close to the seawater level. Not only trunk growth but leaf emergence was found responding to the seasonal pattern of salinity that we found a synchronization between the rates of trunk growth and leaf emergence in *A. alba* trees. These seasonal growth patterns are considered a growth strategy of *A. alba* to cope with the salinity fluctuation. Our latest ongoing research exhibits the seasonal growth pattern of other key mangrove species. The research series from this long-term study plot disclose the secret of the growth strategy of mangroves that we characterized them as an ‘opportunistic’ showing high growth rates when the freshwater is abundant in the wet season. This character benefits as an adaptive plasticity to survive and maintain high NPP of the mangrove forest under fluctuation of salinity environment in the tropical coastal areas. A propounded problem of “mangrove zonation” was addressed in that the heterogeneous salinity environments influenced the occurrence of zonation. There is always a mystery of mangrove forests waiting to be solved through our long journey in mangrove study.

Keywords: Forest Productivity; Mangrove; Monsoon climate; Salinity fluctuation; Seasonal growth

**INTERNATIONAL SYMPOSIUM ON A RECENT PROGRESS
IN FOREST ECOLOGY AND MANAGEMENT
2021**

**SESSION 1
FOREST CARBON CYCLE AND CLIMATE CHANGE**

**Wednesday, 10th November 2021
13:45 - 15:00**

ORGANIZER:

THE UNITED GRADUATE SCHOOL OF AGRICULTURAL SCIENCE, GIFU UNIVERSITY

Net Primary Productivity Estimation in the Chronosequence Coastal-mangrove Plantations in Central Thailand

Suthathip Umnouysin^{1*}, Sasitorn Pongpam², Vilanee Suchewaboripont³,
Chadtip Rodtassana², Tanapon Pongsuvarod²

¹ Department of Biology, Faculty of Science, Silpakorn University, Nakhon Pathom 73000, Thailand

² Department of Botany, Faculty of Science, Chulalongkorn University, Bangkok 10330, Thailand

³ The Institute for the Promotion of Teaching Science and Technology, Bangkok 10110, Thailand

*Corresponding Author: umnouysin_s@su.ac.th

SUMMARY

We present net primary productivity (NPP) estimation in chronosequence coastal-mangrove plantation at Bang Pu, Samut Prakarn Province in central Thailand. The chronosequence plantations consist of four *Avicennia alba* plantations with the age of 15, 12, 10, and 8 years old. The NPP estimation was calculated by a summation product of growth increment (ΔY) and litter production (L). The ΔY included the biomass increment of living trees, biomass increment of newly recruited trees, and fine root production from June 2020 to May 2021. We also investigated the coarse woody debris (CWD) flux including necromass and coarse litter production during this period. The results demonstrated that the ΔY and L showed a positive trend with the ages of plantations. Therefore, the NPP decreased with increasing plantation ages, they were 20.33, 22.84, 23.92, 34.00 t/ha/yr for 15-, 12-, 10-, and 8-year plantations, respectively. The ΔY / fine litter ratio was calculated at 0.72, 0.71, 1.11, 1.63 for 15-, 12-, 10-, and 8-year plantations, respectively. The high ΔY /fine litter ratio in the young *A. alba* plantation indicated that the young trees maximized the stand growth with the available leaf budget, and therefore resulted in the relatively high NPP of the young plantation. The proportion of CWD flux to NPP was averaged as 57.9% across the four plantations. It was extremely high in the 10-year plantation (85.0%). The proportions of these chronosequence coastal-mangrove plantations were higher than the mature *A. alba* forest due to a process of self-thinning in the high-density stand of the young plantation. Our study suggests that forest development could occur in the mangrove plantations with the high NPP of young plantations. More accurate NPP estimation is required to assess the potential of mangrove plantations that can provide ecological functions sustaining the carbon dynamics in coastal areas under climate change.

Keywords: Net primary production; Carbon dynamics; Mangrove plantations

Introduction

Mangrove forests significantly contribute to global carbon stock as well-known for the high net primary productivity (NPP) (Alongi, D. M., 2014) and the 'vegetated blue carbon' playing an important role in coastal carbon fluxes (Macreadie, P. I. *et al.*, 2019). The NPP indicates forest productivity and carbon capture in mangrove ecosystems, especially in the vegetative parts (both biomass and necromass), which can be estimated by using the summation method generally including the growth increment and litter production (Komiyama, A. *et al.*, 2008). Forest productivity related to forest dynamics according to forest structure and age that the mature

mangrove forests were reported for the greater tree diameter-size while the young stands usually had higher stem density (Azman, M. S. *et al.*, 2021).

In the last decades, mangrove plantation has been publicly considered as an approach to restoring the coastal mangrove ecosystems, especially the new mudflat areas, with an engagement with several sectors including government, private sectors, and the public. However, the planting campaign usually ran for a short period and frequently lacked post-planting assessment. For successful mangrove rehabilitation, rather than an instant planting in the large area, long-term monitoring is required to protect losing of established plantations (Lee, S. Y. *et al.*, 2019).

Therefore, the chronosequence mangrove plantations are suitable to assess the potential of mangrove plantations in terms of carbon sequestration that will assist the carbon mitigation.

We aim to estimate the NPP of the chronosequence coastal-mangrove plantation (ranging from 8 to 15 years) at Bang Pu, central Thailand by using the summation method including the growth increment and litter production. Moreover, the CWD fluxes were incorporated in the carbon estimation. A more accurate NPP estimation is important to improve an assessment of mangrove plantations in an aspect of the carbon budget that will benefit the planning of mangrove management and conservation under climate change.

Materials and Methods

The study site is the chronosequence coastal-mangrove plantations at Bang Pu Recreation Center (13°31'N 100°39'E), Samut Prakarn Province in central Thailand. The chronosequence plantations are dominated by *Avicennia alba* with the stand ages of 15, 12, 10, and 8 years old since first planted in 2006.

At each stand, the four study plots (10 m × 10 m) were established. We measured stem diameter at breast height (DBH) and height (H) in June 2020 (t_1) and May 2021 (t_2). Newly recruited trees (DBH reached 4.5 cm) were also recorded at t_2 . The aboveground biomass (W_{Top}) and root biomass (W_R) were calculated using the common allometric equations for mangrove species (Komiya, A. *et al.*, 2005). Fine root production (FRP) was estimated from the fine root production rates in the 15- and 10-year plantations by using the ingrowth core method (0-30 cm depth) during July 2019 – July 2020 (unpublished data). The FRP rate was calculated as 0.03 t ha⁻¹ yr⁻¹ for all stand ages. Growth increment (ΔY) was calculated based on approach 1 of Clark, D.A. *et al.* (2001); ΔY included the biomass increment of living trees present at t_2 (ΔB), biomass increment of newly recruited trees (N), and FRP, as shown in equation (1).

$$\Delta Y = \Delta B + N + FRP \quad (1)$$

Litterfall was collected monthly from 12 litter traps each stand then oven-dried at 80°C to a constant mass. The litterfall was weighed separately into fine litter (leaves and reproductive organs) and coarse litter (branches and woody parts). The annual

litter production (L) of each stand was calculated by summing monthly litterfall from June 2020 to May 2021.

Net primary production (NPP) was calculated by a summation of ΔY and L, as shown in equation (2).

$$NPP = \Delta Y + L \quad (2)$$

Dead trees were recorded in May 2021 (t_2). The mortality rate was estimated using a logarithmic model by Miura, M. *et al.* (2001). The necromass of aboveground, leaf, and root components was estimated using the common allometric equations (Komiya, A. *et al.*, 2005). An annual flux of coarse woody debris (CWD) was obtained by summing necromass excluding leaf and coarse litter production.

Results and Discussion

The tree density across the chronosequence plantations ranged from 975 to 1813 stems ha⁻¹, which were purely *A. alba* trees. The density tended to increase with decreasing stand ages (Table 1). However, the tree size showed an opposite trend that the largest tree sizes were found in 15-year plantation followed by the younger stands.

Table 1: Forest structure of living trees in June 2020 and dead trees in May 2021

	15- year	12- year	10- year	8- year
Living tree				
Tree density (stems ha ⁻¹)	975	1700	1813	1800
Average DBH (cm)	20.5	13.6	12.2	11.0
Average H (m)	11.1	9.23	9.34	7.32
Dead tree				
Number of dead trees (stems ha ⁻¹)	50	200	363	500
Average DBH (cm)	16.0	9.39	10.8	8.57
Average H (m)	5.60	6.14	8.02	5.81
Mortality rate (%)	5.26	14.2	22.3	28.8

The mortality rate increased with decreasing stand ages, which the highest number of dead trees were found in the 8-year plantation with the highest mortality rate (28.8%) (Table 1). During forest development, the self-thinning process occurs in a high-density stand due to the resource competition supporting tree growth under constrained environments (Kamara, M. and M. Kamruzzman, 2020; Kamruzzman, M. *et al.*, 2018).

The ΔB and ΔY showed a positive trend with increasing stand ages (Table 2). The ΔY ranged from 8.02 to 20.26 t ha⁻¹ yr⁻¹. The newly recruited trees were only found in the youngest plantation where the highest mortality rate was observed. Fine litter production ranged from 10.66–12.40 t ha⁻¹ yr⁻¹ (Table 2), which shared the high proportion of 86–91% of total litter production. The NPP was subsequently calculated as 20.33, 22.84, 23.92, 34.00 t ha⁻¹ yr⁻¹ for 15-, 12-, 10-, and 8-year plantations, respectively. It is remarkable that the lower NPP was found in the older plantation ages consistent with other studies (Azman, M. S., *et al.*, 2021; Sahu, S. K. and K. Kathiresan, 2019).

The ΔY /fine litter ratio varied across stand ages, which were 0.72, 0.71, 1.11, 1.63 for 15-, 12-, 10-, and 8-year plantations, respectively. It was suggested as 1:1 in mangrove ecosystems (Day, Jr., J. W. *et al.*, 1987). The ratios obtained from our study were higher compared to the study in a subtropical mangrove forest in Japan reported as 0.41 (Ohtsuka, T. *et al.*, 2019). However, our results showed that the young stand ages had higher ratios which implies the potential of young mangrove plantations to enhance the stand increment.

Table 2: Biomass increment, fine root production, growth increment, litter production, and net primary production during June 2020 to May 2021

	15- year	12- year	10- year	8-year
Biomass increment of living tree at t_2 (ΔB ; t ha ⁻¹ yr ⁻¹)				
Aboveground	5.85	6.26	8.45	14.55
Root	2.14	2.41	3.34	5.62
Total	7.99	8.67	11.79	20.17
Biomass increment of newly recruited trees (N; t ha ⁻¹ yr ⁻¹)				
Aboveground	0.00	0.00	0.00	0.04
Root	0.00	0.00	0.00	0.02
Total	0.00	0.00	0.00	0.06
Fine root production (FRP; t ha ⁻¹ yr ⁻¹)				
	0.03	0.03	0.03	0.03
Growth increment (ΔY ; t ha ⁻¹ yr ⁻¹)				
Aboveground	5.85	6.26	8.45	14.59
Root	2.17	2.44	3.37	5.67
Total	8.02	8.70	11.82	20.26
Litter production (L; t ha ⁻¹ yr ⁻¹)				
Fine litter	11.18	12.22	10.66	12.40
Coarse litter	1.13	1.92	1.44	1.34
Total	12.31	14.14	12.10	13.74
Net primary production (NPP; t ha ⁻¹ yr ⁻¹)				
	20.33	22.84	23.92	34.00

Table 3: Annual coarse woody debris (CWD) flux

	15- year	12- year	10- year	8-year
Necromass production (t ha ⁻¹ yr ⁻¹)				
Aboveground (except for foliage)	6.70	6.03	12.59	9.33
Root	2.78	3.13	6.30	4.97
Total	9.48	9.16	18.89	14.30
Coarse litter production (t ha ⁻¹ yr ⁻¹)				
	1.13	1.92	1.44	1.34
CWD flux (t ha ⁻¹ yr ⁻¹)				
	10.61	11.08	20.33	15.64

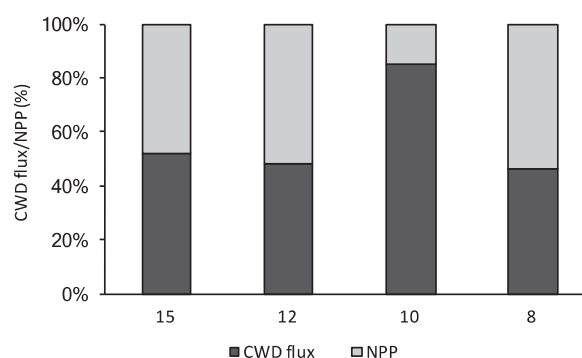


Figure 1: Proportion of the CWD flux to net primary production (NPP)

The young plantation (10-year) had the highest necromass (excepting leaf mass), particularly the aboveground part as shown in Table 3. The average DBH of dead trees in this stand was larger than that of the 8-year plantation; however, the youngest plantation had the highest number of dead trees (Table 1). The CWD fluxes were high in the younger plantations (10- and 8-year) with approximately 1.5 to 2 times compared to the older plantations (Table 3). While the proportions of necromass production to the CWD flux were high in all stands (83–93%). Our findings confirmed the high CWD flux in the younger stands. Although, the younger stands could produce relatively high stand increment. The residence time of aboveground woody components was relatively short due to high mortality rates of the dense stand, which were reported in tropical forests under disturbed conditions (Muller-Landau, H. C. *et al.*, 2021).

The proportion of CWD flux to NPP was averaged as 57.9% across all stand ages; the proportion of the 10-year plantation was

exceptionally high as 85.0% (Figure 1). In a secondary mangrove forest under natural rehabilitation (on an estuary of the Trat River in eastern Thailand), Umnouysin, S. *et al.*, (2017) reported an average proportion of CWD flux to NPP as 24.8%. It is apparently lower than that of the present study suggesting the significance of CWD fluxes in the chronosequence plantation along with the coastal areas. The high CWD fluxes assume the accelerated stand dynamics under the development of mangrove plantations.

Conclusions

We demonstrated that the chronosequence mangrove plantations had different vegetation structures leading to the different magnitudes of NPP. The highest NPP was found in the young plantations in consistence with the trends of mortality rate and CWD flux. We confirmed that the CWD flux is substantial for NPP estimation in mangrove plantations during forest development. Our findings will be beneficial for management planning for mangrove restoration to enhance the capacity of carbon storage on the coastal areas.

Acknowledgment

This study was supported by the Toyota Motor Thailand Co., Ltd. We are grateful to the staff of Bang Pu Recreation Center, which is under the supervision of the Quartermaster Department of the Royal Thai Army, and the staff of the Foundation for Environmental Education for Sustainable Development (FEED), Thailand.

References

- Alongi, D. M. (2014) Carbon cycling and storage in mangrove forests. *Annual Review of Marine Science*, 6:195–219.
- Azman, M. S., Sharma, S., Shaharudin, M. A. M., Hamzah, M. L., Adibah, S. N., Zakaria, R. M., MacKenzie, R. A. (2021) Stand structure, biomass and dynamics of naturally regenerated and restored mangroves in Malaysia. *Forest Ecology and Management*, 482: 118852.
- Clark, D. A., Brown, S., Kicklighter, D. W., Chambers, J. Q., Thomlinson, J. R., Ni, J. (2001) Measuring net primary production in forest: concepts and field methods. *Ecological Applications*, 11(2):356–370.
- Day, Jr. J. W., Conner, W. H., Ley-Lou, F., Day, H., Navarro, A. M. (1987) The productivity and composition of mangrove forests, laguna de Términos, Mexico. *Aquatic Botany*, 27:267–284.
- Kamara, M., Kamruzzaman, M. (2020) Self-thinning process, dynamics of aboveground biomass, and stand structure in overcrowded mangrove *Kandelia obovata* stand. *Regional Studies in Marine Science*, 38:101375.
- Kamruzzaman, M., Ahmed, S., Paul, S., Rahman, M. M., Osawa, A. (2018) Stand structure and carbon storage in the oligohaline zone of the Sundarbans mangrove forest, Bangladesh. *Forest science and technology*, 14(1):23–28.
- Komiyama, A., Ong, J.E., Pongparn, S. (2008) Allometry, biomass, and productivity of mangrove forests: a review. *Aquatic Botany*, 89:128–137.
- Komiyama, A., Pongparn, S., Kato, S. (2005) Common allometric equations for estimating the tree weight of mangrove. *Journal of Tropical Ecology*, 21:471–477.
- Lee, S. Y., Hamilton, S., Barbier, E. B., Primavera, J., Lewis, R. R. (2019) Better restoration policies are needed to conserve mangrove ecosystems. *Nature Ecology & Evolution*, 3:870–872.
- Macreadie, P. I. *et al.* (2019) The future of Blue Carbon science. *Nature Communications*, 10:3998. <https://doi.org/10.1038/s41467-019-11693-w>.
- Miura, M., Manabe, T., Nishimura, N., Yamamoto, S. (2001) Forest canopy and community dynamics in a temperate old-growth evergreen broad-leaved forest, south-western Japan: a 7-year study of a 4-ha plot. *Journal of Ecology*, 89:841–849.
- Muller-Landau, H. C., Cushman, K. C., Arroya, E. E., Cano, I. M., Anderson-Teixeira, K. J., Backiel, B. (2021) Patterns and mechanisms of spatial variation in tropical forest productivity, woody residence time, and biomass. *New Phytologist*, 229:3065–3087.
- Ohtsuka, T., Tomotsune, M., Suchewaboripont, V., Iimura, Y., Kida, M., Yoshitake, S., Kondo, M., Kinjo, K. (2019) Stand dynamics and aboveground net primary productivity of a

- mature subtropical mangrove forest on Ishigaki Island, south-western Japan. *Regional Studies in Marine Science*, 27:100516.
- Sahu, S. K., Kathiresan, K. (2019) The age and species composition of mangrove forest directly influence the net primary productivity and carbon sequestration potential. *Biocatalysis and Agricultural Biotechnology*, 20:101235.
- Umnouysin, S., Sangtiew, T., Pongparn, S. (2017) Zonal distribution of coarse woody debris and its contribution to net primary production in a secondary mangrove forest. *Ecological Research*, 32:51–60.

Relationships between Carbon Stocks and Trees Biodiversity in Production Forest of Register 24, Lampung Province

Christine Wulandari ^{1*}, Samsul Bakri ², Yanfa Ghiyats Ghifari ³,
Destia Novasari ¹, Lia Mulyana ¹, Azhary Taufiq ¹,
Nindya Tria Puspita ¹ and Imawan Abdul Qohar ¹

¹ Magister Program of Forestry, Faculty of Forestry, The University of Lampung

² Magister Program of Environment, The University of Lampung

³ Forestry Department, Faculty of Agriculture, The University of Lampung

*Corresponding Author: christine.wulandari@fp.unila.ac.id

SUMMARY

Many studies stated declining of forest biodiversity will have an impact on decreasing carbon stocks. Based on this condition, it will be necessary to adapt the climate change for maintaining the carbon stock. The availability of sufficient carbon stock will affect the environment condition surrounded the forest. Generally, research that has been done is the correlation between trees biodiversity based on number of species and trees growth phase. Specific study in West Nusa Tenggara, Indonesia mentioned that carbon stock is influenced by wood of trees, not by number of trees species. Based on this research results, the important question is how to maintain carbon stock sufficiency in such production forests in Indonesia because community allow for logging? Research conducted in October 2018 at Register 24 forest area in Lampung Province. This study objectives are to be examined whether trees in production forest of Register 24 are correlated with carbon stocks, and how recommendations can be made to maintain this carbon stock adequacy because trees cutting is permitted in this type of forest.

Keywords: Carbon stock; Trees biodiversity; Production forest

Introduction

Deforestation and forest burning are the causes of damage to resources and the environment, which will indirectly result in a decrease in the forest area. Damage to resources and the environment will have an impact on increasing the earth's temperature, this is related to the carbon absorption process carried out by the vegetation on the land (Erly *et al.*, 2019). Vegetation has the ability in the process of photosynthesis (Rizki *et al.*, 2016). The process of photosynthesis in plants can convert carbon dioxide into glucose and oxygen through the absorption of CO₂ and water with the help of sunlight (Prihatmaji *et al.*, 2016; Hatulesila *et al.*, 2018). The more types of plants, the higher the value of carbon absorbed by plants on the land. So that the diversity of plant species will also affect the amount of carbon in an area.

The vegetation of a forest area generally has several phases, including the phases of trees, poles, saplings, and undergrowth. The tree phase is the largest carbon store. This is in line with the results of research conducted, which states that woody trees aged 6-9 years will have the ability to

absorb carbon more optimally (Supriadi & Adiansyah, 2013). This will indirectly influence the condition of Production Forests because in Indonesia's production forest policy it is permissible to cut down trees. One of the existing production forests in the Lampung area is the forest area of register 24 which is included in the management area of the Bukit Punggur Forest Management Unit (FMU), Lampung.

The FMU of the Bukit Punggur Model, Way Kanan Regency is determined by the Decree of the Minister of Forestry Number SK. 439/Menhut-II/2012 covering an area of ±41,126 ha. The dominant plants in the Bukit Punggur FMU are marawan (*Hopea mangarawan*), medang (*Litsea firmaho*), tenam (*Shorea platycloda* V.Sb.) cempaka (*Beilschielda* sp.), Benda (*Arthocarpus* sp.), Bungur (*Lagerstroemia* spp.), puspa (*Schima* spp.), rasamala (*Altingia excelsa*), rattan (*Calamus* sp.), forest orchids and ferns. Animals in the Bukit Punggur FMU forest area are gibbons (*Symphalangus syndactylus*), monkeys (*Presbytis melalopus*), snakes (*Phyton* sp.), eagles (*Heliastur* sp.), parrots (*Gracula*), sambar deer (*Cervus unicolor*), deer

(*Muntiacus muntjak*), tiger (*Panthera tigris sumatrae*), root tiger (*Felis bengalensis*), sun bear (*Helarctos malayanus*), tapir (*Tapirus indicus*), and pangolin (*Manis javanica*) (KPH Bukit Punggur, 2015). Production forest in FMU of Re-gister 24 is managed under the Social Forestry program, namely the Community Forest scheme. Thus this forest is managed on a community basis. This means that this forest must provide ecological benefits for forest sustainability and also have economic benefits for community income and the FMU.

One way to maintain ecological sustainability through the conservation of biodiversity is to preserve the function of carbon sequestration and storage. Research conducted by Susilo, A (2019) that monoculture forests such as teak forests or industrial plantation forests have low biodiversity but high carbon stocks. The diversity of plant species in a forest will also support the sustainability of the income of the community managing it (Wulandari et al., 2021). Thus, the diversity of species in a forest location will support ecological and economic functions towards sustainability.

Several studies have found that tree diversity also affects the amount of tree carbon stored in forest areas. In addition, tree density and species are positively correlated with changes in carbon storage (Chairul et al., 2016; Banjarnahor et al., 2018; Erly, et al., 2019). Supriadi & Adiansyah (2013) and Markum (2013) added that the thickness of the wood in a tree also affects the amount of carbon in the area. Therefore, this study aims to examine whether trees in Register 24 production forest are correlated with a carbon stock and to develop recommendations to maintain adequate carbon stock in Register 24 production forest because tree cutting is allowed in this type of forest.

Research Methods

1. Research time and place

This research was conducted in October 2018. Data collection was carried out in the Register 24 forest area which is the Bukit Punggur FMU, Way Kanan Regency, Lampung Province. The study was conducted using the Stratified Sampling method in the Register 24 Forest Area.

2. Research Objects and Tools

The object in this study is a tree. The tools used in this study were a tape meter to measure diameter, a Christian hypsometer to measure tree height, an observation sheet (tally sheet), scissors to cut undergrowth, an oven to remove the moisture content of undergrowth and litter, a digital scale with gram units for weighing. undergrowth and litter, cameras for documentation, ropes for plot measurements, GPS for downloading plot coordinates, and a laptop for data processing and making research reports.

3. Research methods

a. Vegetation data

According to Ambarwati (2018) vegetation data in the form of undergrowth, saplings, poles, and trees, namely the number of each species found in the measuring plot with a size of 20 m x 20 m. Vegetation data is used to determine the INP in the Forest Area Register 24, Way Kanan Regency, Lampung.

b. Plot measuring

Determination of measuring plots as many as 16 plots were carried out using the Stratified Sampling method which is a carefully selected sampling method so that it is relevant to sampling data that has been grouped by altitude class (Bhaskara, 2018). Altitude ranges from 550-950 m above sea level.

Table 1: Number of plots in research area

Height Class	Height	Total Plot
1	550 – 650 m asl	4
2	651 – 750 m asl	4
3	751 – 850 m asl	4
4	851 – 950 m asl	4
Total		16

c. Sample plot

The shape of the sample plot used in this study is a square with a size of 20 m x 20 m which is used for biomass data collection (Bhaskara, 2018). The size of the plot to measure each phase of plant growth can be seen in Figure 1.

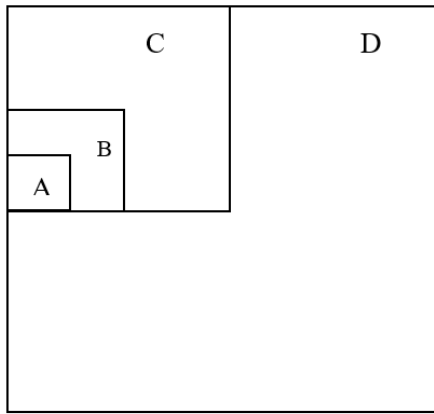


Figure 1: Plot for biomass data collection.

- A: It is a plot measuring 2 m x 2 m, used for sampling litter and undergrowth with a height of <1.5 m.
- B: This is a 5 m x 5 m sample plot, used for saplings with a diameter of <10 cm and a plant height of >1.5 m.
- C: This is a sample plot measuring 10 m x 10 m, used for pole level with a diameter of 10-20 cm.
- D: This is a sample plot measuring 20 m x 20 m, used for tree-level with a diameter of > 20 cm.

4. Data collection

a. Tree biomass

Biomass data were collected using a non-destructive method (not cutting down trees) on each tree in the 20 m x 20 m plot. Trees taken for biomass calculation must be accompanied by data on tree species, diameter, and height of the tree. Biomass measurements were carried out at the tree phase in the 20 m x 20 m plot, the sapling phase in the 5 m x 5 m plot, and the pole phase in the 10 m x 10 m plot.

b. Importance value index

According to Winardi (2014), it is necessary to carry out a vegetation analysis to determine the dominance of a vegetation type over other species in a stand by using the Important Value Index (INP). The INP calculation provides data on the dominant tree species in research areas.

The amount of the Important Value Index (INP) in vegetation can be calculated based on Indiyanto (2016) with the following equation.

$$K = \frac{\text{Number of species-n}}{\text{The total area of the sample plot}} \quad (1)$$

$$KR = \frac{\text{Species density-n}}{\text{Whole species density}} \times 100\% \quad (2)$$

$$F = \frac{\text{The number of sample plots found for a species-n}}{\text{Total Plot}} \quad (3)$$

$$FR = \frac{\text{Frequency of a species-n}}{\text{Frequency of whole species}} \times 100\% \quad (4)$$

$$D = \frac{\text{The total area of the base area}}{\text{The total area of the whole plot}} \quad (5)$$

$$DR = \frac{\text{The dominance of a species}}{\text{The dominance of whole species}} \times 100\% \quad (6)$$

Based on this equation, to calculate the Important Value Index (INP) in a species comes up with the equation:

$$INP = KR + FR + DR \quad (7)$$

Description :

INP: Determination of the dominance of one species over other species from the total sample plots

KR: Percentage of the number of plant species in question from the total unit area

FR: Percentage of the number of plots where a species is found from the total unit area

DR: Percentage of the main plant species that influence the community in terms of the number of species, size, and dominant growth

5. Biomass estimation

a. Tree biomass

The results of measurements of tree diameter and tree height were analyzed using the existing allometric equations to estimate tree biomass as in Table 2.

b. Stored carbon

Carbon stored in forest vegetation can be estimated using the biomass value obtained from the allometric equation or the BSN equation (2011) which states that the percentage value of carbon content is 47% so that the calculation of stored carbon can be converted into carbon (tons/ha). Calculation of carbon can be done using a conversion factor of 0.47 which is expressed in the following formula.

$$\text{Carbon (C)} = \text{Total Biomass} \times 0,47 \quad (8)$$

Table 2: Allometric equation model

No	Stands Type	Allometric Equation	Source	Location
1	Mahogany	$BK = 0,902 (D^2H)^{0,08}$	(Tim Arupa, 2014)	Dn. Kembangan, Sleman
2	Acacia	$BK = 0,077 (D^2H)^{0,90}$	(Tim Arupa, 2014)	Dn. Kembangan, Sleman
3	Medang	$BK = 0,11 \times 0,51(D)^{2,62}$	(Ketterings, 2001)	Sepunggur, Jambi
4	Clove	$BK = 0,11 \times 0,7(D)^{2,62}$	(Ketterings, 2001)	Sukamantri, Bogor
5	Branched Trees	$BK = 0,11 \rho(D)^{2,62}$	(Ketterings, 2001)	Sepunggur, Jambi
6	Non-branched Trees	$BK = \pi \rho D^2 H / 40$	(Hairiah dkk., 2001)	Rantau Pandan, Jambi
7	Coffee	$BK = 0,281 (D)^{2,06}$	(Nugroho, 2014)	Dn. Kembangan, Sleman
8	Rubber	$BK = 3,42 D^{1,15}$	(Saragih dkk, 2016)	Kabupaten Serdang Begadai

BK = Dry weight (kg/tree),

D = Diameter breast height (cm),

ρ = Wood Specific Gravity (0,7 g/m³) and the density of dead wood (0,4 g/m³)

H = Total plant height (m)

BA = Basal area (cm²)

Results and Discussion

1. Importance Value Index (INP)

The Important Value Index (INP) according to Ambarwati *et al* (2019) is an indicator used to determine the dominant species in a plant community. The Important Value Index leads to the analysis of vegetation, the emphasis of the analysis lies on the species composition. According to Putri and Indriyanto. (2021) species composition in a forest habitat is influenced by the habitat and plant species in the area. The results obtained from research on production forests which are the Bukit Punggur FMU are 14 types of tree phase plants, 8 types of pole phase plants, 10 types of sapling phase plants, and 26 types of seedlings and understorey plants. As a production forest, the management mechanism is different from that of a protected forest. In production forests, logging is permitted as long as it is following the permit granted. In Forest Register 24, the production forest is managed by the community through the Social Forestry Scheme, namely Community Forest (CF). This means that the management of production forests in Register 24 is carried out on a community basis. If logging is required, a permit from the government must be obtained through the Bukit Punggur FMU. Thus, the regulation of sustainability must be a FMU policy that is supported by the community who are members of the CF group, for example in the selection of trees and species that may be cut and will not interfere with the function of the forest ecosystem. If logging is required, a permit from the

government must be obtained through the Bukit Punggur FMU. Thus, the regulation of sustainability must be a FMU policy that is supported by the community who are members of the CF group, for example in the selection of trees and species that may be cut and will not interfere with the function of the forest ecosystem. If logging is required, a permit from the government must be obtained through the Bukit Punggur FMU. Thus, the regulation of sustainability must be a FMU policy that is supported by the community who are members of the CF group, for example in the selection of trees and species that may be cut and will not interfere with the function of the forest ecosystem.

1.1. Trees

Trees are cambium plants that have a diameter of more than 20 cm and a height of more than 5 m. Tree phase measurements were carried out on plots measuring 20 m x 20 m. The data obtained in the tree phase contained 14 plant species which can be seen in Table 3.

The results obtained from the study were found 14 plant species in the tree phase. The dominant tree species for the tree phase in all altitude classes were rubber (*Hevea brasiliensis*). This species dominates the area with 81 trees. The species with the lowest INP was the jackfruit (*Artocarpus heterophyllus*) with 1 tree. The dominating species are Multi Purpose Tress Species (MPTS) with 10 species, while for forestry there are only 4 species.

Table 3: INP tree phase at the research site

No	Local name	Scientific name	INP (%)
1	Karet	<i>Hevea brasiliensis</i>	128.03
2	Pulai	<i>Alstonia scholaris</i>	23.66
3	Medang	<i>Phoebe hunanensis</i>	4.42
4	Jengköl	<i>Archidendron pauciflorum</i>	31.81
5	Durian	<i>Durio zibethinus</i>	15.60
6	Akasia	<i>Acacia auriculiformis</i>	16.84
7	Nangka	<i>Artocarpus heterophyllus</i>	3.31
8	Mangga	<i>Mangifera indica</i>	4.84
9	Kapuk	<i>Ceiba pentandra</i>	4.59
10	Cengkeh	<i>Syzygium aromaticum</i>	19.36
11	Pinang	<i>Areca catechu</i>	6.78
12	Petai	<i>Parkia speciosa</i>	18.73
13	Tangkil	<i>Gnetum gnemon</i>	5.15
14	Mangium	<i>Acacia mangium</i>	16.86
Total			300

Source: Primary data (2019).

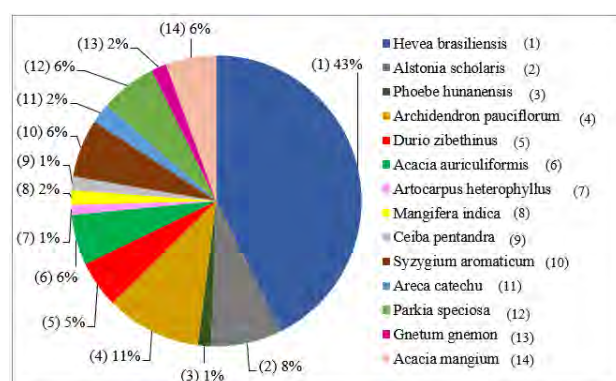


Figure 2: The tree phase significance value index.

The percentage of dominant plant species in the tree phase can be seen in Figure 2. The species with the largest INP is rubber (*Hevea brasiliensis*) which has an INP percentage of 128.03%. Zhafira *et al.* (2019) in his research explains that rubber plants in the research location are the dominating species while forestry plant types include acacia (*Acacia sp.*), mahogany (*Sweitenia mahagoni*), jackfruit (*Arthocarpus heterophyllus*), durian (*Durio zibethinus*), avocado (*Persea americana*) and pulai (*Alstonia scholaris*). The dominant rubber plant (*Hevea brasiliensis*) in this location was caused by the National Movement for Land and Forest Rehabilitation (GNRHL) program in 2003-2004.

1.2. Pole

The pile phase was measured on a 10m x 10m plot. The pole phase in question is a plant that

has a diameter of 10-19 cm. Phase INP calculation results poles obtained 8 plant species (Table 4).

The INP results obtained by the pole phase amounted to 8 species consisting of 6 species of MPTS plant species and 2 types of forestry plants. The dominant species in the four altitude classes were rubber (*Hevea brasiliensis*) with a total of 91 trees. Species that have the lowest INP values are medang (*Phoebe hunanensis*) and pulai (*Alstonia scholaris*) with only 1 tree each.

The species that dominates the pole phase is the same as the dominant species in the tree phase, namely rubber plants (*Hevea brasiliensis*). In the pole phase, rubber plants have an INP of 156.31% which tends that rubber is grown in monoculture. According to Supriadi *et al.* (2018) that forestry crops and other types of rubber MPTS found in the field are generally planted as land boundaries.

1.3. Stake

The stake phase was measured on a 5m x 5m plot. Saplings can be defined as plants that are more than 1.5 meters tall and <10 in diameter cm. The results of the INP calculation at the stake phase can be seen in Table 5.

Table 4: INP of the poles phase at the research site

No	Local name	Scientific name	INP (%)
1	Karet	<i>Hevea brasiliensis</i>	156.31
2	Medang	<i>Phoebe hunanensis</i>	7.91
3	Jengköl	<i>Archidendron pauciflorum</i>	14.89
4	Pulai	<i>Alstonia scholaris</i>	6.33
5	Cengkeh	<i>Syzygium aromaticum</i>	58.83
6	Jambu bol	<i>Syzygium malaccense</i>	6.91
7	Durian	<i>Durio zibethinus</i>	31.33
8	Petai	<i>Parkia speciosa</i>	17.49
Total			300

Source: Primary data (2019).

Table 5: INP of the stake phase in research areas

No	Local name	Scientific name	NIP (%)
1	Kopi	<i>Coffea canephora</i>	97.12
2	Cengkeh	<i>Syzygium aromaticum</i>	95.21
3	Karet	<i>Hevea brasiliensis</i>	51.58
4	Durian	<i>Durio zibethinus</i>	8.09
5	Jambu biji	<i>Psidium guajava</i>	10.82
6	Jengkol	<i>Archidendron pauciflorum</i>	9.26
7	Sawo	<i>Manilkara zapota</i>	10.34
8	Petai	<i>Parkia speciosa</i>	5.47
9	Waru	<i>Hibiscus tiliaceus</i>	5.42
10	Akasia	<i>Acacia auriculiformis</i>	6.68
Total			300

Source: Primary data (2019).

The species that dominated the sapling phase was the coffee species (*Coffea canephora*) with a total of 42 plants, followed by the clove species (*Syzygium aromaticum*) with a total of 29 plants. Species that have a low INP are forestry plants, namely waru (*Hibiscus tiliaceus*) with 1 plant. The community manages the forest by planting various kinds of MPTS plants. These activities are the main source of income for the farmers managing the CF. According to Amelia *et al.* (2019), currently cloves are a potential commodity to increase farmers' income in Lampung Province because the price of cloves is high enough to reach Rp. 80.000/kg. If the price of cloves continues to increase, the income of clove farmers will be higher.

The species that dominates the sapling phase is coffee (*Coffea canephora*) with a percentage of 92.74%, followed by cloves (*Syzygium aromaticum*) with a percentage of 72.59%. Types of coffee and cloves are intercropping plants that are deliberately planted by farmers because the price of rubber has continued to decline since 2011 until now and greatly affects the income of farmers in meeting daily household needs (Syarif *et al.*, 2016).

1.4. Underplants and seedlings

The understory and seedling phases were measured on plots measuring 2m x 2m. INP data acquisition shows that there are 11 species of seedlings and 15 understory species (Table 6).

Table 6: INP of seedling and understory phases

No	Local name	Scientific name	INP (%)
1	Karet	<i>Hevea brasiliensis</i>	11.80
2	Pakis	<i>Cyclosorus aridus</i>	8.39
3	Kopi	<i>Coffea canephora</i>	10.65
4	Kentangan	<i>Borreria latifolia</i>	11.88
5	Paitan	<i>Axonopus compressus</i>	24.03
6	Jambu bol	<i>Syzygium aqueum</i>	5.19
7	Akasia	<i>Acacia auriculiformis</i>	1.89
8	Haredong	<i>Clidemia hirta</i>	24.26
9	Waru	<i>Hibiscus tiliaceus</i>	4.72
10	Sapat	<i>Macaranga tribola</i>	1.89
11	Jambu biji	<i>Psidium guajava</i>	4.82
12	Rayuta	<i>Euphorbia milii</i>	10.50
13	Rumput kasapan	<i>Hypolytrum nemorum</i>	12.71
14	Senggani	<i>Melastoma candidum</i>	2.39
15	Kirinyuh	<i>Chromolaena odorata</i>	7.79
16	Tekelan	<i>Eupatorium riparium</i>	8.92
17	Alang alang	<i>Imperata cylindrica</i>	8.87
18	Putri malu	<i>Mimosa pudica</i>	2.33
19	Cengkeh	<i>Syzygium aromaticum</i>	3.30
20	Saga	<i>Adenanthera pavonina</i>	4.34
21	Rumput gajah	<i>Penisetum purpureum</i>	3.07
22	Mangga	<i>Mangifera indica</i>	3.07
23	Jengkol	<i>Archidendron pauciflorum</i>	2.43
Total			200

Source: Primary data (2019)

The dominant understory species was Paitan grass (*Axonopus compressus*) with a percentage of 24.03% while the one with the lowest INP was Sapat (*Macaranga tribola*) with a percentage (1.89%) and shy daughter (*Mimosa pudica*) with a percentage (2.33%). Seedling phase plants also found on managed land were rubber (*Hevea brasiliensis*), coffee (*Coffea canephora*), acacia (*Acacia auriculiformis*), jambu bol (*Syzygium aqueum*), waru (*Hibiscus tiliaceus*), jambu biji (*Psidium guajava*), cloves (*Syzygium aromaticum*), saga (*Adenanthera pavonina*), mango (*Mangifera indica*) and jengkol (*Archidendron pauciflorum*). The seedling phase was dominated by rubber tillers (*Hevea brasiliensis*) with an INP percentage of 11.80%. As for forestry plant seedlings, waru

(*Hibiscus tiliaceus*) and saga (*Adenanthera pavonina*) have an INP percentage low, namely 4.72% and 4.39%, respectively.

The existence of MPTS and forestry plants is the intervention of farmers in choosing the desired plant species. According to Bhaskara *et al* (2018) farmers tend to throw away unwanted plants. In line with the research of Wijayanto and Hartoyo (2015) that the consideration of choosing the type of plant is due to considering the technical aspects of cultivation and economic aspects. The cultivation aspect in question is a plant that is easy to plant, easy to maintain, and resistant to pests and diseases. Meanwhile, what is meant by the economic aspect is that farmers are more likely to plant the MPTS type as the superior crop.

2. Biomass and Stored Carbon

Biomass can be defined as the total weight or volume of an organization in a certain area or volume (Bhaskara *et al*, 2018). Tampubolon (2011) defines forest biomass as the total amount of living organic matter above the soil in trees and all parts of the population or community body expressed in dry weight of the kiln per unit area (tonnes/ha). The National Standardization Agency (2011) classifies biomass into 2 types of biomass, the first type is aboveground biomass which includes all parts of trees and understorey plants, and the second type is subsurface biomass which includes plant roots and soil organic carbon. Research on carbon stocks is included in the type of measurement of above-ground biomass which includes the type, height and diameter of trees, forest litter and forest undergrowth.

Carbon (C) is a chemical element with atomic number 6 which includes metal elements and if it is released into the air and bound with oxygen (O₂) it becomes carbon dioxide (CO₂) (Arupa Team, 2014). Carbon is the basic building block of all organics. Agus *et al.* (2011) explained that carbon stock is the total weight of carbon stored in an ecosystem in the form of plant biomass and necromass. Carbon stored in the form of biomass and necromass in a vegetation can be an indicator of the success of forest management. The average carbon stored in each plot is 96.45 tons/ha (Table 7).

Table 7: Value of biomass, stored carbon, and CO₂ uptake.

No Plot	Trees (tons)	Pole (tons)	Stake (tons)	Bottom Plant (tons)	Lite r (tons)	Total (tons)	Stored Carbon (tonnes)	Carbon Sequestration (CO ₂ eq) (tons)
1	8.4	49.0	107.7	0.03	0.23	165.4	77.7	285.36
2	69.1	63.4	140.1	0.04	0.21	272.8	128.2	470.71
3	80.3	38.3	19.2	0.04	0.20	138.2	64.98	238.4
4	186.6	58.4	23.7	0.03	0.19	269.0	126.4	464.1
5	482.1	62.3	12.2	0.05	0.21	556.8	261.7	960.5
6	30.3	78.2	10.1	0.02	0.19	118.8	55.87	205.1
7	76.2	80.2	20.1	0.03	0.22	176.8	83.1	304.9
8	24.6	78.5	36.1	0.02	0.23	139.5	65.6	240.7
9	39.4	67.0	31.1	0.03	0.20	137.8	64.8	237.8
10	31.5	53.5	20.6	0.04	0.21	105.8	49.7	182.6
11	29.3	43.4	26.0	0.02	0.20	99.0	46.5	170.8
12	34.9	129.7	95.0	0.03	0.22	259.9	122.2	448.3
13	34.0	65.9	69.7	0.05	0.22	170.0	79.9	293.2
14	268.6	54.7	52.9	0.04	0.21	375.8	176.6	648.2
15	65.0	47.6	35.7	0.03	0.20	148.6	69.8	256.4
16	24.9	73.4	49.6	0.02	0.22	148.2	69.6	255.7
Quantity (tons)	1485.6	1044.0	749.7	0.5	3.36	3283.3	1	5663.4
Average (tonnes/ ha)	92.8	65.2	46.8	0.03	0.21	112.35	96.4	353.9
Percenta ge (%)	45.2	31.8	22.8	0.02	0.1	100		

Source: Primary data (2019).

The average value of biomass in each plant phase is different, namely in the tree phase 92.8 tons/ha, pole phase 65.2 tons/ha, sapling phase 46.8 tons/ha, and undergrowth phase 0.03 tons/ha. Ha. The difference in the value of biomass in the plant phase is influenced by the number, type of plant, and or plant density (Wulandari *et al*, 2018). The plant phase that contributed the highest biomass value was the tree phase. The biomass value is correlated with the stored carbon value produced, which is an average of 96.45 tons/ha. The high value of biomass in the tree phase is influenced by the diversity of MPTS and forestry tree species. This is in line with a study conducted by Wulandari *et al.* (2021), the potential for carbon stored in complex agroforestry cropping patterns is two times greater than in simple agroforestry cropping patterns. From the point of view of the function of the forest area, which is a

production forest area, it is very vulnerable to tree cutting. On the other hand, from a regulatory point of view, the licensing scheme in the form of CF is very possible to regulate the felling of trees, so that the intensity and quantity of trees cut can be limited and regulated in a sustainable manner.

From a regulatory point of view, the licensing scheme in the form of CF is very possible to regulate the felling of trees, so that the intensity and quantity of trees cut can be limited and regulated in a sustainable manner. The role of these regulations can be carried out by FMUs to manage their areas.

The FMU has the ability with the CF scheme to encourage farmers to use MPTS crops wisely while maintaining plant survival and cultivating other plants according to land conditions, so that the ecological function of the forest area is maintained.

Conclusions and Suggestions

The INP value in the tree phase was dominated by rubber (*Hevea brasiliensis*) which was 128.03%. In the pole phase, rubber (*Hevea brasiliensis*) was still the same with an INP of 156.31%. The sapling phase was dominated by coffee plants (*Coffea canephora*) with an INP of 92.74%. The understorey phase was dominated by Paitan grass (*Axonopus compressus*) with a large INP of 24.03%. The average value of carbon stored in each plot is 96.45 tons/ha. This value shows that there is a linear correlation between tree biomass and carbon stock, the more tree vegetation, the more carbon stock in the forest. Several efforts are needed to balance the rate of carbon release with the rate of carbon sequestration, including the application of CF rules in tree felling by FMUs, enrichment of MPTS plant species and maintaining the existence of existing MPTS plants.

References

- Alyani, D.F. dan Ambarwati, R. Variasi morfologi dan kemelimpahan *Donax faba* (Bivalvia: Donacidae) di Pantai Tengket Bangkalan Madura. *Biotropic The Journal of Tropical Biology*. 2(2): 73 – 84 pp. ISSN 2580-5029
- Ambarwati, A., Duryat., Hidayat, W. 2019. INP Vegetation and Carbon Stored in HKm Bina Wana, Kebun Tebu Subdistrict, West Lampung Regency. *Journal of Tropical Forests* 7(2):112-119.
- Amelia, SM, Hasyim, AI, Situmorang, S. 2019. Efficiency of the Clove (*Syzygium aromaticum*) Marketing System in Pesisir Barat Regency. *JIIA* 7(2):187-194.
- Banjarnahor, K. G., Setiawan, A., and Darmawan, A. 2018. Estimasi Perubahan Karbon Tersimpan di Atas Tanah di Arboretum Universitas Lampung. *Jurnal Sylva Lestari* 6(2): 51–59.
- Bhaskara, DR, Qurniati, R. Duryat, Banuwa, IR 2018. Carbon Stored in Repong Damar Pekon Pahmungan, Pesisir Tengah District, Pesisir Barat Regency *Sylva Lestari Journal*. 6(2): 32-40.
- Chairul, Muchktar, E., Mansyurdin, Maideliza, T., and Indra, G. 2016. Struktur Kerapatan Vegetasi dan Estimasi Kandungan Karbon pada Beberapa Kondisi Hutan di Pulau Siberut Sumatera Barat. *Metamorfosa: Journal of Biological Sciences* 3(1): 15–22.
- Erly, H., Wulandari, C., Safe'i, R., Kaskoyo, H., Winarno, G, D. 2019. Species diversity and tree carbon storage at Pemerihan Resort, Bukit Barisan Selatan National Park. *Sylva Lestari Journal*. 7(2): 139-149.
- Hatulesila, J.W., Wattimena, C.M.A., Siahaya, I. 2018. Study on measurement and determination carbon pool in traditional agroforestry system for handling climate change. *International Journal of Forestry and Horticulture (IJFH)*. 4(2): 14-24.
- Indriyanto. 2006. *Ekologi Hutan*. Buku. PT Bumi Aksara. Jakarta. 210 p.
- KPH Bukit Punggur. 2015. Rencana Pengelolaan Hutan Jangka Panjang (RPHJP). Lampung.
- Markum., Arisoelaningsih, E., Suprayogo, D., and Hairiah, K. 2013. Plant species diversity in relation to carbon stocks at Jangkak Watershed, Lombok Island. *J. Agrivita* 35(3): 207–216.
- National Standardization Agency (BSN). 2011. Measurement and Calculation of Carbon Stock. Field Measurement for the Assessment of Forest Carbon Stocks (Ground Based Forest Carbon Accounting). Book. National Standardization Body. Jakarta. 16p.
- Prihatmaji, Y.P., Fauzy, A., Rais, S., Firdaus, F. 2016. Analisis carbon footprint gedung perpustakaan pusat, rektorat, dan lab. MIPA UII berbasis vegetasi eksisting sebagai pereduksi

- emisi gas rumah kaca. Asian Journal of Innovation dan Entrepreneurship. 1 (2): 148-155.
- Putri, SM, and Indriyanto. 2021. Plant Diversity Composing Vegetation of Bengkunt Protected Forest at Resort III KPH Unit I West Coast. Journal of Tropical Forests 9(1): 212-221.
- Rizki, G. M., Bintoro, A., Hilmanto, R. 2016. Perbandingan emisi karbon dengan karbon tersimpan di Hutan Rakyat Desa Buana Sakti Kecamatan Batanghari Kabupaten Lampung Timur. Jurnal Sylva Lestari. 4(1): 89-96.
- Standar Nasional Indonesia No. 7725 Tahun 2011. Penyusunan Persamaan Alometrik untuk Penaksiran Cadangan Karbon Hutan Berdasar Pengukuran Lapangan (ground based forest carbon accounting). Badan Standarisasi Nasional. Jakarta.
- Supriadi., Riniarti, M., Bakri, S. 2018. Rubber Productivity on HKm Jaya Lestari Land, Way Kanan Regency, Lampung Province. Journal of Forestry Research 1(1): 36-43.
- Supriadi, B., Adiansyah, J.S. 2013. Pendugaan Cadangan Karbon Areal Reklamasi Pertambangan: Studi Kasus PT. Newmont Nusa Tenggara. *Lingkungan Tropis*. 7(1): 1-9.
- Susilo, A. 2019. Hubungan Antara Cadangan Karbon dengan Keragaman Hayati: Studi Kasus di Taman Nasional Meru Betiri.
- Syarifa, LF, Agustina, DS, Nancy, C., and Supriadi, M. 2016. The Impact of Low Rubber Prices on Socio-Economic Conditions of Rubber Farmers in South Sumatra. Indonesian J. Nat. ruby. res. 34(1): 119-126.
- Tampubolon, TH 2011. Biodiversity in the education forest of USU Tongkoh, Karo Regency. Essay. University of Northern Sumatra. Medan.
- Wijayanto, N. and Hartoyo, APP 2015. Agroforestry-Based Biodiversity. Proceedings of the National Seminar on Indonesian Biodiversity Society 1(2): 242-246.
- Wulandari, C., Bintoro, A., Rusita, Santoso, T., Duryat, I Kaskoyo, H., Erwin., and Budiono, P. 2018. Community forestry adoption based on multipurpose tree species diversity towards to sustainable forest management in ICEF of the University of Lampung, Indonesia. Biodiversity, 19(3):1102-1109.
- Wulandari, C., Harianto, SP, Novasari, D. 2021. Estimation of Carbon Stock in Simple Agroforestry Cropping Patterns and Complex Agroforestry in KPH Batutegei, Tanggamus Regency. Wilderness Journal 4(2):113-126
- Wulandari, C., Bakri, S., Riniarti, M., and Supriadi, S. 2021. Fostering the sustainability of community fo restry program: case study In lampung-Sumatra. *J. Forestry Ideas* 1(61): 210-232.
- Zhafira, G., Wulandari, C., Rusita., Bakri, S. 2019. The Effect of Altitude on the Production of Community Fo rest Rubber Sap in Way Kanan Regency. National Seminar on Biology 4, Bandung 25 April 2019:181-184 Pg.
- Winardi, F. 2014. *Nilai Kandungan Karbon dan Indek Nilai Penting Jenis Vegetasi Mangrove di Perairan Desa Mantang Baru Kecamatan Mantang Kabupaten Bintan Provinsi Kepulauan Riau*. Skripsi. Universitas Riau. Riau. 86 p.

The Effects of Climate Change on Indonesian Forests

Komariah^{1*} and Umami Marfu'ah²

¹ Dept. of Soil Science, Faculty of Agriculture, Sebelas Maret University, Indonesia

² Research Group of Climate Change and Land Resource Management, Sebelas Maret University, Indonesia

*Corresponding Author: komariah@staff.uns.ac.id

SUMMARY

Climate change phenomenon has led to the warmer temperature of air, hence resulted in higher evapotranspiration from the ecosystem, including forest ecosystem. Especially the forests in Indonesia, which lays in the tropical monsoonal area, the impact of climate change attributes to the increase intensity of drought, as well as higher air temperature. Warmer air will increase air capacity to hold moisture rapidly hence lowering the water table position. The high air temperature is the most important variable and increasing the forest fire, especially in Indonesia. The risk even higher with the logging activity since it opens the canopy, produces drier microclimate and debris thus increases inflammability. Besides increasing the forest fire incidences, higher temperature also decreased the geographic suitability of some vegetation and fruit tree in the forest hence threatening the habitat of predator such as orangutan and some insect species. Many insect species are very sensitive to changes in temperature and humidity, thus the particular insect species shift to the pole ward or higher elevation. However, at the same time, many phytophagous insects are quickly adapting to the new plant host and environment, which frequently lead to insect outbreak to the surroundings. The early warning systems based on fire danger is urgent to mitigate the fire disaster, as well as forcing the forest management agency to reassess policy and strategy. Since forest fire indirectly affects the loss off agricultural yield due to water resources decline, modification of planting and harvest as well as crop selection can help to mitigate the impact of climate change on forest and surroundings ecosystems.

Keywords: *Climate Change; Forest Fire; Fire Disaster; Forest Ecosystem; Early Warning System*

Introduction

Forest disturbance is a problem of both local and global concern. The characteristic of forests in Indonesia are tropical rainforests that have humid characteristics, high annual rainfall, and high evapotranspiration and are green forests. However, with climate change and human intervention in recent decades, forests have been damaged by wildfires, droughts and insect outbreaks that strongly impacts to the ecosystem of the forest to provide ecosystem services to society. Weather and climate including temperature, precipitation, wind and atmospheric moisture are critical aspect of this phenomenon (Flannigan *et al.* 2013). The disturbance of forest have direct effects in biodiversity, loss of property and the carbon emission. This paper reviews the effects of climate change in forest in Indonesia and the mitigation.

The Effects of Climate Change in Forest Fire

Indonesian forest in Kalimantan have

experienced in fires since at least the 17th century (Bowen *et al.* 2001). Fires in tropical rain forests are considered endemic, but the frequency of occurrence is rare and in intervals of hundreds or even thousands of years, because historical records and soil profiles show that fires have unprecedented, even in wetter forests (Cochrane 2003). In 1982-83 Indonesia experienced tropical rainforest fires on a large scale, about 3.6 million hectares of land was affected (Tacconi 2003). Although tropical rainforests are notoriously humid, always wet and are green forests, the fires have repeated in 1987, 1991, 1994, and 1997-98 (Bowen *et al.* 2001) since then the extent, intensity and frequency of fires increased in each year to the year and showed yearly hotspot distribution (Syauфина 2018). During the incident, the most severe fires occurred in the period 1997-98 affecting 11.7 million hectares in Sumatra, Kalimantan, Papua (Goldammer 2002) and hot spots increased periodically every year. These large fires correlate with *El Nino* events (Slik 2004) and climate change (Flannigan *et al.* 2013) that are causing rising temperatures and a long drought in Indonesia. In the

period 1979-2003 the annual average fire duration on a global scale increased to 18% and experienced longer fires more than doubled (Jolly *et al.* 2015).

Factors that increase the risk of forest fires in Indonesia are logging, distance from rivers that are too far away, the development of road and settlement projects and the occurrence of increased temperatures due to climate change (Syaufina 2018). Land clearing by logging increases the fire potential because it opens the canopy, resulting in a dry microclimate so that climate change and increased temperatures can cause dry conditions to increase the occurrence of burning due to biomass (Herawati and Santoso 2011). Rising temperatures due to climate change drastically and rapidly can increase the potential for forest fire activity (Pechony and Shindell 2010). Temperature is the most important variable affecting annual wild land fire activity, with warmer temperatures leading to increased fire activity. Almost the entire world is expected to warm during this century and wildfires may be a reflection of this rise in temperature (Flannigan *et al.* 2013). GISS (Goddard Institute for Space Studies) climate simulation predict a significant warming over the forthcoming century. Rapidly rising temperatures and regional drying reverse the recent fire activity decline, driving a rapid increase after ~ 2050. Population growth, and to a lesser extent, land-cover change, reduces the increase in fire activity, but does not reverse the long-term trend.

The reasons for the positive relationship between temperature and wildfires are three. First, warmer temperatures will increase evapotranspiration, as the atmosphere's ability to withstand moisture increases rapidly with higher temperatures, thereby lowering the position of the water table and reducing fuel moisture unless there is a significant increase in rainfall. Second, warmer temperatures translate into more lightning activity which generally leads to increased ignition. Third, warmer temperatures can lead to an extension of the fire season (Flannigan *et al.* 2013). Weather conditions are also critical drivers of fire activity, and it is generally the co-occurrence of optimal fire weather (hot, low humidity, and windy) with already dry fuels due to anomalously dry climate that promotes fire spread (Williams and Abatzoglou 2016). The combination of a warmer climate with carbon dioxide fertilization may cause more frequent and more severe fires in the western area. Global circulation models suggest that the

length of the fire season, as expressed by measure such as temperature, drought, degree days, and fire weather indices likely longer. Projection of the effects of climatic change on fire regimes have been of two types: mechanistic models that explicitly represent fire weather, fire behavior and fire effects at sub regional scales and statistical models at regional to continental scale often linked to out from global circulation models (Seidl *et al.* 2017).

The Effects of Climate Change in Forest Drought

Tropical rainforests experience an annual dry period, but in the last 10 years tropical rainforests in Indonesia experienced periods of abnormal dry weather over a long period of time and caused unbalanced hydrological conditions (Stocker 2014). Tropical droughts are multi-year climate cycles that are inter-annual, making long-term trends difficult to predict (García-garcía and Ummenhofer 2015), but there have been many detection models that show the frequency and intensity of droughts in various tropical forest regions increasing in this century including in Indonesia (Zhang *et al.* 2015). Based on predictions using The Climate Change Risk and Adaptation Assessment (CCRAA) approach, rainfall intensity on the island of Java in 2011-2040 is rarely greater than 300 mm so the potential increase in drought hazard index (DHI) is very possible because the increase in drought that occurs can reach 45% (Fitriyanto *et al.*). Droughts occur from shifts in climate patterns that are affected by rising temperatures over a long period of time so that transpiration and evaporation rates can increase, this can limit periods of rainfall. El-nino is one of the main causes of drought in tropical rainforests. In the severe El-nino drought in 1997-1998, forests in East Kalimantan experienced drought-related tree deaths between 7.3 and 22.1%, this occurred because understory light conditions changed thus affecting the competition of tree species and the specific composition of canopy trees (Slik 2004).

Drought on tropical rainforest ecosystem influence tree mortality in Indonesia. In Kalimantan forest Drought contributes to stem deaths of about 30% but the estimated contribution to basalt areas die and biomass is higher at 52% and 63% respectively (Nieuwstadt and Sheil 2005). Mortality of tropical trees has been widely observed in both

natural droughts and throughfall exclusion experiments. Some mortality lags one or more years after a drought. Some mortality lags one or more years after a drought. Vulnerability varies among species, sizes, ages, growth rates, and locations, with tree vigor the best predictor of individual mortality. They also have keystone ecological roles, providing substrates for epiphytes, cavities for hole-nesting species, and favorable microclimates for understory plants (Corlett 2016).

Droughts also cause decreased diameter growth in tropical forests especially on large trees, based on Bonal *et al.* 2016 This cannot be explained in diameter measurements and photosynthesis alone, but changes in carbon allocation in trees show that there is a large decrease in carbon sequestration by tropical forests in years of drought. Diameter is an important factor in tree mortality during drought, mortality is much higher in trees with large diameters in East Kalimantan, trees with dbh greater than 20 cm experience death up to 26.5% and trees with dbh less than 20 cm have a lower mortality rate of 17.2% (van Nieuwstadt 2002). On observations in central Kalimantan, tree deaths in peat-swamp forests were higher ($6.13\% \text{ yr}^{-1}$) than healthy forests ($4.26\% \text{ yr}^{-1}$) during observations in the 2 years after drought, in the dry season showed a higher mortality rate than the rainy season (Nishimua *et al.* 2007). Wood density could be another explanation of the higher mortality rates among these pioneer trees. Strong negative relation between wood density and tree drought mortality. This relationship can be explained by the fact that wood density is an important determinant of xylem water transport properties and whole plant water relations (Slik 2004).

The Effects of Climate Change in Insect Outbreak

Distributions of organisms are often defined by climatic factors, such as temperature and precipitation. Many insect species, and phytophagous insects in particular, show relatively rapid responses to the rising temperatures by shifting their geographic range boundaries poleward or to higher elevations. Most insects are very sensitive to changes in temperature, which may affect their activity, development, phenology, and survival directly, or indirectly through host phenology shifts

or effects of temperature on host chemistry. At the same time, many phytophagous insects are able to quickly adapt to new environments, provided their host plants are present. Switching to new hosts may occur among non-specialist herbivores, and can be the first consequence of the strong selection on colonizers (Battisti, A., Stastny, M., Netherer, S., Robinet, C., Schopf, A., Roques, A., & Larsson 2009). Long periods of low precipitation deplete soil moisture in turn causing water stress and low xylem pressure in trees which allow beetles (especially *Dendroctonus* spp.) to colonize cambial tissue. An outbreak of beetles in stressed trees can spread to healthy trees and causing significant mortality to accumulate woody fuels, which greatly increases the hazard of a stand replacing fire and subsequent beetle attack on dead and damaged trees. Such a cascade of spatial and temporal patterns of disturbance makes it difficult to achieve conservation goals for plant and animal species, especially those associated with late successional forest structure.

Climate Change Mitigation for Forestry

The most needed and urgent treatment is for early detection of drought development in a region (Flannigan *et al.* 2016) and followed by a continuous monitoring of its effects. A variety of passive and active satellite sensors, including those measuring optical reflectance, microwave backscatter, thermal signals, gravitational field, near-surface relative humidity, and atmospheric CO₂ concentrations, can be used to detect drought and monitor impacts (Campoy *et al.* 2020).

Yield losses can be at least partially mitigated through management practices, such as modification of planting and harvest dates. However, recent research suggests that climate change over the last 20 years is already having a deleterious impact on agricultural production, and the ability of existing water resources to keep pace with future climate impacts is in question. Even with proactive management, our results suggest increased drying, driven primarily by increases, will likely have significant ramifications for globally important regions of agricultural production in the Northern Hemisphere mid-latitudes (Cook *et al.* 2014).

Many species, and insects in particular, have specific temperature requirements that may

render them sensitive to new temperature regimes. Therefore, our ability to predict changes in species distributions and their potential community impacts, as well as to evaluate suitable management strategies, would benefit from focusing on the mechanisms that drive correlations between climatic factors and survival of organisms (Battisti, A., Stastny, M., Netherer, S., Robinet, C., Schopf, A., Roques, A., & Larsson 2009).

Conclusion

Climate change has led to more intensive forest fire, increased drought hazard index hence higher trees mortality, as well as increased insect outbreak in Indonesian forest. Among the mitigation measures are by usage of futuristic technology, such as satellite monitoring and management practice strategies.

References

- Battisti, A., Stastny, M., Netherer, S., Robinet, C., Schopf, A., Roques, A., & Larsson S. 2009. Expansion Of Geographic Range In The Pine Processionary Moth Caused By Increased Winter Temperatures. *Appl Sci.* 2009(6):2008–2009.
- Bonal D, Burban B, Stahl C, Wagner F, Hérault B, Wagner F. 2016. The response of tropical rainforests to drought — lessons from recent research and future prospects. :27–44. doi:10.1007/s13595-015-0522-5.
- Bowen MR, Bompard JM, Anderson IP, Guizol P, Gouyon A. 2001. ANTHROPOGENIC FIRES IN INDONESIA : A VIEW FROM SUMATRA FOREST FIRES AND REGIONAL HAZE.
- Campoy J, Campos I, Plaza C, Calera M, Bodas V, Calera A. 2020. Estimation of Harvest Index in Wheat Crops Using A Remote Sensing-Based Approach. *F Crop Res.* 256(November 2019):107910. doi:10.1016/j.fcr.2020.107910.
- Cochrane MA. 2003. Fire science for rainforests. 421(February):913–919.
- Corlett RT. 2016. The Impacts of Droughts in Tropical Forests. *Trends Plant Sci.* 21(7):584–593. doi:10.1016/j.tplants.2016.02.003. <http://dx.doi.org/10.1016/j.tplants.2016.02.003>.
- Fitriyanto MS, Supangat A, Ramadhan MR. Developing and Applying Climate Information for Supporting Adaptation in South East Asia Indonesian Case Study : Climate Projections and Drought Hazard Assessments in East Java Province.
- Flannigan M, Cantin AS, De Groot WJ, Wotton M, Newbery A, Gowman LM. 2013. Global wildland fire season severity in the 21st century. *For Ecol Manage.* 294:54–61. doi:10.1016/j.foreco.2012.10.022. <http://dx.doi.org/10.1016/j.foreco.2012.10.022>.
- Flannigan MD, Wotton BM, Marshall GA, de Groot WJ, Johnston J, Jurko N, Cantin AS. 2016. Fuel moisture sensitivity to temperature and precipitation: climate change implications. *Clim Change.* 134(1–2):59–71. doi:10.1007/s10584-015-1521-0.
- García-garcía D, Ummenhofer CC. 2015. Multidecadal variability of the continental precipitation annual amplitude driven by AMO and ENSO. :526–535. doi:10.1002/2014GL062451.Received.
- Goldammer GJ. 2002. Fire Situation in Indonesia. (26):37–45.
- Herawati H, Santoso H. 2011. Tropical forest susceptibility to and risk of fire under changing climate: A review of fire nature, policy and institutions in Indonesia. *For Policy Econ.* 13(4):227–233. doi:10.1016/j.forpol.2011.02.006. <http://dx.doi.org/10.1016/j.forpol.2011.02.006>.
- Jolly WM, Cochrane MA, Freeborn PH, Holden ZA, Brown TJ, Williamson GJ, Bowman DMJS. 2015. Climate-induced variations in global wildfire danger from 1979 to 2013. *Nat Commun.* 6(May):1–11. doi:10.1038/ncomms8537. <http://dx.doi.org/10.1038/ncomms8537>.
- van Nieuwstadt MGL. 2002. Trial by fire : Postfire development of a tropical dipterocarp forest. :142. <http://www.library.uu.nl/digiarchief/dip/diss/2002-0927-111146/inhoud.htm>.
- Nieuwstadt MGLVAN, Sheil D. 2005. Drought , fire and tree survival in a Borneo rain forest , East Kalimantan , Indonesia. :191–201. doi:10.1111/j.1365-2745.2005.00954.x.
- Nishimua TB, Suzuki E, Kohyama T, Tsuyuzaki S. 2007. Mortality and growth of trees in peat-swamp and heath forests in Central Kalimantan after severe drought. *Plant Ecol.* 188(2):165–177. doi:10.1007/s11258-006-9154-z.

- Pechony O, Shindell DT. 2010. Driving forces of global wildfires over the past millennium and the forthcoming century. *Proc Natl Acad Sci U S A*. 107(45):19167–19170. doi:10.1073/pnas.1003669107.
- Seidl R, Thom D, Kautz M, Martin-Benito D, Peltoniemi M, Vacchiano G, Wild J, Ascoli D, Petr M, Honkaniemi J, *et al.* 2017. Forest disturbances under climate change. *Nat Clim Chang*. 7(6):395–402. doi:10.1038/nclimate3303. <http://dx.doi.org/10.1038/nclimate3303>.
- Slik JWF. 2004. El Niño droughts and their effects on tree species composition and diversity in tropical rain forests. *Oecologia*. 141(1):114–120. doi:10.1007/s00442-004-1635-y.
- Stocker T. 2014. *Climate change 2013: the physical science basis: Working Group I contribution to the Fifth assessment report of the Intergovernmental Panel on Climate Change*. Cambridge university press.
- Syaufina L. 2018. Forest and land fires in Indonesia: Assessment and mitigation. In: *Integrating Disaster Science and Management: Global Case Studies in Mitigation and Recovery*. Elsevier Inc. p. 109–121. <http://dx.doi.org/10.1016/B978-0-12-812056-9/00008-7>.
- Tacconi luca. 2003. Fires in Indonesia: causes, costs and policy implications. *Fires Indones causes, costs policy Implic.*(38). doi:10.17528/cifor/001552.
- Williams AP, Abatzoglou JT. 2016. Recent Advances and Remaining Uncertainties in Resolving Past and Future Climate Effects on Global Fire Activity. *Curr Clim Chang Reports*. 2(1):1–14. doi:10.1007/s40641-016-0031-0.
- Zhang KE, Castanho ADDEA, Galbraith DR, Costa MH, Malhi Y, Longo M, Knox RG. 2015. The fate of Amazonian ecosystems over the coming century arising from changes in climate, atmospheric CO₂, and land use. :1–19. doi:10.1111/gcb.12903.

Tropical Montane Forest Ecotone Dynamics in the Context of Climate Change: Case Study in the Doi Suthep-Pui National Park, Thailand

Sutheera Hermhuk ^{1*}, Dokrak Marod ²

¹ Faculty of Agricultural Production, Maejo University, Thailand

² Faculty of Forestry, Kasetsart University, Thailand

*Corresponding Author: h.sutheera@gmail.com

SUMMARY

Recently, climate changes are the most argument topics, particular relating to adaptation and migration of plants in the mountain ecosystem. This study aimed to clarify the forest dynamics; particular sapling and tree stages related to micro-climate changes in a permanent plot along altitudinal gradient (ranged from 900 to 1,100 m above sea level). A permanent transect plot (30 m × 600 m) was established at forest ecotone (FE) between deciduous dipterocarp forest (DDF) and lower montane forest (LMF). All trees with diameter at breast height (DBH > 4.5 cm) were tagged, measured and identified. The monitoring was done every two years since 2012 to 2016. The micro-climatic factors were automatic recorded, and the amount of rainfall was received from meteorological station. All tree (DBH > 4.5 cm) were analyzed to detect the dynamics relating to the micro-climate changes. The results showed environmental changes strongly impact on species coexisting, particular the in FE between DDF and LMF, where the intermediate environmental factors were found. High mortality rate was mostly found in the dominant species of LMF (evergreen species), and positively significant related to decreased rainfall and increased temperature. It indicated that drought conditions had strongly influenced on tree mortality, particular evergreen species. However, the deciduous species of DDF had increased their density, particular at the FE zone, indicating they had high adapted to drought resistance and may be occupied the forest ecotone, instead of LMF species. Thus, the knowledge on coexisting species based on their niches along the altitudinal gradient is useful for the restoration program, particular, in the mountain ecosystem.

Keywords: *Trees diversity; Ecological niche; Environmental gradient*

Introduction

Long-term ecological research (LTER) based on permanent plots may provide the knowledge on forest dynamics, especially tree regeneration, relating to their environmental changes (tree density, basal area, recruitment and mortality in tree density) (Sherman, R. E. *et al.*, 2012). Many sites of LTER plots in Thailand displayed the important outputs such as change of forest cover during successional stage, dynamics of forest structure and spatial distribution related to environmental factors (Bunyavejehwin, S. *et al.*, 2001). Although studies have covered almost all forest types, few have documented the forest ecotone between lowland and upland forest along altitudinal gradients. At present time, many research topics such as; forest biodiversity, forest biomass, carbon storage and forest succession from shifting cultivation etc. were done in both UMF and LMF.

For instant, in Doi Inthanon National Park (the top of mountain in Thailand) set up the permanent plot and focused on forest diversity, ecological niche of dominance species, biomass and carbon storage, diversity of plant species structure along altitudinal gradient (Teejuntuk, S. *et al.*, 2002; Khamyong, S. *et al.*, 2003). In addition, at Doi Suthep-Pui National Park which mainly covered by LMF, also found the reported on species composition and distribution (Marod, D. *et al.*, 2014), seedling dynamics in forest gap and plant functional traits of seedling from dominant species for restoration of this forest type. The results of this research should support natural resources management, especially the selection of trees for restoration programs in mountain ecosystems.

Materials and methods

1. Data collection

All studies were conducted at forest

ecotone between DDF and LMF (latitude 18° 47' 4"N and longitude 98° 54' 58"E) at Doi Suthep-Pui National Park, Chiang Mai province. A Transect permanent plot, 50 m × 600 m (3 ha), was established in 2012 which ranged from 900 to 1,100 m above sea level. Subplots of 10 m × 10 m were divided (total 300 subplots). All tree species with diameter at breast height (DBH) larger than 1 cm were tagged, DBH measured, identified and analyzed only tree stage (DBH > 4.5 cm). Monitoring was done every two year since 2012 to 2018. In addition, the micro-climatic factors, temperature and light intensity, were automatically measured since 2012 by Hobo Data Loggers. The data loggers were set up in three lines, and 50 m adjacent distant for each logger in each line (total 36 loggers). In addition, the amount of rainfall was also analyzed based on the data from Doi Suthep-Pui National Park Meteorological station.

2. Data analysis

To evaluate the dominant of sapling species in the area, the importance value index (IVI) (Whittaker, R. H. 1975). The forest dynamics were characterized using annual mortality rate (M) and recruitment rate (R) (Sherman, R. E. *et al.*, 2012) of selected species which had more than 100 individuals, were used for Generalized linear model (GLM) analysis to detect the relationship between micro-climatic changes based on R program version 3.2 (Team, 2013).

Results and Discussions

Within the 1.8 ha permanent plot, there were 165 species, 118 genera and 59 families. In addition, tree density and basal area were 1,190 individual/ha and 29.56 m²/ha, respectively. The dominant families, based on species number, were Fagaceae, Phyllanthaceae, and Fabaceae with species numbers of 15, 12, and 10, respectively. These dominant families also had a high total BA (m²), particularly, the family of Fagaceae and Dipterocarpaceae and family of Fagaceae, Rubiaceae and Lauraceae, which had high total stem density, which was the highest tree density found in FE zone. The species of *Quercus brandisiana* (32.34 %) was ranked first of dominant species (based on IVI) followed by *Dipterocarpus obtusifolius* (17.73 %), *Wendlandia paniculata*

(17.34 %), *Litsea martabanica* (17.05 %), *Schima wallichii* (15.86 %), *Lithocarpus garrettianu* (12.20 %), *Castanopsis acuminatissima* (11.40 %), *Castanopsis tribuloides* (8.90 %), *Shorea obtuse* (7.96 %), *Dipterocarpus tuberculatus* (6.96 %).

The forest dynamics of trees in the 1.8 ha permanent plot, fluctuated among periods during 2012-2016. The basal area tended to increase during the first period, 2012–2014, (29.97 m²/yr to 32.34 m²/yr), contrasting with the second period, 2014–2016 (Table 1). It mainly due to sized dependent mortality, particular in the small size class (DBH < 10 cm) (Figure 5). However, the highest of species number was found in 2016 (102 species). However, it varied among periods. The mortality and recruitment rate had high fluctuated among study period. Trees mortality rate increased about three times for trees DBH ≥ 4.5 cm. In addition, the recruitment rate also tended to decrease about seven times in second period.

Table 1 Summary data of forest dynamics in the forest ecotone permanent plot

	2012	2014	2016
Basal area (m ² /ha)	29.97	32.34	31.86
Loss (m ² /ha)	0.54	1.51	
Gain (m ² /ha)	2.91	1.03	
Species Number (ha)	98	99	102
Density (individual/ha)	1,263	1,697	1,673
Mortality rate (%/yr)	0.80	2.81	
Recruitment rate (%/yr)	15.57	2.12	

The results from GLM analysis for detecting the relationship between forest dynamics, mortality and recruitment rate, showed that only, mortality rate of both trees and saplings had significant highly correlated to decreasing of rainfall and increasing of temperature. In particular, long drought period was found in the second period, it showed negatively affected by low decreasing rainfall ($p < 0.05$); the rain-free days less than 52 days (2014 = 158 days and 2016 = 106 days) and had positively related to the increasing of temperature ($p < 0.01$).

Considering to species dynamics based on their characteristics, evergreen and deciduous species, net trees mortality and recruitment rate of dominant deciduous species group of DDF were relatively balanced (less than 10%/yr) such as

Aporosa villosa, *Aporosa nigricans*, *Dipterocarpus obtusifolius*, *Quercus branisiana*, *Rothmannia sootepensis*, and *Wendlandia paniculata* (Figure 1). In contrast, the dominant evergreen species group of LMF had high fluctuated on the net mortality and recruitment rate. The mortality had highly negatively relationship to decreased rainfall ($p < 0.05$), particular high increased in the second period such as *Castanopsis tribuloides*, *Castanopsis acuminatissima*, *Litsea martabarnica*, *Tarennoidea wallichii*, *Schima wallichii*, *Myrsine seguinii*, and *Persea gamblei* (Figure 1). Indicating that the drought conditions had strong influenced on evergreen species mortality, and may be induced more deciduous species which high adapted to drought resistance to replace at the forest ecotone.

Thus, the climatic conditions are the main environmental factors for plant regeneration, especially in sapling stage that is sensitive to the changes (Frelich, L. E. 2002). This result study also clarified that the changed of rainfall and temperature were the key factors in the survival of saplings for coexisted species of LMF and DDF along the altitudinal gradients similar to Martin, H. P. *et al.* (2007). Deciduous species well adapting to drought condition by showed high recruitment rate and can be explant up to the high altitude, in contrast with evergreen species, most of them die due to micro-climate changes.

Conclusions

The environmental changes strongly impact on species coexisting, particular the in FE between DDF and LMF, where the intermediate environmental factors were found. High mortality rate was mostly found in the dominant species of LMF (evergreen species), and positively significant related to decreased rainfall and increased temperature. Indicating that drought conditions had strongly influenced on tree mortality, particular evergreen species. However, the deciduous species of DDF had increased their density, particular at the forest ecotone zone, indicating they had high adapted to drought resistance and may be occupied the forest ecotone, instead of LMF species.

Acknowledgment

This research was supported by the Center for Advanced Studies in Tropical National Resources (CASTNaR), Kasetsart University, Bangkok, Thailand. We would like to thank the head of the Doi Suthep-Pui National Park, Chiang Mai Province and his assistants for their supports during field works. Special thanks to all of my team, students from the Thai Forest Ecological Research Network (T-FERN).

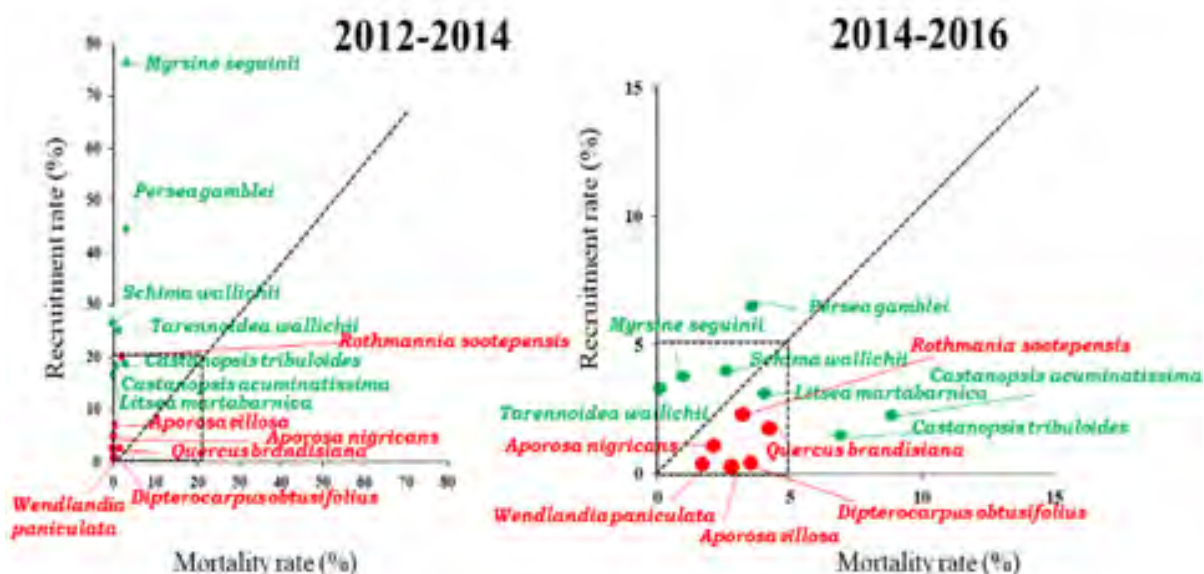


Figure 1 Relationship between recruitment and mortality rates of dominant tree species during study period

Reference

- Bunyavejchewin, S., Baker, P. J. Lafrankie J. V. and Ashton, P. S. (2001). Stand structure of a seasonal dry evergreen forest at Huai Kha Khaeng Wildlife Sanctuary, western Thailand. *Natural History. Bulletin of the Siam Society*, 49: 89–106.
- Frelich, L. E. (2002). *Forest dynamics and disturbance regimes: studies from temperate evergreen-deciduous forests*. Cambridge University Press, UK.
- Khamyong, S., Lykke, A. M., Seramethakun, D., Barfod A. S. (2003). Species composition and vegetation structure of an upper montane forest at the summit of Mt. Doi Inthanon, Thailand. *Nordic Journal of Botany*, 23(1): 83-97.
- Marod, D., Sangkaew, S., Panmongkal, A., Jingjai, A. (2014). Influences of environmental factors on tree distribution of lower montane evergreen forest at Doi Sutep-Pui National park, Chiang Mai Province. *Thai Journal of Forestry*, 33 (3): 23-33.
- Martin, H. P., Sherman R. E. and Fahey, T. J. (2007). Tropical montane forest ecotone: climate gradients, natural disturbance, and vegetation zonation in the Cordillera Central, Dominican Republic. *Journal of Biogeography*, 34 (10): 1792–1806
- Sherman, R. E., Fahey T. J., Martin P. H. and Battles, J. J. (2012). Patterns of growth, recruitment, mortality and biomass across an altitudinal gradient in a neotropical montane forest, Dominican Republic. *Journal of Tropical Ecology*, 28: 483–495.
- Teejuntuk, S., Sahunalu, P., Sakurai K., and Sungpalee, W. (2002). Forest structure and tree species diversity along an altitudinal gradient in Doi Inthanon National Park, Northern Thailand. *Tropics* (2): 85-102.
- Whittaker, R. H. (1975). *Communities and Ecosystem*, second eds. McMil Publication. New York, USA.

Effect of Climate Changes on Dry Evergreen Forest Dynamics in Sakaerat Biosphere Reserve, Northeastern Thailand

Wongsatorn Phumphantang^{1*}, Dokrak Marod¹

¹ Department of Forest Biology, Faculty of Forestry, Kasetsart University, Bangkok 10900, Thailand

*Corresponding Author: fns_pon@hotmail.com

SUMMARY

Long-term ecological research based on large permanent plot can explore the forest dynamics in relation to environmental changes. This study aimed to detect the tree distribution related to environments as well as clarifying tree demography, mortality and recruitment, in response to drought conditions in the dry evergreen forest (DEF) at Sakaerat Biosphere Reserve (SBR), northeastern Thailand. In 2010, a 16 ha permanent plot was established and all trees with diameter at breast height (DBH) ≥ 4.5 cm were tagged, measured, recorded their coordinates and identified to species level. Tree monitoring was in 2015 and 2020 which included new trees with a DBH ≥ 2 and 1 cm, respectively. Within the permanent plot, topographic factors and soil properties were collected to investigate tree distribution using canonical correspondence analyses (CCAs). The climate change based on the Standardized Precipitation-Evapotranspiration Index (SPEI), a drought index, was constructed using meteorological data from SBR since 2010–2020. In 2020, a total of 81,728 individuals (≥ 1 cm DBH) comprising 204 species 156 genera and 62 families were found. The stem density and basal area were 5,108 individual/ha and 30.16 m²/ha, respectively. According to the important value index, *Hydnocarpus ilicifolia*, *Hopea ferrea* and *Walsura pinnata* were the dominant species in the community. Topographic factors (elevation and slope), soil textures and soil nutrients based on CCAs were determined tree distribution ($p < 0.05$). In addition, tree species characteristics can be divided into two groups, drought and moist preferred groups which were distributed under sandy and clay texture, respectively. The mortality and recruitment rates of trees DBH ≥ 4.5 cm during 2010–2020 were mostly balanced (1.96 and 1.93 %/year, respectively); nevertheless, the rates varied among periods. According to SPEI, humid conditions were widespread, particularly in extended humid conditions during the second period. Higher mortality of favored dry species such as *Arytera littoralis* and *Nephelium hypoleucum* was influenced by these circumstances, demonstrating that tree species in the DEF had distinct adaptations to climate change. Hence, our knowledge supports the species ecological niche and can be applied to forest conservation and reforestation program based on suitable species selection.

Keywords: IC-GUI2; Format and layout; International symposium; Soluble protein; Hoover Dam

Introduction

The long-term ecological research (LTER) with large scale permanent plot is imperious to understand the impacts of past disturbances and predicting the effects of future changes on tropical forests (Feeley, K. J. *et al.*, 2011). The general characteristics of the forest communities cannot be detected by small scale plot because heterogeneity in environments is disregarded (Miura, M. *et al.*, 2001). Demographic responses to natural disturbances, such as drought condition, will differ among tree species and especially for tree establishment will be diverse based on the heterogeneity of the environments (Körner, C., 2004; Feeley, K. J. *et al.*, 2011).

In Thailand, there are not many LTER with large scale permanent plots regarding dry evergreen forest (DEF). This forest type cover approximately twenty percent of protected area (Pongpattananurak, N., 2014) and usually located between deciduous and evergreen forest, which they appeared in mixed plant species. Thus, the LTER in the DEF using the large permanent plot should be established, to detect how plant species respond to environmental changes. This study aimed to detect the tree distribution related to environments as well as clarifying tree demography, mortality and recruitment, in response to drought conditions in the dry evergreen forest

Materials and Method

1. Study site

The study was conducted in the DEF at the Sakaerat Biophere Reserve (SBR) Wang Nam Khiao district (14°30'N, 101°56'E), Nakhon Ratchasima province, northeastern Thailand. The altitudinal range is from 250 to 762 m asl. The climate is tropical with rainfall mainly occurring from July to October, while less rain falls in the remaining 8 months. The mean annual rainfall is ca. 1,100 mm/year and the mean monthly temperature is 27.3°C. The geology and soils are characterized by Triassic and Cretaceous sandstone formations from the Phra Wihan formation of the Korat group, overlain by shallow to moderately deep red-yellow podzol (Bunyavejchewin, S., 1999). The total area of SBR is approximately 81 km². The SBR is bordered by extensive agricultural areas and human residences (Trisurat, Y., 2010). In the past, the natural forest was diminished due to encroachment and illegal logging. Forest types comprise DEF, DDF and mixed deciduous forest, MDF, which DEF mostly occupied in the area. However, many restoration areas were implemented both inside and outside the SERS since 1994, then, the forest cover was increased. Additionally, man-made fires generally find in the DDF and MDF during the dry season.

2. Plot establishment and investigation

In 2010, a 16 ha permanent plot was established and was divided into subplots of 10 m × 10 m, total of 1,600 subplots. All trees with DBH greater than 4.5 cm were tagged, measured and identified. Tree monitoring was in 2015 and 2020. Especially in 2020, all trees with DBH over than 1 cm were included. In this study, tree distribution was focused only 2020 data with tree over than 1 cm DBH, but the forest dynamics was investigated on all three-census data with tree greater than 4.5 cm DBH.

3. Environmental collection

The elevation of every corner of all subplots (10 m × 10 m) were collected based on digital elevation model. The elevation of SBR plot ranged from 420-475 m asl.

Sampling plots were established within the permanent plot using a grid structure (50 m × 50

m) (Delgado-Baquerizo, M. *et al.*, 2020). Soil samples were conducted using disturbed soil samples from the surface (0–15 cm depth) with total of 64 points. The soil samples were analyzed for soil physical and chemical properties in laboratory.

4. Data analysis

Canonical Correspondence Analysis (CCA) was performed to correlate tree community and environments. The CCA ordination were done at the scale of 50 m × 50 m (John, R. *et al.*, 2007). The species abundance matrix was total basal area for each species. Only species with < 10 individuals/quadrate in all quadrats were excluded from the analysis (De Souza, J. P. *et al.*, 2007). The Monte Carlo permutation test was analyzed, to evaluate the statistical significance of the environmental variables (5% confidence level with 999 random permutations). Only the significant variables were then selected. All analyses were done using the vegan package by R software version 3.6.1.

To examine drought events, the standardized precipitation-evapotranspiration index (SPEI) (Vicente-Serrano, S. M. *et al.*, 2010) was purposed through the SPEI package (Beguería, S. *et al.*, 2017) in R software version 3.6.1, using the meteorological data from SBR since 2010–2020, including precipitation data, mean temperature and the station's latitude. In this study, the Hargreaves method for computing PET was chosen. This approach decreases the effort required to obtain meteorological variables such as air humidity, radiation, and wind speed (Rascón, J. *et al.*, 2021). Finally, the 12-month SPEI was chosen because it can distinguish between long-term dry and wet periods, making it more reflective of drought's effects on hydrologic regimes (Moreira, E. *et al.*, 2018).

The parameters of forest dynamics were described followed standard methods as purposed by (Condit, R. *et al.*, 1999), for calculating mortality (M) and recruitment (R) following the equations:

$$M = \frac{\ln n_0 - \ln S_t}{t}$$

and

$$R = \frac{\ln n_t - \ln S_t}{t}$$

where the census interval is t , and the population sizes at time 0 and time t are n_0 and n_t . The number of survivors at time t is S_t , with the number of

recruits is $n_t - S_t$. Furthermore, the analysis of variance and the Tukey test was used to determine differences among censuses for tree density.

Results and Discussion

1. Ordination of tree community

Tree species fluctuate between environments, according to the CCA ordination plot (Figure 1). *Hopea ferrea*, *Walsura pinnata* and *Memecylon ovatum*, the most abundant species with the higher IVI of the plot, were unaffected by any of the environments. However, the other species had a different relationship with their environments. For example, higher levels of sandy soil were found in *Nephelium hypoleucum*, *Arytera littoralis*, *Melodorum fruticosum* and *Azelia xylocarpa*. Sandy soils are characterized as good drainage soil, which characterizes as the drier condition of the plot. In contrast, species of *Syzygium siamense* and *Vatica harmandiana* were linked to high silty soil, magnesium, and a lower elevation. Moreover, *Murraya paniculata* was found in an area with a higher proportion of clayey soil. Clayey soil and silty soil can hold more total water than other soil types (Finch, H. J. S. *et al.*, 2014), which describes the moist condition of the area. Therefore, this explained the two groups of species that distribution in the different of environments.

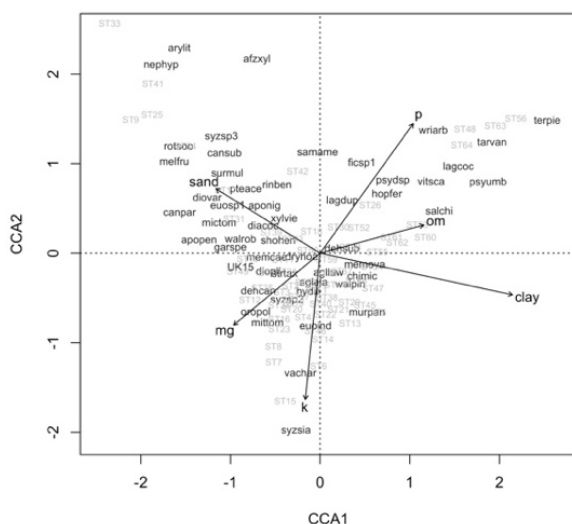


Figure 1: Ordination plot by CCA of tree species of the dry evergreen forest in Sakaerat Biosphere Reserve. Only top 60 % of species were shown.

2. Climate change

On a 12-month time scale, the SPEI values oscillate between -1.3 and 2.0 (Figure 2). In the SBR, the most moderately wet years were observed in 2012, 2014 and 2019, as well as an extremely wet year in 2017–2018. A moderate drought, on the other hand, occurred only in 2016. As a result, the SBR was largely impacted by wet events during the period of the 10 years, with occasional drought.

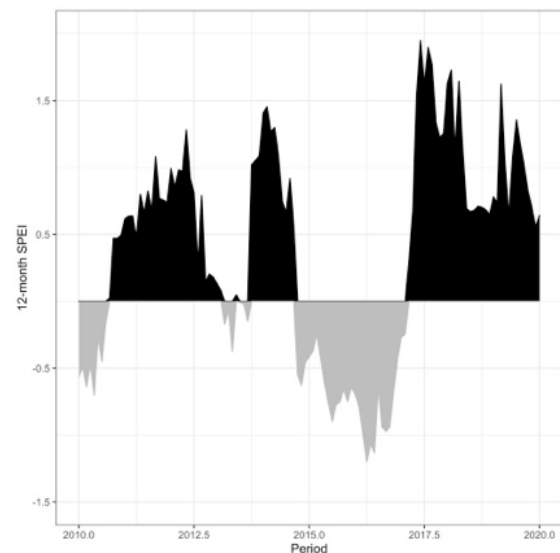


Figure 2: SPEI 12-month for the 2010–2020 period in Sakaerat Biosphere Reserve.

3. Forest dynamics

The summary of forest dynamics for ten-year period was shown in Table 1. The number of species tend to decline, which is most likely to the result of random fluctuation. It found that almost 100% of the species that became locally disappear had only one individual, and most of them are called pioneer species, such as *Micromelum minutum*. The density and basal area were quite balanced, which peak in 2015. In the first period, around 80% of the gain in basal area was belonged to growth of surviving trees, and the rest is from new recruit. But in the second period, loss of basal area was found due to a high number of dead trees, causing a reduction of basal area in 2020. The net mortality and recruitment were quite similar (1.96 and 1.93 %/year, respectively). In the 1st period, recruitment showed higher than mortality (2.56 and 2.00 %/year, respectively). And then, both rates were reduced, which mortality was greater than recruitment (1.88 and 1.27 %/year, respectively).

Table 1: Summary table of forest dynamics (≥ 4.5 cm DBH) in the permanent plot in Sakaerat Biosphere Reserve

	2010	2015	2020	2010 - 2020
Sp. richness	184	172	167	
Density (N/ha)	23,329	23,975	23,253	
BA (m ² /ha)	27.85	28.39	28.32	
Loss	2.11	2.05	2.08	
Gain	2.65	1.98	2.32	
M (%/year)	2.00	1.88	1.96	
R (%/year)	2.56	1.27	1.93	

The difference in tree density across three censuses, 2010, 2015, and 2020, was evaluated using a one-way ANOVA. The density of trees differed statistically significantly among census years ($F(2, 4797) = 4.52, p < 0.05$). In 2015 (14.98 ± 4.77 individual/subplot), the density was higher than in 2010 (14.58 ± 4.74 individual/subplot). In comparison to 2015, it declined in 2020 (14.53 ± 4.47 individual/subplot). However, there was no statistically significant difference in tree density between 2010 and 2020. Tukey post-hoc analyses revealed that the increase from 2010 to 2015 was statistically significant ($p < 0.05$), as was the difference between 2015 and 2020 ($p < 0.05$) (Figure 3).

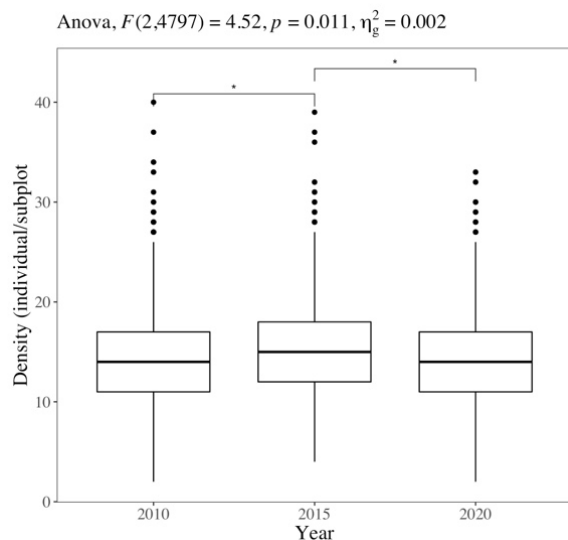


Figure 3: Tree density among three censuses in the permanent plot in Sakaerat Biosphere Reserve.

During the 10 years, the study site was primarily subjected to humid events. These factors largely influenced the forest's dynamics, particularly tree density, which has a direct impact on

recruitment. The recruitment rate was higher than the mortality rate in the first period, indicating that the wet in 2012 and 2014 may have allowed the trees to establish rapidly. This corresponds to a considerable increase in tree density between 2010 and 2015. The mortality rate was more equitably spread in the second period, although the recruitment rate was lower than in the first. According to the SPEI, there is a drought, which will be followed by highly wet conditions. Because of the drought, the death rate should be higher during this time. This suggests that the first period's extremely wet conditions may have played a role since they can buffer the negative effects of short-term severe drought, reducing mortality (Zhang, Q. *et al.*, 2017). This could be the cause for the relatively stable mortality in the second period. Nevertheless, limited storage reserves for tree regeneration, low vacant space for growing, and competition among trees (Maza-Villalobos, S. *et al.*, 2013) may have led to the reduction in recruitment in the second period. This is consistent with the fact that tree density declined statistically significantly in 2020.

Conclusions

Climate changes had influenced on forest dynamics. Net recruitment and mortality rates were almost similar. However, the recruitment of the second period was decreased doubly when compared to the first period. Our knowledge supports the species ecological niche and can be applied to forest conservation and reforestation program based on suitable species selection.

Acknowledgment

This research was financially supported by the Royal Golden Jubilee Ph.D. Programme (Grant No. PHD/0144/2561), through the Thailand Research Fund and the National Research Council of Thailand.

Reference

- Beguería, S., Vicente-Serrano, S. M., and Beguería, M. S. (2017). Package 'spei'. *Calculation of the Standardised Precipitation-Evapotranspiration Index*.
- Bunyavejchewin, S. (1999). Structure and dynamics in seasonal dry evergreen forest in

- northeastern Thailand. *Journal of Vegetation Science*, 10(6): 787-792.
- Condit, R., Ashton, P. S., Manokaran, N., LaFrankie, J. V., Hubbell, S. P., and Foster, R. B. (1999). Dynamics of the forest communities at Pasoh and Barro Colorado: comparing two 50-ha plots. *Philosophical Transactions of the Royal Society of London. Series B: Biological Sciences*, 354(1391): 1739-1748.
- De Souza, J. P., Araujo, G. M., and Haridasan, M. (2007). Influence of soil fertility on the distribution of tree species in a deciduous forest in the Triângulo Mineiro region of Brazil. *Plant ecology*, 191(2): 253-263.
- Delgado-Baquerizo, M., Reich, P. B., Bardgett, R. D., Eldridge, D. J., Lambers, H., Wardle, D. A., Reed, S. C., Plaza, C., Png, G. K., and Neuhauser, S. (2020). The influence of soil age on ecosystem structure and function across biomes. *Nature communications*, 11(1): 1-14.
- Feeley, K. J., Davies, S. J., Perez, R., Hubbell, S. P., and Foster, R. B. (2011). Directional changes in the species composition of a tropical forest. *Ecology*, 92(4): 871-882.
- Finch, H. J. S., Samuel, A. M., and Lane, G. P. F. (2014). Soils and soil management. *Lockhart & Wiseman's Crop Husbandry Including Grassland*, 9th ed.; Elsevier: Amsterdam, The Netherlands: 37-62.
- John, R., Dalling, J. W., Harms, K. E., Yavitt, J. B., Stallard, R. F., Mirabello, M., Hubbell, S. P., Valencia, R., Navarrete, H., and Vallejo, M. (2007). Soil nutrients influence spatial distributions of tropical tree species. *Proceedings of the National Academy of Sciences*, 104(3): 864-869.
- Körner, C. (2004). Through enhanced tree dynamics carbon dioxide enrichment may cause tropical forests to lose carbon. *Philosophical Transactions of the Royal Society of London B: Biological Sciences*, 359(1443): 493-498.
- Maza-Villalobos, S., Poorter, L., and Martínez-Ramos, M. (2013). Effects of ENSO and temporal rainfall variation on the dynamics of successional communities in old-field succession of a tropical dry forest. *PloS one*, 8(12): e82040.
- Miura, M., Manabe, T., Nishimura, N., and Yamamoto, S. i. (2001). Forest canopy and community dynamics in a temperate old-growth evergreen broad-leaved forest, south-western Japan: a 7-year study of a 4-ha plot. *Journal of Ecology*, 89(5): 841-849.
- Moreira, E., Russo, A., and Trigo, R. M. (2018). Monthly prediction of drought classes using log-linear models under the influence of NAO for early-warning of drought and water management. *Water*, 10(1): 65.
- Pongpattananurak, N. (2014). Prioritizing forest complexes of Thailand using landscape metrics. *Thai Journal of Forestry*, 33(2): 61-76.
- Rascón, J., Gosgot Angeles, W., Quiñones Huatangari, L., Oliva, M., and Barrena Gurbillón, M. Á. (2021). Dry and Wet Events in Andean Populations of Northern Peru: A Case Study of Chachapoyas, Peru. *Frontiers in Environmental Science*, 9: 54.
- Trisurat, Y. (2010). Land use and forested landscape changes at Sakaerat environmental research station in Nakhon Ratchasima province, Thailand. *Ekológia (Bratislava)*, 29(1): 99-109.
- Vicente-Serrano, S. M., Beguería, S., and López-Moreno, J. I. (2010). A multiscalar drought index sensitive to global warming: the standardized precipitation evapotranspiration index. *Journal of climate*, 23(7): 1696-1718.
- Zhang, Q., Shao, M. a., Jia, X., and Wei, X. (2017). Relationship of climatic and forest factors to drought-and heat-induced tree mortality. *PloS one*, 12(1): e0169770.

**INTERNATIONAL SYMPOSIUM ON A RECENT PROGRESS
IN FOREST ECOLOGY AND MANAGEMENT
2021**

**SESSION 2
ECOLOGY OF TROPICAL TO TEMPERATE FORESTS**

**Wednesday, 10th November 2021
15:20 - 16:05**

**ORGANIZER:
THE UNITED GRADUATE SCHOOL OF AGRICULTURAL SCIENCE, GIFU UNIVERSITY**

Mast Seeding and Associated Resource Dynamics in *Fagus* Species

Qingmin Han^{1*}, Daisuke Kabeya¹, Yoshiyuki Inagaki²,
Akira Kagawa³, Günter Hoch⁴, Atsuhiko Iio⁵

¹ Department of Plant Ecology, Forestry and Forest Products Research Institute (FFPRI)

² Shikoku Research Center, FFPRI

³ Department of Wood Properties, FFPRI

⁴ Department of Environmental Sciences - Botany, University of Basel

⁵ Faculty of Agriculture, University of Shizuoka

*Corresponding Author: qhan@ffpri.affrc.go.jp

SUMMARY

Mast seeding or masting is a well-known phenomenon in temperate and tropical forests and a reproductive trait that generally exists in afforestation tree species. Although its evolutionary significances have been well demonstrated, its physiological mechanism remains poorly understood. Using long-term field investigation and stable isotopic technology, we demonstrated that nitrogen is the key resource that limits masting events in *Fagus crenata*, whereas stored starch plays a role as a “pinch-hitter” when asynchrony of carbon supply and demand occurs.

Keywords: Allocation; Beech; Carbohydrate; Masting; Nitrogen; Reproduction; Stable isotope; Starch; Storage

Introduction

Natural forests occupy one third of the earth’s land surface and account for two third of dry matter production among terrestrial plants. However, its natural regeneration is often impeded by low seed availability, especially in mast seeding species that refers to the synchronous intermittent production of large seed crops in a population of perennial plants (Kelly 1994). Moreover, reproduction is a key life-history event in respect of maintaining biodiversity by providing energy to pollinators and predators. However, the physiological mechanism of masting remains poorly understood (Isagi *et al.* 1997, Satake and Iwasa 2000). Here, we represent related results achieved from resource dynamics of non-structural carbohydrate (NSC) and nitrogen (N) in *Fagus* species using both natural and pulse-labelling isotopic approach.

Results

1. Nitrogen dynamics in relation to masting

Nitrogen demand for masting events was estimated from litter traps monitored in two *Fagus crenata* stands located at 900 m and 1500 m elevation (Han *et al.* 2014). Average N amount in fruit litter (cupules and nuts) was about equivalent to the N quantity in leaf litters in a full masting year (Fig. 1), indicating that masting events consumes

substantial N resources in mature forests.

In the same stands, a significant reduction in individual N storage pools following was observed after the full masting, which was followed by years of replenishment of this stored N pool. These results provide direct evidence of a decline in stored nutrients after a mast event in mature forests. In addition, significant decreases in leaf litter N were found in the years following masting events, indicating that the N storage pool was reduced as a result of fruiting and this prevented allocation of N to leaves in subsequent years. Together with our previous finding that floral buds have two-fold higher N content than leaf buds (Han *et al.* 2008), preferential allocation of resources to seeds in the

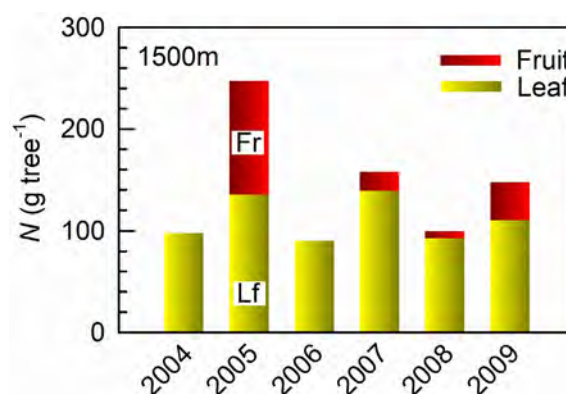


Figure 1: Inter-annual variations in the amount of nitrogen (N) in fruit and leaf litters in a *Fagus crenata* stand located at 1500 m elevation.

most year reduced the availability of resources for flower primordium formation, and this may have accounted for the poor seed production in the following year that is a typical character of masting event (Hilton and Packham 2003). These results indicate that masting affects N cycle dynamics in mature *F. crenata* forests.

To further understanding how mature trees acquiring N resources from soil and the influence of masting on N allocation, pulse ^{15}N labeling was applied to fruiting and non-fruiting trees of *F. crenata* in the 900 m stand (Han *et al.* 2017, Han *et al.* 2020). When labelling was conducted in late spring after the leaves have completely unfurled, fruiting leads to greater $^{15}\text{N}_{\text{excess}}$ uptake from the soil during the first month following application (Fig. 2). Moreover, cupules absorbed more $^{15}\text{N}_{\text{excess}}$ even than leaves in fruiting trees, whereas $^{15}\text{N}_{\text{excess}}$ in leaves was about the same between fruiting and non-fruiting trees. On the other hand, half of ^{15}N was recovered in nuts at the end of the growing season. These results indicate that ^{15}N uptake was driven by

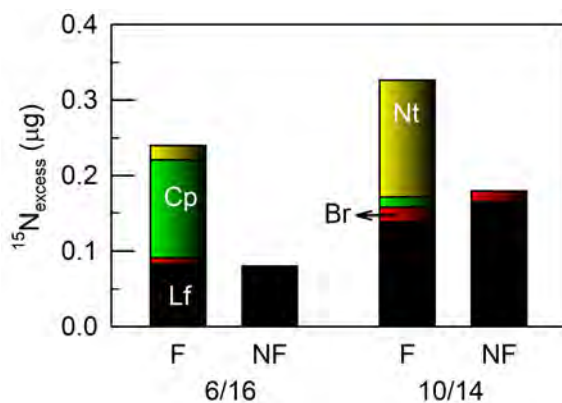


Figure 2: Pulse labelling-derived isotopic nitrogen ($^{15}\text{N}_{\text{excess}}$) for leaves (Lf), current-year branches (Br), cupules (Cp) and nuts (Nt) represented at current-year shoot level averaged from three-year-old branches sampled from upper crowns of fruiting trees (F) and (b) non-fruiting trees (NF) of 89-90-year-old *Fagus crenata*. Values shown are mean \pm SE ($n = 3$). The date of ^{15}N labelling was 31 May 2011.

sink strength. In addition, translocation of N from cupules and senescing leaves contributed also to nut ripening. Together with the effect of N level on flowering gene expression (Miyazaki *et al.* 2014) and validation of both N and carbon in the resource budget model to explore the proximate mechanism

of masting (Abe *et al.* 2016), these results demonstrate that N is the key limiting resource for masting events in *F. crenata*.

2. NSC dynamics in relation to masting

Mature trees store substantial amounts of NSC, mainly starch and soluble sugar, in wood organs (Hoch *et al.* 2003). At the whole-tree level, NSC buffers the asynchrony of carbon supply and demand, and thus plays important functions in plant growth and survival (Chapin *et al.* 1990, Kozłowski 1992, Hartmann and Trumbore 2016). Its role in reproduction remains poorly understood because it is difficult to discriminate NSC storage from new photo-assimilate in mature tall trees. We validated that bulk leaf $\delta^{13}\text{C}$ measured with high temporal resolution could be used as a proxy for new photo-assimilate (Han *et al.* 2016). Using this proxy, and parallel measurements of seasonal $\delta^{13}\text{C}$ pattern in fruits of *F. crenata*, we found that fruit production relies on NSC storage until the middle of the growing season then shifts to new photo-assimilates (Han *et al.* 2016), at which time growth of branch and stem have finished (Kabeya *et al.* 2017). These results complemented our previous finding using a large-scale, continuous ^{13}C labeling technique in a mature forest (Hoch *et al.* 2013), from which seeds of three deciduous tree species were demonstrated to be produced by new photo-assimilate but not by NSC storage.

In order to elucidate whether masting depletes the individual NSC storage pool, seasonal and inter-annual variations in NSC concentrations in branchlets, stems and coarse roots of *Fagus crenata* were measured in the aforementioned stands over five years after the full masting event (Kabeya *et al.* 2021). Individual NSC storage pools decreased after leaf fall in the year of the full masting and replenishment was then observed in the next 2-3 years in both stands. In addition, temporary reduction in starch concentration in summer due to moderate fruiting was found in coarse roots and stems (Fig. 3), but could not be detected after leaf fall, indicating refilling of NSC storage pool during the growing season. These results indicate that whether a decrease in NSC storage caused by masting occurs or not depends on the quantity of fruit production. This also highlights the importance of timing in detecting masting-related NSC variations.

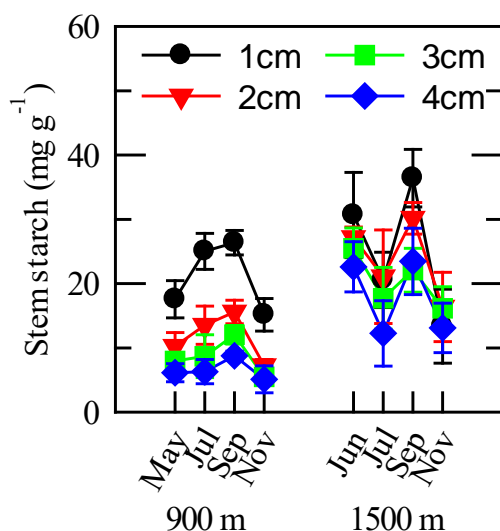


Figure 3: Seasonal variations in starch concentrations for stem cores of different depths starting from the cambium at the 900m and 1500m sites in 2007, a year with moderate fruiting at the 1500 m site only. Values represent the mean \pm SE for three to five individuals.

This fruiting related reduction in starch concentration in summer was found in all sampled stem cores, representing tree rings formed 20 years ago (Fig. 3). Starch is stored in ray and axial parenchyma, and new photo-assimilates are mixed with old NSC in older rings (Richardson *et al.* 2013, Richardson *et al.* 2015, Furze *et al.* 2018). Our results provide the first evidence that starch in deep sapwoods is available for masting events, which is consistent with it being accessible for tree growth and metabolism. Together with a higher starch storage pool in roots than in branchlets, these results indicate that starch stored in roots and stems is available and supports life-history traits such as masting events, as a “pinch-hitter” when asynchrony of carbon supply and demand occurs.

Acknowledgment

The authors would like to thank Professor Emeriti of Y. Kakubari and Ch. Körner for various supports, members of FFPRI and University of Shizuoka who has helped field investigation. This work was supported by JSPS KAKENHI (C18580155, B21380103, B25292094, A26251042, 17H03837, 20H00436), OECD Co-operative Research Program, and Grant for Environmental Research Projects from The Sumitomo Foundation (113250).

Reference

- Abe T, Tachiki Y, Kon H, Nagasaka A, Onodera K, Minamino K, Han Q, Satake A (2016) Parameterisation and validation of a resource budget model for masting using spatiotemporal flowering data of individual trees. *Ecology Letters* 19:1129-1139.
- Chapin FS, Schulze E-D, Mooney HA (1990) The ecology and economics of storage in plants. *Annual Review of Ecology and Systematics* 21:423-447.
- Furze ME, Trumbore S, Hartmann H (2018) Detours on the phloem sugar highway: stem carbon storage and remobilization. *Current Opinion in Plant Biology* 43:89-95.
- Han Q, Kabeya D, Iio A, Inagaki Y, Kakubari Y (2014) Nitrogen storage dynamics are affected by masting events in *Fagus crenata*. *Oecologia* 174:679-687.
- Han Q, Kabeya D, Iio A, Kakubari Y (2008) Masting in *Fagus crenata* and its influence on the nitrogen content and dry mass of winter buds. *Tree Physiology* 28:1269-1276.
- Han Q, Kabeya D, Inagaki Y (2017) Influence of reproduction on nitrogen uptake and allocation to new organs in *Fagus crenata*. *Tree Physiology* 37:1436-1443.
- Han Q, Kabeya D, Inagaki Y (2020) Reproduction affects partitioning between new organs of a pulse of ^{15}N applied during seed ripening in *Fagus crenata*. *New Forests* 51:739-752.
- Han Q, Kagawa A, Kabeya D, Inagaki Y (2016) Reproduction-related variation in carbon allocation to woody tissues in *Fagus crenata* using a natural ^{13}C approach. *Tree Physiology* 36:1343-1352.
- Hartmann H, Trumbore S (2016) Understanding the roles of nonstructural carbohydrates in forest trees – from what we can measure to what we want to know. *New Phytologist* 211:386-403.
- Hilton GM, Packham JR (2003) Variation in the masting of common beech (*Fagus sylvatica* L.) in northern Europe over two centuries (1800-2001). *Forestry* 76:319-328.
- Hoch G, Richter A, Körner C (2003) Non-structural carbon compounds in temperate forest trees. *Plant, Cell & Environment* 26:1067-1081.
- Hoch G, Siegwolf RTW, Keel S, Körner C, Han Q (2013) Fruit production in three masting tree

- species does not rely on stored carbon reserves. *Oecologia* 171:653-662.
- Isagi Y, Sugimura K, Sumida A, Ito H (1997) How does masting happen and synchronize? *Journal of Theoretical Biology* 187:231-239.
- Kabeya D, Iio A, Kakubari Y, Han Q (2021) Dynamics of non-structural carbohydrates following a full masting event reveal a role for stored starch in relation to reproduction in *Fagus crenata*. *Forestry Research* 1:doi:10.48130/fr-2021-0018.
- Kabeya D, Inagaki Y, Noguchi K, Han Q (2017) Growth rate reduction causes a decline in the annual incremental trunk growth in masting *Fagus crenata* trees. *Tree Physiology* 37:1444-1452.
- Kelly D (1994) The evolutionary ecology of mast seeding. *Trends in Ecology and Evolution* 9:465-470.
- Kozłowski TT (1992) Carbohydrate sources and sinks in woody plants. *The Botanical Review* 58:107-222.
- Miyazaki Y, Maruyama Y, Chiba Y, Kobayashi MJ, Joseph B, Shimizu KK, Mochida K, Hiura T, Kon H, Satake A (2014) Nitrogen as a key regulator of flowering in *Fagus crenata*: understanding the physiological mechanism of masting by gene expression analysis. *Ecology Letters* 17:1299-1309.
- Richardson AD, Carbone MS, Huggett BA, Furze ME, Czimczik CI, Walker JC, Xu X, Schaberg PG, Murakami P (2015) Distribution and mixing of old and new nonstructural carbon in two temperate trees. *New Phytologist* 206:590-597.
- Richardson AD, Carbone MS, Keenan TF, Czimczik CI, Hollinger DY, Murakami P, Schaberg PG, Xu X (2013) Seasonal dynamics and age of stemwood nonstructural carbohydrates in temperate forest trees. *New Phytologist* 197:850-861.
- Satake A, Iwasa Y (2000) Pollen coupling of forest trees: forming synchronized and periodic reproduction out of chaos. *Journal of Theoretical Biology* 203:63-84.

Anchorage and Stability Characteristic of Forest Tree Species in Tropical Region and a Suitable Wind Damage Assessment Mode for Planted Forest in Vietnam

Nguyen Trong Minh^{1,2,3,*}, Fukui Sho¹, Iwama Shintaro¹,
Dang Thinh Trieu⁴, Koyano Kaita¹, Hizomi Mizunaga¹

¹ Faculty of Agriculture, Shizuoka University, Japan

² The United Graduate School of Agriculture, Gifu University, Japan

³ Faculty of Silviculture, Vietnam National University of Forestry, Vietnam

⁴ Silviculture Research Institute, Vietnam

*Corresponding Author: minhnguyen1408@gmail.com

SUMMARY

Wind is considered as a major disturbance agent in forests and plays an important role in the dynamics of many forest ecosystems. This study focused on two purposes, including i) to investigate the anchorage and stability of forest tree species related to wind damage by conducting pulling experiments to determine the mechanical tree resistance to over-turning for 17 tree species in planted and natural forest in Vietnam; ii) to examine the efficiency of using a fluid model in complex topography to evaluate the wind hazard model by identifying the most important predictor variables (e.g. stand attributes, topographic and wind speed) in this model, in the tropical zone. This study found that the tree stability was strongly affected by tree characteristics and site conditions, in which the hazard ratio increased as tree size increased, and was driven by tree species, site, and buttress. We applied an empirical method combining airflow simulations, and historical records of wind disturbance within a GIS in middle Vietnam. The wind damage probability of planted forest (*Acacia* hybrid) was associated with stand characteristics, wind velocity, and topographic characteristics found in the test model. Higher damage probabilities were found in stands with taller tree height, on higher slopes, and with higher wind speed. Our results, therefore, provide evidence for using fluid models in complex topography to establish the wind hazard model.

Keywords: Anchorage and stability; Tropical zone; Wind hazard model; Fluid model; Complex topography

Introduction

Strong tropical storms that occur in Asia cause serious natural disturbances to forest ecosystems because wind-induced damage can substantially change forest ecosystem functions, owing to changes in forest structure (Gardiner 2007). Many researches were conducted to discuss the impacts of wind damage in detail for many different regions, forest types, and the factors affecting the levels and types of damage. However, there are limited researches related to wind damage on forest in the sub- and tropical zone (Gardiner 2021). Therefore, we processed this research with the main focus on increasing the understanding of processes behind the occurrence of wind-induced damage in the tropical region.

In this research, the anchorage and stability of trees were studied by applying the Cox regression model, and based on relationships between maximum turning moment (TM_{max}) and site characteristics, tree species, tree weight (TW), and tree size (multiplied tree height (H) and square of diameter at breast height (DBH2) for 17 forest tree species in planted and natural forest, in North and Mid of Vietnam. The impact of these factors on the stiffness index, with a GLMM, was also investigated. Besides that, we conducted a study in 2017 to present an analysis of wind damage data at a regional scale in the *A. hybrid* plantation forest, using an empirical method. The main objectives of this study

were to examine the efficiency of using a fluid model in complex topography to evaluate the wind hazard model by identifying the most important predictor variables for statistical modeling of the probability of wind risk. Our research on integrating GIS, aerodynamics, and satellite image analysis to establish a logistic model to clarify affected factors to determine wind hazard for *A. hybrid* plantations is the first such approach in Vietnam. The results will contribute towards knowledge relating to mechanistic models of tree failure, and the further development of mechanistic wind damage risk models.

Material and methods

1. Study on anchorage and stability

Four research sites were selected to conduct tree-pulling experiments in Vietnam located in the north of Vietnam (Dai Lai, Cuc Phuong) and central Vietnam (Thanh Hoa, Quang Tri). Pulling experiments using wire and robe were conducted according to Nguyen et al. 2021 to detect the TM_{max} of trees. Table 1 indicated the pulled tree information for a total of 107 pulling trees.

The TM_{max} , stiffness index (SI), and buttress index (BHI) were shown in Eq.1, Eq.2, and Eq.3 as follows:

$$TM_{\max} = F \times H_{\text{cable}} (\cos\alpha \sin\beta + \sin\alpha \cos\beta) + TW \times G \quad (1)$$

$$SI = TM_{\max} / \beta \quad (2)$$

$$BHI = BH / BL \quad (3)$$

Where: F (kgf) is the maximum load, α (degree) is the angle between the wire and the horizontal line from the anchor tree's stem base, β (degree) is the mean stem angle from the original position of the stem at the maximum force, and H_{cable} (m) is the attached wire height; BH is buttress height; BL is buttress length.

The “coxme”, “glmm” and “lme4” packages were selected to investigate factors impacted on the risk of tree failure and SI in R. All model formulation were presented in Table 2.

2. Study on wind hazard for *A. hybrid* plantation

The area of interest, located in Quang Tri, Vietnam, measures an area of 10×10 km² with an elevation ranging 37–550m and is located in yellow soil (Ferralsols). There were four main data processing: i) tree height estimation to predict the dominant height (H_{dom}) of *A. hybrid* stands, ii) prediction of wind properties via RIAM-COMPACT, iii) estimation of wind damage by classifying LANDSAT-8 images, and iv) wind risk model for *A. hybrid* plantations (Figure 1).

Tree height estimation: Two data groups, included a training dataset (70% of total sample plots,

77 plots with a size of 1000m²) and an evaluation dataset (30% of total sample plots, 33 plots), were used for estimated the tree height growth curve in R software applied with the ‘rstan’ package. After validating participated equations, the most suitable equation was used for calculating H_{dom} for *A. hybrid* plantation, then to build the Digital Surface Model (DSM).

Prediction of wind properties: Windspeed and wind turbulence were estimated using RIAM-COMPACT (Uchida 2008) at an approximate height of 10 and 15 m above the canopy. The research used 30×30m grid data from DSM topography. Power law of 1/7 of wind profile, an initial wind speed of 10 ms⁻¹, and a buffer zone with a distance of 2.5km were used as parameters for the simulation.

Estimation of wind damage locations: The ‘randomForest’ package in R was used for building the classification model, in which damage condition (damage or no damage) was the response variable, while the predictor variables were shown in Table 3.

Predicting the wind damage in *A. hybrid* plantations: A logistic regression (Collett 2003) was used to assess the probability of wind disturbance, in which, predictor variables were calculated using ArcGIS and then input to R to predict damage probability (Table 3).

Table 1. Description of sample trees in the tree pulling experiments

Site	Species	Dbh (Std) (Unit: cm)	H (Std) (Unit: m)	Number of trees (Unit: trees)	Forest type
<i>Dai Lai</i>	<i>A. hybrid</i>	11.2-23.1	19.9-26.2	12	Plantation
	<i>P. caribaea</i>	8.6-22.7	6.6-19.7	12	Plantation
	<i>E. urophylla</i>	9.8-25.9	14.6-27.3	12	Plantation
<i>Thanh Hoa</i>	<i>A. hybrid</i>	13.2 - 29.9	11.8 - 23.5	5	Plantation
	12 species	13.2 - 29.9	11.8 - 23.5	17	Natural
<i>Cuc Phuong</i>	<i>Parashorea</i> & <i>Pometia</i>	7.5-24.4	9.2-25.0	19	Natural
<i>Quang Tri</i>	<i>A. hybrid</i>	8.9-22.4	8.6-24.6	30	Plantation

Table 2. The model formulation for predicting the hazard ratio of tree failure and the stiffness index (SI)

Model code	Model formulation	Regression model types
(1.1)	$h(t,x) = h_0(t)\exp(a \cdot X_i)$	The Cox regression
(1.2)	$h(t,x) = h_0(t)\exp(a \cdot X_i + c_{\text{site}})$	The Cox regression
(1.3)	$h(t,x) = h_0(t)\exp(a \cdot X_i + b \cdot \text{Species})$	The Cox regression
(1.4)	$h(t,x) = h_0(t)\exp(X_i \otimes \text{Species})$	The Cox regression
(1.5)	$\lg SI = a \cdot X_i + b$	GLMMs
(1.6)	$\lg SI = a \cdot X_i + c_{\text{site}}$	GLMMs
(1.7)	$\lg SI = a \cdot X_i + b \cdot \text{Species}$	GLMMs

In which: X_i is an explanation factor; c_{site} is the random effect; \otimes represents the interaction between explanatory variables and species; $h(t,x)$ is the hazard function; t is considered as the moment of tree failure.

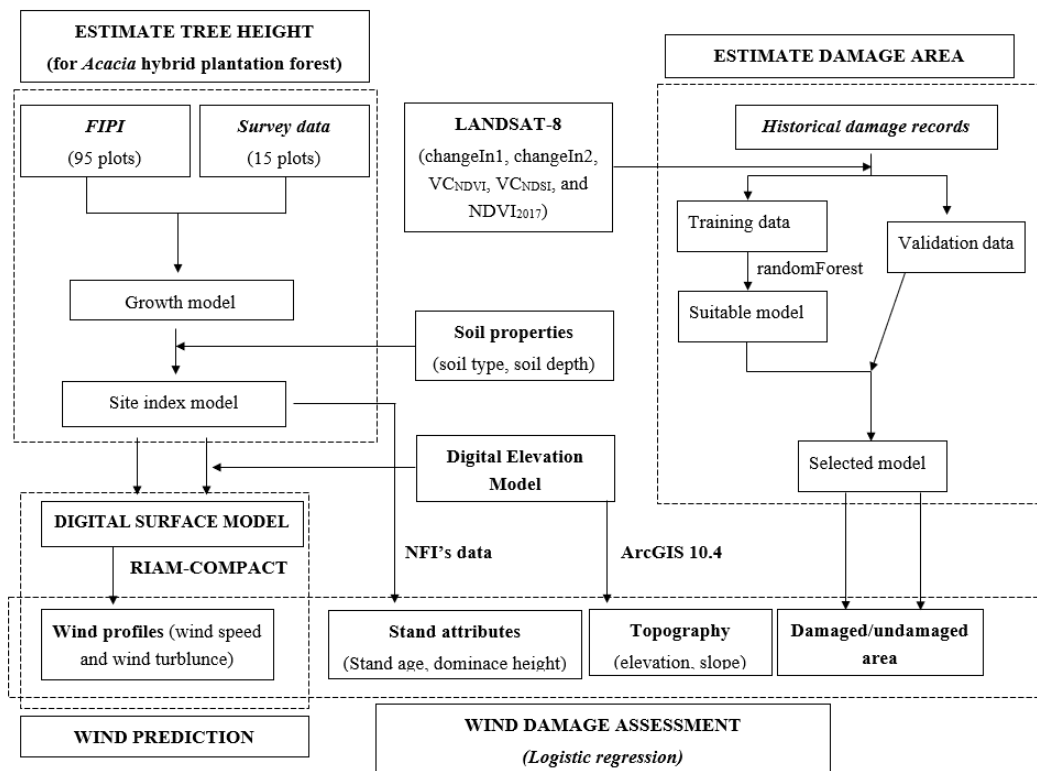


Figure 1. The flowchart describes data processing in this study

Table 3. The model form used for estimating the wind damage probability

Mode code	Model form
1.7	$\text{logit}(p) \sim a + b \times \text{Age} + c \times H_{\text{dom}} + d \times \text{WS}(\text{WS}_3)$
1.8	$\text{logit}(p) \sim a + b \times \text{Age} + c \times H_{\text{dom}} + d \times \text{Turbulence intensity}$
1.9	$\text{logit}(p) \sim a + b \times \text{Age} + c \times H_{\text{dom}} + d \times \text{Elv} + e \times \text{Slo}$
1.10	$\text{logit}(p) \sim a + b \times \text{Age} + c \times H_{\text{dom}} + d \times \text{WS}(\text{WS}_3) + e \times \text{Turbulence intensity} + f \times \text{Elv} + g \times \text{Slo}$

Note: p is the probability of a stand being disturbed; Age is the stand age; H_{dom} is the dominant height of a stand; Elv is elevation; Slo is the slope; and a, b, c, d, e, f, g are the parameters of model.

Results and discussion

1. Anchorage of forest tree species in the tropical region

Effects of tree characteristic on the risk of tree failure: Significant correlations were found between the risk of tree failure and explanatory factors (e.g. tree size, TW, H and DBH with a highly statistically significant coefficient ($p < 0.05$)), in which, the risk of failure can reduce with an increase of these factors. The best model was selected in which tree size was the most suitable indicator for estimating the risk of tree failure. This pulling test confirmed the effect of tree size on TM_{max} , as suggested by previous in which tree stability increased substantially with an increase in tree size (Ribeiro et al. 2016).

Effects of site on the risk of tree failure: Results on the tested model showed that the difference between sites was significant, in which, the hazard ratio was higher in Thanh Hoa than in Dai Lai. The

differences related to soil type and thickness and strongly affected the estimated TM_{max} . The main soil type in Dai Lai was Ferralic Acrisols with a thickness of around 70 cm, whereas in Thanh Hoa the one was Ferralsols derived from basalt with thickness from 30 to 50 cm. This study also provided a graph of TM_{max} for A. hybrid by groups of soil type (Figure 2).

Effects of species on the risk of tree failure: It was found that species have a significant impact on the risk of failure. A difference was clearly seen between *E. urophylla* and A. hybrid, with a probability of tree resistance being lower in *E. urophylla* ($p < 0.05$) (Figure 3a). The survival probability dramatically reduced around 30 kNm for all species in the selected mode. However, there was no significant difference between *P. chinensis* and *P. pinata* when the pulling experiment was conducted in the natural forest (Figure 3b). The findings were following Ribeiro (2016) in which TM_{max} varied among species groups in the Amazon forest based on tree size (e.g. DBH).

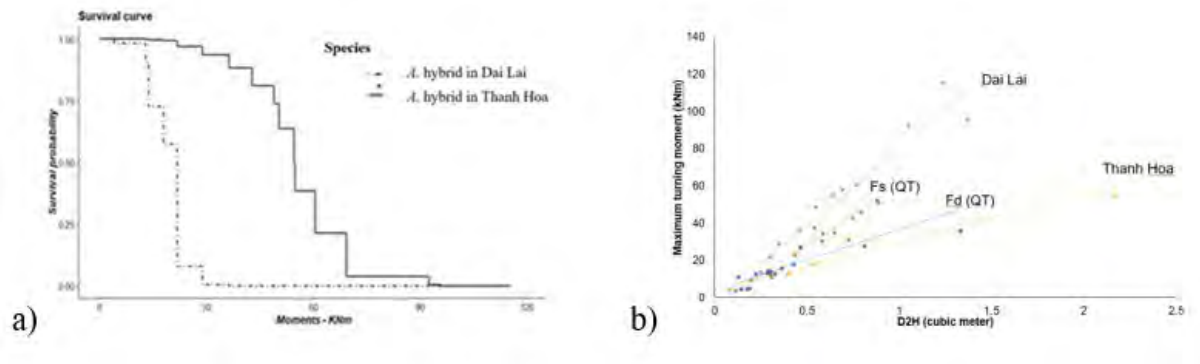


Figure 2. The hazard ratio related to sites (a) and TM_{max} by groups of soil type for *A. hybrid* (b).

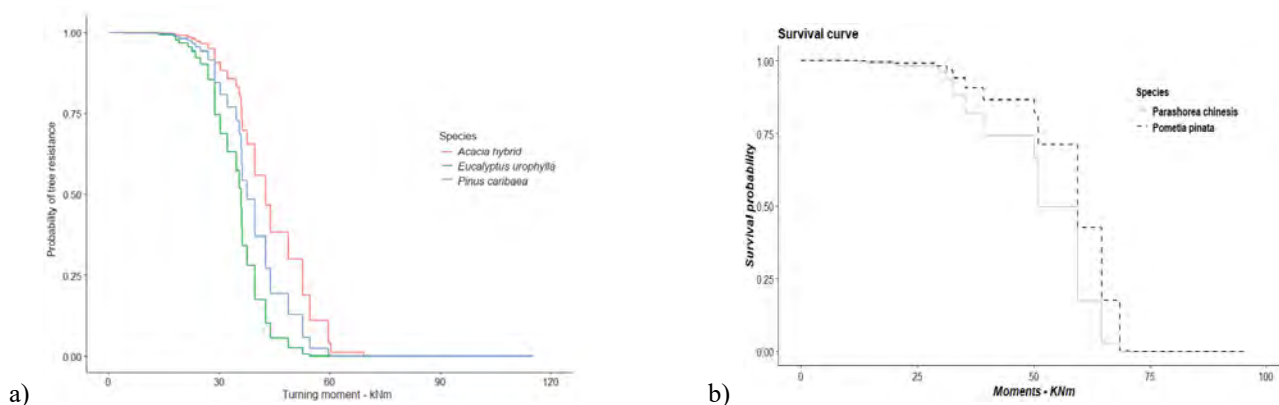


Figure 3. Species effects on the probability of tree resistance in Dai Lai in plantation forest (a) and in Cuc Phuong in natural forest (b).

Effects of tree characteristic on SI: Tree size, tree species were also strongly associated with SI. The SI was increased with the increase of tree size (positive estimated parameters; not shown here). The change of these factors led to the change in SI, in which SI increased with an increase in tree size and showed clear differences among species groups. The current results agree with the findings of Kamimura's research (2012). However, together with site effects, the current study proposed scientific evidence for the impact of species. The SI was also strongly dependent on species groups, for example, *A. hybrid* had a high SI value compared with *P. caribaea* (Figure 4a). This signal was clearly seen in recorded videos while pulling these tree species. The *P. caribaea*' stem still continued to curve, while that of *A. hybrid* was uprooted or broken. Figure 4b presents images of *P. caribaea* stem and tap-root of *E. urophylla* under maximum load in the pulling test.

Effects of buttress on TM_{max} and SI: The buttress was associated with TM_{max} and SI, and strongly affected tree stability along with effects of tree size, in which TM_{max} and SI increase with the increase of BHI. This suggests that the existence of buttress affected the tree resistance to uprooting or breaking the stem and supported the tree stability (positive Coef., Table 4), whereas this one decreases the angle of the stem at the TM_{max} in the pulling experiment. The model including BH and tree size was the best model for SI and then shows the buttress role as one of the critical factors for

root anchorage. These results, therefore, were clear evidence for the impacts of the buttress and were contributed to predicting the TM_{max} and SI. These findings also confirm the discussion of Crook (1996), in which the author found that the buttress height was one main factor contributing to the root anchorage of the tree.

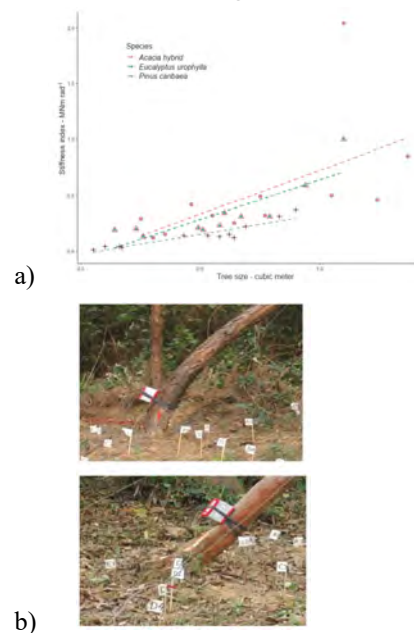


Figure 4. Stiffness index varied among tree species (a) and the flexible stem of *P. caribaea* (upper image) and tap-root broken of *E. urophylla* (lower image) (b).

Table 4. The effect of buttress characteristic on TM_{max} and stiffness index

Variables	Turning moment			Stiffness index (SI)		
	Coef.	Sig.	AIC	Coef.	Sig.	AIC
Intercept	11.24	0.02(*)	126.32	-0.82	0.03(*)	40.06
Tree size	32.42	0.00(*)		2.60	0.00(*)	
BH	0.84	0.83		0.69	0.05(*)	
Intercept	8.80	0.04(*)	121.69	-0.81	0.04(*)	41.04
Tree size	29.83	0.00(*)		2.81	0.00(*)	
BHI	4.81	0.06(.)		0.45	0.06(.)	

BH is buttress height; BHI is buttress index; Coef. is the regression coefficient; Confidence level: '*' 0.05; '.' 0.1.

2. Wind hazard model for A. hybrid plantation forest

By examining five components extracted from the LANDSAT 8 images at the times before and after typhoon Doksuri 2017 hitting Vietnam, the study provided a good qualitative classification for estimating damaged or undamaged areas, with high overall accuracy (95.83%) and kappa index (0.88) (Figure 5). The results from image classification, therefore, meet the aim of detecting the disturbance areas caused by strong wind of the typhoon and then were used to provide a dataset for building a wind hazard model.

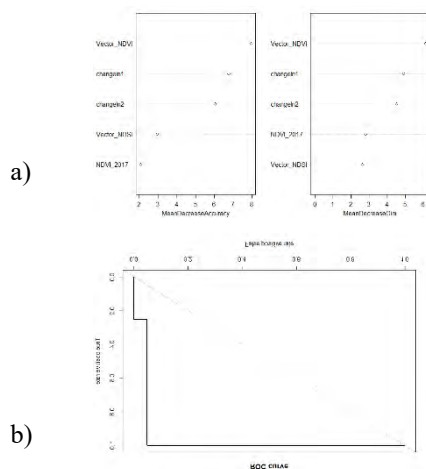


Figure 5. The importance of variables (a) and ROC curves (b) of the model created using the Random Forest algorithm.

The final model for predicting wind damage risk selected using the lowest AIC value, included Sty, A, H_{dom} , WS_3 , Elv, and Slo. In this model, WS_3 was calculated as the wind direction from south to north, and the height at 15 m above the canopy. The model showed that H_{dom} , WS_3 , and Slo were associated with high damage probabilities,

whereas stand age and elevation seemed to be less susceptible (Table 5). Stands growing on soil type F_s were more likely to be stable against wind damage than those on soil type F_d (there was a significant difference, between the two soil types, $p < 0.5$). Since it had the lowest AIC value, the south direction was considered to be the wind flow direction, which was used for predicting wind speed when validating the final model.

Table 5. Estimated model coefficients of the generalized linear model for the probability of occurrence of wind damage.

Explanatory variable	Height above canopy at 15m (AIC = 309.66)		
	Coef.	SE	Sig.
(Intercept)	8.869	2.946	0.003**
Sty F _s [§]	-0.809	0.334	0.015*
A	-0.919	0.329	0.005**
H_{dom}	3.009	1.050	0.004**
WS_3	0.252	0.152	0.097.
Slo	0.043	0.021	0.044*
Ele	-0.007	0.002	0.003*

[§]: Soil type F_d was used as the basis for comparison.

Confidence level: '***' 0.001; '**' 0.01; '*' 0.05; '.' 0.1.

Classification performance tests showed that the wind damage probability model performed moderately. A higher probability of wind disturbance for taller trees/stands, higher wind speeds, and forests on higher slopes was found. The inclusion of stand age had a negative effect on damage probability ($p < 0.05$). Increasing stand age, therefore, may lead to a decrease in wind damage because of the decline in H/DBH (Gardiner 2013).

The taller stands (tree height) were more

likely sensitive to wind damage ($p < 0.05$). If a tree is taller, it is more likely to fall over because it is less stable (Dhubhain et al. 2001). In the current study, H_{dom} was selected since it was better than other factors as a measure of wind vulnerability (Gardiner 2013).

The current study found a significant wind speed predictor (WS_3 at 15 m high above the canopy), with increasing WS_3 leading to a greater probability of wind damage. Higher wind speed causes more damage in a stand (Schindler et al. 2012). The results concurred with the findings of Uchida (2008), in which the forest stands were damaged not only by wind speed enhanced by terrain conditions but also by the fluctuations in wind velocity.

Concerning soil type, the results showed that the stands on F_s were more likely to be stable in a tropical storm than those on F_d ($p < 0.05$). To validate the model result on the effect of soil type, the physical stability TM_{max} of *A. hybrid* was compared on both soil types. The data analysis revealed that TM_{max} in the model of tree failure was governed by tree size and soil type, and the stability of trees in F_d was smaller than those in F_s with the same tree size (Figure 2b). Therefore, the effect of soil type on modeling forest wind damage was supported by this mechanistic measurement. The coincidence of the statistical model from satellite image with mechanistic measurement suggested the effectiveness of the model as the evaluating factor related to the wind damage.

Conclusion

The results provided the Cox hazard proportion that can be used to predict the risk of tree failure and also showed a comparison of anchorage between forest tree species in a tropical zone. The data analysis revealed that the hazard ratio in the model of tree failure and SI were governed by tree size attributes, and varied among tree species and site properties. In addition, the current study analyzed the wind damage probability in complex terrain for *A. hybrid* plantation forests in Vietnam by integrating an aerodynamics model for simulating wind speed, wind disturbance records, and GIS data at a landscape level. The wind hazard ratio of *A. hybrid* plantations was associated with stand characteristics, wind velocity, and topographic characteristics. The combination of GIS, satellite

images, and a wind condition prediction model enabled an analysis of wind damage prediction concerning stand and topography.

Acknowledgments

The authors would like to thank the community of Dai Lai, Lang Chang District, Cuc Phuong, and Quang Tri for their cooperation, and the local government officers for their kind support. The study was financially supported by the Laboratory of Silviculture, Faculty of Agriculture, Shizuoka University. The authors would like to thank the students of the Silviculture Laboratory for their help in the statistical approach and their support of the experiment.

Reference

- Crook, M. J., Ennos, A. R., & Banks, J. R. (1997). The function of buttress roots: a comparative study of the anchorage systems of buttressed (*Aglaia* and *Nephelium ramboutan* species) and non-buttressed (*Mallotus wrayi*) tropical trees. *Journal of Experimental Botany*, 48(314), 1703–1716.
- Dhubháin, A., et al. (2001). The initial development of a windthrow risk model for *Sitka* spruce in Ireland. *Forestry* 74: 161–170.
- Gardiner, B. (2021). Wind damage to forests and trees: a review with an emphasis on planted and managed forests. *Journal of Forest Research*, 26:4, 248-266.
- Gardiner, B. et al. (2013). *Living with Storm Damage to Forests*. European Forest Institute, Joensuu.
- Kamimura, K., et al. (2012). Root anchorage of hinoki (*Chamaecyparis obtuse* Sieb. Et Zucc. Endl.) under the combined loading of wind and rapidly supplied water on soil: analyses based on tree-pulling experiments. *European Journal of Forest Research* 131: 219 – 227.
- Nguyen, et al. (2021). Anchorage and stability of three major plantation forest species in Vietnam. *Journal of Tropical Forest Science* 33(1), 30–40
- Quine, C & Gardiner B. (2007). Understanding how the interaction of wind and trees results in windthrow, stem breakage and canopy gap formation. Pp 103–155 in Johnson E & Miyanishi K (eds) *Plant Disturbance Ecology*:

- The Process and the Response*. Elsevier, Amsterdam.
- Ribeiro, G.H., et al. (2016). Mechanical vulnerability and resistance to snapping and uprooting for Central Amazon tree species. *Forest Ecology and Management* 380: 1–10.
- Schindler, D., et al. (2012). Wind effects on trees. *European Journal of Forest Research* 131: 159–163.
- Uchida, T. & Ohya, Y. (2008). Micro-siting technique for wind Turbine generators by using large-eddy simulation. *Journal of Wind Engineering and Industrial Aerodynamics* 96: 2121–2138.

Hybrid Breakdown as a Result of Up-regulated Expression of Defense-related Genes in the Hybrid Seedlings of Japanese Flowering Cherry

Momi Tsuruta^{1*}, Chunlan Lian², Yuzuru Mukai³

¹ Department of Forest Molecular Genetics and Biotechnology, Forestry and Forest Products Research Institute

² Asian Research Center for Bioresource and Environmental Sciences, Graduate School of Agriculture and Life Sciences, The University of Tokyo

³ Faculty of Applied Biological Sciences, Gifu University

*Corresponding Author: m.tsuruta.lfme@gmail.com

SUMMARY

Knowledge of post-zygotic hybrid incompatibility is essential to understanding speciation. Although the genes and molecular mechanisms involved in hybrid incompatibility are being elucidated in model plants and crops, the information on woody non-model plants is lacking. In the seedlings of a cross between the most famous ornamental cherry cultivar *Cerasus* × *yedoensis* ‘Somei-yoshino’ and its closely related wild species *Cerasus itosakura*, we discovered a hybrid incompatibility characterized by a phenotype in which growth stops after the expansion of the first true leaves and eventually dies. To elucidate the molecular mechanisms related to this seedling necrosis, we performed a comprehensive expressed genes analysis on normal-growth and necrotic weak-growth (SW) hybrid seedlings. The RNA-seq results showed over 1,500 differentially expressed genes (DEGs) specified for the SW. Numerous genes associated with plant defense response, such as pathogenesis-related genes, and several receptor-like protein kinases were included in SW-specific up-regulated DEGs. The Gene Ontology (GO) enrichment analysis also showed the significant association of “defense response” in SW seedlings. On the contrary, the reduction of genes expression related to photosynthesis was also observed in the SW. Our results suggest that an excessed defense-related gene expression suppresses the other physiological activities, resulting in growth failure as an autoimmune response in hybrid cherry seedlings.

Keywords: Autoimmunity; Defense response; Hybrid necrosis; Somei-yoshino; Transcriptome

Introduction

Flowering cherry (Rosaceae, *Cerasus*) is one of the most famous ornamental trees in Japan. More than 10 wild species are distributed in small-island Japan and their habitats often overlap. Since the 18th century, various cultivars have been produced, many of which are originated from interspecific hybridization (Ohba, H. *et al.*, 2007; Kato, S. *et al.*, 2014). Because no physiological interspecific incompatibility has been observed before fertilization, frequent pollen transfer has been observed among cherry species. Thus, flowering cherry is considered to be a taxon with low barriers to interspecific hybridization. Nevertheless, distinct morphological and genetic differentiation of each species has been observed (Ohba, H. *et al.*, 2007; Kato, S. *et al.*, 2014). Understanding how speciation

is maintained despite the frequent interspecific gene flow requires elucidating the mechanism of post-zygotic reproductive isolation, such as hybrid sterility, weakness, necrosis, and hybrid breakdown (hybrid incompatibility that occurs in later generation after F₁).

In the model plants *Arabidopsis* and rice, genes underlying the post-zygotic reproductive isolation have been identified (Bombliet, K. *et al.*, 2007; Yamamoto, E. *et al.*, 2010). Here, the genes derived from other lineages interacted with another locus located in a cluster of receptor-like kinase (RLK) genes with leucine-rich repeat (LRR) domain. The RLKs are associated with the recognition of external stimuli, such as various pathogens, and precipitate downstream defense responses. These excessive defense reactions resulted in the hybrid seedling growth failure as an autoimmune response. Currently, the involvement of defense-related genes

and autoimmunity in hybrid incompatibility has been observed in several plant taxa (Wan, W.L. *et al.*, 2021). However, these studies are limited to herbal model plants and crops, and knowledge about hybrid incompatibility in woody species remains lacking.

In our previous study, we observed that the lethal growth failure (necrotic) phenotype appeared in about half of the seedlings from crosses between cherry cultivar *Cerasus* × *yedoensis* (Matsum.) Masam. et S.Suzuki ‘Somei-yoshino’ and wild cherry species *C. itosakura* (Siebold) Masam. et S.Suzuki (Tsuruta, M. and Y. Mukai, 2015). ‘Somei-yoshino’ is thought to have originated from a cross between two wild species, *C. speciosa* (Koidz.) H.Ohba and *C. itosakura* (Ohba, H. *et al.*, 2007; Kato, S. *et al.*, 2014; Shirasawa, K. *et al.*, 2019). Given that the seedlings from the crossing of ‘Somei-yoshino’ and *C. itosakura* can be considered as a backcross progeny at the species level, the seedling growth failure may therefore be due to hybrid breakdown. In the present study, to accumulate knowledge on the physiological mechanisms of hybrid necrosis in tree species, we conducted a comprehensive gene expression analysis for the normal-growth (SN) and necrotic weak-growth (SW) seedlings. We clarified the physiological mechanism responsible for the lethal hybrid seedlings of flowering cherries. Here, we also attempted to show that the autoimmune response due to high expressions of defense-related genes is a common causal phenomenon in hybrid incompatibility even in forest woody plants.

Materials and Methods

1. Normal and necrotic plant materials

We artificially pollinated *C. itosakura* (pollen donor) to ‘Somei-yoshino’ (seed parent). The

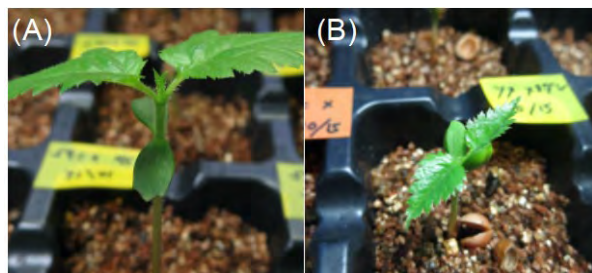


Figure 1: The normal-growth (A) and necrotic weak-growth phenotypes (B) of the hybrid seedlings approximately two weeks after germination.

pollination procedures and seed handling protocols followed the methods described in the work of Tsuruta and Mukai (2015). After three months of wet and chilling incubation, seeds were planted on a vermiculite bed. Of the 31 germinated seedlings, 12 (38.7%) grew normally, and 13 (41.9%) showed the lethal phenotype. The phenotype was characterized as the plants that grew until the emergence of first true leaves but failed to further develop (Fig. 1). Finally, the SW seedlings died after several weeks or a month. Additionally, we collected naturally pollinated seeds from a wild cherry tree, *C. jamasakura* (Siebold ex Koidz.) H.Ohba, and seedlings were obtained after treating the seeds as described above. The necrotic phenotype was never observed in these wild seedlings. Approximately two weeks after germination, SN, SW, and control wild cherry (CJ) seedlings were collected with three replicates each, immediately frozen by liquid N₂, and stored at –80 °C until RNA extraction.

2. RNA extraction and sequencing

From the seedling samples, total RNA was extracted using the modified CTAB method. The qualified RNAs were used for further analysis. RNA-seq was performed following Macrogen’s regular workflow (Macrogen Inc, Seoul, South Korea). Briefly, high-throughput sequencing libraries were constructed using the TruSeq stranded mRNA Library Kit (Illumina, San Diego, CA, USA) following the quality control of RNA. Each library was sequenced by the Illumina platform (NovaSeq6000) at 100 or 150 bp pair-end reads.

3. RNA-seq data processing and identification of DEG

The sequenced reads were first analyzed with fastp (Chen, S. *et al.*, 2018) for quality checking and trimming of low-quality base and read. The genome sequence of ‘Somei-yoshino’ (Shirasawa, K. *et al.*, 2019) was used as a reference. The genome consists of two phasing contigs derived from ancestral *C. itosakura* (CYE_SPA) and *C. speciosa* (CYE_SPE). The clean reads were mapped to the reference genomes using bowtie2 (Langmead, B. and S.L. Salzberg, 2012). Uniquely mapped reads were used for gene expression quantification with featureCounts (Liao, Y. *et al.*, 2014). The differentially expressed genes (DEGs) between the two treatments of CJ, SN, and SW were identified using a TCC-GUI pipeline (Su, W. *et al.*, 2019).

Significant DEGs that were common in CJ vs. SW and SN vs. SW but not present in CJ vs. SN were determined as SW-specific DEGs.

4. Annotation of DEGs and Enrichment Analysis

Gene information, such as annotations, BLAST results, InterPro, Gene Ontology (GO) terms, and GO accessions, were searched in the Genome Database for Rosaceae website (<https://www.rosaceae.org>). The R package goseq v1.38.0 (Young, M.D. *et al.*, 2010) was used to identify significantly enriched GO terms in the SW-specific up- and down-regulated DEGs.

Table 1: Gene expression number in each referenced genome for the normal (SN), necrotic weak growth (SW), and wild cherry (CJ) seedlings.

Reference genome	Transcribable gene	Number of expressed gene			
		SN	SW	CJ	All
'Somei-yoshino'	95,076	63,483	63,896	62,580	55,749 (78.8%)
CYE_SPA	48,280	33,097	33,073	31,470	28,484
CYE_SPE	46,796	30,386	30,823	31,110	27,265

Results

1. Gene expression profiling and detection of characteristic DEGs in SW seedlings

From the RNA-seq, over 50 M sequencing reads with 8.1–13.2 G bases per seedling sample were obtained. Over 97.8% of the quality-filtered clean reads were mapped to the 'Somei-yoshino' reference genomes. Of 95,076 transcribable genes in the reference, 70,746 genes (CYE_SPA: 36,392, CYE_SPE: 34,354) were expressed in any seedling. Among genes, 55,749 (86.2%) were commonly expressed in all seedlings (Table 1). TCC analysis determined that 20,005, 22,789, and 5,477 genes were significant DEGs in the comparison of CJ vs. SN, CJ vs. SW, and SN vs. SW, respectively. A total of 1,535 genes (up-regulated: 871, down-regulated: 664) were identified as SW-specific DEGs (Fig. 2).

2. Annotation of DEGs

From the results of the BLAST search, many plant defense-related genes were found in the up-regulated DEGs (Table 2). One is a member of the pathogenesis-related (PR) gene group.

CYE_r3.1SPA8_g020410 and CYE_r3.1SPE8_g024490, paralogs of the basic PR protein 1 of *Arabidopsis* (AT2G14580), were highly up-regulated in SW seedlings. Several other PR genes, such as thaumatin-like protein (TLP), a member of PR5, and Bet v1 superfamily gene belonging to PR10, were also found in the up-regulated DEGs. Another remarkable defense-related gene was a member of RLK. Of the CYE_SPE genome genes, CYE_r3.1SPE4_g004570, which has RLK and LRR domains, was the most up-regulated DEG. Other LRK genes, including cysteine-rich LRK (CRK), were also found in the DEG lists (Table 2).

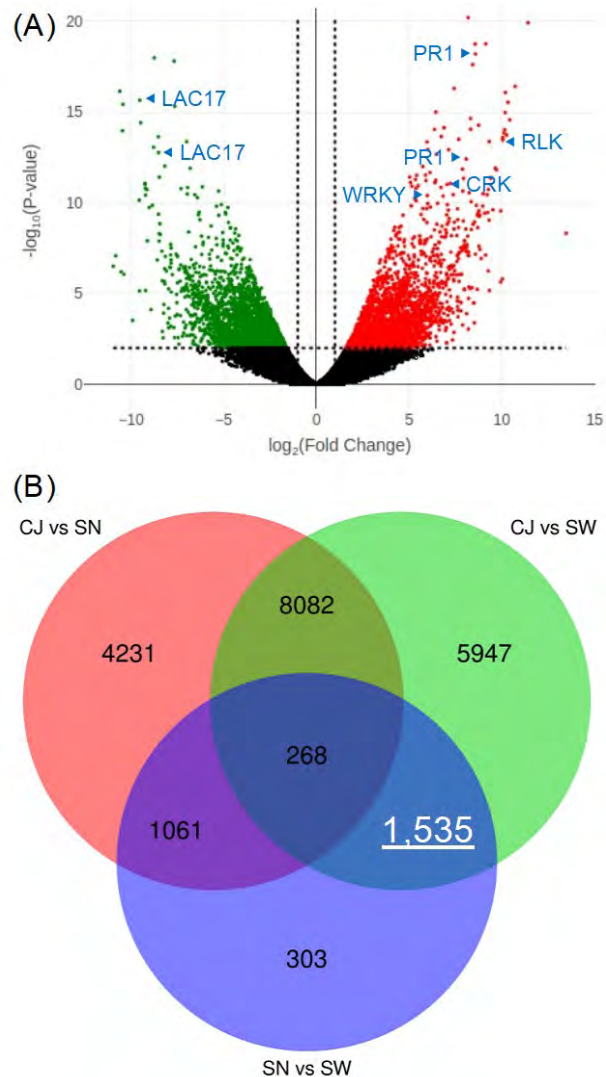


Figure 2: An example for the identification of significantly up- and down-regulated DEGs in the comparison of SN vs. SW (A). Several characteristic DEGs listed in Table 2 are indicated by arrows. Of DEGs, those that were common to CJ vs. SW and SN vs. SW but not present in CJ vs. SN (underlined) were determined as SW-specific DEGs (B).

Additionally, several genes with oxidoreductase activity, such as cytochrome P450 (Cyt_P450) and 2-oxoglutarate and Fe(II)-dependent oxygenase (2OG-FeII), and WRKY transcription factors were listed in the up-regulated DEGs (Table 2).

Table 2: Annotations of defense response-related DEGs listed in the top 15 up-regulated DEGs in the necrotic hybrid seedlings referencing the ‘Somei-yoshino’ CYE_SPA and CYE_SPE genome.

Rank	Gene name	Annotation
<i>CYE_SPA genome</i>		
1:	CYE_r3.1SPA0_g005250	beta-1,3-glucanase 3
2:	CYE_r3.1SPA8_g020410	PR1
3:	CYE_r3.1SPA7_g003390	beta-1,3-glucanase 3
4:	CYE_r3.1SPA7_g003750	beta-1,3-glucanase 3
5:	CYE_r3.1SPA8_g001610	2OG-FeII
6:	CYE_r3.1SPA0_g005180	beta-1,3-glucanase 3
7:	CYE_r3.1SPA0_g139900	beta-1,3-glucanase 3
8:	CYE_r3.1SPA1_g031580	Cupredoxin family protein
9:	CYE_r3.1SPA8_g018610	Plant basic secretory protein
10:	CYE_r3.1SPA1_g027320	WRKY 40
11:	CYE_r3.1SPA7_g003330	beta-1,3-glucanase 3
12:	CYE_r3.1SPA7_g003250	thaumatin like protein (PR5)
13:	CYE_r3.1SPA3_g032850	matrix metalloproteinase
14:	CYE_r3.1SPA4_g001700	CRK
15:	CYE_r3.1SPA0_g084460	Cyt_P450
<i>CYE_SPE genome</i>		
1:	CYE_r3.1SPE4_g004570	RLK
2:	CYE_r3.1SPE0_g157490	Cyt_P450
3:	CYE_r3.1SPE8_g024490	PR1
4:	CYE_r3.1SPE4_g002320	CRK
5:	CYE_r3.1SPE2_g029880	WRKY 70
6:	CYE_r3.1SPE4_g014200	RLK
7:	CYE_r3.1SPE1_g041880	AGD2-like protein 1
8:	CYE_r3.1SPE8_g001690	2OG-FeII
9:	CYE_r3.1SPE1_g036160	Cupredoxin family protein
10:	CYE_r3.1SPE4_g009430	Spo11/DNA topoisomerase VI
11:	CYE_r3.1SPE2_g001950	RLK
12:	CYE_r3.1SPE4_g003590	transcriptional corepressor leunig
13:	CYE_r3.1SPE3_g009100	Coatomer, beta' subunit
14:	CYE_r3.1SPE7_g005730	2OG-FeII
15:	CYE_r3.1SPE0_g133290	Bet_v1-like protein (PR10)

3. Enrichment analysis

From the results of goseq, we determined that 8, 18, and 2 GO terms belonging to biological process (BP), cellular component (CC), and molecular function (MF), respectively, were significantly enriched in the up-regulated DEGs (Fig. 3A). Of the BP terms, “abscisic acid-activated signaling pathway” was the most significantly enriched GO term with a 3.96×10^{-30} FDR level. In addition, “defense response” was identified as the 2nd significantly enriched term in the up-regulated DEG list. As shown in the annotation of up-regulated DEGs, the significant enrichment of several GO

terms, such as “oxidation-reduction process” in BP and “oxidoreductase activity” and “protein kinase activity” in MF was also detected (Fig. 3A).

On the other hand, 13, 14, and 7 GO terms for BP, MF, and CC were significantly enriched in down-regulated DEGs, respectively (Fig. 3B). The photosynthesis-related GO terms, such as “photosynthesis, light harvesting” in BP and “photosystem I reaction center” in CC, were detected as significantly enriched GO terms (Fig. 3B). The “oxidation-reduction process” was also observed in the significant GO enrichment of down-regulated DEGs.

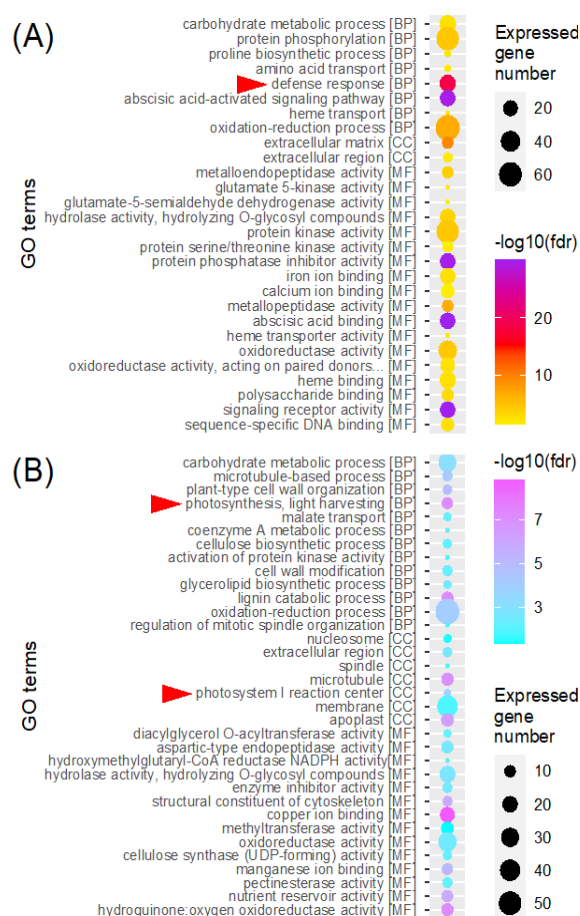


Figure 3: Significantly enriched GO terms detected by goseq in the up- (A) and down-regulated DEGs (B). Significant enrichment of biological process (BP), cellular component (CC), and molecular function (MF) GO terms was represented with a q value (FDR) and the number of DEGs (dot size). The GO term “defense response” and photosynthesis related terms are indicated by red arrows.

Discussion

Through the comprehensive gene expression analysis of hybrid seedlings of ‘Somei-yoshino’ and *C. itosakura*, various genes associated with plant defense response were found in the up-regulated DEG list specified in the growth failure seedlings. In particular, PR1 homologous to *Arabidopsis* basic PR1-like genes was detected as a major up-regulated DEG of SW seedlings in both reference genome analyses. PR1 is expressed by pathogen infection and associated with plant defense (van Loon, L.C. *et al.*, 2006). Another group of detected PR protein, PR5, also referred to as TLP, and Bet v1 family gene, a member of PR10, are also associated with plant defense (van Loon, L.C. *et al.*, 2006).

The RLK gene CYE_r3.1SPE4_g004570 was identified as the most up-regulated DEG in the ‘Somei-yoshino’ SPE genome. RLK which promotes the participation of other defense-related genes triggered an autoimmune response in *Arabidopsis* and rice (Bomblies, K. *et al.*, 2007; Yamamoto, E. *et al.*, 2010). Although the paralog gene of CYE_r3.1SPE4_g004570 did not become DEG in CYE_SPA (data not shown), the RLK gene remains the most likely candidate for triggering hybrid incompatibility in flowering cherries. Meanwhile, other RLKs, CRK, were also found in SW up-regulated DEGs. These genes are also associated with pathogen resistance and cell death in *Arabidopsis* (Yadeta, K.A. *et al.*, 2017). High expressions of genes associated with oxidation-reduction, such as Cyt_P450 and 2OG-FeII, were also found in the SW seedlings. These genes are involved in the detoxification of peroxides and are highly expressed during the immune response in plants. The DEG list included several transcription factors called WRKYs. The WRKYs regulate various biological processes, several of which are highly expressed upon pathogen infection, and up- or down-regulate the expression of themselves, other transcription factors, and downstream defense-related genes (Chen, X. *et al.*, 2019).

The high expression of these series of defense-related genes without pathogen inoculation strongly indicates that an autoimmune response also occurs in the hybrid seedlings of flowering cherry. The excess of these defense responses probably resulted in the reduction of other physiological

activities (Tian, D. *et al.*, 2003). Various gene pathways were significantly suppressed in the SW seedlings. Photosynthesis-related GO terms also showed significant enrichment in the down-regulated DEGs of SW seedlings. These results may be related to growth arrest, but the detailed mechanism is still unknown. Additional detail sampling design for the seedling parts, such as the shoot apex, hypocotyls, and leaves, measurement of the concentrations plant hormones, acting as signaling pathways through defense response, peroxide accumulation, and morphological observation of cell division in the shoot apex will be required for elucidating the growth failure mechanism.

The causative gene of seedling necrosis may still need to be discussed. On the other hand, the up-regulation of defense-related gene expression probably commonly leads to hybrid weakness and hybrid breakdown, which is a phenomenon observed not only in herbal plants but also in woody species.

Acknowledgment

This work was supported by the JSPS KAKENHI, Grant-in-Aid for Early-Career Scientists (JP18K14489).

Reference

- Bomblies, K., Lempe, J., Eppe, P., Warthmann, N., Lanz, C., *et al.* (2007) Autoimmune response as a mechanism for a Dobzhansky-Muller-type incompatibility syndrome in plants. *PLoS Biol* 5: e236.
- Chen, S., Zhou, Y., Chen, Y., Gu, J. (2018) fastp: an ultra-fast all-in-one FASTQ preprocessor. *Bioinformatics* 34: i884-i890.
- Chen, X., Li, C., Wang, H., Guo, Z. (2019) WRKY transcription factors: evolution, binding, and action. *Phytopathol Res* 1: 13.
- Kato, S., Matsumoto, A., Yoshimura, K., Katsuki, T., Iwamoto, K., *et al.* (2014) Origins of Japanese flowering cherry (*Prunus* subgenus *Cerasus*) cultivars revealed using nuclear SSR markers. *Tree Genet Genome* 10: 477-487.
- Langmead, B., Salzberg, S.L. (2012) Fast gapped-read alignment with Bowtie 2. *Nat Methods* 9: 357-359.
- Liao, Y., Smyth, G.K., Shi, W. (2014) featureCounts: an efficient general purpose

- program for assigning sequence reads to genomic features. *Bioinformatics* 30: 923-930.
- Ohba, H., Kawasaki, T., Tanaka, H., Kihara, H. (2007) Flowering cherries of Japan, New edn, Yama-kei Publishers, Tokyo (in Japanese).
- Shirasawa, K., Esumi, T., Hirakawa, H., Tanaka, H., Itai, A., *et al.* (2019) Phased genome sequence of an interspecific hybrid flowering cherry, ‘Somei-Yoshino’ (*Cerasus* × *yedoensis*). *DNA Res* 26: 379-389.
- Su, W., Sun, J., Shimizu, K., Kadota, K. (2019) TCC-GUI: a Shiny-based application for differential expression analysis of RNA-seq count data. *BMC Res Notes* 12: 133.
- Tian, D., Traw, M.B., Chen, J.Q., Kreitman, M., Bergelson, J. (2003) Fitness costs of R-gene-mediated resistance in *Arabidopsis thaliana*. *Nature* 423: 74-77.
- Tsuruta, M., Mukai, Y. (2015) Hybrid seedling inviability locus (*Hls1*) mapped on linkage group 4 of the Japanese flowering cherry, *Cerasus* × *yedoensis* ‘Somei-yoshino’. *Tree Genet Genome* 11: 88.
- van Loon, L.C., Rep, M., Pieterse, C.M. (2006) Significance of inducible defense-related proteins in infected plants. *Annu Rev Phytopathol* 44: 135-162.
- Wan, W.L., Kim, S.T., Castel, B., Charoennit, N., Chae, E. (2021) Genetics of autoimmunity in plants: an evolutionary genetics perspective. *New Phytol* 229: 1215-1233.
- Yadeta, K.A., Elmore, J.M., Creer, A.Y., Feng, B., Franco, J.Y., *et al.* (2017) A cysteine-rich protein kinase associates with a membrane immune complex and the cysteine residues are required for cell death. *Plant Physiol* 173: 771-787.
- Yamamoto, E., Takashi, T., Morinaka, Y., Lin, S., Wu, J., *et al.* (2010) Gain of deleterious function causes an autoimmune response and Bateson-Dobzhansky-Muller incompatibility in rice. *Mol Genet Genomics* 283: 305-315.
- Young, M.D., Wakefield, M.J., Smyth, G.K., Oshlack, A. (2010) Gene ontology analysis for RNA-seq: accounting for selection bias. *Genome Biol* 11: R14.

**INTERNATIONAL SYMPOSIUM ON A RECENT PROGRESS
IN FOREST ECOLOGY AND MANAGEMENT
2021**

**SESSION 3
AGROFORESTRY OF TROPICAL REGION**

**Wednesday, 10th November 2021
16:25 - 17:10**

ORGANIZER:

THE UNITED GRADUATE SCHOOL OF AGRICULTURAL SCIENCE, GIFU UNIVERSITY

Agroforestry System as the Best Vegetation Management to Face Forest Degradation

Maria Theresia Sri Budiastuti^{1*}, Djoko Purnomo¹,
Desy Setyaningrum²

¹ Department of Agrotechnology, Faculty of Agriculture, Universitas Sebelas Maret, Indonesia

² Doctoral Program of Agriculture Science, Faculty of Agriculture, Universitas Sebelas Maret, Indonesia

*Corresponding Author: mariatheresia@staff.uns.ac.id

SUMMARY

Indonesia, as a country with a tropical climate, has a forest area of 94.1 million ha, and in 2019 deforestation reached 3,500,637.7 ha as a result of large-scale illegal logging for many activities. In addition, the area of primary forest has decreased over the last 15 years and is positively correlated with land degradation, carbon sequestration, and plant production. Low carbon sequestration capacity triggers global warming, which impacts the average temperature increase in Indonesia by 0.7°C from 1981 to 2020. Therefore, the restoration of forest functions to support the stability of ecosystems is the first step in forest management planning. Forest management can reduce greenhouse gas emissions, preserve and restore ecosystems that function to support ecological responses. It is proven that carbon emissions from deforestation are the second largest after the energy sector from anthropogenic activities, which is 12-15%. Various efforts to restore the function of the forest are carried out by empowering suboptimal lands as land for agricultural and forest crop production. The suboptimal land area is very high (16,025,000 ha), however, the potential land that can be utilized for agriculture is only limited to 9,358,643 hectares or about 58.4%. One of the efforts to empower suboptimal land is cultivating tree-based plants, known as the agroforestry system. Such systems can maintain water and soil stability, support carbon sequestration, and create microclimate conditions (reduce temperature and maintain soil moisture). In addition, the absorption of soil carbon in the agroforestry system (11.29 t C ha⁻¹ year⁻¹) was higher than in the monoculture system (4.38 t C ha⁻¹ year⁻¹). Agroforestry systems provide options to reduce the impact of global warming, increase crop yields, and support ecosystem stability. Thus, a well-managed and sustainable Agroforestry system is the best vegetation management to overcome the impact of degraded forests.

Keywords: Agroforestry; Forest Degradation; Tree; Vegetation Management

Introduction

Indonesia has a tropical climate and has a forest area of ninth after Australia and Argentina. Indonesia's forests experienced a relatively rapid decline in the area from 2014-2019. In 2019, deforestation reached 3,500,637.7 ha (BPS, 2019). This reflects that the use of forests for various purposes (industry, plantations, agriculture) is experiencing a relatively fast rate and often without considering the function of the forest as a provider of ecosystem services. In addition, several studies have shown that deforestation causes an increase in global warming (Luhass *et al.*, 2021; Reppin *et al.*, 2020; Widianingsih *et al.*, 2019).

The decrease in forest area has a very significant positive correlation with carbon

sequestration capacity (Siarudin *et al.*, 2021). Carbon dioxide emissions in Indonesia increased by 4.7% in 2017 which amounted to 487 million tons (MtCO₂) (Ma *et al.*, 2020). CO₂ emissions triggered an increase in the average temperature of Indonesia's mainland by 0.7°C from 1981 to 2020 (Alfiandy *et al.*, 2020), and increased evaporation from the soil surface (Tahmasebi *et al.*, 2020). CO₂ and temperature are the main factors that affect plant growth, development, and function. Changes in these two factors will affect the productivity, structure, and composition of the ecosystem (Lee *et al.*, 2021; Mosavi *et al.*, 2020). An increase in temperature can cause damage to soil nutrients, decrease microbial activity in the soil, increase the rate of degradation of organic matter in the soil, which ultimately causes soil erosion (Arévalo-

Gardini *et al.*, 2020; Sharma & Anandhi, 2021).

Appropriate management efforts are needed to deal with forest deforestation, namely through well-organized vegetation management. It provides several functions, namely water, and soil conservation, mitigating the impact of global warming and crop production. Vegetation is critical in compensating for the negative effects of deforestation. Therefore, concrete steps are based on the role of trees in rainwater movement (soil and water conservation function), carbon sinks (global warming impact mitigation function), and microclimate support for successful crop production (plant production function).

The integration of trees and crops is an option in vegetation management that benefits the ecosystem. Efforts can be made to reduce the impact of deforestation by increasing carbon sequestration. The potential for increased carbon sequestration can occur in agricultural land and forests through tree-based agricultural cultivation technology (Legout *et al.*, 2020; Trebilco *et al.*, 2013). The agroforestry system provides an option to reduce the impact of deforestation because it is considered capable of increasing carbon sequestration in the soil. This article thoroughly reviews the role of trees in the agroforestry system as a form of management of the impact of deforestation.

1. *The role of agroforestry*

Deforestation causes land degradation, and the approach to solving this problem is an activity that considers the combination of environmental services and human well-being. Agroforestry is an important option to reverse the impacts of deforestation and associated ecosystem functions (Kurniatun Hairiah *et al.*, 2020; Noordwijk *et al.*, 2019). In particular, agroforestry plays an important ecological role, including land conservation (maintaining soil and water resources), carbon sinks, and supporting crop production.

The availability of suboptimal land in Indonesia is very high and reaches 16,025,000 hectares with the categories of critical (9,454,000 hectares) and very critical (4,553,000 hectares) (BPS, 2018). However, the potential of land that can be used for agriculture is only 58.4%, namely 91,904,643 hectares. The soil in suboptimal land has low quality, which is caused by several limiting factors such as sloping topography, low nutrients,

organic matter, low soil moisture content, too low or too high pH, and even accumulation of metal elements that are toxic to plants. (Keshavarz *et al.*, 2017). Suboptimal land characteristics are improved through the application of tree-based agriculture (Agroforestry).

1.1 *The role of agroforestry as a rainwater regulator (Soil and water conservation function)*

Conversion of forest to agriculture disrupts the ecological function of the forest in absorbing rainwater and preventing erosion. Forest conversion can impair the performance of hydrological systems associated with infiltration. Various efforts to restore the function of the forest are carried out by empowering sub-optimal lands as land for agricultural and forest crop production (Tschora & Cherubini, 2020). An agroforestry system supported by high tree diversity can maintain high infiltration rates and can have a positive impact on hydrological function through (1) green canopy cover at tree and understory level, (2) soil surface roughness, (3) litter in the soil surface, and (4) water absorption by trees and vegetation (Nöldeke *et al.*, 2021; Rothé *et al.*, 2019). Tree canopy cover > 80% qualifies as an “infiltration friendly” land use, due to higher rainfall but relatively low erosion rates (Suprayogo *et al.*, 2020). In agroforestry systems with a higher number of perennial crops have lower erosion rates than annual crops (Chofyan & Andriani, 2020).

Agroforestry has a function as land conservation so that it can be used to improve suboptimal land quality (van Noordwijk, 2021). Several studies show that agroforestry systems can be used to increase soil fertility because it is supported by an increase in the diversity of fungi and soil microorganisms. The diversity of fungi and soil microorganisms plays a role in improving the physical and chemical properties of the soil (Arévalo-Gardini *et al.*, 2020).

The most extensive suboptimal land in Indonesia is a peatland. Indonesia's peatlands contain 77% of the total tropical peat carbon stores. Poor peatland management can lead to degraded land, forest, and land fires. Land-use conversion of about 10 million ha of peatland results in annual emissions of 132-159 Mt C year⁻¹ from peat oxidation and will increase greenhouse gas emissions (Corradini *et al.*, 2020). Agroforestry is

one alternative that can be proposed for peat restoration activities. Research result (Binhar *et al.*, 2020) that peatlands and marginal lands can be used for the cultivation of lowland rice, corn, and soybeans with an agroforestry system. This system causes the diversity of land to increase so that the ecological conditions and land structure become better. Thus, agroforestry is beneficial in reducing water and wind erosion, increasing soil nutrition.

Agroforestry plays a role in soil and water conservation; this is supported by an increase in biodiversity. Such systems can contribute to biodiversity conservation and minimize homogenization (Marconi & Armengot, 2020). Agroforestry is considered a distinctive “land sharing” strategy as it supports biodiversity conservation and agricultural production (Betts *et al.*, 2017). Vegetation diversity in agroforestry systems increases beetle species (De Beenhouwer *et al.*, 2016), bird (Clough *et al.*, 2009) and natural enemies (Staton *et al.*, 2021). These variations may affect the potential for biodiversity conservation of different taxa.

Soil microbial community in agroforestry system is higher than monoculture system. Mycorrhizal diversity in agroforestry systems is very high because tree shade affects the efficiency of mycorrhizal bioinoculants, phosphate solvents and rhizobacteria (Shukla *et al.*, 2018). The agroforestry system increases the abundance of heterotrophic bacteria and fungi (Afolabi & Muoghalu, 2018). Agroforestry can also maintain microbial diversity important for soil health and productivity (Dobo *et al.*, 2018).

1.2 Role of agroforestry as carbon sequestration (Mitigation function of global warming)

Agroforestry systems are considered the most effective in carbon sequestration (Theresia & Budiastuti, 2020). Tree-based farming systems have the capacity to absorb carbon dioxide from the atmosphere above the ground, such as stems, branches, and leaves, and below ground, namely the root system, (Percival *et al.*, 2020; Santosa *et al.*, 2021) and can reduce greenhouse gas emissions (Lipper *et al.*, 2010). Soil carbon absorption in the agroforestry system was higher at 11.29 t C ha⁻¹ year⁻¹ than the monoculture system at 4.38 t C ha⁻¹ year⁻¹. Agroforestry systems with various trees and

vegetation have the highest carbon stocks of 108.9 Mg ha⁻¹ (Siarudin *et al.*, 2021). Carbon stocks are related to species density and diversity (Brancalion & Chazdon, 2017; Riwidiharso *et al.*, 2020).

1.3 The role of Agroforestry as a microclimate support (plant production function)

Agroforestry plays a role in maintaining microclimate conditions such as light, wind stability, temperature and humidity. This is caused by trees as climate support (Budiastuti *et al.*, 2020). High temperatures above 30°C cause the photosynthesis mechanism, leaves, and flowers to be damaged, affecting plant physiology and yields (Tschamtkke *et al.*, 2011). Tree-soil-plant interactions in agroforestry systems have a function in agricultural production. For example, a coffee plantation with the use of shade trees to support less than optimal environmental conditions (Sarmiento-Soler *et al.*, 2020). The role of agroforestry in coffee plantations can improve the microclimate, increase soil nutrients and diversify income and increase food security (Phondani *et al.*, 2020). The agroforestry system increases cocoa by 31% and this increase is due to a decrease in the environmental temperature in the system (Kaba, Out-Nyanteh, & Abunyewa, 2020).

2. The best vegetation management

Agroforestry is a sustainable land use approach that can combine three main roles in supporting agricultural activities (rainwater management: soil and water conservation function, carbon sink, microclimate support). Trees as a supporter of the agroforestry system and become part of forest management. Trees in agroforestry systems are assumed to provide ecosystem benefits as forests (Asante *et al.*, 2021) because it plays a role in providing ecosystem services and functions, and is able to create a microclimate that reduces temperature and heat stress, maintains soil moisture and produces nitrogen (Budiastuti *et al.*, 2018).

Tree root systems stabilize hillsides and riverbanks, reducing the risk of landslides (K. Hairiah *et al.*, 2021). Agroforestry will control the reactivation of landslides if the arrangement of trees and plants is based on morphological units formed from previous landslides (Purwaningsih *et al.*, 2020). The role of trees also supports the function of agroforestry to maintain biodiversity, namely

increasing the abundance and diversity of microorganisms and pollinator (Campera *et al.*, 2021). Trees support ecosystem biodiversity (Rosenstock *et al.*, 2019) and is a major component in the water, nutrient and carbon cycle (Van Den Berge *et al.*, 2021).

Conclusions

Agroforestry has three main functions, namely regulating rainwater (soil and water conservation), absorbing carbon (mitigating the impact of global warming), and supporting microclimate (plant production). These three functions are supported by vegetation. Agroforestry systems provide options to reduce the effects of global warming, increase crop yields, and support ecosystem stability. Thus, a well-managed and sustainable agroforestry system is the best vegetation management that can overcome the impact of deforestation.

Reference

- Afolabi, O. O., & Muoghalu, J. I. (2018). Effect of pesticides on microorganisms involved in litter decomposition in cacao plantation in Ile-Ife, Nigeria. *Agroforestry Systems*, 92(2), 511–524. <https://doi.org/10.1007/s10457-016-0032-y>
- Alfiandy, S., Permana, D. S., Nurjaman, A. W., Kurnia, W. G., Prastika, L., Panggabean, H., Rahman, M. S. D. P., Wulandari, S., Setiawan, H., & Hendrawan, A. (2020). Analisis Iklim Provinsi Sulawesi Tengah berdasarkan Data Pemantau Cuaca Otomatis BMKG. *Buletin GAW Bariri*, 1(1), 1–11.
- Arévalo-Gardini, E., Canto, M., Alegre, J., Arévalo-Hernández, C. O., Loli, O., Julca, A., & Baligar, V. (2020). Cacao agroforestry management systems effects on soil fungi diversity in the Peruvian Amazon. *Ecological Indicators*, 115(April), 106404. <https://doi.org/10.1016/j.ecolind.2020.106404>
- Asante, W. A., Ahoma, G., Gyampoh, B. A., Kyereh, B., & Asare, R. (2021). Upper canopy tree crown architecture and its implications for shade in cocoa agroforestry systems in the Western Region of Ghana. *Trees, Forests and People*, 5, 100100. <https://doi.org/10.1016/j.tfp.2021.100100>
- Betts, M. G., Wolf, C., Ripple, W. J., Phalan, B., Millers, K. A., Duarte, A., Butchart, S. H. M., & Levi, T. (2017). Global forest loss disproportionately erodes biodiversity in intact landscapes. *Nature*, 547(7664), 441–444. <https://doi.org/10.1038/nature23285>
- Binhar, Sugianto, & Zainabun. (2020). Evaluasi Tingkat Kesesuaian Lahan Gambut Sebagai Alternatif Pengembangan Tanaman Pangan di Kecamatan Kota Subulussalam. *Jurnal Ilmiah Mahasiswa Pertanian*, 5, 551–563.
- BPS. (2019). *Angka Deforestasi Indonesia*. Badan Pusat Statistik.
- Brancalion, P. H. S., & Chazdon, R. L. (2017). Beyond hectares : four principles to guide reforestation in the context of tropical forest and landscape restoration. *Restoration Ecology*, 1–6. <https://doi.org/10.1111/rec.12519>
- Budiasuti, S., Purnomo, D., Supriyono, Yunindanova, M. B., Mahardini, P. C. A., & Utami, R. R. (2018). Land management strategy for cocoa cultivation at home gardens. *IOP Conference Series: Earth and Environmental Science*, 200(1). <https://doi.org/10.1088/1755-1315/200/1/012005>
- Campera, M., Balestri, M., Manson, S., Hedger, K., Ahmad, N., Adinda, E., Nijman, V., Budiadi, B., Imron, M. A., & Nekaris, K. A. I. (2021). Shade trees and agrochemical use affect butterfly assemblages in coffee home gardens. *Agriculture, Ecosystems and Environment*, 319(November 2020), 107547. <https://doi.org/10.1016/j.agee.2021.107547>
- Chofyan, I., & Andriani, D. I. (2020). Soil erosion in agroforestry development in South Bandung Region, Indonesia. *Journal of Physics: Conference Series*, 1469(1). <https://doi.org/10.1088/1742-6596/1469/1/012122>
- Clough, Y., Dwi Putra, D., Pitopang, R., & Tschardtke, T. (2009). Local and landscape factors determine functional bird diversity in Indonesian cacao agroforestry. *Biological Conservation*, 142(5), 1032–1041. <https://doi.org/10.1016/j.biocon.2008.12.027>
- Corradini, E., Dreibrodt, S., Erkul, E., Groß, D., Lübke, H., Panning, D., Pickartz, N., Thorwart, M., Vött, A., Willershäuser, T., Wilken, D., Wunderlich, T., Zanon, M., & Rabbel, W. (2020). Understanding wetlands stratigraphy:

- Geophysics and soil parameters for investigating ancient basin development at lake duvensee. *Geosciences (Switzerland)*, 10(8), 1–35.
<https://doi.org/10.3390/geosciences10080314>
- De Beenhouwer, M., Geeraert, L., Mertens, J., Van Geel, M., Aerts, R., Vanderhaegen, K., & Honnay, O. (2016). Biodiversity and carbon storage co-benefits of coffee agroforestry across a gradient of increasing management intensity in the SW Ethiopian highlands. *Agriculture, Ecosystems and Environment*, 222, 193–199.
<https://doi.org/10.1016/j.agee.2016.02.017>
- Dobo, B., Asefa, F., & Asfaw, Z. (2018). Effect of tree-enstet-coffee based agro-forestry practices on arbuscular mycorrhizal fungi (AMF) species diversity and spore density. *Agroforestry Systems*, 92(2), 525–540.
<https://doi.org/10.1007/s10457-016-0042-9>
- Dollinger, J., & Jose, S. (2018). Agroforestry for soil health. *Agroforestry Systems*, 92(2), 213–219. <https://doi.org/10.1007/s10457-018-0223-9>
- Hairiah, K., Prayogo, C., Kurniawan, S., & Sudarto. (2021). Adaptation to and mitigation of climate change in the Bangsri Micro-watershed, East Java, Indonesia. *IOP Conference Series: Earth and Environmental Science*, 648(1).
<https://doi.org/10.1088/1755-1315/648/1/012128>
- Hairiah, Kurniatun, van Noordwijk, M., Sari, R. R., Saputra, D. D., Widiyanto, Suprayogo, D., Kurniawan, S., Prayogo, C., & Gusli, S. (2020). Soil carbon stocks in Indonesian (agro) forest transitions: Compaction conceals lower carbon concentrations in standard accounting. *Agriculture, Ecosystems and Environment*, 294(February), 106879.
<https://doi.org/10.1016/j.agee.2020.106879>
- Keshavarz, M., Maleksaeidi, H., & Karami, E. (2017). Livelihood vulnerability to drought: A case of rural Iran. *International Journal of Disaster Risk Reduction*, 21(December 2016), 223–230.
<https://doi.org/10.1016/j.ijdrr.2016.12.012>
- Lee, H. H., Kim, S. U., Han, H. R., Hur, D. Y., Owens, V. N., Kumar, S., & Hong, C. O. (2021). Mitigation of global warming potential and greenhouse gas intensity in arable soil with green manure as source of nitrogen. *Environmental Pollution*, 288.
<https://doi.org/10.1016/j.envpol.2021.117724>
- Legout, A., Hansson, K., van der Heijden, G., Laclau, J. P., Mareschal, L., Nys, C., Nicolas, M., Saint-André, L., & Ranger, J. (2020). Chemical fertility of forest ecosystems. Part 2: Towards redefining the concept by untangling the role of the different components of biogeochemical cycling. *Forest Ecology and Management*, 461(September 2019), 117844.
<https://doi.org/10.1016/j.foreco.2019.117844>
- Luhás, J., Mikkilä, M., Kylkilähti, E., Miettinen, J., Malkamäki, A., Pätäri, S., Korhonen, J., Pekkanen, T. L., Tuppurä, A., Lähäntinen, K., Autio, M., Linnanen, L., Ollikainen, M., & Toppinen, A. (2021). Pathways to a forest-based bioeconomy in 2060 within policy targets on climate change mitigation and biodiversity protection. *Forest Policy and Economics*, 131(October 2020).
<https://doi.org/10.1016/j.forpol.2021.102551>
- Ma, Z., Chen, H. Y. H., Bork, E. W., Carlyle, C. N., & Chang, S. X. (2020). Carbon accumulation in agroforestry systems is affected by tree species diversity, age and regional climate: A global meta-analysis. *Global Ecology and Biogeography*, 29(10), 1817–1828.
<https://doi.org/10.1111/geb.13145>
- Marconi, L., & Armengot, L. (2020). Complex agroforestry systems against biotic homogenization: The case of plants in the herbaceous stratum of cocoa production systems. *Agriculture, Ecosystems and Environment*, 287(September 2019), 106664.
<https://doi.org/10.1016/j.agee.2019.106664>
- Mosavi, S. H., Soltani, S., & Khalilian, S. (2020). Coping with climate change in agriculture: Evidence from Hamadan-Bahar plain in Iran. *Agricultural Water Management*, 241(April), 106332.
<https://doi.org/10.1016/j.agwat.2020.106332>
- Nöldeke, B., Winter, E., Laumonier, Y., & Simamora, T. (2021). Simulating agroforestry adoption in rural Indonesia: The potential of trees on farms for livelihoods and environment. *Land*, 10(4).
<https://doi.org/10.3390/land10040385>
- Noordwijk, M. van, Coe, R., & Sinclair, F. L. (2019). *Sustainable development through trees on farms*: (Meine van). WORDS AGROFORESTRY.

- Percival, L. M. E., Bond, D. P. G., Rakociński, M., Marynowski, L., Hood, A. V. S., Adatte, T., Spangenberg, J. E., & Föllmi, K. B. (2020). Phosphorus-cycle disturbances during the Late Devonian anoxic events. *Global and Planetary Change*, 184.
<https://doi.org/10.1016/j.gloplacha.2019.103070>
- Phondani, P. C., Maikhuri, R. K., Rawat, L. S., & Negi, V. S. (2020). Assessing farmers' perception on criteria and indicators for sustainable management of indigenous agroforestry systems in Uttarakhand, India. *Environmental and Sustainability Indicators*, 5, 100018.
<https://doi.org/10.1016/j.indic.2019.100018>
- Purwaningsih, R., Sartohadi, J., & Anggri, M. (2020). Trees and crops arrangement in the agroforestry system based on slope units to control landslide reactivation on volcanic foot slopes in Java, Indonesia. *Land*, 9(9).
<https://doi.org/10.3390/LAND9090327>
- Reppin, S., Kuyah, S., de Neergaard, A., Oelofse, M., & Rosenstock, T. S. (2020). Contribution of agroforestry to climate change mitigation and livelihoods in Western Kenya. *Agroforestry Systems*, 94(1), 203–220.
<https://doi.org/10.1007/s10457-019-00383-7>
- Riwidiharso, E. D. Y., Santoso, S., Sudiana, E., Yani, E. D. Y., Nasution, E. K., Aprilliana, H., & Chasanah, T. (2020). *Insect diversity in various distances to forest edge in small nature reserve : A case study of Bantarbolang Nature Reserve , Central Java , Indonesia*. 21(10), 4821–4828.
<https://doi.org/10.13057/biodiv/d211048>
- Rosenstock, T. S., Wilkes, A., Jallo, C., Namoi, N., Bulusu, M., Suber, M., Mboi, D., Mulia, R., Simelton, E., Richards, M., Gurwick, N., & Wollenberg, E. (2019). Making trees count: Measurement and reporting of agroforestry in UNFCCC national communications of non-Annex I countries. *Agriculture, Ecosystems and Environment*, 284(April), 106569.
<https://doi.org/10.1016/j.agee.2019.106569>
- Rothé, M., Darnaudery, M., & Thuriès, L. (2019). Organic fertilizers, green manures and mixtures of the two revealed their potential as substitutes for inorganic fertilizers used in pineapple cropping. *Scientia Horticulturae*, 257(April), 108691.
<https://doi.org/10.1016/j.scienta.2019.108691>
- Santosa, E., Susila, A. D., Widodo, W. D., Nasrullah, N., Ruwaida, I. P., & Sari, R. (2021). Exploring fruit tree species as multifunctional greenery: A case of its distribution in Indonesian cities. *Sustainability (Switzerland)*, 13(14), 1–23. <https://doi.org/10.3390/su13147835>
- Sarmiento-Soler, A., Vaast, P., Hoffmann, M. P., Jassogne, L., van Asten, P., Graefe, S., & Rötter, R. P. (2020). Effect of cropping system, shade cover and altitudinal gradient on coffee yield components at Mt. Elgon, Uganda. *Agriculture, Ecosystems and Environment*, 295(March 2019), 106887.
<https://doi.org/10.1016/j.agee.2020.106887>
- Sharma, A., & Anandhi, A. (2021). Temperature based indicators to develop adaptive responses for crop production in Florida , USA. *Ecological Indicators*, 121, 107064.
<https://doi.org/10.1016/j.ecolind.2020.107064>
- Shukla, A., Kumar, A., Chaturvedi, O. P., Nagori, T., Kumar, N., & Gupta, A. (2018). Efficacy of rhizobial and phosphate-solubilizing bacteria and arbuscular mycorrhizal fungi to ameliorate shade response on six pulse crops. *Agroforestry Systems*, 92(2), 499–509.
<https://doi.org/10.1007/s10457-017-0070-0>
- Siarudin, M., Rahman, S. A., Artati, Y., Indrajaya, Y., Narulita, S., Ardha, M. J., & Larjavaara, M. (2021). Carbon sequestration potential of agroforestry systems in degraded landscapes in west Java, Indonesia. *Forests*, 12(6), 1–13.
<https://doi.org/10.3390/f12060714>
- Suprayogo, D., Azmi, E. N., Ariesta, D. A., Sutejo, Y. A., Hakim, A. L., Prayogo, C., & McNamara, N. P. (2020). Tree and plant interactions in the agroforestry system: Does the management of coffee intensification disrupt the soil hydrological system and pine growth? *IOP Conference Series: Earth and Environmental Science*, 449(1). <https://doi.org/10.1088/1755-1315/449/1/012045>
- Tahmasebi, T., Karami, E., & Keshavarz, M. (2020). Agricultural land use change under climate variability and change: Drivers and impacts. *Journal of Arid Environments*, 180(May), 104202.
<https://doi.org/10.1016/j.jaridenv.2020.104202>
- Theresia, M., & Budiastuti, S. (2020). *Agroforestri Sebagai Bentuk Mitigasi Perubahan Iklim terkait dengan pencemaran gas , khususnya CO*

- 2 , yang sulit terurai di atmosfer sehingga menghalangi pemantulan kembali sinar matahari yang mengakibatkan suhu bumi meningkat (Zhang et al ., 2018). pad. 2020, 23–29.
- Trebilco, R., Baum, J. K., Salomon, A. K., & Dulvy, N. K. (2013). Ecosystem ecology: Size-based constraints on the pyramids of life. In *Trends in Ecology and Evolution* (Vol. 28, Issue 7, pp. 423–431).
<https://doi.org/10.1016/j.tree.2013.03.008>
- Tschora, H., & Cherubini, F. (2020). Co-benefits and trade-offs of agroforestry for climate change mitigation and other sustainability goals in West Africa. *Global Ecology and Conservation*, 22.
<https://doi.org/10.1016/j.gecco.2020.e00919>
- Van Den Berge, S., Vangansbeke, P., Baeten, L., Vanhellemont, M., Vanneste, T., De Mil, T., Van den Bulcke, J., & Verheyen, K. (2021). Biomass Increment and Carbon Sequestration in Hedgerow-grown Trees. *Dendrochronologia*, 70(October 2020), 125894.
<https://doi.org/10.1016/j.dendro.2021.125894>
- van Noordwijk, M. (2021). Agroforestry-based ecosystem services: Reconciling values of humans and nature in sustainable development. *Land*, 10(7).
<https://doi.org/10.3390/land10070699>
- Widianingsih, N. N., David, W., Pouliot, M., & Theilade, I. (2019). Land use, income, and ethnic diversity in the margins of Hutan Harapan – A rainforest restoration concession in Jambi and South sumatra, Indonesia. *Land Use Policy*, 86(April), 268–279.
<https://doi.org/10.1016/j.landusepol.2019.05.006>
- Syukri, D., Thammawong, M., Naznin, A. H., Kuroki, S., Tsuta, M., Yoshida, M., Nakano, K. (2018) Identification of a freshness marker metabolite in stored soybean sprouts by comprehensive mass-spectrometric analysis of carbonyl compounds. *Food Chemistry*, 269:588-594.
- Tuan, Le Anh and Ken Hiramatsu (2020) Hydraulic Investigation of Piano Key Weir. *Review in Agricultural Science* 8: 310-322.
- UGSAS-GU (2020) Newsletter of the United Graduate School of Agricultural Science, Gifu University. http://www.ugsas.gifu-u.ac.jp/eng/news/file/UGSAS_GU_NEWSLETTER_9_2020%20_ENG.pdf, (accessed 05/31/2020).
- Zaki, Muhamad Khoiru, Keigo Noda, Kengo Ito, Komariah, Sumani, and Masateru Senge (2020) Adaptation to Extreme Hydrological Events by Javanese Society through Local Knowledge. *Sustainability* 12(24): 10373-10373.

Contribution of Forest Resources in Shifting Cultivation System to Livelihood Diversification in Mountain Villages of Northern Laos

Cahyo Wisnu Rubiyanto^{1*}, Isao Hirota²

¹ United Graduate School of Agricultural Science, Gifu University

² Faculty of Applied Biological Sciences, Gifu University

*Corresponding Author: wr.cahyo@yahoo.com

SUMMARY

Drastic globalization is being serious in Southeast Asia especially for local people who still depending on shifting cultivation in mountain villages. Shifting cultivation system provides a lot of activities, not only for subsistence but also commercial purposes including collection forest products such as Non-Timber Forest Products (NTFPs). In this study, to understand the contribution of forest resources to livelihood diversification, we focused on historical dynamics of livelihood transition show the pattern of household livelihood strategy in mountain villages of northern Laos. Field survey was carried out in Sone district, Houaphan province. We chose 4 villages in three different conditions of road accessibility; poor (Bong village), middle (Houay Su and Houay Sanguan village), and good (Houay Lao) accessibility, to know the influence of road development on agriculture and forest resources and to compare how different livelihood strategies local people chose. This study revealed that in first stage after village establishment local people were still maintained subsistence activities combined with NTFPs collection. NTFPs collection plays an important role for cash in poor and middle accessibility villages and it was considered to be selected as a livelihood activity to increase investment in local communities. The results showed that diversity of income positively correlated to total income and suggested that the pattern of livelihood diversification in this area tended to be progressive.

Keywords: *Road accessibility; Livelihood transition; Combination of livelihood activities; Cross-border trade; Southeast Asia*

Introduction

Local people in mountain villages of Southeast Asia who still depend on shifting cultivation are experiencing drastic changes from the impact of globalization. In northern Laos, our research focus, road development project was bigger than central or southern Laos, contributes 60% of national road development project. The construction of this road has rapidly reformed local communities into market-oriented activities (Hirota *et al*, 2014). As a result, diversification of forest products collection is the mainstay of local people as income-generating livelihoods.

Although infrastructure facilities such as roads have encouraged the formation of and change in livelihood structure from subsistence-based to market-oriented or farm to non-farm (Nguyen and Yokoyama, 2019), its diversification is questionable. In order to understand current situation of their livelihoods, it is better for us to elaborate the livelihoods that have been changing in the past twenty years and explore their contribution to livelihood diversification (Rubiyanto and Hirota, 2021). To

explain this, we have to look at their situation from two aspects, the historical aspect and the economic aspect. The historical aspect can understand the changing livelihood transition, while the economic aspect help us to understand the contribution of their livelihood to livelihood diversification. From this study, we aim to explored the livelihood activities and its history from the first stage before local people are allocated near the main road, and investigate the factors of livelihood diversification in mountainous villages of Northern Laos.

Methods

Study site

We chose Sone district in Houphan province, northern Laos as study site because there was big road construction. Sone is also one of the most forested district which enclosed by a conservation area. Four sample villages were selected in this study based on their road accessibility such as Bong village (poor accessibility), Houay Su and Houay Sanguan village (middle accessibility), and Houay Lao village (good accessibility). Besides road accessibility, we also used other criteria including the

same ethnic groups and similar livelihood activities to know the influence of road development on agriculture and forest resources and to compare how different livelihood strategies local people chose (see Table 1). The four villages were also established in the early 2000s. The data collection took place at two points in time, specifically in April-June 2018, and January to March 2019.

Table 1. Characteristics of villages survey

Village Name	Ethnic Group	No. of Household Interviewed	Main Livelihood	Accessibility
Bong	Hmong	32	Upland rice, livestock raising, NTFPs collection	Poor
Houay Su	Hmong	38	Upland rice, maize cultivation livestock raising, NTFPs collection	Middle
Houay Sanguan	Hmong	35	Upland rice, livestock raising, NTFPs collection	Middle
Houay Lao	Hmong	20	Upland rice, maize cultivation, livestock raising, NTFPs collection	Good

Data collection and analysis

A total 125 semi-structured household interview were used to collect data of basic information of household and their characteristics including explore their history of land use and livelihoods change. We identified their livelihood activities that can generate income and can be followed by an interview about past activities; upland rice cultivation, paddy rice cultivation, cultivation of maize, cultivation of other cash crops, red mushroom collection, and other NTFPs collection. We ask starting and ending year of each livelihood activity, and accumulate the household number to village level. The percentage of the number of household in each livelihood activity to the number of total sample households in each village in each year was calculated to know the trend of livelihood transition in village level along road improvement after establishment of villages (See table 2).

We asked the sources of household income and the amount of income which each household obtained within one year from each survey period. Then, we calculated the income sources diversity by using Simpson index and we explored the relationship between its diversity and total income. Income diversity and total income were selected as dependent variables, and we carried out multiple linear regression to identify direction of livelihood strategy of each household. In this study we selected 13 variables into the analysis as independent variables to

represent basic household condition, subsistence and economic livelihood activities.

Results and Discussion

Change of rice cultivation

The area of upland rice cultivation gradually decreased from establishment of village to recent year in all villages, as 84 % of the households in Bong village, 71 % of the households in Houay Sanguan villages and 95 % of the households in Houay Lao village reported a decrease compared to past. Surprisingly, this decrease in villages with poorer accessibility occurred with an increase in the expansion of paddy rice, while in village with better access, the households have still maintained upland rice without paddy rice. Shifting from upland rice to paddy rice can be accomplished from richer households because they were able to buy and reclaim new paddy field. Ducourtieux and Castella (2006) revealed that households who shift to paddy field from upland field, they could become to allocate their labor for other activities such as NTFPs collection, cultivation of cash crops or raising livestock.

Change of cash crop cultivation

The ratio of household with maize increased until the year of road pavement in all villages, but showed decreased after the year of road pavement, except in Houay Lao village. In Houay Lao village, the ratio increased and continue to cultivate maize due to the low price fluctuation and located in good access.

Ratio of household with other cash crops increased after the pavement of road. Local people started to cultivated other cash crops as choices of income diversification. The introduction of cash crops in this study was observed from aspects of environmental degradation, increasing influence from global market and influence from outsider such as local government and NGO. Coffee was reported as a crop which highly contribute to area of other cash crop land, where newly introduced and get supported from international organization, especially in Houay Su and Houay Lao village. Other cash crops were also cultivated because some of species became to decrease during around 15 years and partly disappeared already several years before the survey. As a results, the land for “new cash crops” in this area were established.

Table 2. Changes of main livelihood activities in study area

Year	Improvement of infrastructure and its impacts	Rice cultivation in upland and paddy field	Cultivation of cash crops	Collection of forest products
- 2000	Poor main road access	Upland rice cultivation as main livelihood	Opium was main income source	N/A
2001- 2010	Bong villages established in 2001, and other villages established in 2003. Road opened for walking and opening access to Vietnamese market (2002) Upgrade main road for motor bike (2002) Upgrade main road for car and truck (2004) Market access to China (2010)	Start of reclamation for paddy field in Bong and Houay Sanguan villages (2003) Start of reclamation for paddy field in Houay Su village (2005)	Introduction of maize in Bong village where the most frontier village in Sone district adjacent to Vietnam border. (2003) Introduction of maize in Houay Lao village (2005) in Houay Su village (2007)	Start of commercial collection of NTFPs in all villages, especially for <i>Mak Sam Sip and On Ling</i> (2003) Start of commercial collection of <i>Mak Naeng</i> and <i>Mak Lok Lek</i> (2005) Start of commercial collection of red mushrooms in Houay Su village through Chinese merchant (2010)
2011-	Introduction of electricity in Houay Sanguan village (2011), Houay Lao village (2014), Houay Su village (2016), Bong village (2017). Pavement of main road from Vietnam to center district (2013-2017), Opening access to local market in Sone district (2013).		Introduction of maize in Houay Sanguan village (2012) Introduction of coffee in Houay Su and Houay Lao villages. First cultivation of <i>Mak naeng</i> and <i>Mak Lok Lek</i> (2016) Introduction of cassava by Vietnamese merchant in Bong village (2018).	Start of commercial collection of red mushrooms in Bong, Houay Sanguan and Houay Lao villages (2015)

Note: Year of first cultivation of pineapple in Houay Sanguan village is unclear.

Change of forest products collection and their contribution to livelihood diversity

The ratio of household with NTFPs increased from the village establishment. The most important NTFPs were *Mak Sam Sip* and *On Ling* in the beginning of village establishment followed by *Mak Naeng* and *Lok Lek*. These products were substantial part of local or cross-border trade. The ratio of household with red mushroom drastically increased after the year of road pavement except in Houay Su villages because one household had relatives with Chinese merchants and the influence expanded to other villagers. It is reported that red

mushroom was important exportation products to bring the highest value among all NTFPs in cross-border trade of China (Phounviosuk *et al*, 2013) This study showed that commercialization of NTFPs, especially for new NTFPs such red mushrooms, related to road accessibility to village, and road development brought drastic change of local livelihood activities in forest.

The relationship between income diversity and total income, which dominate with forest resources, showed positive relationship. Regression results showed that upland and paddy rice were not significantly related to income diversity in all villages.

Maize had contributed to income diversity and total income for household in village with poorer accessibility. Other cash crops showed positive effect on income diversity in Houay Lao village, this indicates that cash crop can be an important strategy for income diversity. In addition to diversifying income, it is also important for household survival in overcoming shocks. This study highlighted that NTFPs contribute both positively and negatively to income diversity. However, if the households much more collect red mushrooms, it showed much less income diversity. Although red mushrooms were highly contributed to total income, this study suggests keeping maintain other NTFPs is needed to diversify their income.

Conclusion

This study explored the history of livelihood transition and analysis household strategy to livelihood diversification. This study revealed that in the beginning of village establishment local people were still maintained subsistence activities combined with NTFPs collection in shifting cultivation systems. NTFPs collection were considered to play an important role for cash poorer accessibility villages such in Bong, Houay Su, and Houay Sanguan village and it was considered to be selected as a livelihood activity to increase investment in local communities. The results showed that diversity of income positively correlated to total income and suggested that the pattern of livelihood diversification in this area tended to be progressive.

Acknowledgment

We thank to the all staff of Department of Agricultural and Forestry Office in Sone district and all villagers for the cooperation.

References

- Ducourtieux, O and Castella, J. 2006. Land reforms and impact on land use in the uplands of Vietnam and Laos: Environmental protection of poverty alleviation? In: *Colloque international Les frontières de la question foncière – At the frontier of land issues*, Montpellier.
- Hirota, I., Koyama, T and Ingray, P. 2014. Mountainous livelihood in northern Laos: Historical transition and current situation of swidden village. In: *Integrated Studies of Social and Natural Environment – Advances in Asian human-environmental research* (S. Yokoyama *et al.*, eds.). pp. 39-59. Springer. Tokyo.
- Ngoc, N and Yokoyama, S. 2019. Driving force for livelihood structure changes in Vietnam's northwestern mountainous region: A case study on Yen Chau district, Son La province. *Tropics*, 27:81-97.
- Phounvisouk, L., Zuo, T and Chee Kiat N. 2013. Non-timber forest products marketing: Trading network of trader and market chain in Luang Namtha province, Lao PDR. *IOSR Journal of Humanities and Social Science (IOSR-JHSS)*, 18: 48-57.
- Rubiyanto, C.W. and Hirota, I. 2021. A review on livelihood diversification: Dynamics, measurement, and case studies in Montane Mainland Southeast Asia. *Reviews in Agricultural Science*, 9:128-1

Agroforestry Practice in Volcano Prone Area: Findings from Mount Merapi Indonesia

Zuhud Rozaki ^{1*}, Nur Rahmawati ¹, Oki Wijaya ¹,
Atikah Fajriyah Mubarak ¹, Masateru Senge ¹, Mohd Fauzi Kamarudin ²

¹ Department of Agribusiness, Universitas Muhammadiyah Yogyakarta

² Universiti Teknikal Malaysia Melaka

*Corresponding Author: zaki@umy.ac.id

SUMMARY

Mount Merapi is one of the most active volcano in Indonesia. Despite the risk and hazard, people still staying in this volcano, many of them are working as farmers. Agroforestry is the agriculture system that being practiced as economic contributor and also become volcano disaster mitigation strategies. The presentation talk about agroforestry practices and challenges in Mount Merapi risk and hazard prone area of Indonesia. Agroforestry has been practiced by farmers in Mt. Merapi risk and hazard prone area from older generation. Each area in Mount Merapi has different type of agroforestry such as agrisilviculture, silvopasture, and agrosilvopasture. In the village of Glagaharjo, Yogyakarta, this system has been used for land restoration or conservation. 139 agroforestry adopters were chosen from 269 respondents that have been randomly interviewed from four different areas around Mount Merapi. Statistical descriptive method using values of mean and percentage were used. Additionally, multinomial Logistic regression was utilized to understand the model. The findings of the study shows that the trend of agroforestry is increasing, especially in Glagaharjo, after the 2010 eruption. Agroforestry system are also found to be practiced for mitigation strategies in facing Mount Merapi hazards and risk, especially for crop protection, and land and water conservation. Promoting agroforestry as one of the coping strategies in facing Mount Merapi hazards and risk is important as indicated by the results of this study. Additionally, the gender perspectives on agroforestry also will be presented.

Keywords: *Agroforestry; Mount Merap; Agriculture; Farmers' lives*

Introduction

As an active volcano, Merapi often erupts. This mountain is located in Central Java and covers three regencies (Boyolali, Klaten and Magelang) and the Special Region of Yogyakarta that covers one regency (Sleman). Hardiansyah *et al.* (2020) explain that Hhistorically, many people live in the area of Merapi because the land is fertile. Beside the perceived danger of being a disaster prone area, people who live in Mt. Merapi , enjoys the economic blessing such as fertile land as well as tourists visit. As stated by Dove (2008), people won't move from Merapi because of economic motivation and assets preservation (Nofrita & Krol, 2014).

At Merapi, most people are farmers, dairy farmers and sand miners, respectively (Paton *et al.*, 2013) and many felt that it is important for them to keep these livelihoods (Bakkour *et al.*, 2015). Antriandarti, Ferichani, and Ani (2013) explain that people in Merapi prone area need to develop their abilities, skills and knowledge in agriculture because

many of them are practicing AF. This system is a land use management system in which trees or shrubs are grown around or among crops or pastureland. This intentional combination of agriculture and forestry has varied benefits, including increased biodiversity and reduced erosion. Jaza Folefack, Ngo Njiki, and Darr (2019) suggest that using AF or mix cropping could increase yields without over utilizing the natural forest. This practice is suitable for mountainous area. Some areas in the world also use this method to cope and conserve the land that is prone to the volcano eruption disaster (Utami *et al.*, 2018). In Merapi, AF is practiced for the reason of restoring the land that was impacted by previous volcano eruptions (Fitria & Banowati, 2018).

Suryanto *et al.* (2011) explain that AF has a high level of diversity and as such, can increase land productivity. Lasco *et al.*, (2014) stated that that AF systems have emerged as having the potential to enhance the resilience of smallholders to disaster risk area. AF consists of several types and

each has its own characteristics regarding economic the contribution and benefits environmentally (Henley, 2008). In Merapi itself, this system has been practiced since a long time ago and continued to the current generation. This study aims to describe the AF practices and challenges in the Merapi prone area.

Research Method

1. Study area

This study was conducted in Merapi prone area which area coverage includes all different direction of Merapi, East (Jemowo Village, Tamansari Subdistrict, Boyolali Regency), North (Tlogolele Village, Selo Subdistrict, Boyolali Regency), West (Krinjing Village, Dukun Subdistrict, Magelang Regency) and South (Glgaharjo Village, Cangkringan Subdistrict, Sleman Regency) respectively. National Agency for Disaster Management (BNPB) classified the hazard level of Merapi based on the radius with the top of Merapi ring 1 (0-5 km), ring 2 (6-10 km), ring 3 (10-15 km) and ring 4 (16-20 km) (BNPB 2010). This study was taken in ring 2 because this area is the closest area to Merapi that AF can be practiced. Meanwhile ring 1 is owned by the government and is therefore prohibited for AF practice.

2. Sampling procedure and data collection

There are three main variables in this study: demographic, AF characteristics, and AF contributions. These variables or indicators were measured with Likert scale and descriptive statistics. These research instruments were analysed using the validity and reliability tests. Subsequently, in-depth interviews and observations were done to complement the findings.

3. Data Analysis

To present the results, descriptive method is used. Mean, frequency, and percentage were used to describe the variables, and also to know the different characteristics among four different areas. Variables with Likert scale have been tested through the validity and reliability tests. Additionally, logistic multinomial regression analysis was used to analyse quantitative data to identify the best set of quality independent variables (selected demographic and AF characteristics) predicting the dependant

variable (AF contribution).

Results and Discussion

1. Demographics of respondents

From a total 139 respondents, male farmers represent 80.58%. Regarding age, 79% of respondents are in the age range of 28-40 and 41-53 years old. 12.95% respondents are more than 64 years old, this age is categorized in non-productive age. As with other countries, Indonesia also is faced with the issue of ageing farmers since young people are not interested to agriculture.

According to the Dinis *et al.* (2019), education level is important for adoption of agriculture system including adopting AF system. The majority of Education of respondents' is elementary school, which is 53.96%. The education of four research areas are still dominated by elementary school graduated respondents. In Jemowo and Tlogolele, only 5.71% and 7.14 respectively has Diploma or University certificate.

In terms of farming experience, 25.9% of the respondents has 21-30 years' of experience. and 16.55% respondents have experiences more than 41 years. For AF experience, the distribution are quite similar with 0-10 years' of experience and farming experience is 17.99%. As for the family number of 2-4, 81% of the participants are in this category.

2. AF characteristics

a. AF type

There are three types of AF system that are being practiced by people in Merapi prone area which are: agrisilviculture, silvopasture, and agrosilvopasture. These three types are found to match the people's need, besides the available natural resource. Agrisilviculture combine food crops and trees (Etshekape *et al.*, 2018), silpasture combines tree and livestock (Santiago-Freijanes *et al.*, 2018), and agrosilvopasture combining food crops, trees and livestock (Russo, 1996). Each area of Merapi has their own type of AF. Jemowo (East) is dominated by silvopasture, followed by agrosilvopasture and agrisilviculture respectively. Meanwhile in Tlogolele (North), it is dominated by agrisilviculture, because this area is higher and the land is suitable for vegetables. Hence, applying agrisilviculture benefitted the farmers. Glagaharjo

has the same trend with Jemowo, which is dominated by silvopasture. This area is not suitable for vegetables like Tlogolele.

b. AF trends

AF easiness based on all areas are quite similar which is around 4 in mean (Figure 1). This system has already been practiced from respondents' parents of grandparents. Therefore, they feel that AF is not difficult to be practiced. The average of land size is less than half hectare. Jemowo has the lowest average of land size while Tlogolele has the highest average of land size.

The distance of AF plot to home varies and the average distance is less than 1 km. The Merapi mountainous area is challenging. Having farm land far from home is taking time and more efforts from the farmers. AF plots which are less than 1 km is a good distance. In term of land fertility, Tlogolele is most fertile as compared to others. This is proven by the vegetables planted there. The lowest land fertility is in Glagaharjo, an area more known as sand producer due to the much deposit of sands from eruption. Additionally, Glagaharjo is the most severe damage from Merapi previous eruptions. Therefore, this area has highest trend in the increasing of AF practice. Farmers plant trees to conserve the land after the volcano eruption swept away their land.

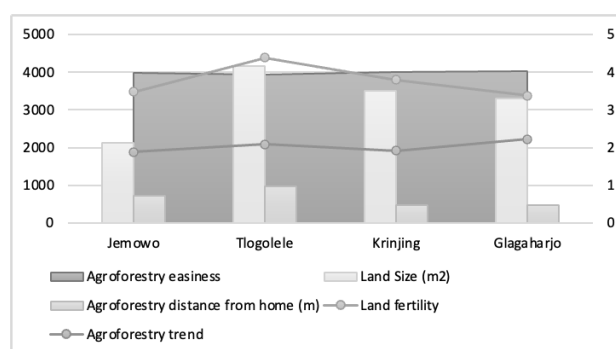


Figure 1. AF Characteristics

c. AF contribution

AF contribution in Merapi prone area varies which include as a food supplier, farming income, land restoration/conservation, water conservation and crop protection. AF adopters have their own reasons to adopt this system based on the farmers needs and environmental conditions. AF to supplies food for Jemowo with a mean of 3.66. This system can help to generate income is more felt in Krinjing with a mean of 3.56. Glagaharjo has highest mean on land restoration/ conservation caused by the

severe damage from previous volcano eruptions. Through AF, they can restore and conserve the Glagaharjo land. AF also leads to conservation of water. Krinjing shows the highest mean in water conservation. Additionally, trees from AF practices can protect the food crops with the highest mean in Glagaharjo. Kiyani *et al.* (2017) stated that, AF adoption can increase the income, improves soil fertility, and conserves water and soil.

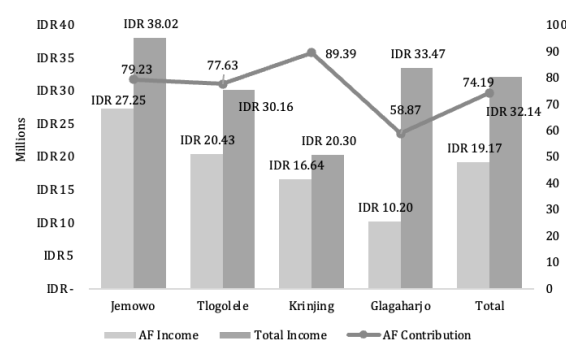


Figure 2. Average AF Income per Year in Millions

d. Family income from AF

Family income from AF consists of farming activities and livestock. Through Figure 2, it can be seen that the average income per year from AF practices are not much and ranges from IDR 10 million to IDR 28 million, or about IDR 0.8 million to 2.5 million per month. However, AF is like agriculture whereby the income is uncertain and will be worse when eruption happened such asin Glagaharjo. In this are, some land were burnt away by Merapi eruption. When this event happens,, all farmers are in high risk. This study too found that AF practices are the farmers' main livelihood. Additionally, some farmers are practicing AF as a second livelihood. The contribution of AF income varies from around 58% to 90%. Glagaharjo shows the lowest AF income contribution because the farmers are losing their farm land, and many prefer to work as a sand miner (Rahman *et al.* 2016).

Conclusions

AF practices in Merapi prone area have been started from the older generations. Therefore, the current generation felt that AF practices are not difficult as they are used to the system. There are three types of AF that people are practicing: agrisilviculture, silvopasture, and agrosilvopasture. This study shows that AF provide food or income

and can become one of the mitigation strategies for Merapi hazards. The AF system can become the method for land and water conservation, and most importantly as coping strategies for Merapi hazards and risks. Additionally, crops is used as protection from the Merapi hazards. Increasing this system practices in Merapi prone area will bring good benefits for all parties. The challenge of this system is education of AF for farmers in the Merapi prone area. This is important to increase this system practices and support the prevention actions against Merapi hazards in the future. Understanding the contribution of AF will lead more farmers to adopt this system.

Acknowledgment

The authors would like to deliver big gratitude to Universitas Muhammadiyah Yogyakarta for supporting this research through internal research grant.

Reference

- Antriandarti, E., Ferichani, M., & Ani, S. W. (2013). Sustainability of Post-Eruption Socio Economic Recovery for the Community on Mount Merapi Slope through Horticulture Agribusiness Region Development (Case Study in Boyolali District). *Procedia Environmental Sciences*, 17, 46–52.
<https://doi.org/10.1016/j.proenv.2013.02.010>
- Bakkour, D., Enjolras, G., Thouret, J. C., Kast, R., Mei, E. T. W., & Prihatminingtyas, B. (2015). The adaptive governance of natural disaster systems: Insights from the 2010 mount Merapi eruption in Indonesia. *International Journal of Disaster Risk Reduction*, 13, 167–188.
<https://doi.org/10.1016/j.ijdrr.2015.05.006>
- BNPB (Badan Nasional Penanggulangan Bencana). (2010). Peta zonasi bahaya (jarak radius 20 km) dari Puncak Gunungapi Merapi (Hazard Map of Merapi within 20 km radius). In *BNPB (Badan Nasional Penanggulangan Bencana)* (Issue November). <https://bnpb.go.id/>
- Dinis, I., Simões, O., Cruz, C., & Teodoro, A. (2019). Understanding the impact of intentions in the adoption of local development practices by rural tourism hosts in Portugal. *Journal of Rural Studies*, 72(November 2018), 92–103.
<https://doi.org/10.1016/j.jrurstud.2019.10.002>
- Etshekape, P. G., Atangana, A. R., & Khasa, D. P. (2018). Tree planting in urban and peri-urban of Kinshasa: Survey of factors facilitating agroforestry adoption. *Urban Forestry and Urban Greening*, 30, 12–23.
<https://doi.org/10.1016/j.ufug.2017.12.015>
- Fitria, A., & Banowati, E. (2018). Partisipasi Masyarakat terhadap Pelestarian Hutan Lereng Merapi Melalui Program Agroforestri Kopi di Desa Tlogolele Kecamatan Selo. *Edu Geography*, 6(3), 162–169.
- Hardiansyah, Muthohar, I., Balijepalli, C., & Priyanto, S. (2020). Analysing vulnerability of road network and guiding evacuees to sheltered areas: Case study of Mt Merapi, Central Java, Indonesia. *Case Studies on Transport Policy*, 8(4), 1329–1340.
<https://doi.org/10.1016/j.cstp.2020.09.004>
- Henley, D. (2008). Natural resource management: Historical lessons from Indonesia. *Human Ecology*, 36(2), 273–290.
<https://doi.org/10.1007/s10745-007-9137-2>
- Jaza Folefack, A. J., Ngo Njiki, M. G., & Darr, D. (2019). Safeguarding forests from smallholder oil palm expansion by more intensive production? The case of Ngwei forest (Cameroon). *Forest Policy and Economics*, 101(January), 45–61.
<https://doi.org/10.1016/j.forpol.2019.01.016>
- Kiyani, P., Andoh, J., Lee, Y., & Lee, D. K. (2017). Benefits and challenges of agroforestry adoption: a case of Musebeya sector, Nyamagabe District in southern province of Rwanda. *Forest Science and Technology*, 13(4), 174–180.
<https://doi.org/10.1080/21580103.2017.1392367>
- Lasco, R. D., Delfino, R. J. P., Catacutan, D. C., Simelton, E. S., & Wilson, D. M. (2014). Climate risk adaptation by smallholder farmers: The roles of trees and agroforestry. *Current Opinion in Environmental Sustainability*, 6(1), 83–88.
<https://doi.org/10.1016/j.cosust.2013.11.013>
- Nofrita, S., & Krol, B. G. C. M. B. (2014). The Livelihood Analysis in Merapi Prone Area After 2010 Eruption. *Indonesian Journal of Geography*, 46(2), 195.
<https://doi.org/10.22146/ijg.5790>
- Paton, D., Okada, N., & Sagala, S. (2013). Understanding Preparedness for Natural

- Hazards: Cross cultural comparison. *Journal of Integrated Disaster Risk Management*, 3(1), 18–35. <https://doi.org/10.5595/idrim.2013.0051>
- Russo, R. O. (1996). Agrosilvopastoral Systems: A Practical Approach Toward Sustainable Agriculture. *Journal of Sustainable Agriculture*, 7(4), 5–16.
https://doi.org/10.1300/J064v07n04_03
- Santiago-Freijanes, J. J., Pisanelli, A., Rois-Díaz, M., Aldrey-Vázquez, J. A., Rigueiro-Rodríguez, A., Pantera, A., Vityi, A., Lojka, B., Ferreiro-Domínguez, N., & Mosquera-Losada, M. R. (2018). Agroforestry development in Europe: Policy issues. *Land Use Policy*, 76(March), 144–156.
- <https://doi.org/10.1016/j.landusepol.2018.03.014>
- Suryanto, P., Hamzah, M. Z., Mohamed, A., & Alias, M. A. (2011). Silviculture Agroforestry Regime: Compatible Management in Southern Gunung Merapi National Park, Java, Indonesia. *International Journal of Biology*, 3(2).
<https://doi.org/10.5539/ijb.v3n2p115>
- Utami, S. N. H., Purwanto, B. H., & Marwasta, D. (2018). Land Management for Agriculture After The 2010 Merapi Eruption. *Planta Tropika: Journal of Agro Science*, 6(1), 32–38.
<https://doi.org/10.18196/pt.2018.078.32-38>

**INTERNATIONAL SYMPOSIUM ON A RECENT PROGRESS
IN FOREST ECOLOGY AND MANAGEMENT
2021**

KEYNOTE SPEECH 2

**Thursday, 11th November 2021
12:00 - 13:20**

ORGANIZER:

THE UNITED GRADUATE SCHOOL OF AGRICULTURAL SCIENCE, GIFU UNIVERSITY

Masting Impact on Canopy Structure and Photosynthesis in Beech Forests

Does Masting Perform as Gap?

Atsuhiko Iio

Agricultural faculty, Shizuoka University

Corresponding Author: iio.atsuhiro@shizuoka.ac.jp

SUMMARY

Small openings formed in forest canopy are called “gaps”. Gap formation promotes tree regeneration and growth, and thus is important event for determining species composition and productivity of future forest. In addition to normal gap formed by tree death, forest canopy provides various types of gap; e.g., transient openings formed by inter-species variations in leaf phenology (seasonal or phenological gap) and by insect outbreak. The variety of gap increases spatio-temporal heterogeneity of forest structure and environments (i.e., niche partitioning), which should play an important role for maintenance of species diversity and productivity in forest ecosystem. However, studies for transient gaps are generally limited compared with those for normal gap, probably because of difficulty for detecting such transient impact on forest structure and function.

Masting is synchronous intermittent production of large seed crops in perennial plant populations. In *Fagus crenata* forests, masting event generally occurs for 5 to 10 years intervals. This unique characteristic has attracted interest of plant ecologists, and its ecological meaning and physiological mechanisms have been investigated. On the other hand, several studies have shown that heavy masting reduces leaf amount of canopy layer, most likely because of the high resource demands of fruit production, implying that masting can perform as transient gap. However, there are no studies evaluating masting event from such aspect. I therefore examined masting-dependent changes in canopy structure at *Fagus crenata* forest, and evaluated its impact on within-canopy light environment and photosynthesis, with eco-physiological process-based model that can describe changes in canopy structure at small branch scale.

Masting markedly reduced leaf area of sunlit part of canopy due to decreases in individual leaf area and shoot length of fruit-bared branches. Heavy masting event decreased stand leaf area index (LAI) by half, but LAI returned to pre-masting level in following year. There were no clear differences in leaf photosynthetic capacity between mast and non-mast years. Model simulation revealed that heavy masting drastically changes productive structure of beech forest so that canopy photosynthesis decreased by half but photosynthesis in sub-canopy and understory layer increased two-three folds. When comparing masting with normal gap formation, canopy photosynthesis was 20 % higher for masting than for normal gap formation, because masting reduced leaf area only in the upper part of canopy, which relieved significant leaf self-shading within the canopy and thus improved light use efficiency of photosynthesis, especially in the middle and lower part of the canopy. Masting may contribute to extend longevity not only for understory vegetations but also for shaded branches in the lower part of the canopy, which largely differs with impact of normal gap.

Keywords: *Masting; Fagus crenata; Gap; Structural heterogeneity; Canopy photosynthesis*

Forest Tree Breeding in Hokkaido, Japan

So Hanaoka

Hokkaido Regional Breeding Office, Forest Tree Breeding Center, Forestry and Forest Products
Research Institute, Forest Research and Management Organization, National Research and
Development Agency

Corresponding Author: sohana@affrc.go.jp

SUMMARY

Forest tree breeding in Japan commenced in the 1950s with the selection and preservation of trees of Japanese main forestry species, such as *Cryptomeria japonica*, *Chamaecyparis obtusa*, *Pinus densiflora*, *Abies sachalinensis*, *Larix kaempferi*, *Picea glehnii*, etc. Progeny test sites of first generation-plus trees have been established, and the selection of second generation-plus trees commenced in the 2000s based on tree growth and wood traits. In Hokkaido Prefecture, the northern part of Japan, variety development of second generation-plus trees of *A. sachalinensis*, *L. kaempferi*, *Picea glehnii*, etc. are required. However, it is important to reveal the heritability of target traits as the first step of variety development. Therefore, I have studied the heritability of tree growth and the wood strength of those species. In this symposium, I will introduce the results of *Picea glehnii*. Also, reducing the time and labor for trait measurement (phenotyping) is also an issue to promote forest tree breeding. Recently, accurate and quantitative data have been required to combine genome and phenotype data. Therefore, technological development of phenotyping is also one of my works. I will introduce some of my results using UAV and AI.

Picea glehnii is an evergreen conifer species mainly distributed in Hokkaido. The forest area of *P. glehnii* is about 180,000 ha, which is the third largest in Hokkaido. In my study, tree height and DBH data from six progeny test sites were analyzed and higher heritability of tree height (0.16–0.77) and DBH (0.05–0.72) was revealed. Also, the heritability of wood strength was estimated from the stress wave velocity data at 26–28 years after planting, and its heritability was 0.38–0.96. From these results, it was concluded that the growth and wood strength of *P. glehnii* can be improved through breeding. Therefore, I selected 120 individuals of the second generation-plus trees based on breeding values (Best linear unbiased prediction (BLUP) values). These trees will be planted in seed orchards, and improved seedlings will be distributed in the future. Also, I studied the heritability of stem straightness, in other words, resistance to stem or basal bending due to snow damage. Environmental effect mainly explained those variations, and heritability was not necessarily high (0.025 and 0.012 for stem and basal bending, respectively). But some genetic effects were detected, and I selected some superior trees resistant to stem or basal bending.

Regarding the technological development of phenotyping, I have developed a tree height measurement application from the digital surface model, constructed by UAV images. Also, I have developed an AI (object detection) model to detect cones on the tree crown of *A. sachalinensis*. These techniques will be utilized in the near future.

Keywords: Heritability; Best linear unbiased prediction (BLUP); Variety development, Phenotyping; *Picea glehnii*

**INTERNATIONAL SYMPOSIUM ON A RECENT PROGRESS
IN FOREST ECOLOGY AND MANAGEMENT
2021**

**SESSION 4
FOREST HYDROLOGY AND BIOGEOCHEMISTRY**

**Thursday, 11th November 2021
13:40 - 14:40**

ORGANIZER:

THE UNITED GRADUATE SCHOOL OF AGRICULTURAL SCIENCE, GIFU UNIVERSITY

Seasonal Variations of Dissolved Organic Carbon Concentrations and Fluxes in an Evergreen Broadleaved Subtropical Forest in Central Japan

Siyu Chen^{1*}, Ruoming Cao², Shinpei Yoshitake³, Toshiyuki Ohtsuka^{2,4}

¹ School of Environment and Life Science, Nanning Normal University, China

² River Basin Research Center, Gifu University, Japan

³ Faculty of Education and Integrated Arts and Sciences, Waseda University, Japan

⁴ United Graduate School of Agricultural Science, Gifu University, Japan

*Corresponding Author: siyu9053@163.com

SUMMARY

Most studies of dissolved organic carbon (DOC) hydrological fluxes were established in deciduous and coniferous forests, little is known about the origin, dynamic, and fate of DOC in the evergreen broad-leaved forest ecosystems, which are distributed widely in the subtropical and warm-temperate regions of East Asia. Thus, we examined the variations of DOC concentration in throughfall, stemflow, and litter leachate in an evergreen broadleaved subtropical forest in Central Japan for nearly three years (Jun, 2016 – Apr, 2019), and calculated the DOC fluxes of different forest hydrological fluxes to figure out the seasonal change patterns of DOC. All forest hydrological fluxes were highly enriched in DOC compared to bulk precipitation. DOC concentrations in throughfall were significantly higher in spring (Mar-May) than the other seasons, while DOC concentration in stemflow were highest in summer. However, DOC concentrations in bulk precipitation and litter leachate did not show a statistically seasonal variation. Monthly DOC concentrations in stemflow and litter leachate were significantly related to that in throughfall, thus the monthly DOC concentration change pattern of stemflow and litter leachate was similar to that of throughfall. Furthermore, monthly throughfall DOC concentration was positively correlated to dry weights of litterfall and flower, suggesting the canopy exchanges (leaf emergency, leaf fall and florescence) had a great impact on throughfall DOC concentration and had indirect impacts on DOC concentrations in stemflow and litter leachate. DOC fluxes variations in all hydrological fluxes were well described by bulk precipitation amounts, furthermore, DOC fluxes in throughfall were also significantly controlled by its DOC concentrations. DOC fluxes in throughfall and litter leachate showed a similar seasonal pattern, which were highest in summer or spring and lowest in winter, these seasonal trends suggest that the increases in bulk precipitation can result in proportional increased in DOC fluxes input to the forest floor. The results of our study suggest that canopy changes still have significant effects on DOC concentration and DOC fluxes, despite there is no clear leaf and leafless season in the evergreen forest.

Keywords: Seasonal Variation; DOC; Throughfall; Carbon Vertical Transport; Stemflow

Introduction

Evergreen broad-leaved (*Lucidophyllous*) forests are distributed widely in the subtropical and warm-temperate regions of East Asia. Numerous studies have quantified and characterized fluxes of DOC in the forest ecosystems at local, regional, or national scale (Borken *et al.*, 2011; Buckingham *et al.*, 2008b; Van den Berg *et al.*, 2012), but most studies were established in deciduous and coniferous forests (Michalzik *et al.*, 2001, Kindler *et al.*, 2011, Camino-Serrano *et al.* 2014), little is known about the origin, composition, and fate of DOC in the evergreen broad-leaved forest ecosystems.

Considering the highest average NPP has been reported for evergreen broad-leaved species occupying mesic temperate environments in Japan, it may also be a large contributor of DOC flux inputs to the soil. Beyond that, previous studies found that canopy structure is an important controlling factor on throughfall patterns, broad-leaved deciduous canopies have been shown to influence throughfall patterns during the leafed season (Keim *et al.* 2005; Staelens *et al.* 2006b). Moreover, some study assumed that the multiple layers within the forest canopy and differences in canopy phenology might complicate throughfall patterns in tropical forests (e.g., Germer *et al.* 2006; Zimmermann *et al.* 2009;

Zimmermann and Isenbeer 2008). Although there is no clear leafed and leafless season in evergreen forest, the changes of canopy phenology still have impacts on the dynamics of DOC concentration in throughfall, stemflow and litter leachate. To test the hypothesis, we evaluated the variations of DOC concentrations in throughfall, stemflow, and litter leachate of this evergreen forest, and quantified the annual contribution of DOC from different forest hydrological flux to the DOC input to the forest floor, aims to figure out the seasonal change patterns of DOC.

Materials and Methods

The study site Mt. Kinka (35°26' N, 136°47' E, the peak is 329 m) is located in Gifu Prefecture, central Japan. Almost all areas (597 ha) of Mt. Kinka consist of secondary natural forests (93%) and artificial coniferous forests (2%). In particular, the lower slopes of Mt. Kinka are covered by secondary evergreen broad-leaved forests that predominated by *Castanopsis cuspidata*, which were mainly recovered after the World War II.

Samples of bulk precipitation, stemflow, throughfall and litter leachate were collected twice a month. Litterfall and flower were collected in using litter traps (1 m² area) that was set near the each throughfall collector for a total of nine litter traps. Litterfall and flower were collected once a month.

Results and Discussions

There was a definite difference in DOC concentration among precipitation, throughfall, stemflow and litter leachate at both annual and monthly scale (Table 1, Fig. 2), and the order of the DOC concentrations in this study was always: litter leachate > stemflow > throughfall > precipitation. The results are similar to those reported in other forest ecosystems (Michalzik *et al.* 2001, Solinger *et al.*, 2001, Chen *et al.* 2017). It is generally assumed that the wash-off from the canopy, including branches and trunks and leaching from the leaves are the two major sources of DOC in throughfall and stemflow. The tree species and canopy structures can greatly alter the amount, spatiotemporal patterning, and chemical properties of bulk precipitation via the vertical transport processes (Levia *et al.*, 2011; Pypker *et al.*, 2011). Previous studies in subtropical forests reported that DOC concentration in

throughfall and stemflow ranged in 5–11 mg L⁻¹ and 6–43mg L⁻¹, respectively (Van Stan and Stubbins, 2018), the annual mean DOC concentration in throughfall (6.62 ± 1.31 mg L⁻¹ in 2017, 6.10 ± 1.48 mg L⁻¹ in 2018) and stemflow (11.95 ± 3.28 mg L⁻¹ in 2017, 12.26 ± 3.71 mg L⁻¹ in 2018) in this study consistent with previous reports. There was rare research investigated the DOC concentration in litter leachate in the subtropical evergreen broadleaved forest. However, the annual mean DOC concentration in litter leachate (19.88 ± 4.20 mg L⁻¹ in 2017, 26.98 ± 8.09 mg L⁻¹ in 2018) was within the range of those investigated in the temperate forest ecosystems (20–40 mg L⁻¹, Michalzik *et al.* 2001), but at low level.

Table1 Mean annual volume-weighted dissolved organic carbon (DOC)_i concentration (mg L⁻¹), hydrological flux (mm), DOC_i flux (kg ha⁻¹ yr⁻¹), net DOC flux (kg ha⁻¹ yr⁻¹), pH and EC (mS m⁻¹) in bulk precipitation, stemflow, throughfall and litter leachate from January 2017 to December 2018.

		Bulk Precipitation	Stemflow	Throughfall	Litter leachate
DOC concentration (mg L ⁻¹)	2017	2.78 ± 0.40	11.95 ± 3.28	6.62 ± 1.31	19.88 ± 4.20
	2018	2.27 ± 0.16	12.26 ± 3.71	6.10 ± 1.48	26.98 ± 8.09
Hydrological flux (mm)	2017	1864	67.72	1353.12	1506.87
	2018	2157	74.14	1487.68	1702.93
DOC flux (kg ha ⁻¹ yr ⁻¹)	2017	38.71 ± 4.20	9.01 ± 1.28	72.98 ± 5.15	307.84 ± 37.97
	2018	54.03 ± 8.90	8.70 ± 1.56	82.01 ± 3.55	372.19 ± 54.61
net DOC flux (kg ha ⁻¹ yr ⁻¹)	2017	38.71 ± 4.20	6.08 ± 2.61	48.20 ± 12.47	216.69 ± 72.46
	2018	54.03 ± 8.90	5.66 ± 3.64	51.87 ± 11.19	301.21 ± 79.81
pH	2017	5.69 ± 0.22	5.02 ± 0.21	5.35 ± 0.19	5.49 ± 0.23
	2018	6.14 ± 0.16	5.19 ± 0.25	5.77 ± 0.14	5.50 ± 0.29
EC (mS m ⁻¹)	2017	4.41 ± 0.34	4.90 ± 0.36	5.17 ± 0.35	5.89 ± 0.55
	2018	1.35 ± 0.07	3.87 ± 0.95	4.01 ± 0.98	6.92 ± 2.24

The concentrations of DOC in throughfall were significantly higher in spring (Mar-May) than the other seasons. And monthly throughfall DOC concentration was positively correlated to dry weights of litterfall and flower. Additionally, Nitta and Ohsawa (1997) reported that leaf fall of *Castanopsis* had a high peak in May simultaneously with leaf emergence. The results observed in evergreen forest in this study are consistent with those of a previous report that seasonal effects on metabolic processes (such as changes in biological activity and dry deposition) can affect the concentrations of most nutrients in throughfall, with the highest in leaves fall season in deciduous forest (Parker, 1983). Because stemflow is considered as a concentrated version of throughfall (McColl, 1970) and a significant relation was detected for the monthly concentrations of DOC between throughfall

and stemflow ($r = 0.482$, $p < 0.05$), the highest seasonal DOC concentration of stemflow was found in summer, monthly change pattern of stemflow was similar to that of throughfall. Beyond that, significant and positive relationships were found in and litter leachate vs. in throughfall ($r = 0.590$, $p < 0.05$). Taken together, we supposed that the canopy exchanges (leaf emergency, leaf fall and florescence) had a great impact on throughfall DOC concentration and had indirect impacts on DOC concentrations in stemflow and litter leachate.

The amounts of bulk precipitation that reaches the forest floor, decomposition of litterfall, and microbial activity are the major determinants of the concentrations of DOC in litter leachate (Kalbitz *et al.*, 2000; Long *et al.*, 2015). In this study, monthly DOC concentration in litter leachate was positively correlated to temperature ($r = 0.672$, $p < 0.001$), suggesting a significant biological control on the DOC leaching from litterfall, which confirming the results in previous studies in both laboratory experiments and field studies (Andersson *et al.* 2000; Kalbitz *et al.* 2000; Solinger *et al.*, 2001). Beyond that, numerous studies found that litter leachate DOC concentration showed a positive response to the litterfall dynamics in temperate

forests (Casals *et al.* 1995; Currie *et al.* 1996; Michalzik and Matzner 1999). Statistically significant correlation $r = 0.388$, $p < 0.01$) was also found between litter leachate DOC concentration and litterfall at monthly scale in this study. Additionally, the statistically significant correlation found between monthly litter leachate DOC concentration and flower ($r = 0.474$, $p < 0.05$). As we know, there was no previous research reported the correlation between litter leachate DOC concentration and flower, we supposed that the amount of flower might also be an important source of DOC on the forest floor during the flower season.

In forest ecosystems, the forest floor has been identified as a primary source for DOC (Cronan and Aiken, 1985, Currie *et al.*, 1996, Qualls and Haines, 1991). At the study site, the annual DOC fluxes input to the forest floor was $307.84 \pm 37.97 \text{ kg}^{-1} \text{ ha}^{-1} \text{ yr}^{-1}$ in 2017, and $372.19 \pm 54.61 \text{ kg}^{-1} \text{ ha}^{-1} \text{ yr}^{-1}$ in 2018, respectively, which were comparable to the highest values recorded in temperate forests ($100\text{--}482 \text{ kg}^{-1} \text{ ha}^{-1} \text{ yr}^{-1}$, Michalzik *et al.* 2001, Fujii *et al.* 2001), nevertheless, it was much higher than that reported in another evergreen broadleaved forest in Japan ($149.4 \text{ kg}^{-1} \text{ ha}^{-1} \text{ yr}^{-1}$, Fujii *et al.*, 2011), this result may be explained by the differences of annual precipitation amounts, vegetation types (lignin concentration, C/N ratio), the amounts of litterfall (Godde *et al.* 1996, Currie and Aber 1997, Michalzik *et al.* 2001, Fujii *et al.* 2001) and even the difference of throughfall, considering 15.58 % of total annual DOC fluxes was provided by throughfall in 2017. And most of total annual DOC fluxes was from litter leachate (70.02%, $216.69 \pm 72.46 \text{ kg}^{-1} \text{ ha}^{-1} \text{ yr}^{-1}$ in 2017; 72.87%, 301.21 ± 79.81

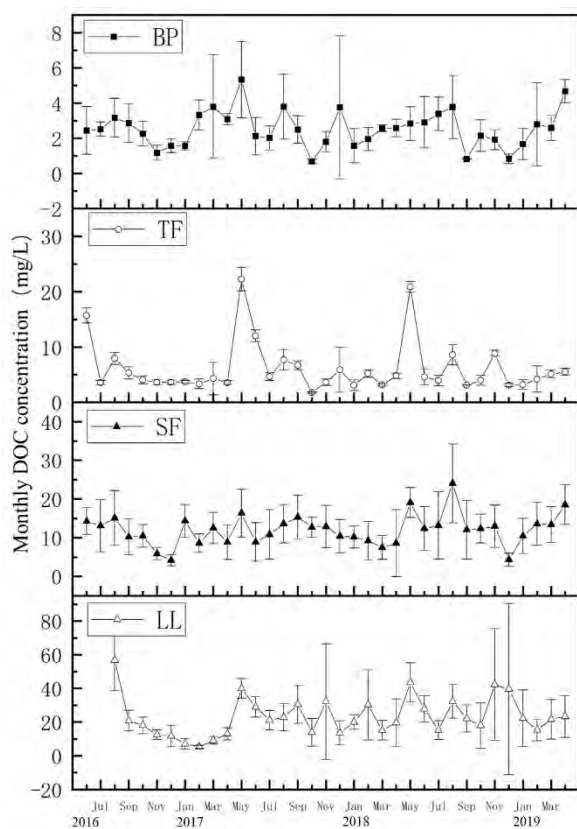


Fig. 1 Monthly DOC concentration (mg/L) of bulk precipitation (BP), throughfall (TF), stemflow (SF) and litter leachate (LL) from June 2016 to April 2019.

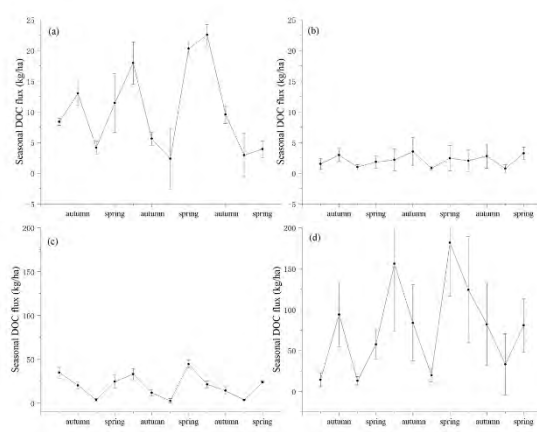


Fig. 2 Seasonal DOC flux (kg/ha) of bulk precipitation (BP), throughfall (TF), stemflow (SF) and litter leachate (LL) from autumn in 2016 to spring in 2019.

kg⁻¹ ha⁻¹ yr⁻¹ in 2018), while stemflow only attributed 1.97% of total annual DOC fluxes (6.08 kg⁻¹ ha⁻¹ yr⁻¹) in 2017, indicating that the major source of DOC input to soil depends on litter decomposition.

Conclusions

The dynamics of DOC concentration and fluxes throughfall, stemflow and litter leachate in the studied evergreen broadleaved forest in a subtropical region showed some differences from that in deciduous forest in temperate regions, where DOC has been intensively studied. DOC concentrations of all hydrological fluxes are not hydrologically controlled. Significant positive correlations were found among monthly DOC concentrations in throughfall, stemflow and litter leachate. DOC concentrations in throughfall and stemflow exhibited a similar pattern. Moreover, monthly DOC concentration in throughfall, stemflow and litter leachate positively responded to the canopy changes (litterfall and flower), these results demonstrating that canopy change is one of the main controls of DOC concentrations in throughfall, stemflow and litter leachate.

DOC fluxes variations in all hydrological fluxes were well described by bulk precipitation amounts, furthermore, DOC fluxes in throughfall were also significantly controlled by its DOC concentrations. DOC fluxes in throughfall and litter leachate showed a similar seasonal pattern, which were highest in summer or spring and lowest in winter, these seasonal trends suggest that the increases in bulk precipitation can result in proportional increased in DOC fluxes input to the forest floor.

Together, the results of our study suggest that canopy changes still have significant effects on DOC concentration and DOC fluxes, despite there is no clear leaf and leafless season in the evergreen forest. Although litter leachate was the primary source of DOC inputs to forest floor, throughfall DOC flux affected the litter leachate DOC flux in the study site, thus, evaluating the proportion of DOC fluxes from different hydrological fluxes input to the forest floor help us understand the dynamics of DOC in the forest ecosystem better.

Acknowledgment

The authors would like to thank Prof. T. Otsuka for helpful advice. Special thanks for field assistance and laboratory assistance provided by individuals at the River Basin Research Center, Gifu University, Japan: Dr. R. Cao, Prof. F.S. Li. And suggestions by Pro. Yoshitake at Faculty of Education and Integrated Arts and Sciences, Waseda University.

Reference

- Borken, W., Ahrens, B., Schulz, C., and Zimmermann, L. (2011). Site-to-site variability and temporal trends of DOC concentrations and fluxes in temperate forest soils. *Glob. Change Biol.* 17, 2428–2443.
- Buckingham, S., Tipping, E. and Hamilton-Taylor, J. (2008). Concentrations and fluxes of dissolved organic carbon in UK topsoils, *Sci. Total Environ.*, 407(1), 460–470.
- Camino-Serrano, M., *et al.* (2014), Linking variability in soil solution dissolved organic carbon to climate, soil type, and vegetation type, *Global Biogeochem. Cycles*, 28, 497–509, doi:10.1002/2013GB004726.
- Chen, S., Yoshitake, S., Iimura, Y., Asai, C. and Ohtsuka, T. (2017). Dissolved organic carbon (DOC) input to the soil: DOC fluxes and their partitions during the growing season in a cool-temperate broad-leaved deciduous forest, central Japan. *Ecol. Res.* 32(5), 713–724.
- Fujii, S., Garling, T., and Kitamura, R., (2001). Breaking habitual defecting by a temporary structural change. In: Presented at Ninth International Conference on Social
- Germer, S., Elsenbeer, H. and Moraes, J. (2006). Throughfall and temporal trends of rainfall redistribution in an open tropical rainforest, south-western Amazonia (Rondônia, Brazil). *Earth Surf Process Landf* 10(3), 383–393. Dilemmas, June 29–July 3, 2001, Chicago.
- Godde, M., David, M. B., Christ, M. J., Kaupenjohann, M., Vance, G. F. (1996): Carbon mobilization from the forest floor red spruce in the northeastern USA. *Soil Biol. Biochem.* 28, 1181–1189.
- Kalbitz K, Solinger S, Park, J-H., Michalzik, B., and Matzner, E. (2000). Controls on the

- dynamics of dissolved organic matter in soils: A review. *Soil Sci* 165:728–736.
- Keim, R.F., Skaugset, A.E., and Weiler, M. (2005). Temporal persistence of spatial patterns in throughfall. *J Hydrol* 314:263–274.
- Kindler, R., Siemens, J.A.N., Kaiser, K., Walmsley, D.C., Bernhofer, C., Buchmann, N., Cellier, P., Eugster, W., Gleixner, G., GrÜNwald, T., Heim, A., Ibrom, A., Jones, S.K., Jones, M., Klumpp, K., Kutsch, W., Larsen, K.S., Lehuger, S., Loubet, B., McKenzie, R., Moors, E., Osborne, B., Pilegaard, K.I.M., Rebmann, C., Saunders, M., Schmidt, M.W.I., Schrumpf, M., Seyfferth, J., Skiba, U.T.E., Soussana, J.-F., Sutton, M.A., Tefs, C., Vowinkel, B., Zeeman, M.J. and Kaupenjohann, M. (2011). Dissolved carbon leaching from soil is a crucial component of the net ecosystem carbon balance. *Glob Chang Biol* 17(2), 1167–1185.
- Levia, D.F., Keim, R.F., Carlyle-Moses, D.E. and Frost, E.E. (2011). Throughfall and stemflow in wooded ecosystems. In: *Forest Hydrology and Biogeochemistry*, 216, 425–443.
- Long G Q, Jiang Y J, Sun B. Seasonal and inter-annual variation of leaching of dissolved organic carbon and nitrogen under long-term manure application in an acidic clay soil in subtropical China[J]. *Soil & Tillage Research*, 2015, 146:270–278.
- McColl, J. G. (1970). Properties of some natural waters in a tropical wet forest of Costa Rica. *BioScience* 20, 1096–1100. doi: 10.2307/1295415
- Michalzik, B., Kalbitz, K., Park, J.-H., Solinger, S., and Matzner, E. (2001). Fluxes and concentrations of dissolved organic matter - a synthesis for temperate forests. *Biogeochemistry* 52:173–205.
- Staelens, J., De Schrijver, A., Verheyen, K., and Verhoest, N.E.C. (2006). Spatial variability and temporal stability of throughfall water under a dominant beech (*Fagus sylvatica* L.) tree in relationship to canopy cover. *J Hydrol* 330(3–4), 651–662.
- Solinger, S., Kalbitz, K., and Matzner, E. (2001). Controls on the dynamics of dissolved organic carbon and nitrogen in a Central European deciduous forest. *Biogeochemistry* 55:327–349.
- Parker GG (1983) Throughfall and stemflow in the forest nutrient cycle. *Adv Ecol Res* 13:57–133
- Van den Berg, L. J. L., Shotbolt, L. and Ashmore, M. R. (2012). Dissolved organic carbon (DOC) concentrations in UK soils and the influence of soil, vegetation type and seasonality, *Sci. Total Environ.*, 427, 269–276, doi:10.1016/j.scitotenv.2012.03.069.
- Zimmermann, A., Zimmermann, B.E., and Isenbeer, H. (2009). Rainfall redistribution in a tropical forest: spatial and temporal patterns. *Water Resour Res* 45:W11413.
- Zimmermann, B.E., and Isenbeer, H. (2008). Spatial and temporal variability of soil saturated hydraulic conductivity in gradients of disturbance. *J Hydrol* 361:78–95.

Difference of Water and Material Dynamics between Coniferous Plantation and Deciduous Secondary Forest Watershed - Focusing on Dissolved Organic and Inorganic Carbon

Taketo Uemura ^{1*}, Takeo Onishi ², Toshiyuki Otsuka ³,
Ken Hiramatsu ²

¹ Graduate School of Natural Science and Technology, Gifu University

² Faculty of Applied Biological Sciences, Gifu University

³ River Watershed Research Center, Gifu University

*Corresponding Author: a4522002@edu.gifu-u.ac.jp

SUMMARY

To clarify the effects of coniferous plantation on the hydrological processes and the associated material dynamics in the forest watershed, the dynamics of Dissolved Organic Carbon (DOC) and Dissolved Inorganic Carbon (DIC), whose quantity and quality strongly depend on the water flow paths, were investigated by paired catchment study between coniferous plantation (CP) watershed (0.60 km²) and deciduous broad-leaved secondary forest (DB) watershed (0.72 km²). Stream discharge, DOC, DIC, Cl⁻, NO₃⁻, SO₄²⁻, Na⁺, K⁺, Mg²⁺, Ca²⁺ concentrations, and fluorescence characteristics of DOC were measured at the outlet of each watershed. In addition, we applied the same chemical analysis on throughfall, soil water at the depth of 10 cm and 50 cm, and spring water as a substitute for groundwater, collected in each watershed. Daily concentrations of DIC, Na⁺, and Ca²⁺ of which main source can be considered bedrock, were clearly higher in the DB watershed than in the CP watershed, while concentrations of DOC and NO₃⁻, derived from organic decomposition near the soil surface, were slightly higher in the CP watershed than in the DB watershed. The ratio of DIC to DOC (DIC/DOC) was higher in DB watershed than in CP watershed, suggesting the contribution of component with high DIC content is significant in DB watershed. During rainfall runoff periods, DOC and NO₃⁻ concentrations significantly increased with peak runoff in both watersheds. On the other hands, DOC were sometimes higher than DIC in CP watershed, while DOC were always lower than DIC in DB watershed. These observations suggest that the ratio of runoff components flowing through the near surface zone tend to be higher in CP watershed during rainfall events. To demonstrate this hypothesis, we conducted the End-Members Mixing Analysis (EMMA) using throughfall, soil water, and spring water (groundwater) as end-members to determine the contribution rate of each component.

Keywords: Paired catchment study; DOC; DIC; Flow path; EMMA

Introduction

Coniferous plantation, one of the anthropogenic alterations of forest ecosystems, affects the hydrological processes in forest watersheds. For example, the ratio of discharge to precipitation is lower in evergreen coniferous plantation watersheds than in natural deciduous broad-leaved forest watersheds, caused by differences in interceptional evaporation or evapotranspiration cause differences in watershed water runoff (Hisada *et al.*, 2011; Nagasaka *et al.*, 2015). These differences in hydrological processes also affect material dynamics, such as carbon, nitrogen, and inorganic ions through water flow. Some studies on forest hydrology have reported much information about water quality dynamics in

rainfall-runoff processes, and changes in discharge and solution concentrations in stream water. However, few studies have focused on the effects of anthropogenic forest alteration on ecosystem functions and the relationship between hydrological processes and material dynamics.

To evaluate the effects of coniferous plantation on material dynamics, it is necessary to elucidate formation mechanisms of water quality based on water flow paths. Paired catchment study between coniferous plantation and natural forest watersheds will serve for this purpose. To estimate the flow paths, substances that show characteristic dynamics depending on hydrological processes are used as tracers, and the interrelationships between their quantitative or qualitative dynamics and hydrological variables are evaluated. Recently, the

dynamics of Dissolved Organic Carbon (DOC), such as humic substances, and Dissolved Inorganic Carbon (DIC), such as dissolved carbonic acid, have been actively studied due to the growing interest in carbon cycle research, then their runoff process based on water flow paths well understood (e.g. Boyer *et al.*, 1996; Hinton *et al.*, 1998; Sakamoto *et al.*, 1999; Katsuyama and Ohte, 2002; Kawasaki *et al.*, 2002; Ohte and Kawasaki, 2004; Haga *et al.*, 2007a; Haga *et al.*, 2007b; Tsurita and Ishizuka, 2013). These studies showed that DOC concentrations increase during rainfall and snowmelt period, when runoff components passing through near the soil surface with rich organic matter predominate. Moreover, DIC is supplied by dissolution of CO₂ in soil air, deep soil, or leaching from bedrock. Thus, dissolved carbon dynamics in stream water can be an effective indicator for estimating water runoff processes.

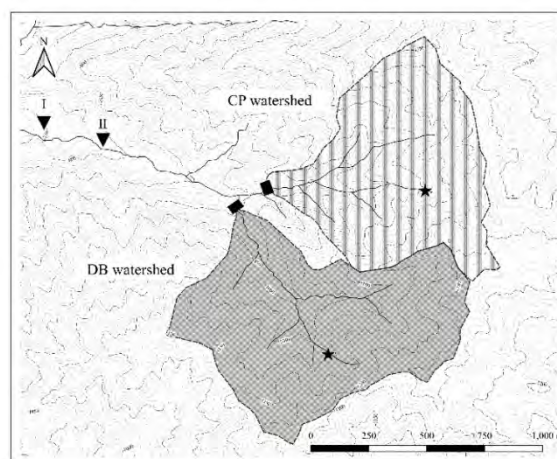
Hooper *et al.* (1990) and Christophersen *et al.* (1990) proposed a method called End-Members Mixing Analysis (EMMA), which assumes that stream water is formed by the mixing of source water, such as groundwater and soil water in the watershed. EMMA is useful for estimating the flow paths in the watershed, since the contribution of each source water can easily calculate from the concentrations of substances in the stream water and source water.

In this study, to clarify the effects of coniferous plantation on water and material dynamics, we conducted the pair catchment study between coniferous plantation (CP) watershed and natural secondary deciduous broad-leaved forest (DB) watershed. We quantified the differences in water and material dynamics in CP and DB watershed. In addition, we compared material dynamics focusing on DOC and DIC, and estimated the differences in water flow paths by EMMA.

Site Description

The study was conducted in paired catchments located in Kuraiyama Experimental Forest, Gifu Field Science Education and Research Center, Faculty of Applied Biological Sciences, Gifu University (Figure 1). The northern watershed has 0.60 km², an average slope of 32.5°, with an elevation ranging from 926 to 1278 m. Coniferous plantations, mainly Japanese cedar (*Cryptomeria japonica*) and cypress (*Chamaecyparis obtusa*)

cover 65% of the watershed, deciduous broad-leaved forests 28%, and natural coniferous forests 2%. Coniferous plantation is 50 to 60 years old. The southern watershed has 0.72 km², an average slope of 33.1° and is located at 909 to 1278 m elevation. The vegetation is a mixture of secondary deciduous broad-leaved forests such as *Quercus crispula* and *Magnolia obovata*, and natural coniferous trees such as *Tsujopsis dolabrata* and *Chamaecyparis pisifera*. The mixed forest covers 91% of the watershed. The geology and soil type in both watersheds is Nohi rhyolite and brown forest soil respectively. Thus, this site can be regarded as paired catchment with similar climatic and geological conditions. A v-notch weir has been installed at the outlet of each watershed, and stream discharge has been monitored. The annual precipitation is about 2,500 mm, with high rainfall during warm season from May to November. The mean annual air temperature is about 10°C.



I: Rainfall collecting point, II: Air temperature and air pressure observation point, ★: Throughfall, soil water and spring water collecting point.

Figure 1: Study Site

Methods

1. Hydrological observation

Precipitation was measured using a tipping bucket rain gauge installed at the outlet of DB watershed. In addition, we obtained precipitation data observed at AMEDAS Funayama Station, Takayama City, Gifu Prefecture, to supplement missing periods. Stream temperature and pressure were measured at the v-notch weir in each watershed using pressure logger (HOBO U20 model Water Level Logger). Using the same type of logger, air temperature and pressure was measured at the downstream of the study site (elevation is 780 m).

The measurement intervals were every 5 minutes from May 22, 2020 to December 4, 2020, every 10 minutes from December 4, 2020 to April 14, 2021, and every 3 minutes from April 14, 2021 to August 31, 2021. The stream water level was calculated using the observed water and air pressure, and converted to stream discharge by applying weir formula.

$$Q = Ch^{5/2}$$

$$C = 1.357 + \frac{0.004}{h} + \left(0.14 + \frac{0.2}{W^{1/2}}\right) \left(\frac{h}{B} - 0.09\right)^2 \quad (1)$$

where Q is stream discharge (m^3/s), C is the flow coefficient ($m^{1/2}/s$), h is the overflow depth (m), B is the weir width (m), and W is the height from the riverbed to the bottom of the weir notch (m).

2. Water sampling

Streamwater samples were collected at the outlet of each watershed using two automatic water sampler (ISCO 6712 model). While one sampler collects water once a day (CP: at 13:00, DB: at 12:00), another collects water once in a 2-hour when stream water level rises during rainfall period. Sampling started in May 22, 2020, and stopped during winter season (December 5, 2021 to February 28, 2021).

To quantify how water quality change in hydrological processes, we collected rainfall outside the forest (P), throughfall (TF), soil water (10 cm and 50 cm depths), and spring water (SP) as a surrogate index of groundwater. Rainfall was collected by three 10 L collection bottles, with a 21 cm diameter funnel, at the office (elevation is 750 m). To inhibit microbial activity, 10 mL of 0.1 mg/L CuBr solution was added to the collection bottles. Furthermore, glass wool was placed in the funnel neck, and a mesh bag covered the top of funnel, to prevent possible contaminations. For throughfall and soil water collection, we set up one experimental slope in each watershed. Throughfall was collected by collection bottles same as rainfall. Soil water was sampled by the tension lysimeter (DIK-8392) at 10 cm and 50 cm depths. In each experimental slope, we placed collectors on the upper, middle, and lower point of the slope. Spring water was collected at one spring point located near the experimental slope in each watershed. Sampling started in May 2021, with a biweekly sampling interval.

3. Chemical analysis

Water samples were filtered through a 0.7 μm pore glass fiber filter (Whatman GF/F) or a 0.45 μm pore syringe filter (ADVANTEC DISMIC®-25CS), and kept refrigerated until analysis. DOC and DIC concentrations were analyzed using total organic carbon analyzer (SHIMADZU TOC-L, TOC-V). Na^+ , K^+ , Mg^{2+} , Ca^{2+} , Cl^- , NO_3^- , and SO_4^{2-} concentrations were measured by ion chromatograph (DKK-TOA ICA-2000).

4. Estimate of the origin of runoff water

We estimated the origin of runoffwater during rainfall events by End-Members Mixing Analysis (EMMA). EMMA assumes that streamwater chemistry is determined by the mixing of source water, such as rainwater, soil water, and groundwater. First, we select two materials as tracer. Then concentrations of these tracer in streamwater and each source water (end-member) are plotted on the same graph called mixing diagram. In the graph, streamwater would be plotted in a polygon connecting each end-member, and the plot position reflects the contribution rate of each end-member. In case of using three end-members, the contribution rate to streamwater is calculated by the next equation.

$$f_1 + f_2 + f_3 = 1$$

$$C[A]_1f_1 + C[A]_2f_2 + C[A]_3f_3 = C[A]_{st} \quad (2)$$

$$C[B]_1f_1 + C[B]_2f_2 + C[B]_3f_3 = C[B]_{st}$$

where $C[A]$ and $C[B]$ are the concentrations of the two tracers A and B , f is the contribution rate of each component, subscripts 1, 2, and 3 indicate the end-members, and st is the stream water. In this study, rainfall component (rainfall and throughfall), soil water component (10 cm and 50 cm depth) and groundwater component (spring water) were selected as the end-members, assuming that these components contribute to streamwater. We applied the EMMA to streamwater during rainfall runoff period collecting in July 2, and August 9, 2021. Two different tracers were selected from the nine materials potentially utilized for tracers. Thus, total of 36 combinations of two chemical compositions were tested. For the most promising tracer combinations, we calculated each component contribution rate, and the applicability of EMMA were verified. The tracer concentrations for each end-member were the arithmetic mean of the water samples collected in May to September 2021. For rainfall, throughfall and soil water, the arithmetic

mean of the upper, middle, and lower slope concentrations were used.

Table 1: Solute concentrations for both watersheds
Means \pm standard deviations are shown.

		CP	DB
DOC	(mgC/L)	0.6 ± 0.4	0.4 ± 0.2
DIC	(mgC/L)	1.1 ± 0.2	1.8 ± 0.4
Na ⁺	(mg/L)	1.9 ± 0.4	2.6 ± 0.5
K ⁺	(mg/L)	0.4 ± 0.2	0.5 ± 0.1
Mg ²⁺	(mg/L)	0.1 ± 0.0	0.1 ± 0.0
Ca ²⁺	(mg/L)	0.6 ± 0.1	1.3 ± 0.3
Cl ⁻	(mg/L)	0.8 ± 0.2	0.7 ± 0.2
NO ₃ ⁻	(mg/L)	1.0 ± 0.5	0.9 ± 0.2
SO ₄ ²⁻	(mg/L)	0.6 ± 0.4	0.9 ± 0.1

Results

1. Daily concentrations of streamwater

The streamwater concentrations from May 22, 2020, to August 31, 2021 are shown in Table 1. DIC concentrations were clearly higher in DB watersheds with 1.8 ± 0.4 mgC/L than CP watershed with 1.1 ± 0.2 mgC/L. On the other hand, DOC concentrations were slightly higher in CP watershed

with value 0.6 ± 0.4 mgC/L than in DB watershed with value 0.4 ± 0.2 mgC/L. The ratio of DIC to DOC concentration (DIC/DOC) was 2.0 ± 0.2 in CP watershed and 5.6 ± 3.0 in DB watershed, with higher values in DB watershed. Among other dissolved ions, Na⁺, and Ca²⁺ showed clear difference in concentration, with higher concentrations in the DB watershed. Similar to DOC concentration, NO₃⁻ concentration was slightly higher in the CP watershed.

2. Concentration dynamics during rainfall period

From the start of sampling in May 2020 to August 2021, 11 peaks in CP watershed, and 14 peaks in DB watershed out of 14 rainfall events were collected. The significant increase in DOC and NO₃⁻ concentrations was observed in both watersheds at all rainfall runoff events. These increase roughly paralleled to the timing of the stream discharge increase. DIC, Na⁺, and Ca²⁺ concentrations, which showed clear differences between two watersheds, didn't show significant changes in concentrations, although in many cases there was a slight decrease in concentration as the runoff peak occurred. Due to the rapid rise in DOC concentration, DIC/DOC

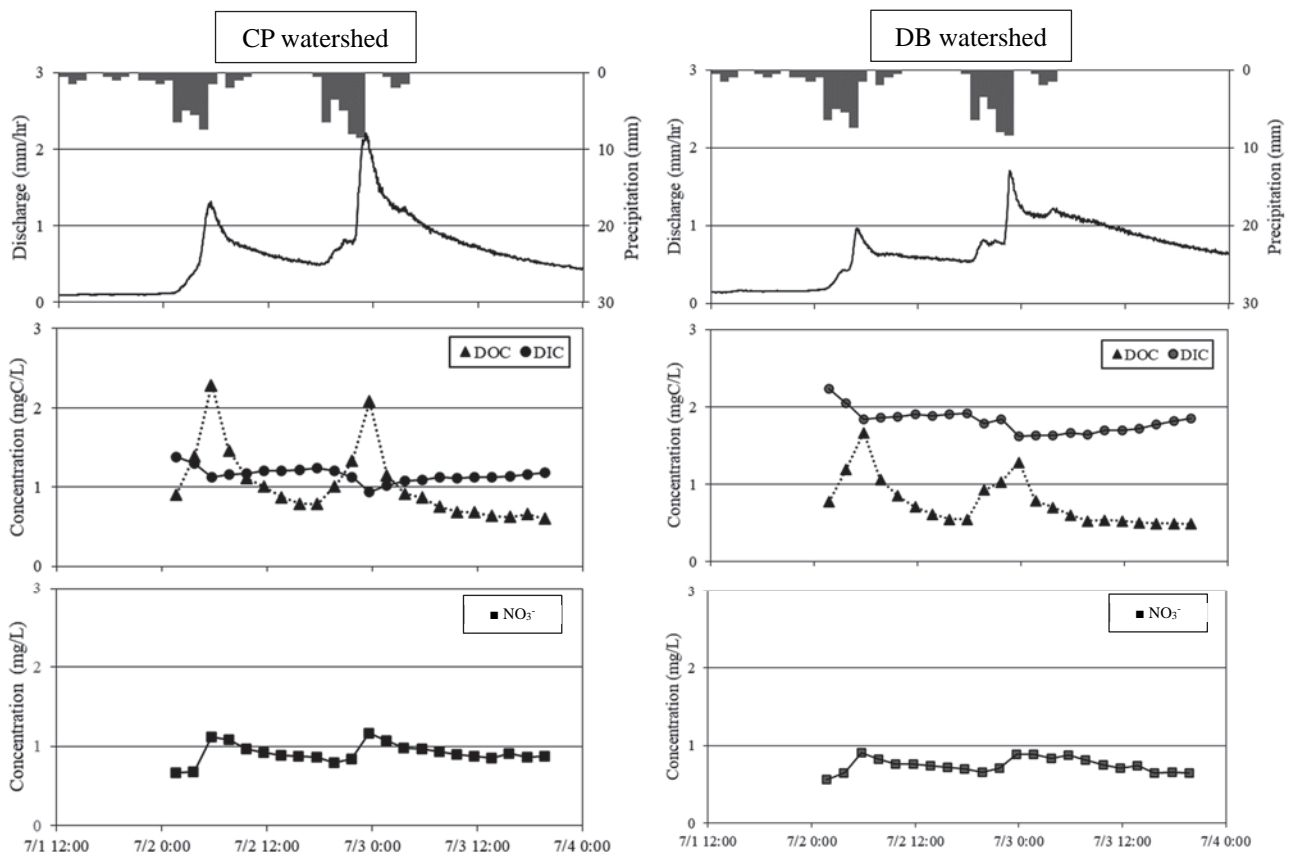


Figure 2: Comparison of discharge, DOC, DIC and NO₃⁻ concentrations between CP and DB watershed during rainfall period (July 2, 2021). Left side is CP watershed, and right side is DB watershed.

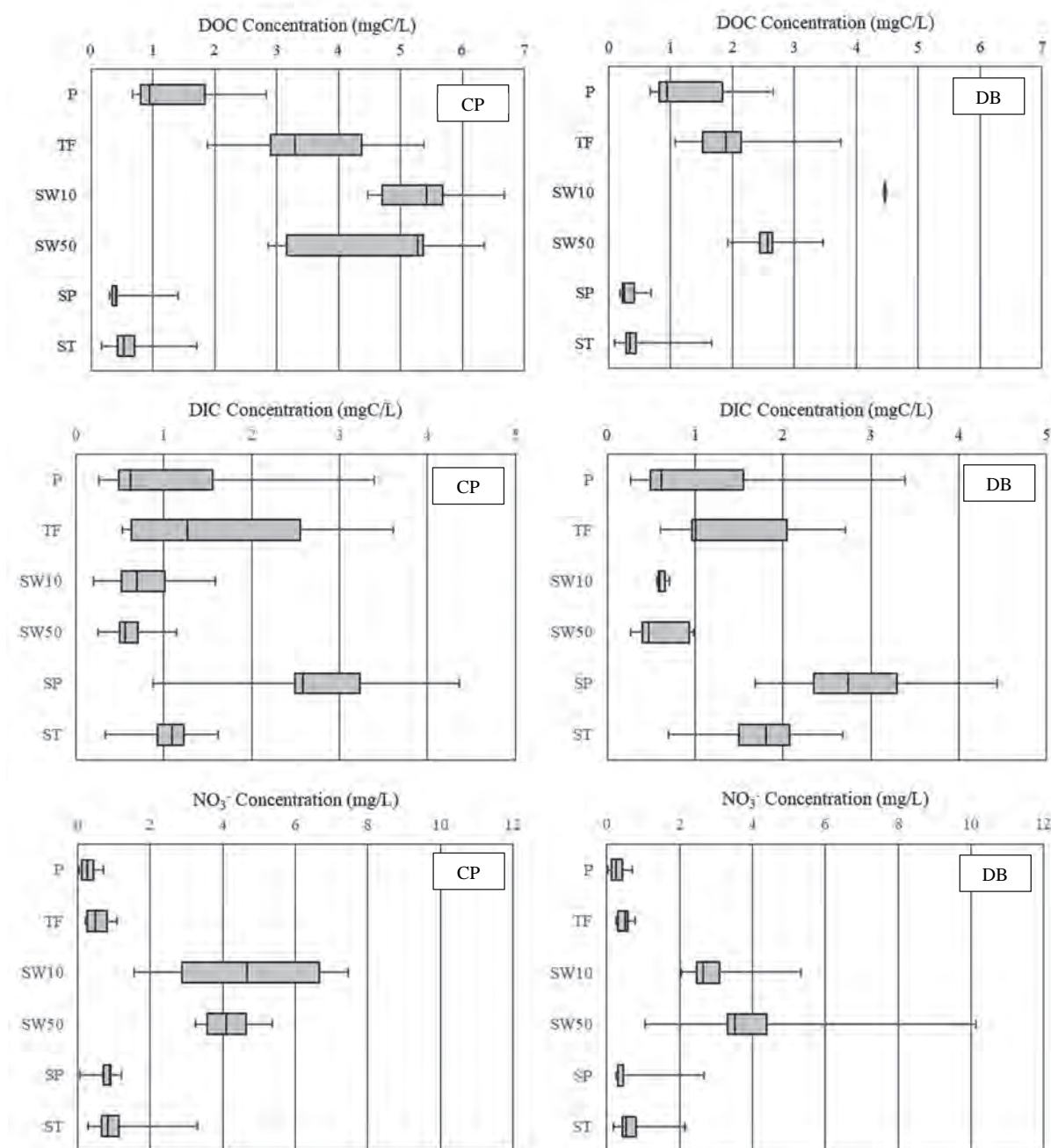


Figure 3: Variations of DOC, DIC, and NO_3^- concentrations. Left side is CP watershed, and right side is DB watershed. P: Rainfall ($n = 8^*$), TF: Throughfall (CP: $n = 9^{**}$, DB: $n = 9^{***}$), SW10: 10 cm depth soil water (CP: $n = 6$, DB: $n = 6$), SW50: 50 cm depth soil water (CP: $n = 6$, DB: $n = 6$), SP: Spring water (CP: $n = 11$, DB: $n = 7$), ST: Streamwater (CP: $n = 322$, DB: $n = 359$).

*: For NO_3^- , $n = 6$. **: For NO_3^- , $n = 4$. ***: For NO_3^- , $n = 6$.

during rainfall runoff became smaller in both watersheds. In CP watershed, however, DOC concentration was sometimes higher than DIC concentration. In contrast, in DB watershed, DOC concentration was always lower than the DIC concentration. Variation of DOC, DIC and NO_3^- concentrations during the rainfall events on July 2, 2021, are shown in Figure 2.

3. Variation of concentrations in rainfall, throughfall, soil water, spring water, and streamwater

Variation of DOC and DIC concentrations in the different water are shown in Figure 3. Variability in dissolved carbon concentrations was similar in CP and DB watersheds. DOC concentrations were increased in the rainfall, throughfall, soil water, and the highest concentration is observed in surface soil water. Then decreased

slightly in 50 cm depth soil water, the lowest concentrations were observed in spring water. Stream water showed a slight increase in concentration compared to spring water. On the other hand, DIC concentration decreased through the process from rainfall to soil water, and the lowest concentration was observed at 50 cm depth of soil water. Then significantly increased in spring water to a maximum concentration. In stream water, DIC concentrations were lower than spring water, but almost same or higher than rainfall and soil water. The trend of high concentrations in soil water and rapid decrease in spring water was also observed in NO_3^- . However, in some cases, NO_3^- concentrations were not detected in rainfall and throughfall. This result was different from previous study in this site (Ashik, 2021), thus there is uncertainty in the concentration values, Na^+ , Mg^{2+} , and Ca^{2+} increased from soil water to spring water, which was similar to DIC pattern.

4. Estimation of the contribution ratio of each end-member in runoff water

We found that DOC and NO_3^- were commonly able to represent the occurrence and variability of rainfall-runoff concentrations in both watersheds. Note that NO_3^- concentrations of rainfall components are uncertainly, and the number of data is small.

For example, Figure 4 shows the mixing diagrams for event on July 2, 2021, using throughfall, 10 cm soil water, and spring water as end-members. In both watersheds, the streamwater plots were distributed around the spring water. During peak runoff, however, the plots moved toward the straight line connecting throughfall and soil water end-member. As stream discharge diminished, the plots were again plotted near the spring water. This trend was also observed in the case of using rainfall or 50 cm depth soil water as the end-member, and in the event of August 9, 2021.

We calculated the contribution rate for Figure 4 and found that before the occurrence of the peak runoff, the contribution of spring water was the largest, accounting for more than 80 % of the stream runoff. When the runoff volume increased, the contribution of the throughfall and soil water component increased, while spring water contribution relatively decreased. The contribution rate of spring water during peak runoff was 48% in

CP watershed and 30 % in DB watershed. After the rainfall stopped, contribution of the spring water increased again. The increment in the contribution rate during peak runoff was more pronounced for the throughfall component, which in some cases exceeded the spring water contribution rate. The mean contribution rate of throughfall was 9 % in CP watershed and 23 % in DB watershed. Furthermore, the maximum contribution rate of the throughfall was 40 % in CP watershed and 69 % in DB watershed, with the contribution of throughfall in the forest being higher in DB watershed. Soil water component had the smallest contribution among the three components, ranging from 2 to 12 % in CP watershed and 0 to 6 % in DB watershed. In CP watershed, soil water contribution persisted for some time during the runoff recession period, while in DB watershed was almost didn't have contribution in the late recession period. Furthermore, the contribution of soil water components was always about 5% higher in CP watershed than in DB watershed. The mean contribution rate of spring water is 87 % in CP watershed and 81 % in DB watershed and tended to

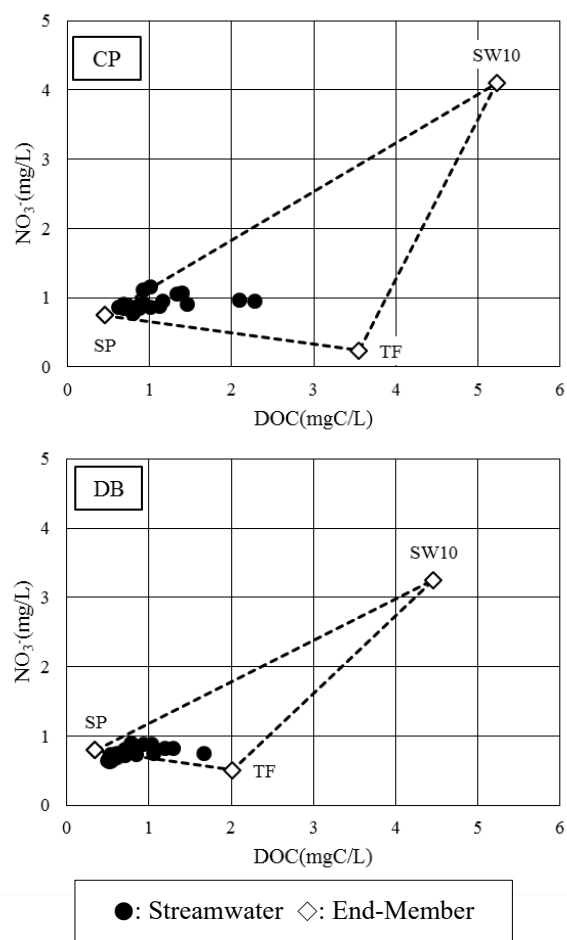


Figure 4: Mixing diagram on July 2, 2021 rainfall period

be relatively low in the DB watershed. The same trend of variation in the contribution of each end-member was observed on August 9.

Discussion

Generally, DIC, Na^+ , Mg^{2+} , and Ca^{2+} concentrations are higher in deeper soils and in runoff components which experiences long contact time with the bedrock. In contrast, DOC and NO_3^- mainly produced in the near surface soil due to plant litter deposition and microbial decomposition of organic matter. In the study site, DOC and NO_3^- concentrations were maximum in soil water, while DIC, Na^+ , and Ca^{2+} concentrations in spring water were significantly higher, indicating that DOC and NO_3^- decline, and increasing reaction of DIC, Na^+ , and Ca^{2+} occur during the process from surface soil to spring water. This trend is commonly found in CP and DB watersheds, suggesting that the sources of dissolved materials are similarly distributed regardless of vegetation in this site.

The fact that concentration of materials mainly derived from the bedrock is high, and DIC/DOC ratio in DB watershed is high suggest that the contribution of runoff components which have a long contact time with the deep soil and bedrock, such as groundwater, is significantly large in DB watershed than in CP watershed. The increase in DOC and NO_3^- concentrations linked to runoff peaks during rainfall period proves that rainfall runoff is formed by component passing through near the soil surface with high DOC and NO_3^- . Large increase of DOC concentrations in CP watershed during rainfall suggests that near-surface flow paths during rainfall in CP is much dominant then in DB, and the contribution of near-surface component to stream water is greater. The difference in the contribution of near-surface flow paths and deep soil or matrix flow paths may create long-term and short-term differences in material dynamics between watersheds.

EMMA using DOC and NO_3^- explained the occurrence of rainfall runoff due to the mixture of three components: rainfall, soil water, and spring water. Both DOC and NO_3^- are extremely high in soil water, and rainfall components or spring water is relatively low. The tracers used in EMMA are required to have sufficient concentration differences between each end-members (Hooper *et al.*, 1990).

Since DOC and NO_3^- meet this requirement and show clear concentration variations during rainfall-runoff events, they can be used as tracers for EMMA. On the other hand, Na^+ and SO_4^{2-} , which have been used as tracer in some studies, such as Katsuyama *et al.* (2001), couldn't explain peak runoff in our study site. This is probably due to the fact that the concentration variation during rainfall runoff is smaller than those of DOC and NO_3^- .

The shift of stream water plots on the mixing diagram indicates that the streamwater chemistry approaches that of the rainfall and soil water components as rainfall runoff occurs. During recession period of runoff, the contribution of rainfall and soil water components stops or decreases, then streamwater chemistry returns to near the spring water. A similar trend has been reported in the forested watersheds of the headwaters of the Shimanto River in Japan (Shinomiya *et al.*, 2014). Therefore, the stream water during rainfall runoff can be explained by the mixture of rainfall, soil water, and spring water, and the peak rainfall runoff is caused by the increased contribution of rainfall and soil water components.

The contribution rate of each end-member suggests that the contribution of soil-water component might be greater in CP watershed than DB watershed during rainfall-runoff events, which supports the hypothesis that near-surface flow paths are more prone to occur in CP watershed. Moreover, the contribution of soil water components is continuously observed even in recession period. The contribution of draining water from soil into stream should significantly contribute to entire rainfall runoff event. In the DB basin, the contribution of throughfall component was larger than that of spring water component, then we found no evidence of significant contribution of groundwater component in DB watershed. Since the contribution rates of spring water and throughfall components vary in a complementary, the relatively high contribution rate of throughfall might have caused a decrease in the contribution rate of spring water. Katsuyama *et al.* (2000) reported that the contribution of the rainfall component was approximately 20 to 40 %. However, our results were much higher than this value. For rainfall and throughfall, microbial activity in the collection bottles was considered to have an effect. We found algae floating in some samples regardless of the addition of CuBr. Therefore, there is

uncertainty in the concentration values of rainfall components. Furthermore, it is also possible that the end-member and tracer are chosen incorrectly.

For further improvement of accuracy of EMMA, silicate, which is leached during the chemical weathering process of bedrock minerals and is rarely used by organisms, can be used as a tracer.

Acknowledgment

We would like to acknowledge the support provided by members of the Laboratory of Watershed Management, Laboratory of Otsuka, River Watershed Research Center, Laboratory of Montane Forest Ecology and Management, Mr. Akinori Tsuzuki and Mr. Masaya Aoki, Gifu Field Science Education and Research Center, Gifu University. We also would like to acknowledge Professor Kosugi, Kyoto University, and Professor Katsuyama, Kyoto Prefectural University, for the proposal of EMMA.

References

- Ashik, T. (2021) Paired catchment study of nitrogen dynamics in cool-temperate broadleaved deciduous and evergreen coniferous forests, central Japan. Master's thesis of Graduate School of Natural Science and Technology, Gifu University.
- Boyer, E.W., Hornberger, G.M., Bencala, K.E., and McKnight, D. (1996) Overview of a simple model describing variation of dissolved organic carbon in an upland catchment. *Ecological Modelling*. 86: 183-188.
- Christophersen, N., Neal, C., Hopper, R.P., Vogot, R.D. and Anderson, S. (1990) Modelling streamwater chemistry as a mixture of soilwater End-Members – a step towards second-generation acidification models. *J. Hydrol.* 116: 321-343.
- Haga, H., Nishida, K. and Sakamoto, Y (2007a) Effects of flow paths on dissolved organic carbon concentrations in a forest stream. *Journal of Japan Society on Water Environment*. 30(10): 573-578.
- Haga, H., Nishida, K. and Sakamoto, Y (2007b) Dissolved organic carbon concentrations in a forest stream and hydrological processes in a hillslope during storm flow periods. *Journal of Japan Society on Water Environment*. 30(11): 657-660.
- Hinton, M.J., Schiff, S.L., and English, M.C. (1998) Sources and flowpaths of dissolved organic carbon during storms in two forested watersheds of the Precambrian Shield. *Biogeochemistry*. 41: 175-197.
- Hisada, S., Senge, M., Ito, K. and Maruyama, T. (2011) Comparison of characteristics of water balance between evergreen coniferous and deciduous broad-leaved forest. *I D R E Journal*. 271: 1-7.
- Hooper, R.P., Christophersen, N. and Peters, N.E. (1990) Modelling streamwater chemistry as a mixture of soilwater End-Members – an application to the Panola Mountain catchment, Georgia, U.S.A. *J. Hydrol.* 116: 321-343.
- Katsuyama, M., Ohte, N., Uchida, T., Asano, Y. and Kimoto, A. (2000) Effects of the Differences of Hydrological Processes on the Streamwater Chemistry. *J. Japan Soc. Hydrol. & Water Resour.* 13(3): 227-239.
- Katsuyama, M., Ohte, N., and Kobashi, S. (2001) A three-component End-Member analysis of streamwater hydrochemistry in a small Japanese forested headwater catchment. *Hydrological Processes*. 15: 249-260.
- Katsuyama, M. and Ohte, N. (2002) Determining the sources of stormflow from the fluorescence properties of dissolved organic carbon in a forested headwater catchment. *Journal of Hydrology*. 268: 192-202.
- Kawasaki, M., Ohte, N., Nambu, K., Hobara, S., Okazaki, R., Katsuyama, M. and Kim, S. (2002) The dynamics of DOC in the hydrological process in a forested watershed. *Japanese Journal of Limnology*. 63: 31-45.
- Nagasaka, A., Nagasaka, Y. and Ishikawa, Y. (2015) Export of stream dissolved organic carbon and inorganic nitrogen at two headwater catchments with different forest types in central Hokkaido, Japan. *Bulletin of the Hokkaido Forestry Research Institute*. 52: 11-22.
- Sakamoto, T., Takahashi, M., Terajima, T., Nakai, Y., and Matsuura, Y. (1999) Comparison of the effects of rainfall and snowmelt on the carbon discharge of a small, steep, forested watershed in Hokkaido, northern Japan. *Hydrological Processes*. 13: 2301-2314.

- Shinomiya, Y., Yamada, T., Inagaki, Y., Yoshinaga, S. and Torii, A. (2014) Evaluation of annual nitrate nitrogen load and its runoff processes in a forested catchment in the Shimanto River headwaters. *Journal of Japan Society on Water Environment*. 37(3): 91-101.
- Tsurita, T. and Ishizuka, S. (2013) Dissolved organic- and inorganic- carbon dynamics in a small watershed of Japanese cedar and cypress plantation in northern Kyushu. *Kyushu J. For. Res.* 66: 97-98.

Estimating of Run off Using SCS-CM Model in Gunung Bromo Education Forest Discharging to Kalijirak River

Dwi Priyo Ariyanto ^{1,2,*}, Tio Egar Nurhutomo ³,
Mujiyo ¹, Komariah ¹

¹ Soil Science Department, Faculty of Agriculture, Universitas Sebelas Maret, Indonesia

² Forestry Education and Training Center, Universitas Sebelas Maret, Indonesia

³ Students of Agrotechnology Study Program, Faculty of Agriculture, University of Sebelas Maret Surakarta

*Corresponding Author: dp_ariyanto@staff.uns.ac.id

SUMMARY

This study aims to calculate the effective runoff volume estimation at Gunung Bromo Education Forest of Universitas Sebelas Maret, Indonesia based on the SCS-CN formula. Based on the formula used, a slope map and land cover map are needed as the basis for calculating the volume of runoff. Slope map is classified into 5 classes and land cover map is divided into 6 land cover. Overlay process is carried out to get the final result of the land map unit. Field surveys were carried out to obtain data on slopes, types of cover, and laboratory analysis was carried out to obtain soil texture data. The results showed that the estimated research location had an effective area of 83.69 hectares or about 62% and a runoff volume of 696,321.45 m³. The results of this study can be used as basic data to make an appropriate hydrological management plan.

Keywords: Forest; KHDTK Gunung Bromo; Land cover; Runoff; SCS-CN model

Introduction

Watershed management of is an important aspect as a way to maintain a unity of upstream and downstream areas, due to the reciprocal relationship between the two. Medawaty, Iriani & Nuraeni (2014) explained that several watersheds in Indonesia have decreased river conditions, due to the not optimal management of land function impacts into settlements from local natural resources that cause land degradation. Many phenomena are characteristic of the occurrence of degradation. According to (Isrun, 2009) the characteristics of land degradation include the discharge of river water in the dry season is very low, acceleration of sedimentation in lakes and irrigation networks, as well as a decrease in water quality. Therefore, watershed management needs to be done in order to provide benefits.

The increasing biophysical function of watersheds in the form of land cover today from forest areas to plantations, agriculture, and settlements resulted in changes to the water system conditions. Optimization of forest area will affect the availability of water in sub-sub-watersheds forests can significantly affect watershed water systems, although the optimal cover area (forest) in each

region varies depending on the biophysical watershed (Hanifiyani, 2015) The purpose of forest management by taking into account hydrological data is to maintain sustainable water management, so that hydrological data can be explored for optimal hydrological governance on land, as well as a reference for the prevention of adverse impacts resulting from runoff.

Gunung Bromo Education forest is an area that has a corrugated topography in which the river flows. However, there is no information regarding the effective contribution of Gunung Bromo Education Forest volume that can be donated to sub-watershed Kaljirak through runoff in the area. One of the models used to predict the volume of runoff of a watershed by the SCS-CN (Soil Conservation Service Curve Number) method. This study aims to knows the effective area estimate of Gunung Bromo Education Forest, the volume of runoff contributed to sub-watershed Kalijirak, and the influence of the environment along with the relationship of runoff volume parameters.

Materials and Methods

The research of runoff volume was conducted at Gunung Bromo Education Forest (or in Indonesian named KHDTK Gunung Bromo UNS)

located in Karanganyar District, Central Java Province, Indonesia, from December 2020 to January 2021. Primary data is obtained through field observation surveys, as well as laboratory analysis. Rainfall data was taken from Jumantono weather station which 6 km from Gunung Bromo Education Forest between 2009 to 2018. The determination of the sample point is done by purposive sampling of the results of land unit obtained from the overlay of land cover maps and slope maps. The land cover map was obtained from Forestry Education and Training Center. The slope map of the slope is processed from Indonesian Geospatial Information Agency in scale of 1:25,000.

Sampling is done by sampling the soil continuously in the topsoil layer (depth 0 - 20 cm) using a hoe in each land unit specified. Overlaying the map using a scale of 1:12,000 produces a land unit map with 16 sample points. Observations observed in the field in the form of data type closure, land management, and hydrological conditions. While the data in the laboratory analysis in the form of soil texture which is then collected for calculation using SCS-CN equation to obtain an estimate of runoff volume at the research site. Estimating runoff volume using the SCS-CN method is supported by the potential retention value of the runoff area.

Results and Discussion

1. Wide effective volume runoff KHDTK Gunung Bromo

The delineation process is made with the principle of topographic data extraction to obtain input values determining the characteristics of watershed hydrology (Purwono, Hartanto, Prihanto, & Kardono, 2018). Overland flow or flow runoff, to know the form of runoff flow and the area intended water when covering based on relief form topography or soil height. The direction of runoff by using the D8 algorithm method. Determination of topographic direction based on pixel algorithm based on height and then compared between 1 pixel to 8 pixels around it (Indarto, Wahyuningsih, Usman, & Rohman, 2008). After obtaining the results area of water catchment, then calculate the area using calculate geometry.

Determination of the effective area value of each land unit by combining or intersect effective wide of Gunung Bromo Education Forest area. The

results of the broad analysis of Catchment Area are presented in Table 1.

Table 1: The effective runoff area per land unit

Land Unit	Land area ha	Effective runoff area	
		ha	%
Mixed (25-45%)	18,36	14,40	78
Mixture (>45%)	12,14	11,10	91
Mahogany (25%-45%)	1,70	1,70	100
Mahogany (>45%)	1,97	1,97	100
Season (25%-45%)	6,53	5,52	84
Season (>45%)	3,64	3,44	94
Former nursery (>45%)	3,10	3,10	100
Pinus (<8%)	0,96	0,95	99
Pinus (9%-15%)	1,79	0,68	38
Pinus (16%-24%)	5,35	1,86	35
Pinus (25%-45%)	38,45	14,16	37
Pinus (>45%)	26,89	1,02	38
Mahogany Pine (<8%)	0,12	0,01	1
Mahogany Pine (9%-15%)	3,87	1,68	43
Mahogany Pine (25%-45%)	12,86	10,31	80
Mahogany Pine (>45%)	11,81	11,81	100

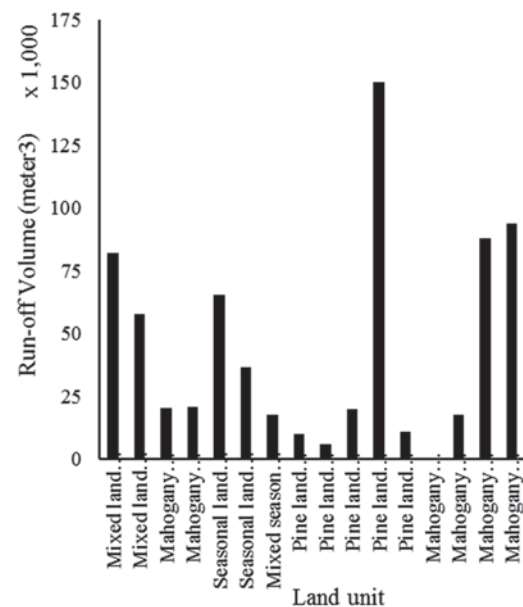


Figure 1: Graph of effective runoff volume per year

2. Effective runoff volume

The main purpose of effective runoff volume estimation is to obtain specific and reliable information for hydrological management of a land area. Factors that affect the volume of runoff include factors of land use type, factors of land management, hydrological condition factors, factors of soil hydrology group. The data obtained is then used for the SCS-CN equation and generates the average value of runoff volume per year per SPL region and

is presented in Figure 1.

The total effectiveness of the average runoff volume of Gunung Bromo Education Forest in the last 10 years was able to account for the volume of runoff by 63% with the total effective volume of 698,334.95 m³ of the total catch of runoff volume of Gunung Bromo Education Forest (1,117,264.34 m³). This is because the contour shape of the soil on Gunung Bromo Education Forest is hilly, causing the runoff volume does not lead to sub-watershed Kalijirak. According to Bambang, 2010, runoff comes from the highest points and moves towards the lower points in a perpendicular direction with contour lines.

3. Effect of environmental parameters on effective runoff volume

There is an environmental influence from the results of runoff volume value where after statistical tests, it is obtained that the environmental results that affect the magnitude of the runoff volume value of each land unit is the influence of land cover and the influence of slope. According to (Sarminah *et al.*, 2018) different levels of vegetation density types, can suppress the rate of surface runoff, so the tighter the heading of vegetation covering the surface, the lower the rate of surface runoff. While on the slope in accordance with the statement (Suryanto & Wawan, 2017) slope has an impact on the rate of surface flow the more tilted a land, the higher the runoff rate influenced by gravitational forces. The results of One Way Anova test that showed the influence of land cover environment and land slope on the volume of runoff effectively then tested further DMRT statistics (Table 2).

Table 2: The Effect of land cover on effective runoff volume per year

Land Cover	Runoff volume (mm/m ²)
Former Nursery	115.81a
mixture	231.61a
mahogany	431.60ab
A season	485.20ab
Pinus-Mahogany	829.60bc
Pinus	1,036.76bc

DMRT test results of land cover presented in Table 3 showed a noticeable difference in each of the 6 types of land cover to the volume of effective runoff, where the type of land cover used seedlings have the lowest end runoff volume contributor factor

with a total of 115.81 mm / m²/ year, and the highest runoff volume contributor cover at pine land cover with 1036.76 mm / m²/ year. There is a noticeable difference in the type of cover of pine-mahogany and pine land against former seedlings and mixtures, and mahogany and land land a season there is no real difference to other land cover. This is because according to (Verrina, Anugrah, & Sarino, 2013) land that has dense vegetation, rainwater that falls will be stuck to vegetation and seep into the soil, so that runoff flows small, so there are other factors that affect the volume of runoff. The conditions in this study are not uniform slope levels on each land cover that makes a noticeable difference to the value of runoff volume.

Table 3: Effect of slope on effective runoff volume per year

Slope	Runoff volume (mm/m ²)
3 (16%-24%)	179,83a
2 (9%-15%)	324,47a
1 (0%-8%)	359.66ab
4 (25%-45%)	802,97bc
5 (>45%)	934,67c

DMRT test results of land slope class presented in table 4.18 show a noticeable difference in each of the 5 classes of land slope to the volume of effective runoff. where the slope of the land class 3 (16%-24%) has the lowest runoff volume contributor factor with a total of 179.83 mm/m²/year, while the highest at slope 5 with a runoff volume of 934.67 mm/m²/year. There is a noticeable difference in each of the 5 grades of slope to the volume of effective runoff whereas in the slope class 3 (16%-24%) and slope 2 (9%-15%) there is a noticeable difference in the slope class 4 (25%-45%) and 5 (>45%), while at a slope of 1 (0%-8%) has a noticeable difference to the slope of 5 (>45%) according to (Suryanto & Wawan, 2017) the slope class of the land has a difference in the angle of weight force (gravity) The difference in weight force is getting bigger in line with the increasing tilt of the ground surface from the horizontal plane. This weight force is an absolute requirement of the process (transportation) of water to a lower height. The conditions in this study are not uniform slope levels on each land cover that causes there to be a noticeable difference in the value of runoff volume that is not in accordance with existing theories.

Conclusions

Effective runoff area of Gunung Bromo Education Forest account for 83.71 ha which flowed 698,334.95 m³ per year. Land cover and slope influence to runoff volume in Gunung Bromo Education Forest.

Acknowledgment

This work was supported by Universitas Sebelas Maret Research Grant (PUT-UNS) financial year 2019-2021.

Reference

- Hanifiyani, mawardah nur. (2015). Analisis hidrologi menggunakan model swat di sub das cilebak kabupaten bandung. Institut Pertanian Bogor.
- Indarto, Wahyuningsih, S., Usman, F., & Rohman, L. (2008). Pembuatan Jaringan Sungai Dan Karakteristik Topografi Das Dari DEM- JATIM. Media Tek Sipil. MEDIA TEKNIK SIPIL, (37), 99–108.
- Isrun. (2009). Analisis tingkat kerusakan lahan pada beberapa sub das di kawasan danau poso. Media Litbang Salteng, 2(1), 67–74.
- Medawaty, I., Iriani, L. Y., & Nuraeni, R. (2014). Penerapan Teknologi Pengolahan Air Secara Terpadu Di Permukiman Kawasan Daerah Aliran Sungai (Das) Studi Kasus : Kawasan Das Citarik , Sub Das Hulu Citarum. Jurnal Permukiman, 9(2), 67–77.
- Purwono, N., Hartanto, P., Prihanto, Y., & Kardono, P. (2018). Teknik Filtering Model Elevasi Digital (DEM) Untuk Delineasi Batas Daerah Aliran Sungai (DAS). Restorasi Sungai: Tantangan Dan Solusi Pembangunan Berkelanjutan, 490–504. Surakarta: Badan Informasi Geospasial.
- Sarminah, S., Prititania, F. S., Kehutanan, F., Mulawarman, U., Kelua, K. G., Hajar, J. K., ... Fax, T. (2018). Iklim di Indonesia merupakan iklim terhadap erosi . Selain curah hujan yang mengetahui Nilai Penting Jenis (NPJ),. Agrifor, XVII, 355–368.
- Suryanto, & Wawan. (2017). Pengaruh Kemiringan Lahan dan Mucuna bracteata terhadap Aliran Permukaan dan Erosi di PT Perkebunan Nusantara V Kebun Lubuk Dalam. Jurnal Online Faperta, 4(Ptpn V), 1–15.
- Verrina, G. P., Anugrah, D. D., & Sarino. (2013). Analisa Runoff Pada SUB DAS Lematang Hulu. Jurnal Teknik Sipil Dan Lingkungan, 1(1).

The Runoff and Sediment Response Due to Land Use Change in the Lubuk Paraku Sub-Watershed

Edwina Zainal^{1*}, Zufrimar¹, Zahrul Umar¹, Irfan Andika S¹

¹ Faculty of Civil Engineering and Planning, Bung Hatta University

*Corresponding Author: edwinazainal@bunghatta.ac.id

SUMMARY

Batang Arau catchment area consists of several tributaries, with the main river being the Batang Arau River. The upstream of the Batang Arau catchment area is Lubuk Paraku sub-watershed which is in the northeast of Padang City, with a catchment area of 25.04 km² approximately. In this study, the land-use change from 2007 to 2017 was identified by Arc-GIS software and examined the impact of land-use changes on runoff response and sediment load. The Rational Method was used to express a relationship between rainfall runoff in the catchment area to analyze the rainfall-runoff response concerning land-use change. The sediment capacity was estimated by the Yang, Ackers & White, and Engelund & Hansen method. The results showed the decreasing of dense forest and the increasing of the runoff and sediment capacity. The rate of runoff is 107.86 m³/s and 121.68 m³/s, in the years 2007 and 2017, respectively. The sediment capacity was 36266.33 t/y and 39730.19 t/y, in the years 2007 and 2017 that estimated by Engelund and Hansen method.

Keywords: Land-use change; Rainfall-runoff analysis; Sediment load; Lubuk paraku

Introduction

The land-use change in the upstream region is recognized to have a significant influence on the hydrological function of the catchment area. The hydrological function of the catchment area is the ability to absorb, hold, store, and slowly drain the water to create a balance of a water system.

Batang Arau catchment area consists of several tributaries, with the main river is the Batang Arau River and one of the major rivers in Padang City. The upstream of the Batang Arau catchment area is Lubuk Paraku which is located in the northeast of Padang City. It is dominated by conservation areas and protected forests such as the Botanical Forest Park Dr. Mohammad Hatta and the Nature Reserves Barisan I (BPDAS Agam Kuantan, 2011). A small part of the Lubuk Paraku is converted by the community into settlements, rice fields, and agricultural areas (Rebecha P., *et al.*, 2015; Endes N D, *et al.*, 2014). It is also a tourist destination area and flyover construction planned area (RPJMD, 2019).

The RPJMD (Local Government Medium-term Development Plans 2019-2024) of Padang City carried out prioritizes economic development, such as tourist areas, and is supported by increasingly improved road access. This development is a response to the increasing of land-

use conversion in the water catchment area. Nurhamidah, *et al.*, (2018) showed the upstream of the Batang Arau catchment area continued to decline due to the land-use conversion. The increasing activity in the upstream area will have an impact on the midstream to the downstream area in the changes of runoff fluctuations and sediment load. Runoff response generally depends on the shapes, length, slopes, perimeter, and areas of the watershed. In the absence of runoff records and other related hydrological information, attempts have been made to relate runoff to the watershed geometry using various techniques.

Sediment in the river channel will cause flood water levels to rise. According to the Padang City Bappeda (2014), the flooding that occurred in Padang City was indicated by the damage of the river bodies in the upstream area.

Base on the description above, it is necessary to identify the runoff and sediment response due to land-use change in the upstream of the Batang Arau catchment area in order to understand the hydrological process and predict the hydrological behavior.

Methods

1. Study area

The Lubuk Paraku sub-watershed (figure 1) is located in Indarung Village, Lubuk Kilangan

District. The area has a slope from gentle (8-16%) to very steep (> 40%) with a dominant hilly topography. The main river of Lubuk Paraku watershed is Lubuk Paraku River, with a length of 10.29 km. The catchment area in the Lubuk Paraku is relatively small, covering an area of 25.04 km² or 14.71% of the Batang Arau watershed total area.

The Lubuk Paraku sub-watershed area dominates by hilly areas, mountains, primary and secondary forests with undulating topography. According to the Regional Development Planning Agency (Bappeda) of Padang City (2014), the land use in the Lubuk Paraku sub-watershed protect forest and tourism forest, such as Bung Hatta Grand Forest Park. In addition, other land uses are fields/moorlands, rice fields, abandoned land and settlements. The soil in this area is intensively washed by rainwater, so the soil surface looks a bit pale and rough.



Figure 1. Batang Arau watershed and Lubuk Paraku sub-watershed

2. Rainfall-runoff analysis

The rainfall data from 2003 until 2017 was taken from the Office of Management of Water Resources of West Sumatera. This study used the maximum daily rainfall data from the Ladang Padi rainfall station. It produces rainfall plan and rainfall intensity at a certain return period.

Determination of land-use change in 2007 and 2017 by Arc-GIS software is used to determine the flow coefficient in the Lubuk Paraku sub watershed in order to estimate the amount of runoff generated by the rainfall plan. It is used in rational formula to estimate the runoff debit.

Table 1. Total Sediment Load Formula

Methods	Formulation
Yang	$\log C_t = 5.435 - 0.286 \log \frac{\omega d_{30}}{v}$ $- 0.457 \log \frac{u_*}{\omega}$ $+ \left(1.799 - 0.409 \log \frac{\omega d_{30}}{v} \right)$ $- 0.314 \log \left(\frac{u_*}{\omega} \right) \log \left(\frac{V \cdot S}{\omega} \right)$ $- \frac{V_{\infty} \cdot S}{\omega}$ $q_w = \gamma_w DV(C_t \times 10^{-6}) \quad (1)$
Ackers and White	$C_t = \left[\frac{G_{gr} d_{50} \left(\frac{\gamma_s}{\gamma} \right)}{D \left(\frac{u_0}{v} \right)^n} \right] \cdot 10^6$ $\rightarrow G_{gr} = C \left(\frac{F_{gr}}{A_1} \right)^{m^{1-n}}$ $\rightarrow F_{gr} = \frac{u_0^n}{\left[\left(g d_{50} \left(\frac{\gamma_s}{\gamma} - 1 \right) \right) \right]^{1/2} \left[\frac{v}{\sqrt{32} \log \left(\frac{v}{g d_{50}} \right)} \right]}$ $q_w = \gamma_w DV(C_t \times 10^{-6}) \quad (2)$
Engelund and Hansen	q_w $= 0.05 \gamma_s r V^2 \left[\frac{d_{50}}{g \left(\frac{\gamma_s}{\gamma} - 1 \right)} \right]^{1/2} \left[\frac{\tau_0}{[(\gamma_s - \gamma) d_{50}]} \right]^{3/2} \quad (3)$
Where:	
Discharge (Q_w)	discharge (m ³ /s)
Wide (W)	width of river (m)
Slope (S)	slope of the riverbed
d_{50}	average particle size of the base material (mm)
Gradation	of basic particle size geometric deviations
Specific Gravity	specific gravity
Concentration (C)	concentration of the load material (ppm/kg)

Source: T A Gunawan, *et al.*, 2019

3. Sediment load analysis

This research compares several methods of estimating the total sediment load, namely Yang Method, Ackers and White's Method, and Method of Engelund and Hansen. Sediment parameter data inventory is done by taking water samples to estimate the concentration of total load sediment. In addition, measurement of river hydraulic parameter is needed, including flow velocity. Tabel 1 shows the formula that used for calculation method.

Result and Discussion

1. Rainfall Analysis

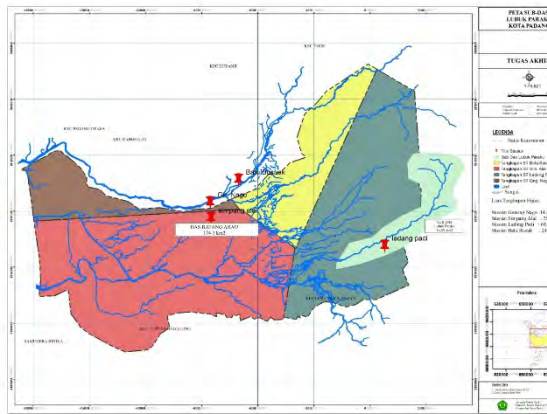


Figure 2. Rainfall Station in Batang Arau catchment area

Figure 1 shows the each rainfall station (Gunung Nago, Batu Busuk, Simpang Alai and Ladang Padi) that may influencing the Batang Arau catchment area on ArcGIS application. According to figure 1, in this study, the average rainfall data was obtained from the maximum daily rainfall data in a given year only from Ladang Padi rainfall station (upstream region). The maximum daily rainfall for fifteen years in the study area is shown in table 2. The highest rainfall occurred on 2006 at 155 mm, while the lowest occurred on 2007 at 75 mm.

The maximum rainfall data was analyzed with a certain return period in order to show the relationship between the magnitudes of the extreme events rainfall to the frequency of occurrence by using a probability distribution. There were four methods that were commonly used, such as the Normal, Log-Normal, Gumbel and Log Pearson III. According to the result and the goodness of fit test of chi-square and the Smirnov-Kolmogorov, the Normal distribution was generally appropriate for the Lubuk Parake watershed.

$$I = \frac{R_{24}}{24} \left(\frac{24}{t} \right)^{2/3} \quad (4)$$

The Monobe equation (4) is used to calculate the rainfall intensity (I in mm/hour). It provides a mathematical relationship between the duration (t in hour) and observed rainfall (R in mm). In the study area, the rainfall intensity is 42.52 mm/hour for 2 year return periods.

Table 2. The Average of The Maximum Daily Rainfall

Year	The Maximum Daily Rainfall (mm)
2003	105
2004	95
2005	118
2006	155
2007	75
2008	80
2009	145
2010	109
2011	118
2012	117
2013	125
2014	125
2015	76
2016	118
2017	122

2. Land-Use Change

Land use is the utilization of land resources by humans for various purposes and activities such as industrial, residential, recreational, transport, and agriculture (Azlini *et al.*, 2015). The Lubuk Paraku watershed is a water catchment and provides water resources for domestic use downstream, industrial, and agricultural. These rivers serve as freshwater sources, irrigation for agriculture purposes, and are for recreational activities (Endes N D, *et al.*, 2014).

Table 3. Land-use Change

Land-use	2007	2017
	Area (km ²)	Area (km ²)
Bare ground	0.84	0.45
Scrub/Shrub	1.92	0.99
Dense forest	16.80	14.77
Dry land farming	0.76	1.06
Paddy field	0.98	1.63
Farm and shrub	0.76	1.28
House	1.88	3.38
Industrial	1.28	1.85

The dense forest in the Lubuk Paraku watershed has been decreased from 16.80 km² to 14.77 km². On the other side, the settlement significantly increased. Table 3 showed a significant association between the increase of development

land use and the decrease of forest areas. In another study by Maryam A, *et al.* (2020), a significant land-use change in the upstream of Batang Arau catchment areas from 2010 to 2018 has been reported, where the Lubuk Paraku area has increased in the settlement and infrastructure.

Inefficient law enforcement has caused many illegal activities, which trespass the forest reserve and riverbank area. The unsustainable developing methods (settlement on a steep slope, recreational, transport, agricultural, soil erosion, landslide, and high sedimentation rate in the riverbed) have created major ecological disturbances in the Lubuk Parau sub-watershed.

3. Runoff analysis

The Rational method was used to estimate surface runoff potential in an ungauged watershed of the upper Batang Arau River basin. The Rational method is used for small watershed areas (C. Thomson, P.E., 2019). The rational formula is shown in equation 5 to estimate the peak of runoff (Q in m^3/sec) at a specific location in a watershed as a function of the drainage area (A in ha), mean rainfall intensity (I in mm/hour), and runoff coefficient (C) for a certain rainfall duration. The peak flow in the study area are summarized in table 4.

$$Q = 0.002778CIA \quad (5)$$

Table 4. Runoff Estimation

Year	Runoff (m^3/s)
2007	107.86
2017	121.68

Land-use changes greatly influence the surface runoff into water bodies. The decreasing of dense forests can cause repeated runoff and erosion into water bodies, particularly during rainfall. The increasing runoff during precipitation due to decreased infiltration rate into the soil caused land changes/landslides (Mufubi A, *et al.*, 2016; Edwina Z, *et al.*, 2016). Open farming has the highest erosion rate estimated, and more than 69% of the rainfall becomes runoff that flows into the river (BY Aminudin, *et al.*, 2005). Furthermore, this study also demonstrates an approach to generate reliable runoff data for vulnerable ungauged river basins.

4. Sediment analysis

Chih Ted Yang (1972) and T A Gunawan *et al.* (2018) explained that sediment load estimation based on the concept of energy exchange, such as the Engelund-Hansen, Yang, and Bagnold method are more accurate, reliable, and simpler than other approaches. The result of the total sediment transport estimation can be seen in table 5. The comparison of the methods has not provided satisfactory results. However, the result shows the highest rate of sediment load by the Engelund and Hansen method.

Tipani U S, *et al.* (2018) has reported that the study area is located in a highland elevation, more than 40% of the total area has an elevation of more than 1000 m and has steep slopes with a gradient greater than 25° . Therefore, the Lubuk Paraku has a high risk of soil erosion and is not suitable for development. It also emerged from the study of Benjamin K K, *et al.* (2020); F M Ziadat, *et al.* (2013), that the rate of soil loss increased with the increase in slope steepness and slope length. In addition, the Lubuk Paraku sub-watershed area is also prone to landslides due to heavy rainfall and heavy runoff. The runoff rates cause an increase in shear stress on the soil surface, leading to increased silt delivery (Syed A A and Hamelmal H, 2016).

Table 5. Sediment Estimation

Year	Total Sediment Load Method (ton/year)		
	Yang	Ackers and White	Engelund and Hansen
2007	2270.95	49.81	36266.33
2017	2286.46	51.64	39730.19

Conclusions

This study investigated the runoff and sedimentation response due to land-use change in the Lubuk Paraku sub-watershed by using the rational method and sediment load estimation. It is evident from the findings of the study that the Lubuk Paraku sub-watershed had land-use change from 2007 to 2017 and affects the generated runoff and sediment load. Soil erosion, landslides, agriculture activities, industrial, residential, and unplanned development associated with land-use change have significantly influenced the Lubuk Paraku sub-watershed. Continuous land-use changes without a

proper development plan and law enforcement may threaten the sustainability of the the Batang Arau watershed.

Reference

- Azlini Razali, Sharifah Norkhadijah Syed Ismail, Suriyani Awang, Sarva Mangala Praveena, and Emilia Zainal Abidin. (2018) Land use change in highland area and its impact on river water quality: areview of case studies in Malaysia. *Springer: Ecological Processes* 7: 19.
- Benjamin K K, Lalit K, and Richard K. (2020) Impact of Land Use/Cover Changes on Soil Erosion in Western Kenya. *MDPI, Sustainability*, 12, 9740.
- BY Aminudin, WY A Wan, UB Cheah, MH Ghulam, M Zulkefli, RB Salama. (2001) Impact of intensive highland agriculture on the ecosystem. *Journal of Tropical Agriculture Food Science*, Vol. 29, No. 1: 69-76
- C. Thomason, P.E. (2019) Hydraulic Design Manual, Texas Department of Transportation.
- Central Management of Regional River Flow (BPDAS) Agam Kuantan. (2011) Identifikasi potensi penyedia, pengguna dan karakter jassa DAS untuk pengembangan cost sharing hulu hilir SWP DAS Arau, Padang.
- Chih Ted Yang. (1972) Unit Stream Power and Sediment Transport. *Journal of the Hydraulics Division*, Vol. 98, Issue 10: 1805-1826
- Edwina Zainal and K. Toshiharu, (2016) Investigation of Long Term Evapotranspiration by Using Hamon Equation Factor and NDVI Data in Forest Plantations Area, *China-USA Business Review*, Vol. 15 No. 10, pp 494-506.
- Endes N. Dahlan, Rebecca P, and Omo Rusdiana. (2014) Pemanfaatan Sumberdaya Air di Sub DAS Lubuk Paraku Sumatera Barat (Water Resourece Utilization in Lubuk Paraku Sub Watershed, West Sumatera). *Media Konservasi*, 19 (1): 30-40.
- F.M Ziadat and A.Y Taimeh. (2013) Effect of Rainfall Intensity, Slope, Land use and Antecedent Soil Moisture on Soil Erosion in an Arid Environment. *Land Degradation & Development*, Vol. 24, Issue 6: 582-590
- Mehdi Habibi and Muttucumaru Sivakumar. (1992) Review of Selected Methods of Sediment Transport Estimation. *11th Australian Fluid Mechanic Conference*. Hobart. 175-178.
- Madhatilah, and Rusli HAR. (2020) Analisis Debit Air Limpasan Permukaan (Run Off) Akibat Perubahan Tata Guna Lahan Pada DAS Kuranji dan DAS Batang Arau Kota Padang. *Junal Bina Tambang*, Vol. 5, No. 1: 178-189.
- Maryam Afifa, Afla Dina, Elvi Roza Syofyan, and Wisafri. (2020) Analisa Debit Andalan Pada DAS Batang Arau Dengan Menggunakan Model Soil and Water Assessment Tool (SWAT). *Jurnal Ilmiah Poli Rekayasa*, Vol. 16, No.1: 34-42.
- Mufubi Agaton, Yudi Setiawan, Hefni Effendi. (2016) Land use/land cover change detection in an urban watershed: a case study of Upper Citarum Watershed, West Java Province, Indonesia. *Procedia Environmental Sciences* Vol. 33:654-660.
- Nurhamidah, Ahmad Junaidi, and Muhammad Kurniawan. (2018) Tinjauan Tata Guna Lahan Terhadap Limpasan Permukaan, Kasus: DAS Batang Arau Padang. *Jurnal Rekayasa Sipil (JRS-UNAND)*, 14(2): 131-138.
- Padang City Government. (2019) Local Government Medium Term Development Medium Plan 2019-2024 (RPJMD Kota Padang).
- Rebecha Prananta, Endes N. Dahlan, and Omo Rusdiana. (2015) Penilaian dan Pemanfaatan Sumberdaya Air Sub DAS Lubuk Paraku Kota Padang, Sumatera Barat (Assessment and Utilization of Water Resource in Lubuk Paraku Sub Watershed, Padang City, West Sumatera). *Jurnal Penelitian Hutan dan Konservasi Allam*, 12 (1): 19-31.
- Syed Ahmad Ali and Hamelmal Hagos. (2016) Estimation of soil erosion using USLE and GIS in Awasa Catchment, Rift valley, Central Ethiopia. *Geoderma Regional*, Vol. 7, Issue 2: 159-166.
- T A Gunawan, A Daud, H Haki, and Sarino. (2019) The Estimation of Total Sediments Load in River Tributary for Sustainable Resources Management. *IOP Conf. Series: Earth and Envrinmental Science* 248/012079
- Tipani U S, Taufiq H, Hartati, Zahrul U. (2018) Kajian Sedimentasi pada Muara Sungai Batang Arau Kota Padang. *Jurnal Ilmiah Rekayasa Sipil* Vol. XV, No.1: 37-44.

**UGSAS-GU & BWEL JOINT POSTER SESSION
ON AGRICULTURAL
AND BASIN WATER ENVIRONMENTAL SCIENCES
2021**

POSTER PRESENTATIONS

**Thursday, 11th November 2021
15:00 - 17:10**

**ORGANIZERS:
THE UNITED GRADUATE SCHOOL OF AGRICULTURAL SCIENCE,
GIFU UNIVERSITY
&
GIFU UNIVERSITY REARING PROGRAM
FOR BASIN WATER ENVIRONMENTAL LEADERS**

Effects of curcumin nanoemulsion on the water vapor permeability and antioxidant activities of chitosan-based films

Fakfan Luangapai¹, Methavee Peanparkdee², and Satoshi Iwamoto^{1,3}

1. Division of Science of Biological Resources, The United Graduate School of Agricultural Science, Gifu University, 1-1 Yanagido, Gifu 501-1193, Japan.
2. Department of Food Science and Technology, Faculty of Agro-Industry, Kasetsart University, Bangkok 10900, Thailand.
3. Department of Applied Life Science, Faculty of Applied Biological Sciences, Gifu University, 1-1 Yanagido, Gifu 501-1193, Japan.

INTRODUCTION

The development of renewable and environmentally friendly resources is critical concerned because non-biodegradable plastic wastes affected environmental issues. Biopolymer materials can be a viable solution by partially substituting non-biodegradable materials and perform as excellent carriers of functional additives. Chitosan (CH), a deacetylated derivative of chitin, is considered as environmentally benign biopolymer. CH has wide range of applications owing to its biocompatibility, biodegradability, and antimicrobial properties. Nevertheless, the chitosan films demonstrate undesirable properties, such as low mechanical strength and high permeability of water vapor transmission, which limit their function and efficiency. To overcome these shortcomings and achieve additional functionalities, several studies have attempted to incorporate hydrophobic lipid compounds in CH films (Peanparkdee *et al.*, 2016).

Curcumin, obtained from the extraction and purification of *Curcuma longa*, has been used as a spice, coloring agent, nutritional supplement, and herbal medicine. It has a wide range of beneficial properties, including antioxidant, anti-inflammatory, anti-cancer, and antimicrobial properties. However, the utilization of curcumin is restricted due to poor solubility and rapid hydrolysis. Numerous approaches have been reported to increase bioavailability of curcumin, such as nanoemulsion, nanoliposomes, and solid lipid nanoparticles. Herein, the study focused on the nanoemulsion technique, a promising approach to overcome dissolubility, stability, and bioactivity of various oil-soluble compounds owing to their small droplet size and high kinetic stability. As effective points of curcumin and nanoemulsion technique, they had high potential to be incorporated with chitosan-based films in order to improve the films' properties (Luangapai *et al.*, 2019).

Hence, this work aimed to develop the capabilities of water vapor permeability and enhance antioxidant activities of the films by incorporating with curcumin nanoemulsion (CurNEs). Thereafter, the effects of CurNEs on the various preparations were determined through physical properties such as color, water vapor permeability (WVP), glass-transition temperature (T_g), and antioxidant activities.

MATERIALS AND METHODS

Preparation of the CH-based films

CH powder (2 g) was dissolved in a 1% acetic acid solution. Glycerol was added to the film-forming solution containing 30% w/w CH powder. The solution was heated in a water bath shaking incubator for 4–6 h at 50 °C and 120 oscillation/min. The sample solutions were ultrasonicated for 15 min. The modified CH films were prepared via four approaches. First, CH in the film-forming solution as the control sample. Second, CH-NE was the film-forming solution blended with CurNEs. The CH and CH-NE film solutions were separately homogenized and cast on a metal plate. CH-CNE and CH-CO were prepared by coating the surface with CurNEs and

curcumin oil. The modified films were conditioned in a chamber for 48 h at 50% relative humidity (RH).

Preparation and characterization of CurNEs

Curcumin powder (70 mg) was dispersed in 10 mL of MCT oil to form the oil phase. Tween 80 and distilled water were mixed at 1:8 to form the aqueous phase. Appropriate proportions of the oil and aqueous phases and ultrasonication times as shown in Table 1. Under the various conditions, the size distributions and zeta potentials of the oil droplets were measured on a Zetasizer Nano ZS (Malvern, UK) at 25 °C.

Table 1 Ratio of oil to aqueous phase and ultrasonication time of curcumin nanoemulsion.

Conditions	Ultrasonic time (min)	Oil: Aqueous phase
CurNE1	15	1:4
CurNE2	30	1:4
CurNE3	90	1:4
CurNE4	120	1:4
CurNE5	15	1:6
CurNE6	15	1:8
CurNE7	15	1:9

Determination of the WVP of CH-based films

The water vapour transmission rate (WVTR) was evaluated, following the test method of ASTM (2007). The film samples were coated over cups (diameter 5 cm) containing silica gel. The film-covered cups were placed in a chamber that was set to 25 °C and 75% RH. WVTRs ($\text{gm}^{-2}\text{d}^{-1}$) of the films were determined from the slope of the regression analysis of the moisture weight gain (Δw) obtained through a film area (A) during a definite period (Δt) upon attaining the steady-state (Eq. (1)). The WVTRs of the films were subsequently calculate WVP via Eq. (2). At least five replications of each modified film were tested ($\text{gmm}^{-2}\text{d}^{-1}\text{kPa}^{-1}$), x is the film thickness (mm), and Δp is the difference between the partial water vapour pressures of the inner (p_1) and outer (p_2) surfaces of the film in the chamber (kPa).

$$\text{WVTR} = \frac{\Delta w}{A \Delta t} \quad \text{Eq. (1)}$$

$$\text{WVP} = \text{WVTR} \frac{x}{\Delta p} \quad \text{Eq. (2)}$$

Determination of the antioxidant activities of CH-based films

The sample (1 mL) was added to the ABTS working solution (4 mL). The mixture was incubated in the dark for 30 min. The ABTS radical scavenging activity (RSA) was calculated employing Eq. (3) and expressed as mmol Trolox/g weight of the dried film:

$$\text{RSA}(\%) = \frac{(A_{\text{control}} - A_{\text{sample}})/A_{\text{control}}}{\text{Trolox}} \times 100 \quad \text{Eq. (3)}$$

where A_{control} and A_{sample} are the absorbance of the blank and sample.

Determination of the color of CH-based films

The color parameters (L^* , a^* , and b^*) of the films were calculated on a spectrophotometer (RM200QC, X-rite, USA).

Six spots were randomly selected on the sample films, and three film samples were utilized for each replication. A white plate used to measure background and standard calibrations.

Determination of the thermal properties of CH-based films

The thermal properties were determined employing a DSC6200/EXSTAR6000 apparatus an inert nitrogen atmosphere at -50 to 150 °C and a heating rate of 10 °C/min.

RESULTS AND DISCUSSION

Size distributions and zeta potential of CurNEs

The mean diameters and zeta potential values of CurNEs are listed in Table 2. CurNE7 exhibited the smallest mean diameter (307.53 ± 6.30 nm) ($p \leq 0.05$). The variety of the size distribution corresponded to the ratio of the oil to the aqueous phases, the increasing adsorption of the concentration of the aqueous phase, the decrease in the interfacial tension, and the formation of fine droplets. CurNE7 exhibited the highest absolute value (-15.43 ± 0.74 mV) ($p \leq 0.05$). Moreover, the ultrasonication time is a crucial factor in preparing NE because prolonged time might increase the temperature from the cavitation-induced thermal effect, thus inducing the deterioration and aggregation of neighboring droplets (Agrawal et al., 2017). Since CurNE7 exhibited a concise ultrasonication time (15 min) and demonstrated higher stability and uniformity compared with the other conditions, it was selected and integrated with the CH films to further investigations.

Table 2 Mean diameters and zeta potential of curcumin nanoemulsion.

Condition	Mean diameter (nm)	Zeta potential (mV)
CurNE1	1023 ± 13.00^a	-0.88 ± 0.36^b
CurNE2	758.7 ± 3.68^b	-0.69 ± 0.26^b
CurNE3	360.67 ± 2.29^c	-0.50 ± 0.33^b
CurNE4	378.20 ± 5.59^d	-0.52 ± 0.48^b
CurNE5	533.23 ± 3.68^c	-0.08 ± 0.21^b
CurNE6	367.50 ± 5.20^{de}	-0.73 ± 0.38^b
CurNE7	307.53 ± 6.30^f	-15.43 ± 0.74^a

*Different letters in the same column indicate significantly different ($p \leq 0.05$).

Determination of the WVP of CH-based films

The CH-NE condition exhibited the lowest WVP (0.049 ± 0.001 gmm $^{-2}$ d $^{-1}$ kPa $^{-1}$), followed by CH-CO, CH-CNE, and CH. The improved WVP of CH-NE might be due to the presence of CurNEs in the inner film structure enhanced the water barrier properties by increasing the tortuosity, thereby generating the resistance of water vapour through the film. Conversely, CH-CNE and CH-CO exhibited higher WVP than CH, however, compared with CH-NE, CH-CNE and CH-CO exhibited lower efficiencies, which were attributed to the weak structural integrities of the surface of the film.

Determination of the antioxidant activities of CH-based films

The CH-NE condition exhibited five times higher antioxidant activity than CH. Moreover, CH-NE exhibited the highest antioxidant activity probably because of the reduction in the droplet size of the CH-incorporated NE, which promoted specific surface interaction, and afforded accelerated and very efficient free radical absorption. Additionally, the reduction in the size of the oil droplets improved the mass transfer and increased the release rate, dispersion, and kinetically stable suspension. Conversely, CH-CNE and CH-CO also demonstrated antioxidant effects, although their effects were

lesser than that of CH-NE because of their lower potential intermolecular interactions and hydrophobicity.

Determination of the color of CH-based films

The color properties can be detected through the L^* , a^* , and b^* values. The L^* , a^* , and b^* coordinates indicate the lightness and darkness, green to red, and yellow to blue colors, respectively. CH-NE exhibited the lowest L^* (76.63 ± 1.75), although it exhibited the highest a^* (10.0 ± 1.94) and b^* (54.58 ± 1.06) values. Thus, the probable appearance of CH-NE could be a yellowish red, whereas CH, CH-CNE, and CH-CO were yellowish green. The color properties might be affected by the method of in corporations.

Determination of the thermal properties of CH-based films

CH exhibited a T_g of ~ 80.71 °C, however, the T_g of the CH-NE film sample shifted to 71.34 °C, whereas those of CH-CNE and CH-CO shifted slightly to 78.82 and 83.42 °C, respectively. It is well known that the T_g is an important criterion for the miscibility of the components. In a completely miscible blend of two compounds, only one T_g was observed. The results indicating good miscibility by performing one T_g and forming of new hydrogen bonding networks appear. Furthermore, the decrease of T_g of CH-NE corresponded to the interaction between CH and CurNEs in the amorphous regions. The modification of CH by small amounts of additives, such as NEs, is induced owing to the plasticization effect, thus increasing the chain mobility in the amorphous regions, and decreasing the degree of crystallinity (Luangapai et al., 2021).

In summary, to develop CH-based films by incorporating CurNEs on various preparations. CH-NE exhibited good appearance, enhanced WVP, and antioxidant activities. Additionally, the thermal analysis revealed that the films exhibited considerable miscibility of the components from CH and CurNEs incorporation. The results initiated and promoted an interesting development as an active ingredient for producing food packaging materials.

Table 3 WVP, antioxidant activities and T_g of CH-based films composited with curcumin nanoemulsion and/or oil.

Samples	WVP (g mm $^{-2}$ d $^{-1}$ kPa $^{-1}$)	mmol Trolox/g film	T_g (°C)
CH	0.130 ± 0.010^a	0.39 ± 0.02^d	80.7
CH-NE	0.049 ± 0.001^d	2.11 ± 0.09^a	71.3
CH-CNE	0.087 ± 0.001^b	0.58 ± 0.03^c	78.8
CH-CO	0.077 ± 0.001^c	0.73 ± 0.00^d	83.4

*Different letters in the same column indicate significantly different ($p \leq 0.05$).

REFERENCES

- Agrawal, N., Maddikeri, L., and Pandit, B. (2017) Sustained release formulations of citronella oil nanoemulsion using cavitation techniques. *Ultrasonics Sonochemistry* 36: 367-374.
- Luangapai, F., Peanparkdee, M., and Iwamoto, S (2019). Biopolymer films for food industries: Properties, applications, and future aspects based on chitosan. *Reviews in Agricultural Science* 7: 59-67.
- Luangapai, F., Peanparkdee, M., and Iwamoto, S Effects of a curcumin nanoemulsion on the physico - chemical properties of chitosan - based films. *International Journal of Food Science & Technology*.
- Peanparkdee, M., Iwamoto, S., and Yamauchi, R (2016). Microencapsulation: A review of applications in the food and pharmaceutical industries. *Reviews in Agricultural Science* 4: 56-65

LAMP-FLP for detection of thiophanate-methyl resistant strains of *Fusarium fujikuroi* in Japan

FangJing Li¹, Ryoji Komura², Chiharu Nakashima², Masafumi Shimizu³, Koji Kageyama⁴ and Haruhisa Suga⁵

1. The United Graduate School of Agricultural Science, Gifu University, Gifu 501-1193, Japan

2. Graduate School of Bioresources, Mie University, Tsu, Mie 514-8507, Japan

3. Fac. of Applied Biological Sciences, Gifu University, Gifu 501-1193, Japan

4. River Basin Research Center, Gifu University, Gifu 501-1193, Japan

5. Institute for Glyco-core Research (iGCORE), Gifu University, Gifu, 501-1193, Japan

INTRODUCTION

Fusarium fujikuroi is the pathogen of rice bakanae disease, which results in 3.0–95.4% yield losses (Gupta et al. 2015). Infected plant often exhibits abnormal stem elongation and yellowish leaves. Gibberellin (GA) production in *F. fujikuroi* is considered as a main factor contributing to symptoms of bakanae disease (Singh and Sunder 2012). In addition to GA, *F. fujikuroi* is known to produce mycotoxin fumonisin (FUM), posing a health risk to mankind and animals (Morgavi and Riley 2007). Based on phylogenetic and GA and FUM production analyses, *F. fujikuroi* is subclassified into GA and FUM groups (G- and F-groups) (Suga et al. 2019). G-group strains produce a high amount of GA and are FUM non-producers, whereas F-group strains produce a little or no GA but a high amount of FUM (Suga et al. 2019).

Thiophanate-methyl (TM), a benzimidazole fungicide, has been used to control *F. fujikuroi* for some decades. Representative benzimidazole fungicides include benomyl, carbendazim, and TM. The mode of action of benzimidazole fungicides is binding to tubulin, the sub-unit of microtubules that involved in cellular processes. Two tubulin genes are presented in *F. fujikuroi* (β_1 -tubulin (gene ID: FFUJ04397) and β_2 -tubulin (FFUJ03388)) (Wiemann et al. 2013).

Due to repeatedly application of benzimidazole fungicides, their resistance has been reported in *F. fujikuroi*. In most cases, resistance is correlated with a point mutation in a β -tubulin gene, which results in an amino acid change at the fungicide binding site. An E198V or F200Y mutation in β_2 -tubulin was discovered to be responsible for carbendazim resistance in Chinese *F. fujikuroi* (Chen et al. 2014). However, there is no report for TM resistance in *F. fujikuroi*.

Clarification of the fungicide resistance mechanism, and development of molecular method for monitoring resistance based on the mechanism, are important for the continuing application and the development of new fungicide. A loop-mediated isothermal amplification-fluorescent loop primer (LAMP-FLP), is detection method of a specific single nucleotide polymorphism (SNP). In recent years, LAMP-FLP has been applied to the detection of fungicide resistance in the *Fusarium* head blight pathogen of wheat (Komura et al. 2018).

In this study, mutations in β_2 -tubulin that correlated with TM resistance were investigated in Japanese *F. fujikuroi*, and a LAMP-FLP method was developed for detection of TM-resistant strains.

MATERIALS AND METHODS

TM sensitivity

A mycelial plug with 4 mm diameter was placed at the center of the sterilized PDA medium supplemented with 0, 0.25, 0.5, 0.75, 1, 10, and 100 $\mu\text{g mL}^{-1}$ TM. Three repeats were

conducted for each concentration. After five days of growth at 25°C, colony radius was measured. The minimum inhibitory concentration (MIC) was determined by the growth ability of the strain, and the half-maximal effective concentration (EC₅₀) were calculated based on the colony radius.

PCR and sequencing

PCR amplification for β_1 -tubulin and β_2 -tubulin was performed using AmpliTaq® DNA Polymerase Kit ((Thermo Fisher Scientific, Waltham, MA, USA)). The PCR products were purified by Nucleospin® Extract Kit II Gel (Macherey-Nagel, Düren, Germany), sequenced by Big-Dye terminator V3.1 with cycle sequencing kits (Thermo Fisher Scientific).

LAMP-FLP reaction

LAMP primers and probe sets were designed according to Komura et al. (2018). The LAMP reaction was performed using an LF-8 detecting instrument (Nippon Gene) at 66°C for 35 min. DNA amplification was measured by the turbidity of the LAMP products. An annealing curve from 95°C to 35°C based on the quenching time was then analyzed, using LF-8 Manager software and the LF-8 instrument. The experiment was repeated twice, for confirmation of result consistency.

RESULTS AND DISCUSSION

TM sensitivity

The TM sensitivities of nine strains (five strains were isolated in this study. Three strains were from Suga et al. (2019)) were investigated (Table 1). The MIC of TM sensitive (TMS) strains were 1.0–10.0 $\mu\text{g mL}^{-1}$ and were higher than 100 $\mu\text{g mL}^{-1}$ in TM resistant (TMR) strains. EC₅₀ in TMS strains (3.3–4.1 $\mu\text{g mL}^{-1}$) was lower than that in TMR strains (7.1–12.7 $\mu\text{g mL}^{-1}$). According to previous study (Suga et al. 2019) and the current results, most of G-group strains were resistance to TM, while no of F-group strains were TM-resistant except for one anomalous strain Gfc1521033 (Table 1). TMR selection pressure might impose on the G-group strains due to bakanae pathogen with high GA production.

Mutation in β -tubulin

Comparison of the β_1 - and β_2 -tubulin sequences between TMS and TMR strains indicated that no amino acid substitution occurred in β_1 -tubulin, and either E198K or F200Y mutation in β_2 -tubulin was detected in TMR strains (Table 1). This result revealed that the mutations in β_2 -tubulin are associated with TM resistance in Japanese *F. fujikuroi*.

β -tubulin as the target site of benzimidazole fungicides has been studied intensively. Previous research suggests that β_1 -tubulin functions on sexual reproduction, whereas β_2 -tubulin is important for vegetative growth (Liu et al. 2013). Y50D mutation in β_1 -tubulin was found responsible to

benomyl resistance in *Fusarium verticillioides* (Liu et al. 2013), while mutations E198V and F200Y in β_2 -tubulin were corresponded to carbendazim resistance in *F. fujikuroi*. Present study also revealed that TM resistance is caused by the mutations in β_2 -tubulin, possibly due to the importance of β_2 -tubulin in vegetative growth.

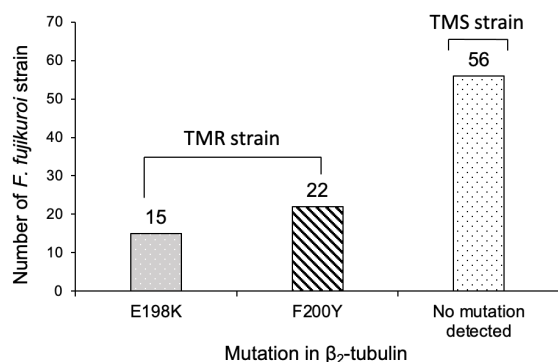


Fig. 1: Thiophanate-methyl resistance and sensitivity and corresponding mutation at positions 198 and 200 in β_2 -tubulin as determined by LAMP-FLP method in *F. fujikuroi*. Fifteen and 22 of 37 TMR strains were detected with E198K and F200Y mutation, respectively. No mutation was detected in 56 TMS strains.

LAMP-FLP analyses

In this study, 93 *F. fujikuroi* strains were used for LAMP-FLP analyses. TM sensitivity of them were previously conducted by Suga et al. (2019). Thirty-seven TMR strains and 56 TMS strains were determined. LAMP-FLP method showed that all of the 37 TMR strains have either of E198K or F200Y mutations, and that none of the 56 TMS strains has these mutations (Fig. 1). LAMP-FLP was successfully detected E198K and F200Y mutations in TMR strains.

Molecular method can monitor the resistance faster than conventional methods. A primer-introduced restriction analysis PCR (PIRA-PCR) was developed to identify E198L and G235G substitution in β_2 -tubulin in carbendazim-resistant *F. fujikuroi* strains (Zhang et al. 2015). However, PIRA-PCR is unable to identify TMR strains in Japanese *F. fujikuroi* as

they have either E198K or F200Y. Previous research indicated that LAMP-FLP was successfully detect F167Y, E198Q, and F200Y in β_2 -tubulin of benzimidazole resistant *F. graminearum* (Komura et al. 2018). LAMP-FLP developed in this study also useful for diagnosis of TM resistance in Japanese *F. fujikuroi*.

REFERENCES

- Chen, Z. H., Gao, T., Liang, S. P. et al. (2014) Molecular mechanism of resistance of *Fusarium fujikuroi* to benzimidazole fungicides. FEMS Microbiology Letters 357: 77-84.
- Gupta, A. K., Solanki, I. S., Bashyal, B. M. et al. (2015) Bakanae of rice – an emerging disease in Asia. Journal of Animal and Plant Sciences 25: 1499-1514.
- Komura, R., Kawakami, T., Nakajima, K. et al. (2018) Simultaneous detection of benzimidazole-resistant strains of *Fusarium* head blight using the loop-mediated isothermal amplification-fluorescent loop primer method. Journal of General Plant Pathology 84: 247-253.
- Liu, S., Duan, Y., Ge, C. et al. (2013) Functional analysis of the beta2 - tubulin gene of *Fusarium graminearum* and the beta-tubulin gene of *Botrytis cinerea* by homologous replacement. Pest Management Science 69: 582-588.
- Morgavi, D. P., and Riley, R. T. (2007) An historical overview of field disease outbreaks known or suspected to be caused by consumption of feeds contaminated with *Fusarium* toxins. Animal Feed Science and Technology 137: 201-212.
- Suga, H., Arai, M., Fukasawa, E. et al. (2019) Genetic differentiation associated with fumonisin and gibberellin production in Japanese *Fusarium fujikuroi*. Applied and Environmental Microbiology 85: e02414-18.
- Singh, R., and Sunder, S. (2012) Foot rot and bakanae of rice: an overview. Review of Plant Pathology 5: 566-604.
- Wiemann, P., Sieber, C. M. K., von Bargen, K. W. et al. (2013) Deciphering the cryptic genome: genome-wide analyses of the rice pathogen *Fusarium fujikuroi* reveal complex regulation of secondary metabolism and novel metabolites. PLoS Pathogens 9: e1003475.
- Zhang, Z., Chen, Z., Hou, Y. et al. (2015) PIRA-PCR for detection of *Fusarium fujikuroi* genotypes with carbendazim- resistance alleles. Plant Disease 99: 1241-1246.

Table 1. Phenotypic and molecular characteristics and thiophanate-methyl sensitivity of strains of *Fusarium fujikuroi*.

Strain	Subgroup ^a	Thiophanate-methyl sensitivity ^b	MIC ($\mu\text{g mL}^{-1}$)	EC ₅₀ ($\mu\text{g mL}^{-1}$) ^c	Amino acid in β_2 -tubulin		Reference
					198 th	198 th	
MAFF235949	G-group	TMS	1<MIC<10	4.07 (0.93)	E	F	Suga et al. 2019
Gfc1524102	F-group	TMS	1<MIC<10	3.85 (0.93)	E	F	This study
Gfc1524502	F-group	TMS	1<MIC<10	3.66 (0.93)	E	F	This study
Gfc0825009	F-group	TMS	1<MIC<10	3.30 (0.93)	E	F	Suga et al. 2019
Gfc1524101	G-group	TMR	100<MIC	12.74 (0.97)	K	F	This study
Gfc1524102Re	G-group	TMR	100<MIC	10.79 (0.98)	K	F	This study
Gfc1524502Re	G-group	TMR	100<MIC	10.55 (0.97)	K	F	This study
Gfc0801001	G-group	TMR	100<MIC	7.09 (0.95)	E	Y	Suga et al. 2019
Gfc1521033	F-group	TMR	100<MIC	9.35 (0.95)	E	Y	H. Watanabe

a The gibberellin and fumonisin groups (G- and F-groups) are subgroups in *F. fujikuroi* (Suga et al. 2019).

b Thiophanate-methyl resistant (TMR) strains grew on PDA with 100 $\mu\text{g mL}^{-1}$ with thiophanate-methyl. Thiophanate-methyl sensitive (TMS) strains did not.

c EC₅₀ for thiophanate-methyl. The correlation coefficient is indicated in parenthesis.

Changes in chlorophyll and carotenoid profiles and gene expression during fruit regreening in Valencia orange

Nichapat Keawmanee^{1,2}, Gang Ma^{2,3}, Lancui Zhang², Masaki Yahata^{2,3}, and Masaya Kato^{2,3*}

1. The United Graduate School of Agricultural Science, Gifu University, 1-1 Yanagido, Gifu-shi, Gifu 501-1193, Japan

2. Department of Bioresource Sciences, Faculty of Agriculture, Shizuoka University, 836 Ohya, Suruga, Shizuoka 422-8529, Japan

3. Graduate School of Integrated Science and Technology, Shizuoka University, 836 Ohya, Suruga, Shizuoka 422-8529, Japan

INTRODUCTION

Citrus fruit accumulate a diversity of pigments at different mature stages. In immature fruit, chlorophylls were massively accumulated in the flavedo. During the maturation, chlorophylls contents decreased rapidly along with the gradual increases in the contents of carotenoids in the flavedo of citrus fruit (Young and Erickson, 1961). In some cultivars, especially Valencia orange, when the fruit is left on the tree till late spring or summer season, the color of the fruit will reverse from orange to green, and this process is called regreening (Caprio, 1956). It was reported that the regreening was correlated with the decreases of carotenoids and the increases of chlorophylls (Thomson et al., 1967). This study aimed to investigate the changes of chlorophyll and carotenoid profiles and gene expression involved in chlorophyll and carotenoid metabolisms in the top and the bottom parts of Valencia orange during the regreening.

MATERIALS AND METHODS

Fruits of 'Valencia orange' (*Citrus sinensis* Osbeck) harvested in April, May, and June from Fujieda farm of Shizuoka University were used as plant materials. After harvest, the flavedos in the top and the bottom parts of the fruit were sampled separately, immediately frozen in liquid nitrogen, and kept at -80 °C until use. Chlorophyll was extracted from flavedos using *N,N*-dimethylformamide and calculated according to Moran's method (1982). The contents of major carotenoids, all-*trans*-vioxanthin (T-vio), 9-*cis*-vioxanthin (C-vio), lutein (Lut), β -cryptoxanthin (β -Cry), and β -carotene (β -Car), were extracted from the flavedos following Kato's method and measured by HPLC (Kato et al., 2004). Regarding gene expression, the total RNA was extracted by using phenol-chloroform according to Kato's method (Kato et al., 2004). The gene expression analysis was carried out by real-time PCR using TaqMan probes and the set of primers for carotenoid biosynthetic genes (*CitPSY*, *CitPDS*, *CitZ-ISO*, *CitZDS*, *CitCRTISO*, *CitLCYb1*, *CitLCYb2*, *CitLCYe*, *CitHYb*, *CitHYe*, and *CitZEP*), chlorophyll biosynthetic genes (*CitGGDR*, *CitCHLH*, *CitCHLM*, *CitCHL27*, *CitPORA*, *CitCS*, and *CitCAO*), and chlorophyll degradation genes (*CitCLH1*, *CitCLH2*, *CitSGR*, *CitPPH*, *CitPAO*, and *CitRCCR*).

RESULTS

The regreening of citrus fruit was observed during the experiment period, especially in June. The color of the flavedo reversed gradually from orange to green, which was related to the increase of chlorophylls contents and decrease of carotenoids contents. In the different parts of the fruit, the result showed that the contents of chlorophyll *a*, *b*, and total chlorophyll in the top part were higher than the bottom part of the flavedo (Fig. 1A). In contrast, the contents of total carotenoid, 9-*cis*-violaxanthin and β -cryptoxanthin were

significantly higher, while the contents of lutein and β -carotene were significantly lower in the bottom part than the top part of the fruit during regreening (Fig. 1B). In this study, the expression of seven chlorophyll biosynthetic genes, six chlorophyll degradation genes, and eleven carotenoid biosynthetic genes was investigated. The up-regulation of chlorophyll biosynthetic genes and down-regulation of chlorophyll degradation and carotenoid biosynthetic genes were observed in the fruit flavedo during regreening. In comparison with the bottom part of the fruit, the expression of genes involved in chlorophyll biosynthesis (*CitCHLH*, *CitCHLM*, *CitPORA*, *CitCS*, and *CitCAO*) was significantly up-regulated in the top part (Fig. 2A), while the expression of chlorophyll degradation genes (*CitCLH2*, *CitSGR*, and *CitRCCR*) was significantly down-regulated in the top part in June (Fig. 2B). The expression of carotenoid biosynthetic genes (*CitPSY*, *CitZDS*, *CitCRTISO*, *CitLCYb1*, *CitLCYb2*, and *CitHYb*) were significantly lower in the top part compared with the bottom part. In contrast, the expression of *CitLCYe* and *CitHYe* in the top part were significantly higher than that in the bottom part in June (Fig. 3).

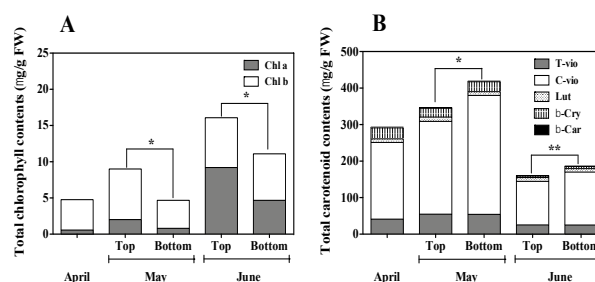


Fig. 1: The contents of chlorophylls (A) and carotenoids (B) in top and bottom parts of fruit flavedo.

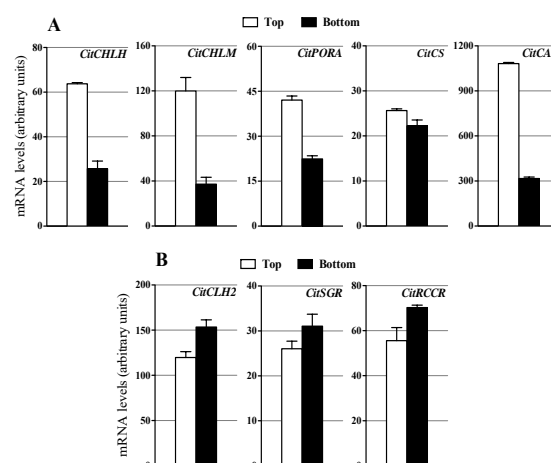


Fig. 2: The expression of genes involved in chlorophyll biosynthesis (A) and chlorophyll degradation (B) in top and bottom parts of fruit flavedo (June).

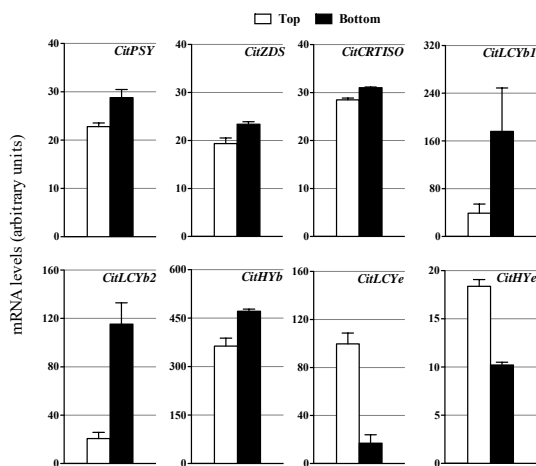


Fig. 3: The expression of genes involved in carotenoid biosynthesis in top and bottom parts of fruit flavedo (June).

DISCUSSION

In general, the citrus fruit turn from green to orange in the winter season. In Valencia orange, when the fruit was left on the tree till spring or summer season, it will reverse from orange to green (Caprio, 1956). In plants, the regreening process was accompanied with the reversion of chromoplasts (carotenoid) to chloroplasts (chlorophyll) and the formation of new chloroplasts (MacKinney, 1961). In the immature fruit, the fruit flavedos accumulated high levels of chlorophyll a, chlorophyll b, and β , ϵ -carotenoids (α -carotene and lutein). In the mature fruit, the contents of chlorophyll a, chlorophyll b, and β , ϵ -carotenoids decreased, and the accumulation of β , β -carotenoids (β -cryptoxanthin, zeaxanthin, all-*trans*-violaxanthin and 9-*cis*-violaxanthin) was observed. (Kato et al., 2004; Ma et al., 2016; Rodrigo et al., 2013). In the present study, the result showed that the contents of chlorophylls were induced, while the contents of carotenoids were decreased in flavedo during the regreening process. Moreover, the regreening was more obviously in the top part than the bottom part of the fruit. Similarly, Coggins and Lewis (1962) reported that the content of chlorophyll was higher in the stem end area than the apical and equatorial area of the flavedo.

The accumulation of chlorophylls and carotenoids was regulated by the expression of genes involved in chlorophyll and carotenoid metabolisms. In citrus fruit, the syntheses of chlorophyll and carotenoid share a common precursor. They are both derived from geranylgeranyl diphosphate (GGPP). The GGPP was converted into chlorophyll a catalyzed by the geranylgeranyl reductase (GGDR) and the tetrapyrrole biosynthetic genes. In the meanwhile, the condensation of GGPP to form phytoene by phytoene synthase (PSY), which was the first key step in the carotenoid biosynthesis (Alós et al., 2006; Ma et al., 2021). During fruit ripening, the expression of chlorophyll biosynthesis genes (*CitGGDR*) was down-regulated, while up-regulation of carotenoid biosynthesis genes (*CitPSY*, *CitPDS*, *CitZDS*, *CitLCYb*, and *CitHYb*) and chlorophyll degradation (*CitPAO*) contributed to carotenoid accumulation in the flavedo of citrus fruit (Kato et al., 2004 and Alós et al., 2006). In this study, the up-regulation of chlorophyll biosynthetic genes (*CitCHLH*, *CitCHLM*, *CitPORA*, *CitCS*, and *CitCAO*) and simultaneous down-regulation of carotenoid biosynthetic genes (*CitPSY*, *CitZDS*, *CitCRTISO*, *CitLCYb1*, *CitLCYb2*, and *CitHYb*) and chlorophyll degradation genes (*CitCLH2*, *CitSGR*, and *CitRCCR*) were observed in the top part during regreening. In addition, the expression of *CitLCYe* was up-regulated in the top part of the fruit. Similarly, Kato et al.

(2004) report that the expression of *CitLCYe* was high in the green fruit and it decreased when the fruit turned orange.

In conclusion, the results presented in this study suggested that the reduction of β , β -xanthophylls (β -cryptoxanthin, zeaxanthin, all-*trans*-violaxanthin, and 9-*cis*-violaxanthin) was related to the down-regulation of carotenoid biosynthetic genes, while the accumulation of chlorophyll was related to the up-regulation of chlorophyll biosynthetic genes and down-regulation chlorophyll degradation genes in the flavedo during the regreening process. In addition, the regreening was more evident in the top part of the fruit than the bottom part, which indicated that the regreening process might start from the top part of the citrus fruit.

ACKNOWLEDGMENTS

This work was supported by KAKENHI Grant Numbers JP20H02976 (to M.K.) from Japan Society for the Promotion of Science (JSPS).

REFERENCES

- Alós, E., Cercós, M., Rodrigo, M.J., Zacarías, L., and Talón, M. (2006) Regulation of color break in Citrus fruits. Changes in pigment profiling and gene expression induced by gibberellins and nitrate, two ripening retardants. *Journal of Agricultural and Food Chemistry* 54: 4888-4895.
- Caprio, J.M. (1956) An analysis of the relation between regreening of Valencia oranges and mean monthly temperatures in Southern California. *Proceedings of the American Society for Horticultural Science* 61: 222-35.
- Coggins, C.W. and Lewis, L.M. (1962) Regreening of Valencia orange as influenced by potassium gibberellate. *Plant Physiology* 37: 625-627.
- Kato, M., Ikoma, Y., Matsumoto, H., Sugiura, M., Hyodo, H., and Yano, M. (2004) Accumulation of carotenoids and expression of carotenoid biosynthetic genes during maturation in citrus fruit. *Plant Physiology* 134: 824-837.
- MacKinney, G. (1961) Coloring matters, In "The Orange, Its Biochemistry and Physiology". (W. B. Sinclair, Ed.) Univ. of Calif. Printing Dept. 302-333.
- Ma, G., Zhang, L.C., Yungyuen, W., Tsukamoto, I., Iijima, N., Oikawa, M., Yamawaki, K., Yahata, M., and Kato, M. (2016) Expression and functional analysis of citrus carotene hydroxylases: Unraveling the xanthophyll biosynthesis in citrus fruits. *BMC Plant Biology* 16: 148.
- Ma, G., Zhang, L.C., Kitaya, Y., Seoka, M., Kudaka, R., Yahata, M., Yamawaki, K., Shimada, T., Fujii, H., Endo, T., and Kato, M. (2021) Blue LED light induces regreening in the flavedo of Valencia orange in vitro. *Food Chemistry* 335: 127621.
- Moran, R. (1982) Formulae for determination of chlorophyllous pigments extracted with *N,N*-dimethylformamide. *Plant Physiology* 69: 1376-1381.
- Rodrigo, M.J., Alquézar, B., Alós, E., Lado, J., and Zacarías, L. (2013) Biochemical bases and molecular regulation of pigmentation in the peel of Citrus fruit. *Scientia Horticulturae* 163: 46-62.
- Thomson, W.W., Lewis, N., and Coggins, C.W. (1967) The reversion of chromoplasts to chloroplasts in Valencia oranges. *Cytologia* 32: 117-124.
- Young, L.B., and Erickson, L.C. (1961) Influence of temperature on color change in Valencia oranges. *Proceedings of the American Society for Horticultural Science* 78: 197-200.

Modified newmark approach for evaluation of earthquake-induced displacement of earthdams

Phuong Le-Hong¹, Shin-ichi Nishimura², and Tatsuro Nishiyama²

1. The United Graduate School of Agricultural, Gifu University, Gifu, Japan

2. Faculty of Applied Biological Sciences, Gifu University, Gifu, Japan

INTRODUCTION

Newmark (1965) proposed a simple approach for evaluating the potential deformation of earth dams and embankments due to earthquake shaking based on a rigid slide block above the slippage surface, known as the conventional Newmark sliding block approach. Due to its simplicity and efficiency, the conventional Newmark approach has been widely applied in practice. The procedure requires that the value of the yield acceleration or yield seismic intensity be determined for the potential failure surface using conventional limit equilibrium methods. The ordinary method of slices, or Fellenius method, is commonly used in the conventional Newmark approach to calculate the factor of safety as well as the yield seismic intensity. However, this method ignores the forces between the slices needed to facilitate the calculation. When compared to the rigorous methods, which take into account the forces between the slices, the factor of safety of the Fellenius method is smaller (Duncan and Wright 1980). Therefore, it can be predicted that the amount of displacement calculated by the conventional Newmark approach will be larger than that calculated by a strict method.

As is known, the acceleration time history data is the acceleration data measured at certain time intervals of an earthquake. At any given time interval, when the seismic acceleration exceeds the yield acceleration, the sliding mass will slip. However, in the conventional Newmark approach used at present, the change in the position of the sliding mass at that interval is not considered much in the analysis. Therefore, the fixed sliding mass position in the conventional Newmark approach may lead to unreliable estimations of seismic slope deformations. Nishimura et al. (2020) considered the changing of the sliding mass position through the re-division of the sliding mass as the sliding mass moves at the time steps of the acceleration time history data. However, they also used the Fellenius method to calculate the earthquake-induced permanent displacement.

In this study, therefore, a modified Newmark approach is proposed to evaluate the seismic displacement of an earth dam based on the changing position of the sliding mass over time. In the proposed procedure, the change in the sliding mass position is taken into account by re-dividing the slip mass in the time step of the slip occurrence. Moreover, a relatively easy method among the strict methods is used, namely, the simplified Bishop method, to evaluate the yield seismic intensity. Seismic displacements are evaluated and compared for the Fellenius and simplified Bishop methods in both conventional and modified Newmark approaches.

THE NEWMARK METHODOLOGY

Factor of safety F_s in the ordinary method of slices, or the Fellenius method, is given by the ratio of resisting moment M_R and driving moment M_D , as

$$F_s = \frac{M_R}{M_D} = \frac{R \sum [C \cdot l + (W \cdot \cos \alpha - u \cdot l - k_h \cdot W \cdot \sin \alpha) \tan \varphi]}{\sum [W \cdot x_g + k_h \cdot W \cdot y_g]} \quad (1)$$

By assigning unity to F_s , the equation can be rearranged in terms of the yield seismic intensity as

$$k_y = \frac{R \sum [C \cdot l + (W \cdot \cos \alpha - u \cdot l) \tan \varphi] - \sum W \cdot x_g}{\sum [W \cdot y_g + W \cdot \sin \alpha \cdot \tan \varphi]} \quad (2)$$

The simplified Bishop method is a stricter method than the Fellenius method, in which normal interaction forces between adjacent slices are assumed to be collinear and the resultant interslice shear force is zero. By considering horizontal seismic intensity k_h , the original formulation by Bishop (1955) can be rewritten as

$$F_s^* = \frac{M_R}{M_D} = \frac{R \sum [c \cdot b + (W - b \cdot u) \tan \varphi] / m_\alpha}{\sum [W \cdot x_g + k_h \cdot W \cdot y_g]} \quad (3)$$

$$m_\alpha = \cos \alpha + \frac{\tan \varphi \cdot \sin \alpha}{F_s}$$

In a manner similar to the Fellenius method, the yield seismic intensity based on the Bishop method is obtained as

$$k_y^* = \frac{R \sum [c \cdot b + (W - u \cdot b) \tan \varphi] / m_\alpha - \sum W \cdot x_g}{\sum W \cdot y_g} \quad (4)$$

As mentioned earlier, the changing position of the sliding mass over the time intervals in the seismic data is ignored in the conventional Newmark sliding block approach. Thus, the values for x_g and y_g in Eqs (2) and (4) do not change along with the other parameters for the slip surface and sliding mass, resulting in yield seismic intensity that does not change over time. In addition, when applying the method of slices (Fellenius or Bishop method) in the conventional Newmark approach, the sliding mass above the slip surface is only subdivided once into vertical slices at the initial static state. However, when the sliding mass moves, the edges of the slice are no longer vertical as they were at first.

A modified Newmark procedure is developed to address the above-mentioned drawbacks. The determination of the yield seismic intensity is carried out in this modified version based on the Fellenius and Bishop methods. The effect of the changing position of the sliding mass during an earthquake on the predicted permanent displacements is also considered.

VERIFICATION

To verify the applicability of the modified Newmark procedure, an agricultural earth-fill dam, the Ijira Dam, 18 m in height and located in Yamagata City, Gifu Prefecture, Japan, was analyzed. This dam was under repair from 2016 to 2017, but this study only focuses on analyzing it before its repair. As a means of verification, the results obtained by the proposed approach were compared with those obtained from the conventional Newmark approach. The input acceleration time history in the horizontal direction, used in this study and based on the EW component of the 2011 off the Pacific coast of Tohoku-Pacific Earthquake.

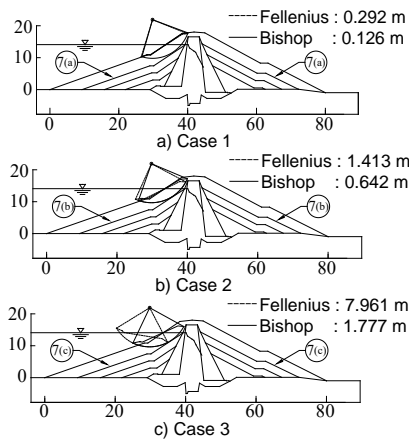


Fig. 1: Sliding displacement results with Conventional Newmark approach

Figure 1 presents the results of the sliding displacement based on the Fellenius and Bishop methods for the three calculation cases when the conventional Newmark approach is applied. It can be seen that, in Case 1, the sliding displacement is small with both Fellenius and Bishop methods. The difference between the two methods is not significant, with the results of the Fellenius method being slightly larger than those of the Bishop method by about 0.16 m. However, in Cases 2 and 3, since the shear strength parameters of soil material No. 7 are assumed to have decreased, the sliding displacements with both methods are larger than in Case 1, especially that of Case 3. The application of the Bishop method yielded smaller results than the Fellenius method, as was analyzed in section 2. Moreover, it was found that, with the conventional Newmark approach, the difference between the Fellenius and Bishop methods is large when the sliding mass moved as much as it did in Case 3 (Fig. 1c). The results of the sliding displacement with the Bishop and Fellenius methods for the three cases are shown in Fig. 2 according to the modified Newmark approach. It can be clearly seen that the results of the Bishop and Fellenius methods have decreased, especially those with the Fellenius method in Case 3. The difference between the Fellenius and Bishop methods is no longer as large as with the conventional Newmark approach. This proves that the re-division of the sliding mass in the modified Newmark approach is effective with both Bishop and Fellenius methods.

According to the design guidelines for land reclamation projects, "reservoir maintenance" (MAFF 2015), it is difficult to give specific values for the allowable settlement of reservoirs, but they include (1) the difference in elevation between the top of the dam and the normal water level (NWL), (2) the difference in elevation between the top of the dam and the designed high water level (HWL), and (3) 1.0 m (taking into account the extra height and freeboard). It can be seen that with hypothetical Cases 2 and 3, when calculating according to the conventional Newmark approach, it is highly possible that the results of the sliding displacement will be larger than the allowable settlement, especially with the Fellenius method. Accordingly, no guarantee can be given for the dam's seismic performance against level 2 earthquake motion. This will lead to a costly, wasteful solution for ensuring the dam's performance against level 2 earthquake motion. However, when applying the modified Newmark approach, the results of the sliding displacement are smaller than the allowable settlement with both Fellenius and Bishop methods for Case 2, and with the Bishop method for Case 3. Therefore, the application of the modified Newmark approach,

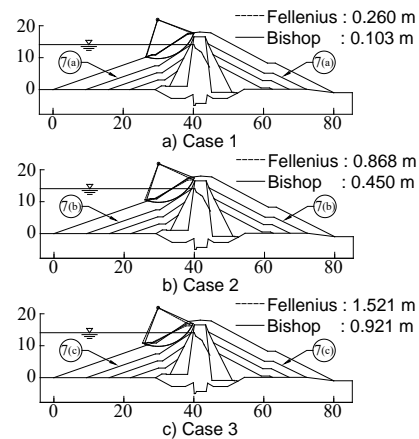


Fig. 2: Sliding displacement results with Modified Newmark approach

combined with the Bishop method, will provide a less conservative design solution.

CONCLUSIONS

In this study, a modified Newmark approach has been presented to evaluate the earthquake-induced permanent displacement of an earth dam based on the changing position of the sliding mass by re-dividing the sliding mass by time steps when slip occurs. Comparing the results of the modified and the conventional Newmark approaches, there is a noticeable difference between the obtained displacements. The difference confirms that ignoring the change in the slip surface position during an earthquake can produce an inconsistent yield seismic intensity (constant value), and result in an overly conservative displacement estimate. Through verification for one agricultural dam, with two hypothetical cases (cases 2 and 3), the displacement results, according to the conventional Newmark approach, may be outside the allowable settlement range with both methods Fellenius and Bishop. But with the modified Newmark approach, the values of that displacement are still within that range with both methods Fellenius and Bishop for case 2 and with the Bishop method for case 3. Thus the modified Newmark approach, combined with the simplified Bishop method, a method that is stricter than the Fellenius method, leads to a more realistic assessment of the permanent displacement in seismic slope stability analyses.

REFERENCES

- Bishop A. W., (1955) The Use Of The Slip Circle in The Stability Analysis of Slopes, *Geotechnique*, Vol. 5, No. 1, pp. 7–17.
- Duncan J. M. and Wright S. G., (1980) The Accuracy of Equilibrium Methods of Slope Stability Analysis, *Engineering Geology*, Vol. 16, No. 1–2, pp. 5–17.
- Ministry of Agriculture, Forestry and Fisheries of Japan (MAFF), (2015) Land Improvement Project Design Guideline "Reservoir maintenance.", pp. 125–129.
- Newmark N. M., (1965) Effects of Earthquakes on Dams and Embankments, *Geotechnique*, Vol. 15, No. 2, pp. 139–160.
- Nishimura S., Nishiyama T., Hiramatsu K., and Senge M., (2020) Newmark's Method Considering Redivision of Sliding Mass: Application to Agricultural Fill Dam, *The Japanese Society of Irrigation, Drainage and Rural Engineering*, Vol. 88, No. 2, pp. 213–218. (In Japanese)

Development of a HS-SPME/GC-MS method for the extraction and identification of the volatile compounds in coffee

Fawzan Sigma Aurum^{1,2}, Teppei Imaizumi¹, Manasikan Thammawong¹ and Kohei Nakano^{1*}

1. The United Graduate School of Agricultural Science, Gifu University, 1 – 1 Yanagido, Gifu, 501-1193 JAPAN

2. Assessment Institute for Agricultural Technology of Bali, Indonesian Agency for Agricultural Research and Development, Ministry of Agriculture, Denpasar, Bali, 80222 INDONESIA

INTRODUCTION

The unique flavor and aroma of coffee can be attributed to its volatile compounds and other metabolites. Volatile metabolites compounds of coffee can be extracted using various methods. Steam distillation and solvent extraction are often used. However, both methods may lead to thermal artifacts (Prososki et al., 2007). Currently, Head Space Solid Phase Micro Extraction (HS-SPME) has been widely employed to extract volatiles of coffee.

Compared to liquid-liquid extraction, such headspace extraction techniques have several advantages, including solvent-free sample preparation, a quick extraction time, a little volume of sample required, and fewer labor requirements. The SPME is based on compound adsorption on a fiber covered with a polymer, commonly known as the extraction phase. Several polymers with varying polarity are presently available, and compound desorption in GC is often accomplished using a thermal technique. Polar chemicals are sorbed on polar fibers, whereas nonpolar compounds are sorbed on nonpolar fibers. Aside from the fiber's composition, numerous additional factors such as extraction temperature and length, equilibration time, desorption time, and agitation can all impact the SPME technique.

A novel SPME-Arrow technology has emerged in recent years. This method employs a greater amount of sorbent material to increase detection limits in SPME fibers, which are less fragile than standard SPME fibers. Since its inception, the SPME-Arrow approach has been used to evaluate the volatile constituent in fish sauce (Song et al., 2019), contaminated water (Kremser et al., 2016), and wastewater (Helin et al., 2015). Based on our literature study, SPME-Arrow has never been utilized for the volatile compound evaluation of roasted coffee.

This research aims to determine the optimum extraction temperature of the SPME arrow using HS-SPME for volatile compounds identification. This study uses coffee from the class of *Coffea Arabica* and *Coffea Canephora P* (Robusta) collected from four famous coffee-producing locations in Indonesia. Volatile profiling was done by the GC-MS system employing an untargeted method. Therefore, to process and extract the informative data, chemometrics modeling was used.

MATERIALS AND METHODS

Materials

Coffee beans from 4 locations in Indonesia of the crop year 2020 were used (Arabica Gayo - Aceh, Arabica Kintamani – Bali, Robusta Lampung – Sumatera, Robusta Jawa – West Java). Sample was roasted in a small batch roaster machine capacity of 500 gram (WE 600I, Indonesia) using controlled temperature at 200°C for 12 minutes, followed by fan-assisted cooling 10 minutes. Coffee was ground into powder followed by screening with Ø 425 µm test sieve (Retsch, UK). Coffee sample was stored at -80°C until further use. The chemical reagent used was 3-heptanone purchased from Sigma-Aldrich (Merck KGaA: St. Louis, Missouri, United States)

Sample preparation and volatile extraction

Coffee powder sample 1 gram was transferred into a 20 mL vial with a laminated PTFE screw cap.

The procedure of extracting the volatile compounds was based on headspace extraction. The internal standard (10 µl of 1 µl/ml 3-heptanone) was spiked to the sample vial before incubation. A thermostatic system was used to incubate the vial. Two optimization temperatures were employed for volatile extraction, i.e., 70°C and 50°C. Firstly, the vials were incubated for 10 minutes. Then, the SPME-arrow needle was injected into the vial for extraction for 10 minutes for both temperature treatments. Volatile extraction was done using SPME-Arrow PDMS (O.D.: 1.1 mm, film thickness: 100 µm, length: 20 mm) purchased from Shimadzu (Shimadzu Corporation, Kyoto, Japan). Prior to extraction, the SPME-Arrow was equilibrated at GC Injector port 250°C for 15 minutes.

GCMS experimentation

The volatile compounds analysis from the coffee head space were performed using a GC 2030 Nexis (Shimadzu, Japan) coupled to a Shimadzu Mass Spectrometer-TQ8040 NX (Shimadzu, Japan) with the column: 30 m x 0.250mm x 1.0 µm DB-5 (Agilent Technology, Inc, US). Injection system: Splitless. Temperature program employed was as follows: 0-4 min (40 °C); 5-25 min at 10 °C/min to 250 °C; hold at 250 °C (5 min). The carrier gas used was Helium with the flow rate at 1.5 ml/min. The molecular fragmentation was obtained by electron ionization (EI) 70eV with scan interval: 1.0 sec. Scan mode employed was full scan, in the range: 40 – 400 amu. Total ion chromatograms (TIC) were processed using the built-in processing software.

Data Processing

The mass spectra from Shimadzu dedicated file were converted to NETcdf for ease of analysis. Then the fragmentation of each compound was compared to the database (NIST17 and open source library at RIKEN PRIME) to identify the compounds. Data deconvolution and alignment was done in MSDIAL using the n-alkane standard (Tsugawa et al., 2015). Furthermore, the identification was accomplished by comparing the retention indices (RI) of volatiles under the experimental condition with the data from the databases. Only compounds with match probability > 80% (considered an acceptable match) were included. Data were normalized by the internal standard followed by data rearrangement in R-Studio.

Multi-variate data analysis was done using Random Forest (RF) in R employing the RandomForest package (Liaw and Wiener, 2002). The features were auto-scaled, the number of trees selected was 250, the number of features tried at each split was 8. The top important metabolites features were selected based on the Decreased Mean Accuracy algorithm from the RF model.

The model was built based on the training samples (N = 6) for each coffee origin. The model was then applied to predict the coffee origin of the validation samples (N = 3). Training and validation samples were coffee from different villages from the same location. The most optimum temperature extraction

method was selected based on the comparison of the accuracy and area under the curve from both models.

RESULTS AND DISCUSSION

Data deconvolution and alignment in MS-DIAL identified 125 references matched and 409 unknown compounds for the coffee volatiles extracted at the temperature of 70° C for 10 minutes. Another extraction temperature, 50° C for 10 minutes, resulted in 112 references matched and 380 unknown metabolites. After removing the redundant features and filtering the detected features with blank, 78 compounds and 77 compounds were determined for 70°C and 50°C extraction temperature, respectively.

Model evaluation was performed using several indicators as indicated in Table 1. Based on the model evaluation, the results of the study showed that extraction temperature at 70°C for 10 minutes performed better than 50°C. Prediction accuracy of the model based on the validation sample was performed by employing a confusion matrix. Out of Bag (OOB), estimate error rate is a way to measure the error prediction of an RF model. Multiclass Area Under the Curve was performed to evaluate the class separation based on the RF model.

Table 1. Random Forest model performance parameter based on the extraction times

Extraction Temp	Prediction Accuracy	OOB Error rate	Multiclass AUC
50°C	91.67%	16.67%	0.972
70°C	100%	0.00%	1.000

Furthermore, the model can be employed to find the important features that lead to the classification. Table 2 shows the top 10 important features for both extraction temperatures. The important volatile compounds were selected based on the Mean Decrease (MD) Accuracy score and Mean Decrease (MD) Gini value. The important metabolites at the extraction temperature of 50°C showed differ to 70° C.

Overall, the composition of the top ten important compounds are from the furans, phenols, pyrazines, and pyridines. These compounds are available in roasted coffee together or bind with hydrocarbons, acids and anhydrides, esters, alcohols, and sulfur compounds. These compounds vary in concentration and sensory potency, which explains why different coffee types have distinct flavors. Furans and

pyrazines, the Maillard-reaction products, are generated by various chemical processes, including heat oxidation of lipids and thermal degradation of carbohydrates.

However, several volatile compounds selected as important features were overlapping in the two treatments. For instance, Ethoxybenzene and 6-Amino-6-methylfulvene which are shared in both treatments. Both compounds are aromatic with a pleasant smell. However, most of the selected features are unique to each treatment. The first important volatile for 50°C, 4-Ethyl-2-methoxyphenol, is included in the phenolic constituent associated with flavor in cooked foods, resulting in a roasted-like aroma. On the other hand, the first important volatile extracted by the 70°C method was from the pyridazine group. It is a heterocyclic aromatic organic compound commonly found in coffee.

The higher extraction temperature shows a higher classification of coffee origin. This result may be associated to the compounds having a higher boiling point. It is commonly understood that brewing coffee at a higher temperature below the water boiling point induced pleasant aroma and flavor.

The performance of the Random Forest model evaluated using several accuracy parameters shows that extracting the volatile at 70°C for 10 minutes results in better classification. Therefore, this information is beneficial for the future study of coffee classification based on volatile metabolites profile.

REFERENCES

- Helin, A., Rönkkö, T., Parshintsev, J., Hartonen, K., Schilling, B., Läubli, T., & Riekkola, M. L. (2015). Solid phase microextraction Arrow for the sampling of volatile amines in wastewater and atmosphere. *Journal of Chromatography A*, 1426, 56–63.
- Kremser, A., Jochmann, M. A., & Schmidt, T. C. (2016). PAL SPME Arrow - Evaluation of a novel solid-phase microextraction device for freely dissolved PAHs in water. *Analytical and Bioanalytical Chemistry*, 408(3), 943–952.
- Liaw A. and M. Wiener. (2002). Classification and Regression by randomForest. *R News* 2(3), 18-22.
- Prososki, R. A., Etzel, M. R., & Rankin, S. A. (2007). Solvent type affects the number, distribution, and relative quantities of volatile compounds found in sweet whey powder. *Journal of Dairy Science*, 90(2), 523–531.
- Song, N. E., Lee, J. Y., Lee, Y. Y., Park, J. D., & Jang, H. W. (2019). Comparison of headspace-SPME and SPME-Arrow-GC-MS methods for the determination of volatile compounds in Korean salt-fermented fish sauce. *Applied Biological Chemistry*, 62(1).
- Tsugawa, H., Cajka, T., Kind, T., Ma, Y., Higgins, B., Ikeda, K., Kanazawa, M., VanderGheynst, J., Fiehn, O., & Arita, M. (2015). MS-DIAL: data-independent MS/MS deconvolution for comprehensive metabolome analysis. *Nature Methods*, 12(6), 523–526.

Table 2. Top ten important volatile compounds of coffee using extraction temperature of 70°C and 50°C based on Random Forest

Volatiles (IUPAC)	Extraction Temperature 50° C					Volatiles (IUPAC)	Extraction Temperature 70° C				
	RI	RT	m/z	MD Accur acy*	MD Gini **		RI	RT	m/z	MD Accu racy*	MD Gini **
4-ethyl-2-methoxy-phenol	1291.1	18.4	137.1	5.231	0.851	2H- Cyclopenta [d]pyridazine	1224.7	17.4	118.1	4.944	0.615
4-Methylthiazole	815.56	9.74	99	5.184	0.973	1-methyl-1H-pyrrole-2-acetonitrile	1120.2	15.7	119	4.707	0.597
Ethoxybenzene	979.0	13.17	94.05	4.866	0.714	Furfural	832.7	10.1	96.0	4.629	0.564
Phenol, 2-methoxy-	1099.44	15.33	109.05	4.302	0.630	3,5-Diethylphenol	1328.6	18.9	150.1	4.612	0.648
2-Heptanol	899.79	11.58	45.5	4.206	0.565	2-Ethyl-4,5-dimethylphenol	1329.1	18.95	150.1	4.431	0.528
2-Furanmethanol-acetate	992.32	13.4	81.05	4.136	0.495	6-Amino-6-methylfulvene	963.0	12.85	107.1	4.264	0.510
6-Amino-6-methylfulvene	964.2	12.8	107.07	4.098	0.587	2,5-dimethyl-1H-Pyrrole	871.6	10.9	94.0	4.081	0.540
2-Ethyl-6-methylpyrazine	1001.6	13.58	121.1	3.966	0.498	3-Hydroxypyridine-monoacetate	1066.08	14.773	95.04	4.015	0.486
2,5-Dimethyl-1H-pyrrole	872.03	10.9	94.05	3.865	0.498	1-Propionylethyl acetate	959.1	12.78	43	3.97	0.563
2-Methyl-5-(methylthio) furan	1234.9	17.5	81.05	3.79	0.505	Ethoxybenzene	979.0	13.17	94.05	3.955	0.471

Note: * Mean Decrease (MD) Accuracy based on Random Forest Model; ** Mean Decrease (MD) Gini based on Random Forest Model

Development of a program for constructing ortholog data set using taxonomic information

Tomoaki Watanabe¹ and Tokumasa Horiike²

1. The United Graduate School of Agricultural Science, Gifu University
2. Department of Bioresource Sciences, Shizuoka University

INTRODUCTION

Orthologs, which are genes derived from speciation, have been used for species phylogenetic inference because their phylogenetic relationships correspond to that of species. The rRNA gene is a typical example of such genes (Woese et al. 1990), but there are also some problems in using it for species phylogenetic inference because the number of rRNA genes in a genome may differ between species. In such a case, the number of the genes is considered to have increased due to gene duplication. Genes derived from gene duplication are called paralogs and genes generated by gene duplication before speciation are called out-paralogs in particular. It has been an important issue to distinguish orthologs and out-paralogs because the phylogenetic relationship of the out-paralogs does not correspond to that of species because out-paralogs remain information of gene duplication (Tekaia 2016). In recent years, with the rapid increase in the amount of available sequence information in databases, the methods of using multiple orthologs for species phylogenetic inference have become popular to reduce the effects of errors in individual ortholog inference and increase the accuracy of the analysis (Gadagkar et al. 2005). However, these are not fundamental solutions to the problem of distinguishing paralogs. Therefore, there is still a strong need for methods to construct highly accurate ortholog datasets that exclude paralogs. Although several programs to construct orthologs datasets are already reported, they were mainly developed for prediction of gene function and consequently allow for the contamination of out-paralogs and especially those in which one gene is deleted after gene duplication (called hidden out-paralogs, Horiike et al. 2016; Train et al. 2017) are prone to contamination. Therefore, the existing programs are not suitable for constructing datasets for species phylogenetic analysis. For these reasons, "Ortholog Finder" which is the first program to construct orthologs data set that can remove out-paralogs and even hidden out-paralogs are developed in previous research (Horiike et al. 2016). Ortholog Finder was able to detect out-paralogs from the phylogenetic tree of candidate ortholog groups using taxonomic information such as out-groups and in-groups. However, there was a limitation in the removal of hidden out-paralogs because the available taxonomic information was limited to two. In addition, there were technical problems such as long running time, inability to handle large-scale analysis, and low maintainability due to using many kinds of development language. Therefore, the purpose of this study was to develop a new ortholog dataset construction program that solves these problems and to evaluate its performance.

METHODS

The ortholog inference of the improved Ortholog Finder is composed of the following five processes. 1) Prediction and removal of horizontally transferred genes from the input sequences (default: off). 2) Calculation of similarity scores between all sequences by the homology search program and normalization of each score (Emms and Kelly 2015). 3) Clustering of genes to create candidate ortholog groups. 4) Phylogenetic tree inference of candidate ortholog groups. 5) Detection and removal of out-paralogs using candidate ortholog

groups phylogenetic trees and taxonomic information. It is also possible to infer the species phylogenetic trees based on the created ortholog dataset (default: on).

We evaluated the performance of the improved Ortholog Finder with evolutionary simulated protein sequences as follows. First, we generated gene phylogenetic trees from the model phylogenetic tree by Zombi (Davin et al. 2019). In this process, gene duplications occurred with a certain probability in each gene tree. Next, we generated protein sequence data based on each gene phylogenetic tree using INDELible (Fletcher and Yang 2009). Then, we randomly deleted the paralogs in each generated homolog group, leaving one. This makes all out-paralogs hidden out-paralogs. Using the sequence data generated by the above process, we executed Ortholog Finder to construct an ortholog dataset (previous version), improved Ortholog Finder, OMA (Altenhoff et al. 2019), and OrthoFinder (Emms and Kelly 2019) programs, respectively. For each ortholog dataset, we calculated "Recall" (proportion of inferred orthologs to all orthologs), "Precision" (proportion of true orthologs to inferred orthologs), "Tree" (proportion of inferred orthologs whose phylogenetic tree matched the species phylogenetic tree), and "Species" (proportion of species phylogenetic trees inferred from the orthologs data set that matched the model phylogenetic tree) for each ortholog dataset. The numbers of iterations for the analyses were set to 100. We also evaluated the performance of the programs using real protein-sequence data provided by Quest for Orthologs (Altenhoff et al. 2016). In this test, the 78 species to be analyzed were selected from three domains: bacteria, archaea, and eukaryotes. The accuracy of ortholog inference was evaluated by the percentage of agreement between the true phylogenetic tree of the species (provided by Quest for Orthologs) and the phylogenetic tree of the inferred orthologs in the test of Quest for Orthologs.

RESULTS AND DISCUSSIONS

The result of the performance tests with simulated protein sequences is shown in Fig. 1. The sequences were generated based on a model species tree with 32 OTU (Operational Taxonomic Unit). The ortholog dataset generated by improved Ortholog Finder has a higher percentage in "Precision" than that generated by the original Ortholog Finder, OMA, and OrthoFinder. This suggests that each ortholog in the improved Ortholog Finder dataset are more reliable than that in the ortholog dataset generated by the other programs. As shown in "Species" of Fig. 1, the phylogenetic tree using the improved Ortholog Finder dataset has the highest percentage of species phylogenetic trees that matched the model phylogenetic tree out of 100 iterations. This suggests that the ortholog dataset constructed by the improved Ortholog Finder can be used to inference the phylogeny of species more accurately than the ortholog datasets generated by the existing programs.

The agreement between phylogenetic trees of each ortholog and the species phylogenetic tree was low overall. However, the accuracy of species phylogenetic inference was much higher in the improved Ortholog Finder, suggesting that the negative effect of such a low agreement percentage on species phylogenetic inference is small. In addition, Recall was also higher in the previous Ortholog Finder than in the improved

Ortholog Finder. This is because the previous Ortholog Finder used only two taxonomic information for ortholog inference and the threshold for ortholog detection was low. Since the threshold of ortholog detection becomes stricter when more taxonomic information is used, the improved Ortholog Finder had lower Recall than the others. However, Fig 1. shows the strict threshold of improved Ortholog Finder leads to accurate species phylogenetic inference. Also, OMA and OrthoFinder are high recall than improved Ortholog Finder. This is because the paralog detection methods are different. OMA uses a comparison of the evolutionary distance of candidate orthologs to detect out-paralogs. A very simple explanation of the principle is that the evolutionary distance between orthologs is smaller than between out-paralogs. OrthoFinder infers the rooted phylogenetic tree of species from the inferred orthogroups and detects paralogs by comparison with the species tree. Both methods cannot accurately detect out-paralogs under the conditions of this evaluation test because duplicate genes must remain in order for out-paralog detection. Therefore, almost all genes are not removed and the Recall is high while Precision is low. This means that the difference in the Recall of each program means that only Ortholog Finder was able to remove more out-paralogs correctly. We constructed an ortholog dataset for "2018's Quest for Orthologs protein dataset" and performed the benchmark test. The results of this test show RF (Robinson Foulds) distance between the species phylogenetic tree for LUCA (Last Universal Common Ancestor) and the phylogenetic trees of orthologs generated by each program (Fig. 2). RF distance is a scale for the similarity between two phylogenetic tree topologies. If the topologies for two phylogenetic trees are closer, the RF distance is smaller. Ortholog Finder has the smallest RF distance to the species phylogenetic tree. This indicates that Ortholog Finder has high accuracy in ortholog inference and is the program that can construct the most suitable ortholog dataset for species phylogeny inference. We evaluated the performance of the program using simulated ortholog data and published sequence data provided by Quest for Orthologs. The results of the performance tests using a simulation program suggest that improved Ortholog Finder can accurately remove paralogs even under severe conditions that many genes that are duplicated before speciation have been deleted differentially. The percentage in "Precision" and "Species" of improved Ortholog Finder (provided ten taxonomic information) was higher than improved Ortholog Finder (provided three taxonomic information), respectively. This result suggests that the accuracy of orthologs inference was further enhanced by using more taxonomic information. Based on the results of the Quest for Orthologs benchmark test, the improved Ortholog Finder showed a smaller RF distance than that of the existing programs. This indicates that the improved Ortholog Finder also can accurately infer orthologs under real conditions where out-paralogs and hidden out-paralogs are mixed. It shows that the improved Ortholog Finder is particularly suitable for constructing ortholog data sets for phylogenetic inference of species, which is our motivation.

REFERENCES

Altenhoff, A. M. et al. (2016) Standardized benchmarking in the quest for orthologs. *Nature Methods* 13:425-430.
Altenhoff, A. M. et al. OMA standalone: Orthology inference among public and custom genomes and transcriptomes. (2019) *Genome Research*. 29
Davín A. A. et al. (2019) Zombi: a phylogenetic simulator of trees, genomes and sequences that accounts for dead lineages. *Bioinformatics* 36.1286-1288.

Emms, D. M. & Kelly, S. (2015) OrthoFinder: solving fundamental biases in whole genome comparisons dramatically improves orthogroup inference accuracy. *Genome Biology* 16.
Emms, D. M. & Kelly, S. OrthoFinder: Phylogenetic orthology inference for comparative genomics. (2019) *Genome Biology*. 20.
Fletcher and Yang (2009) INDELible: A Flexible Simulator of Biological Sequence Evolution. *Molecular Biology and Evolution*. 26. 1879-1888.
Gadagkar S, et al. (2005) Inferring species phylogenies from multiple genes: Concatenated sequence tree versus consensus gene tree. *Journal of Experimental Zoology*, 304:64-74.
Horiike T et al. (2016) Ortholog-Finder: A Tool for Constructing an Ortholog Data Set. *Genome Biology and Evolution*. 8. 446-457.
Tekaia, F. (2016) Inferring orthologs: Open questions and perspectives. *Genomics Insights* 9.
Train et al. (2017) Orthologous Matrix (OMA) algorithm 2.0: more robust to asymmetric evolutionary rates and more scalable hierarchical orthologous group inference. *Bioinformatics*. 33. i75-i82.
Woese C et al. (1990) Towards a natural system of organisms: proposal for the domains Archaea, Bacteria, and Eucarya. *Proceedings of the National Academy of Sciences*. 87: 4576-4579.

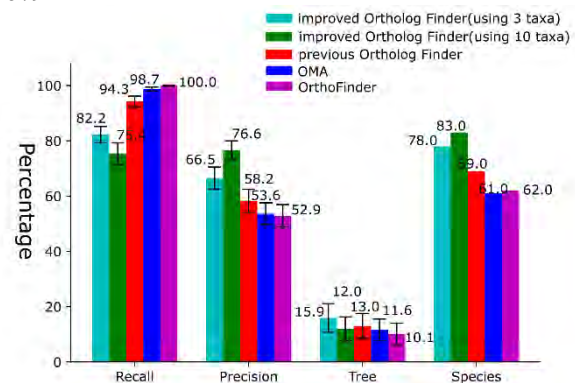


Fig. 1: The result of performance test using simulation sequences based on the 32OTU model tree. For each evaluation item, the results of five different programs are shown. From left to right, the programs are improved Ortholog Finder (provided three taxonomic information), improved Ortholog Finder (provided ten taxonomic information), previous Ortholog Finder, OMA, and OrthoFinder. The vertical axis represents the percentage (%) of each item.

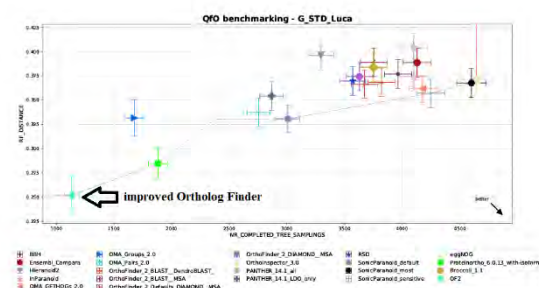


Fig. 2: The result of Quest for Orthologs benchmark test (Generalized Species Tree Discordance Benchmark of Luca). Each program is indicated by a separate mark. (OF2 is a yellow-green diamond). The vertical axis represents the mean Robinson Foulds distance between the species phylogenetic tree and the orthologous phylogenetic tree.

Visualization of low molecule phenol (LMP) and copper naphthenate in oil palm veneer using X-ray microtomography

Ayuni Nur Apsari^{1*}, Eko Sudoyo², Eka Mulya Alamsyah³, Kenji Kobayashi⁴, and Takashi Tanaka⁴

1. The United Graduate School of Agriculture Science, Major of The Utilization of Biological Resources, Gifu University, Yanagido 1-1, Gifu City 501-1193 Japan
2. Research and Development Division, PT Sumber Graha Sejahtera, Sampoerna Strategic Square, North Tower, 21st Floor, Jl. Jend. Sudirman Kav. 45-46, Jakarta 12930, Indonesia
3. Post Harvest Technology Study Program, School of Life Sciences and Technology, Institut Teknologi Bandung, Jalan Ganesha No. 10 Bandung 40132 Indonesia
4. College of Agriculture, Academic Institute, Shizuoka University, Ohya 836, Suruga-ku, Shizuoka, 422-8529 Japan

INTRODUCTION

The abundant of oil palm trunk has a prospective resource for the plywood industry. The oil palm is a monocotyledonous species that has different anatomy with dicotyledonous wood. The anatomy of the oil palm trunk contains around 50% of soft parenchyma tissue and vascular bundles (Schmidt *et al.*, 2016 and Loh *et al.*, 2011).

The prospective veneer material from oil palm has an inferior quality in dimensional stability, low strength, and less durability. However, the oil palm is more porous than the common wood. The anatomy of oil palm makes it easier to absorb the chemical modification such as low molecule phenol (LMP) to enhance the dimensional stability, especially in loose side of the veneer (Loh *et al.*, 2011).

The veneer also needs to be protected from the decay fungi. The copper-based preservative is famous to be used as wood preservative. The recent plywood industry used copper naphthenate to increase their veneer durability, especially to protect veneer surface against staining fungi (Civardi *et al.*, 2016). The Schmidt *et al.* (2011) investigated the mass loss of oil palm wood by fungus *Coniophora puteana* up to 61%. The investigation was done using transmission electron microscopy (TEM), light microscopy, and UV techniques. Those techniques were stained and/or destructed the sample for investigation.

The appropriate techniques are needed to check the quality of the treated oil palm veneer using LMP and copper naphthenate non-destructively and without any additional material (chemically). X-ray microtomography might be the promising technique to perform non-destructive testing to the treated oil palm veneer without any additional material. It gives a high resolution image and can be formed into 3D image to deeply understand the microdistribution of material in wood (Oishi and Tanaka, 2020).

This study was conducted to determine the applicability of X-ray microtomography to visualize the micro distribution of LMP and copper in treated oil palm veneer non-destructively and without any additional material during X-ray scanning.

MATERIALS AND METHODS

Oil palm veneer was treated by LMP (solid content 27.11%) and copper naphthenate (metal content 8%). The LMP treatment was conducted using impregnation process. The pressure was kept at 5 kg/cm² for 30 minutes using pump Krisbow KW20-425. The copper naphthenate treatment was a dipping process for one second. After modification treatment to the veneer, all the veneer (including untreated-veneer) were oven-dried at 103°C for 15 hours. The modification treatment was followed the plywood industrial method.

One oil palm veneer treated by LMP, copper naphthenate, and the untreated oil palm veneer with dimension 10 mm x 100 mm x 2.21 mm were arranged as Fig. 1 for X-ray microtomography scanning. The L4320 lens type with F.O.V 14 mm x 10 mm, and molybdenum X-ray target were used for X-ray scanning. The X-ray tube voltage and tube current were set automatically at 50 kV and 24 mA, respectively. The resolution of the image was 8.800 µm/px (Binning 2), 8 s exposure time, angular step at 0.225° (with 800 projections equaling 180° ÷ 800 = 0.225° angular steps), and the distance between the sample and lens was 8 mm. After scanning, we auto-centered the reconstruction image to minimize the blurry image due to sample shifted during the rotation of the X-ray scanning process.

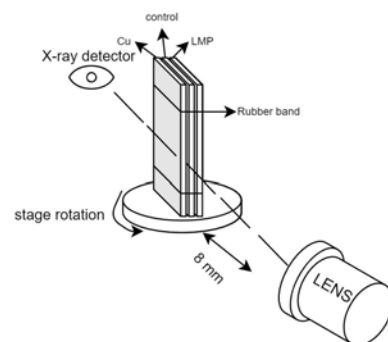


Fig. 1: The schematic of the X-ray microtomography

The gray value plot profile and calculation of it were performed using imageJ 1.48v software to the 2D X-ray image. The deeper observation of the LMP and Cu distribution was performed using VGstudio software, specially using X-ray image stack in 3D form.

RESULTS AND DISCUSSION

The distribution of LMP and Cu in the treated oil palm veneer was successfully visualized using the X-ray microtomography. The difference among LMP treated veneer, copper naphthenate treated veneer, and untreated veneer can be seen clearly from the 2D X-ray image and the gray value plot profile. The 2D image also shows the shrinking and swelling phenomena happened in the treated veneer compared with the size of the untreated veneer.

The micro distribution of LMP mostly in the parenchyma of the LMP treated veneer, and seems distributed evenly in the veneer. The brightness level almost same for all part according to the gray value peak in the plot profile. The micro distribution of the Cu in the copper naphthenate treated veneer can be seen from the brightest color of the vascular bundle's border in the copper naphthenate treated veneer (Fig. 2).

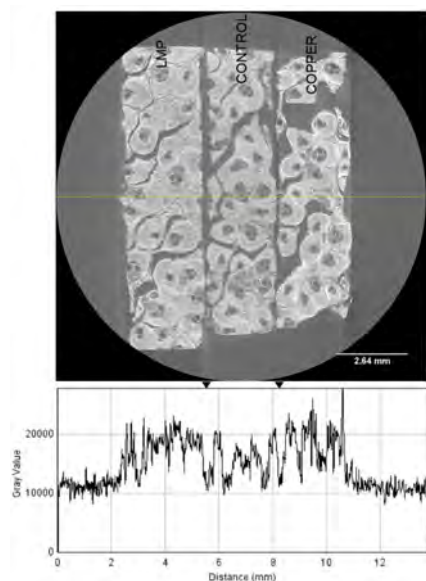


Fig. 2: Two-dimensional (2D) X-ray image of the oil palm veneer. Scale: 2.64 mm

The X-ray image show clearly the swelling phenomenon of the parenchyma in the LMP treated oil palm veneer, and the shrinking phenomenon of parenchyma in the copper naphthenate treated oil palm veneer. The probability of LMP and Cu as the reagent distributed in the treated oil palm veneer can be seen from the peak of the gray value plot profile. The treated veneer has many higher peaks (higher gray value) than the peak of untreated oil palm veneer. The average gray value of copper naphthenate treated veneer was the highest (18900.15441), followed by LMP treated veneer (17973.6965), and the lowest was the untreated veneer's average gray value (15566.27132).

The anatomy of the oil palm different with the anatomy of wood. The oil palm anatomy contains of vascular bundle and parenchyma. The oil palm also has crystalline silica in the parenchyma. The observation from X-ray image stack in 3D form show the existence of the crystalline silica in both treated veneer and untreated veneer (Fig. 3). The parenchyma of oil palm has <20% klason lignin that contaminated with crystalline silica (Tomimura, 1992).

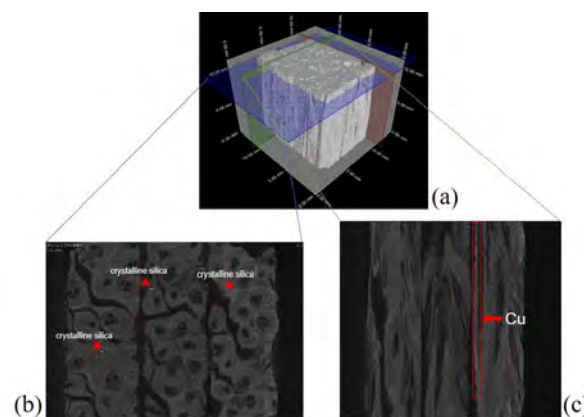


Fig. 3: (a) Up-right-front three-dimensional (3D) X-ray image stack of oil palm veneer, (b) 2D image of transverse section (obtained from the blue cut section of the 3D image, 226% zoom), and (c) 2D image of a radial section (obtained from the green cut section of the 3D image)

ACKNOWLEDGMENTS

The authors express their appreciation to JSPS KAKENHI for funding (Fund No.: 20K06163). We would like to express our big appreciation to Takeshi Arizono for performing and explaining the LMP and copper naphthenate materials and the applied process. We thank PT. Sumber Graha Sejahtera "Sampoerna Kayoe" for providing the material and facility for conducting the LMP and copper naphthenate treatments.

REFERENCES

- Civardi C, Van den Bulcke J, Schubert M, Michel E, Butron MI, Boone MN, et al. (2016). Penetration and effectiveness of micronized copper in refractory wood species. *PLoS ONE*, **11** (9), e0163124. <https://doi.org/10.1371/journal.pone.0163124>
- Loh, Y. F., Paridah, M. T., Hoong, Y. B., and Yoong, A. C. C. (2011). Effects of treatment with low molecular weight phenol formaldehyde resin on the surface characteristics of oil palm (*Elaeis quineensis*) stem veneer. *Materials & Design*, Volume 32, Issue 4, Pages 2277-2283. <https://doi.org/10.1016/j.matdes.2010.11.014>
- Oishi, A., and Tanaka, T. (2020). Development of a nondestructive imaging method for morphological characterization of adhesive bondlines in wood-based materials using x-ray micro-computed tomography. *日本接着学会誌 第57巻 4号 別刷*, **145-151**, 18-24.
- Schmidt, O., Bahmani, M., Koch, G., Potsch, T., and Brandt, K. (2016). Study of the fungal decay of oil palm wood using TEM and UV techniques. *International Biodeterioration & Biodegradation*, Volume 111, Pages 37-44. <https://doi.org/10.1016/j.ibiod.2016.04.014>
- Tomimura, Y. (1992). Chemical characteristics and utilization of oil palm trunks. *Jarq-japan Agricultural Research Quarterly*, **25**, 283-288.

Generalized pollination and floral scent chemistry in the invasive *Coreopsis lanceolata*

Muhammad Arifin¹ and Tomoko Okamoto^{1,2},

1. The United Graduate School of Agricultural Science, Gifu University, Japan
2. Faculty of Applied Biological Science, Gifu University, Japan

INTRODUCTION

The invasive alien species pose threats to the reproduction of native plants due to their ability to compete for local pollinators (Courchamp et al. 2017; Muñoz et al. 2008). The floral traits have been reported to facilitate invasive species successfully colonizing the local plant-pollination web (Gibson et al. 2012; van Kleunen et al. 2015). Therefore, investigation on floral traits as key factors supporting invasiveness is crucial to explain the mechanism of invasiveness.

Coreopsis lanceolata (Asteraceae) is an herbaceous perennial plant native to North America (Samfield et al. 1990). It was introduced to Japan in the 1880s as ornamental plant and later used for landscaping (Suzuki et al. 1990). This species spreads rapidly in Japan and is currently registered as the 100 worst invasive alien species based on the Invasive Alien Species Act. *C. lanceolata* produces numerous flower densities of about 30 capitula per 100 cm² (Zeng et al. 2021). The flowers produce large amounts of seeds as long-distance dispersal strategy, in which the seeds are easily transferred by wind or water. The plants can also use rhizome as short-distance dispersal strategy (Batianoff et al. 2002).

C. lanceolata are self-incompatible. Consequently, seed production has relied on pollinators. However, the floral traits involved in the attraction of pollinators for seed production are overlooked. This study investigated floral traits related to the reproductive biology of *C. lanceolata* in Japan. The aims were to answer the following questions: (i) Which insect assemblages visit *C. lanceolata*? (ii) How important are the volatile compounds for the attraction of visitors?

MATERIALS AND METHODS

Study species and sites- *Coreopsis lanceolata* (Asteraceae) is an herbaceous perennial up to 70 cm in height, which found invading riverbanks, roadsides, and wastelands in almost entire Japan. These plants produce flower head, namely a capitulum (plural capitula), from May to July. The capitulum is composed of numerous ray and disk florets arranged into a whole inflorescence that looks like a single flower. The capitula are bright yellow and 4–6 cm in diameter (Batianoff et al., 2002).

We conducted the study of *C. lanceolata* on three populations in Gifu Prefecture, Japan, from May to July 2021. The populations, namely Ajiki (35°29'47.0"N 136°43'37.1"E; 26 m. asl), Hirai (35°33'20.0"N 136°43'11.6"E; 76 m. asl) and Tsubaki Bora (35°28'18.6"N 136°45'50.4"E; 18 m. asl) were more than 4 km apart each other.

Flower visitor observation and analysis- Flower visitor observations on *C. lanceolata* were conducted on cloudy and sunny days with low wind speeds between 0700h–1830h. All populations were growing on the roadside (300–800 m long). Therefore, transect sampling was performed. We clustered the flowers into four to seven sampling points for each transect and made 10 mins observations of each, in turn. The hand net was used to capture the flower visitors which landed on flower parts. Subsequently, flower visitors were deposited into 30 ml transport tube and kept at -20°C until identification. The stereo

microscope and standard book references were used for identification. We noted the number of attached pollen grain and location of pollen load on specimen's bodies during the identification.

Floral scent collection and analysis- Floral scent collections were conducted from fresh flowers growing in Tsubaki Bora population using a dynamic headspace technique (Raguso et al. 1998). The floral scent collections were captured for two hours during the peak of flower visitor activities in 1000h–1400h. During the collection, two capitula from each individual were enclosed in low-density polyethylene bags. Overall, we sampled six capitula from three individuals. The sorbent cartridge made from Tenax TA (60 mg; mess 80–100; GL Science, Tokyo, Japan) was used to adsorb the volatiles in the headspace.

Collected volatile samples were eluted from the adsorbent with n-hexane (1.5 mL) and were carefully evaporated by N₂ flow until it reached 20 µL at room temperature. A microsyringe was used to take an aliquot of 1 µL sample. As a standard for analysis, 1 µL of n-eicosane (concentration of 10 ng µL⁻¹) was added to the sample. The analysis was performed using gas chromatography-mass spectrometry (GC-MS) (GC-2010, MS: Shimadzu, Tokyo, Japan) installed with Rtx-5sil MS capillary column (30 m × 0.25 mm; film thickness, 250 µm; Restek, Restek Corporation, USA). Helium was used as the carrier gas.

To discover the floral scent compound, we compared the volatiles produced by flowers, branches without flowers, and ambient air. The compounds were discovered and identified by matching the fragments to those in the National Institute of Standards and Technology NIST 05 and NIST 05s libraries. We also estimated retention indices for all compounds using n-alkane standards and compared them to those reported in prior research and the NIST chemistry webbook (<https://webbook.nist.gov/chemistry/>). Emitted rate of each compound was determined by comparing the GC results to the internal standards.

RESULTS & DISCUSSION

Flower visitor assemblages- Species-rich of insects were observed visiting *C. lanceolata*. Overall, we recorded 261 insects belonging to at least 12 families of five orders. The flower visitors were observed diurnally in all populations, in which the peak daily visitation was between 1000h to 1400h. Hymenoptera made the most significant portion of visitation (c 59–66%), followed by Diptera, Lepidoptera, Coleoptera, and others, respectively (Fig. 1). Most of the flower visitors carried pollen on their bodies. Compared to visitors among populations, the halictid and megachilid bees were the most common and important visitors for *C. lanceolata*. The halictid bees, such as *Halictus* spp. and *Lasioglossum* spp. were small to medium in body size, though they effectively carried pollen on whole bodies, mainly on the scopa under the abdomen. This pollen was readily transferred across flowers (Parker et al., 2015). In contrast, the recent studies of *C. lanceolata* in introduced range of China revealed that *C. lanceolata* significantly attracted Apidae, especially *Apis cerana* (c 45% of total specimens), to guarantee seed reproduction (Zeng et

al. 2021). Even though the honeybee *A. cerana* also exist in Japan, surprisingly, our study revealed that *A. cerana* was less abundant as the visitor in all populations (Fig. 1). Instead, halictid and megachilid bees were the most abundant. Further study regarding the insect assemblage's composition surrounding the *C. lanceolata* population probably helps answer these phenomena.

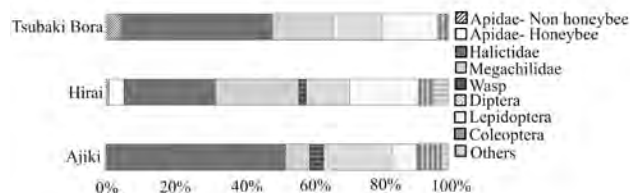


Fig.1: Comparison of flower visitor assemblages of *C. lanceolata* among populations

Most notably, our results highlighted the ability of invasive *C. lanceolata* to conduct the generalist pollination system. The flower of *C. lanceolata* was typically an open plate shape flower in which the pollen and nectar were exposed and easily accessed by the visitors. These results support previous studies that invasive plants attract generalist pollinators for reproduction (Montesinos et al. 2016; Ward et al. 2013). Most of the flower visitors were native species, and this could be a shred of evidence that *C. lanceolata* successfully integrated into the native pollination web (Mommott et al. 2002). The integration with native pollinators was more likely to be a vital key that allowed *C. lanceolata* to produce large seeds, although they were basically self-incompatible.

Table 1. Floral scent chemistry of *C. lanceolata* in Tsubaki Bora population expressed as percent relative peak area

Compounds#	Retention indices	Relative amount (%) (mean \pm SD, N=3)
<i>Benzenoids</i>		
2-Phenylacetaldehyde	1045	7.64 \pm 2.83
Methyl phenylacetate	1176	0.61 \pm 0.65
Methyl salicylate	1195	0.43 \pm 0.41
<i>Monoterpenes</i>		
o-Cymene	1026	1.62 \pm 1.31
(E)-Linalool oxide, furanoid	1087	0.75 \pm 0.70
Z-Verbenol	1165	15.37 \pm 6.85
<i>Sesquiterpenes</i>		
β -Bourbonene	1391	17.90 \pm 8.19
β -Elemene	1394	4.43 \pm 1.13
β -Cedrene	1427	18.05 \pm 4.48
β -Bisabolene	1512	25.01 \pm 3.95
<i>Unidentifieds*</i>		
m/z [43, 119, 41, 109, 81]	1259	1.23 \pm 1.08
m/z [119, 132, 105, 41]	1485	2.54 \pm 1.65
m/z [41, 69, 132, 134, 119]	1682	2.35 \pm 0.80
m/z [43, 58, 71, 57, 59, 41]	1842	2.08 \pm 1.11
Total emission rate (mean \pm SD, ng .h ⁻¹ .capitulum ⁻¹)		4.42 \pm 2.99

#Identification of compound was performed by comparing the similarity of mass spectrum of focal compound in libraries, and Retention Indices (RI) reported in the NIST Chemistry WebBook

*Ion fragments are lined from the stronger for unidentified compounds

Floral scent- The floral scents emitted from *C. lanceolata* were listed in Table 1. The emission rate of floral compounds was 4.42 ± 2.99 ng .h⁻¹.capitulum⁻¹ (N=3). In total, we detected at least 14 unique compounds belonging to benzenoids, monoterpenes, and sesquiterpenes emitted from the flower. Sesquiterpenes were the predominantly abundance volatiles, which collectively made up more than half of the relative amount of volatiles. All of the identified compounds were found in the floral scents of other angiosperms (Knudsen 1993; Knudsen et al. 2006). These compounds are likely to be attractive for general insects. Our study supported the evidence that floral scent is more likely a key component which plays the role for pollinator attraction (Whitehead et al. 2009). However, the identified compounds (Table 1) which we presented here were the preliminary work. Further works on confirmation with the authentic standard compound are needed to determine the compounds.

In conclusion, this study lay the evidence that *C. lanceolata* utilized generalist pollination system to avoid reproductive failure. Moreover, it is noteworthy that the scent profiles play a role in attracting general native visitors to *C. lanceolata*.

ACKNOWLEDGMENTS

The first authors, M.A., would like to express gratitude to The Ministry of Education, Culture, Sports, Science, and Technology (MEXT) Japan for sponsoring a scholarship for Ph.D. study.

REFERENCES

- Batianoff, G. N., & Halford, D. A. (2002) *Coreopsis lanceolata* L. (Asteraceae): Another Environmental Weed for Queensland and Australia. *Plant Protection Quarterly* 17(4): 168–169.
- Courchamp, F., Fournier, A., Bellard, C., Bertelsmeier, C., Bonnaud, E., Jeschke, J. M., & Russell, J. C. (2017) Invasion Biology: Specific Problems and Possible Solutions. *Trends in Ecology and Evolution* 32(1): 13–22.
- Gibson, M. R., Richardson, D. M., & Pauw, A. (2012) Can Floral Traits Predict an Invasive Plant's Impact on Native Plant-Pollinator Communities? *Journal of Ecology* 100(5): 1216–1223.
- Knudsen, J. (1993) Trends in Floral Scent Chemistry in Pollination Syndromes: Floral Scent Composition in Moth-Pollinated Taxa. *Botanical Journal of the Linnean Society* 113(3): 263–284.
- Knudsen, J. T., Eriksson, R., Gershenzon, J., & Ståhl, B. (2006) Diversity and Distribution of Floral Scent. *The Botanical Review* 72(1): 1–120.
- Mommott, J., & Waser, N. M. (2002) Integration of Alien Plants into a Native Flower-Pollinator Visitation Web. *Proceedings of The Royal Society B: Biological Sciences*, 269(1508): 2395–2399.
- Montesinos, D., Castro, S., & Rodríguez-Echeverría, S. (2016) Two Invasive Acacia Species Secure Generalist Pollinators in Invaded Communities. *Acta Oecologica* 74: 46–55.
- Muñoz, A. A., & Cavieres, L. A. (2008) The Presence of a Showy Invasive Plant Disrupts Pollinator Service and Reproductive Output in Native Alpine Species Only at High Densities. *Journal of Ecology* 96(3): 459–467.
- Parker, A. J., Tran, J. L., Ison, J. L., Bai, J. D. K., Weis, A. E., & Thomson, J. D. (2015) Pollen Packing Affects the Function of Pollen on Corbiculate Bees but Not Non-Corbiculate Bees. *Arthropod-Plant Interactions* 9(2): 197–203.
- Raguso, R. A., & Pellmyr, O. (1998) Dynamic Headspace Analysis of Floral Volatiles: A Comparison of Methods. *Oikos*, 81(2): 238–254.
- Samfield, D. M., Zajicek, J. M., & Cobb, B. G. (1990) Germination of *Coreopsis lanceolata* and *Echinacea purpurea* Seeds Following Priming and Storage. *Hortscience* 25(12): 1605–1606.
- Suzuki, K., & Kondo, M. (1990) A Method of Plant Seeding and Maintenance with Wildflower. *Journal of the Japanese Society of Revegetation Technology* 16(3): 46–57.
- van Kleunen, M., Dawson, W., & Maurel, N. (2015) Characteristics of Successful Alien Plants. *Molecular Ecology*, 24(9): 1954–1968.
- Ward, M., & Johnson, S. D. (2013) Generalised Pollination Systems for Three Invasive Milkweeds in Australia. *Plant Biology* 15(3): 566–572.
- Whitehead, M. R., & Peakall, R. (2009) Integrating Floral Scent, Pollination Ecology and Population Genetics. *Functional Ecology* 23(5): 863–874.
- Zeng, J. J., Zhou, B., & Wang, N. (2021) Comparing the Reproductive Biological Characteristics of the Alien Invasive *Coreopsis lanceolata* to Those of the Non-Invasive Alien Congener *Coreopsis tinctoria*. *Plant Species Biology* 36(3): 379–389.

Inhibition effect of different sorbent materials on transfer of cesium and arsenic from contaminated soil to vegetation

Shiamita Kusuma Dewi¹ and Yongfen Wei²

1. The United Graduate School of Agricultural Science, Gifu University, Japan

2. River Basin Research Center, Gifu University, Japan

INTRODUCTION

Arsenic (As) in soil is the major source for arsenic uptake of crops. Inorganic arsenic (As) such as arsenite and arsenate are toxic to humans and is considered a carcinogen by the International Agency for Research on Cancer.

Radio cesium represents in water, soil, and air which threatening human health and the environment. It acts directly on living organisms from external sources, or it becomes incorporated through the food chain or both. The plant forms the base of the food chain. Therefore, it is essential to inhibit its transfer to vegetation.

Due to simplicity, low cost, high effectiveness, and being environmentally friendly, reducing the bioavailability of these heavy metal (iod) in soil by adding promising sorbent materials such as activated carbon, biochar, and wood ash can be considered as an economically feasible approach.

Activated carbon (AC), having a high surface area, and developed porosity, is a low-cost and effective adsorbent for a wide range of pollutants. (Mohan et al., 2006; Marsh et al., 2006). Biochar is an eco-friendly product that has a negative surface charge, high porosity, large specific surface area, and abundance of functional groups on the surface, it has been considered as a low-cost material that can be used in carbon sequestration, soil improvement, waste management, and remediation areas (Wang et al. 2018; Ruan et al. 2019). Wood ash contains organic matter, Ca, Mg, Fe, and other minerals that can immobilize toxic metal (iod) in soil.

In this study, to evaluate the ability of a different types of sorbent on inhibiting arsenic and cesium transfer from contaminated soil to vegetation, pot experiment is designed and carried out.

MATERIALS AND METHODS

Soil and additive samples – the mixture of two commercial products: Gardening soil and Decomposed granite soil mixed in a dry weight ratio of 3:2 was used as soil sample. Five selected sorbent materials including bamboo activated carbon (BAC), wood activated carbon (WAC), coal activated carbon (CAC), biochar, and wood ash, were used in the study. The properties of the samples of soil and sorbents are summarized in Table 1. It can be seen from the table that the properties of soil samples and sorbents are quite different.

Table 1. Properties of soil and sorbents used in this study

Parameter	Soil	BAC	Biochar	Wood Ash	CAC	WAC
pH	6.100	10.200	9.200	11.800	6.700	7.800
EC (mS/m)	81.200	463.000	777.000	463.000	1204.000	95.600
OM (%)	12.361	15.018	37.430	2.244	22.368	18.292
CEC (cmol/kg)	11.530	7.360	6.280	6.390	9.780	8.390
Pore volume (cm ³ /g)	-	0.486	0.477	0.020	0.604	0.549
SSA (m ² /g)	-	1368.800	206.500	4.200	1168.000	1500.900

Note: All value represented the averaged values. EC: electrical conductivity, OM: organic matter, CEC: cation exchange capacity, SSA: specific surface area, BAC: bamboo activated carbon, CAC: coal activated carbon, WAC: wood activated carbon

Pot Experiment (Fig.1) – CsCl and Na₂HAsO₄ solution were uniformly mixed with soil. The contamination concentration of the soil used for the experiment was set as 300 mg kg⁻¹ for arsenic and 50 mg kg⁻¹ for cesium. The soil was well mixed with sorbent materials, and the mixing ratio for each sorbent to the soil was set at 5%. 500 g of contaminated soil was placed in plastic pot and no additive applied soil was used as control for comparison. Each treatment had two replicates. Totally, 48 pots were prepared

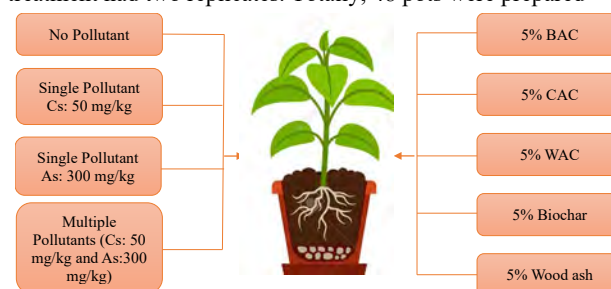


Fig 1. Design of Experiments

Sample analysis – This research experiment was conducted outdoor. Komatsuna was cultivated in greenhouse Gifu University for 73 days and no additional fertilizer was added during the entire growing period. The vegetation was watered with river water and the water leached from the potting soil was collected on harvest day. After harvest, the vegetation was washed and, then further hot-dried in the oven at 80°, followed by shattering by crusher and digested with nitric acid in the autoclave. Arsenic and cesium concentration of the digested sample from the different parts was measured using inductively coupled plasma mass spectrometry (ICP-MS, Agilent 7700X).

Statistical analysis – Statistical analysis are conducted using SPSS 24.0 ($p \leq 0.05$). All data are expressed as means \pm standard errors. Significant differences are determined using one-way analysis of variance (ANOVA) by Tukey's multiple comparisons test.

RESULTS

Plant growth status evaluation – As shown in Table 2., depending on the contaminant(s) the dry weight of harvested komatsuna range from 0.416 to 0.884 g pot⁻¹ (Control; average: 0.618 g pot⁻¹), 0.052-0.295 g pot⁻¹ (Cs: 50 mg kg⁻¹; average: 0.161 g pot⁻¹), 0.055-0.191 g pot⁻¹ (As: 300 mg kg⁻¹; average: 0.103), 0.138-0.287 g pot⁻¹ (AsCs; average: 0.160 g pot⁻¹), respectively. It was found that the contamination of As and Cs suppressed the growth of the most komatsuna, and that only CAC, BAC, WAC addition in AsCs contamination level which increased the dry weight of komatsuna compared to control.

Table 2. Dry weight of plant under different addition of sorbent materials

Treatment		Dry weight (g/pot)	Average (g/pot)
control	No addition	0.416 ± 0.008	0.618
	Bamboo Activated Carbon (BAC)	0.545 ± 0.021	
	Coal Activated Carbon (CAC)	0.731 ± 0.030	
	Wood Activated Carbon (WAC)	0.619 ± 0.274	
	Biochar	0.884 ± 0.045	
	Wood ash	0.513 ± 0.062	
Only Cs:50 mg/kg	Cs	0.295 ± 0.006	0.161
	Bamboo Activated Carbon (BAC)	0.053 ± 0.001	
	Coal Activated Carbon (CAC)	0.243 ± 0.001	
	Wood Activated Carbon (WAC)	0.172 ± 0.083	
	Biochar	0.052 ± 0.008	
	Wood ash	0.150 ± 0.024	
Only As:300 mg/kg	As	0.191 ± 0.073	0.103
	Bamboo Activated Carbon (BAC)	0.113 ± 0.008	
	Coal Activated Carbon (CAC)	0.101 ± 0.000	
	Wood Activated Carbon (WAC)	0.070 ± 0.000	
	Biochar	0.090 ± 0.001	
	Wood ash	0.055 ± 0.009	
Both Arsenic and Cesium	AsCs	0.138 ± 0.000	0.16
	Bamboo Activated Carbon (BAC)	0.165 ± 0.032	
	Coal Activated Carbon (CAC)	0.287 ± 0.067	
	Wood Activated Carbon (WAC)	0.183 ± 0.000	
	Biochar	0.119 ± 0.003	
	Wood ash	0.070 ± 0.011	

Value represents the mean ± SEM. BAC: bamboo activated carbon, CAC: coal activated carbon, WAC: wood activated carbon.

Amount of arsenic and cesium in vegetation and leached water - The amount of Cs and As in the vegetation and leached water under multiple pollutants (contamination level Cs:50 mg/kg and As: 300 mg/kg) is shown in **Fig.2** and **Fig.3**. All sorbent materials were not significantly different compared to the control group. Only the addition of BAC and WAC which significantly decreased the cesium amount in the vegetation. For leached water, BAC and wood ash showed increased As concentration significantly in leached water. While only wood ash treatment showed significantly increased Cs amount in leached water

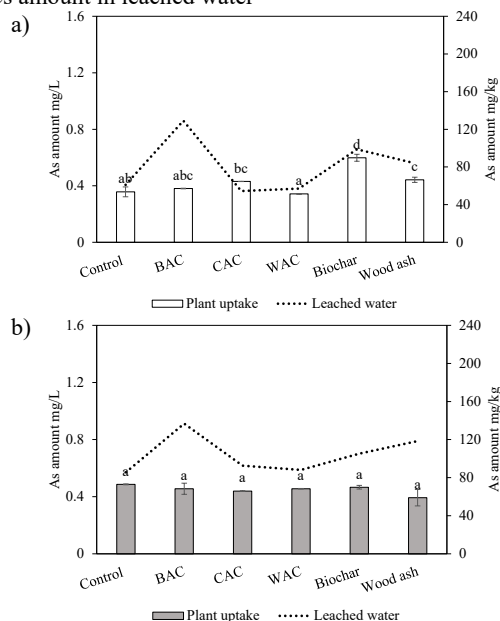


Fig.2 Amount of As uptake by plant and in leached water under (a) single pollutant (As:300 mg/kg), (b) multiple pollutants (As:300 mg/kg; Cs:50 mg/kg)

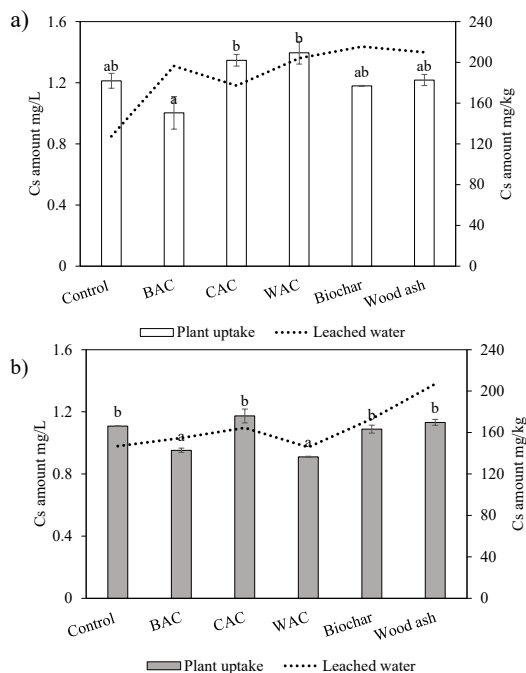


Fig.3 Amount of Cs uptake by plant and in leached water under (a) single pollutant (Cs:50 mg/kg), (b) multiple pollutants (As:300 mg/kg; Cs:50 mg/kg)

DISCUSSION

The addition of different sorbent materials in As contaminated and Cs contaminated soil mostly decreased the dry weight of komatsuna. Compare to control only BAC, CAC, and WAC in AsCs contaminated soil increased the dry weight in AsCs contaminated soil. As shown in **Fig.2** As and Cs concentration in vegetation was no different between control and sorbent materials additive treatment, only BAC and CAC significantly decreased Cs concentration in the plant. This figure indicated that arsenic and cesium were soluble for plant uptake. Arsenic and cesium that are uptaken by plants will suppress the growth of the komatsuna plant. Some researchers also report that at higher concentration, uptake nutrient element inhibits in roots, therefore, the growth of the whole plant hampered and biomass decreased and caused physiological disorders (Wells B, 1997).

For As and Cs concentration in leached water, the most result showed that addition of sorbent materials gave no significant differences between the control and treatment group. Despite of decrease arsenic and cesium amount in leached water, some of addition of sorbent materials tend to increase the amount of As/Cs in it.

CONCLUSION

In summary, all data revealed that adding sorbent materials into contaminated As and Cs soil could be inhibiting As and Cs transfer to plant (BAC and CAC) but also could be allowing the As and Cs soluble to plant uptake and leached water. Further investigation needs to be conducted to investigate the factor that affect the solubility of arsenic and cesium in soil due to the addition of sorbent materials.

Ensemble prediction of solar irradiance in tropical regions

Daiki Harada¹, Naoki Moriai¹ and Tomonao Kobayashi²

1. Graduate School of Natural Science and Technology, Gifu University
2. Faculty of Engineering, Gifu University

INTRODUCTION

Solar irradiance is high in tropical regions (Fig. 1). The introduction of photovoltaic systems in these regions is expected to contribute to the realization of a low-carbon society and the stable supply of electricity. For efficient operation of the power grid to which the photovoltaic system is connected, the predicted value of the solar irradiance by the numerical weather prediction model may be used. In this case, the prediction accuracy of the numerical weather prediction model has a great influence on the efficient operation of the power grid.

In this study, the solar irradiance is predicted by the numerical weather prediction model.

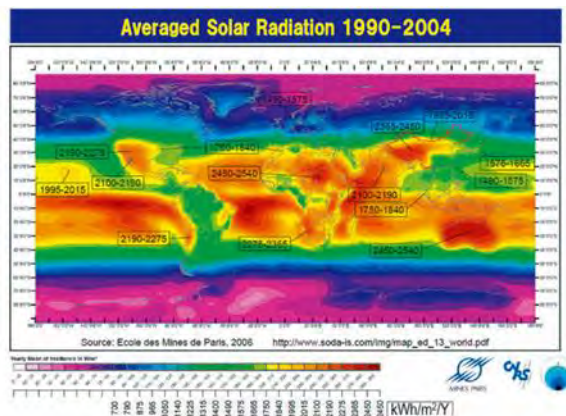


Fig. 1: Distribution of solar irradiance

MATERIALS AND METHODS

In this study, we aim to improve the prediction accuracy of solar irradiance in tropical regions by the Weather Research and Forecasting (WRF) model (Skamarock et al., 2008). WRF has a physical process for calculating clouds, radiation, and etc. In addition, there are several option schemes for each physical process. In order to make accurate calculations, it is necessary to use the appropriate schemes according to the climatic conditions of the target area. In this study, the accuracy of solar irradiance calculation is improved in the following two steps.

Step 1

In this step, appropriate combination of physical process schemes is derived for getting the highest WRF calculation accuracy in the tropics (option optimization). In this study, simulations were performed in two cases (case 1 and case 2). In case 1, a combination of schemes according to Hadrien et al. (2018), which is considered to have high calculation accuracy of solar radiation intensity in Singapore, was set. As case 2, a combination of options modified from case 1 to improve accuracy in Thailand for the six processes of cloud physics process, long wave radiation process, shortwave radiation process, cumulus process, surface process, and planetary boundary layer process. The modification was based on the WRF model optimization method performed by Arasa et al. (2016) for Spain.

Step 2

In this step, ensemble prediction is performed to further improve the accuracy. Ensemble prediction is a method of performing numerical weather prediction with multiple initial values and statistically processing the results. In this study, we set multiple initial times and make predictions using the combination of options optimized in step 1. Specifically, three predicted values can be obtained every day by making predictions for three days including the current day. Of the three, the intra-day forecast, the next-day forecast, and the 2-day ahead forecast are made in order from the newest forecast start time. The method of statistical processing will be examined in the future.

Targets area and computation settings

The calculation area is shown in Fig. 2. In this study, three areas centered on the National Electronics and Computer Technology Center (NECTEC) in Thailand were set, and calculations are performed by two-way nesting. Two-way nesting not only reflects data from a large area to a small area, but also feeds back the calculation results of the small area to the calculation of the large area. The horizontal resolutions of region 1, 2 and 3 are 18 km, 6 km, and 2 km, respectively, and the number of grids was 100 × 100, respectively, and the solar irradiance in whole the year 2017 was calculated. FNL data (3 hour interval, 0.25 ° grid) from the National Centers for Environmental Prediction (NCEP) was used as input data.

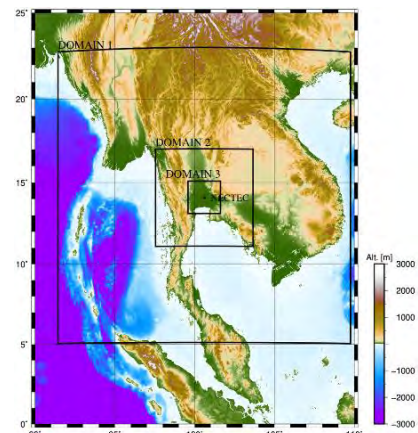


Fig. 2: Target domains for weather forecasting

RESULTS AND DISCUSSIONS

Step 1

Table 1 shows statistical errors of the initial settings (case 1) and the optimal case (case 2). In addition, Fig. 3 shows a time-series diagram comparing the observed and calculated values, and the three days from October 1st to October 7th, 2017 are targeted so that the changes in the values can be clarified. Since the solar radiation intensity peaks at noon, the time-series diagram shows a roughly upward convex change. Small fluctuations indicate the effect of clouds.

By optimizing the options, it can be read that the observed value is approaching. The accuracy of cloud prediction is still low.

Table 1: Annual correlation coefficients and RMSEs between WRF forecasting and observation

	case1	case2
Corr	0.773	0.814
RMSE (W/m^2)	241.5	204.7

Table 2: Annual RMSEs for each prediction

	Intra-Day	Next-Day	2-Day ahead
RMSE(W/m^2)	174.9	175.3	183.3

In addition, the ensemble prediction revealed that the value changes significantly depending on the time when the prediction is started.

Step 2

The statistical error of each predicted value is shown in Table 2, and the time series diagram is shown in Figs. 4 and 5. Each time-series chart is in the three Thai seasons (dry season and rainy season) on behalf of a week. The period was from December 11th to 17th, 2019 and from July 11th to 17th, 2020, respectively.

From Fig. 4, it can be seen that the error of each predicted value is small and the calculation can be performed accurately in the dry season. On the other hand, from Fig. 5, it can be seen that the error of each predicted value is large in the rainy season, and it deviates greatly from the observed value.

CONCLUSIONS

In this study, we improved the accuracy of solar radiation prediction using a numerical weather prediction model. By optimizing the options of the physical process, it is possible to capture the occurrence of clouds to some extent.

REFERENCES

- Arasa, R., I. Porras, A. Domingo-Dalmau, M. Picanyol, B. Codina, M^a Ángeles González, and J. Piñón.: Defining a Standard Methodology to Obtain Optimum WRF Configuration for Operational Forecast: Application over the Port of Huelva, Atmospheric and Climate Sciences, Vol.6, pp.329-350, 2016
- Skamarock, W.C., J. B. Klemp, J. Dudhia, D.O. Gill, D. M. Barker, W. Wang, and J.G. Powers.: A description of the advanced research WRF version 3. NCAR Tech. Note. TN-475+STR, 1-96, 2008
- Verbois, H., R. Huva, A. Rusydi, and W. Walsh.: Solar irradiance forecasting in the tropics using numerical weather prediction and statistical learning, Solar Energy, Vol.162, pp. 265-277, 2018

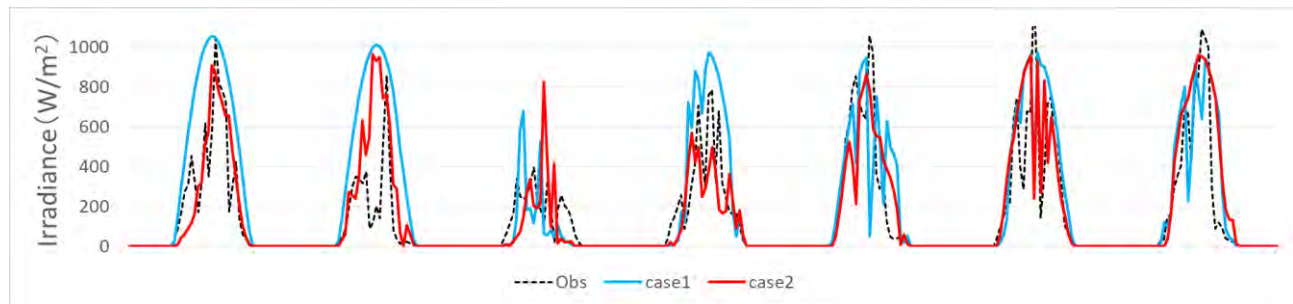


Fig. 3: Solar irradiance (from Oct. 1st, 2017 to Oct. 7th. NECTEC)

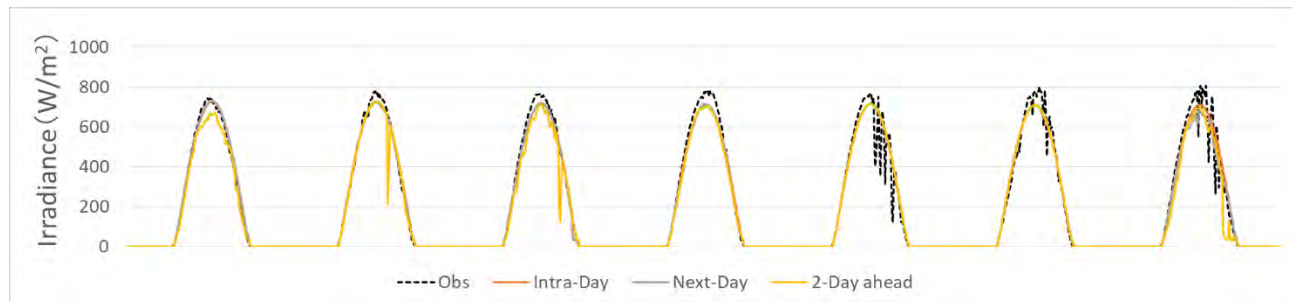


Fig. 4: Ensemble prediction of solar irradiance in the dry season (from Dec. 11th, 2019 to Dec. 17th. NECTEC)

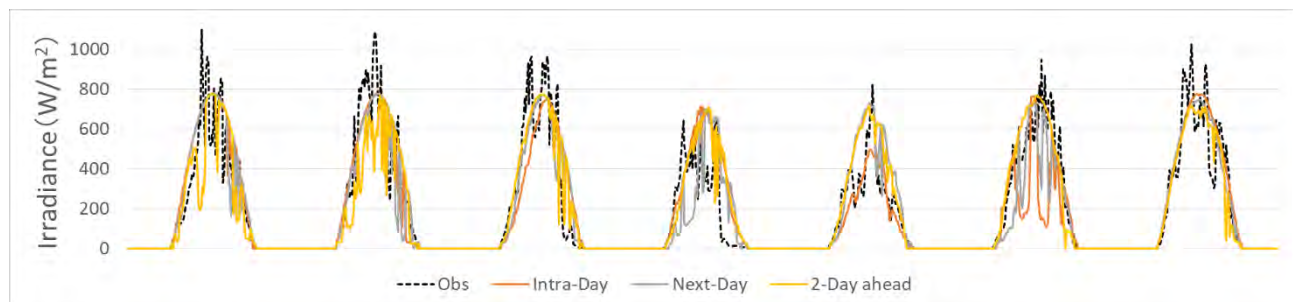


Fig. 5: Ensemble prediction of solar irradiance in the rainy season (from Jul. 11th, 2020 to Jul. 17th. NECTEC)

Short-term prediction of cloud movements with meteorological satellite images processed in spectrum space

Yuto Hara¹, Rina Takada¹, Tomonao Kobayashi¹ and Jun Yoshino¹

1. Gifu University, Gifu, JAPAN

INTRODUCTION

Many photovoltaic (PV) systems are already installed in worldwide in these days. The PV output fluctuates by changing solar irradiance, and then, the PVs which are connected to electric grids cause of instability of power on the grids. One of the ways for avoiding the risk on the grids is that the solar irradiance and PV output are predicted, and the predicted information is utilized for management of the electric grids. There are several methods for prediction of weather and solar irradiance, e.g. numerical weather simulation, and image processing of cloud images. Rerez et al. (2010)^[1] shows prediction errors with several prediction methods as shown in Figure 1. This figure indicates that the statistical error RMSE of the prediction with image processing technique is lower than the one with a numerical weather simulation from the beginning to 6-hour ahead. It means that the image processing technique can predict with higher accuracy than the numerical weather simulation in short-term prediction.

By following to this result, the image processing technique with meteorological satellite images is developed in this study. As the original approach in this study, the satellite images are developed temporally to the future ones in a spectrum space.

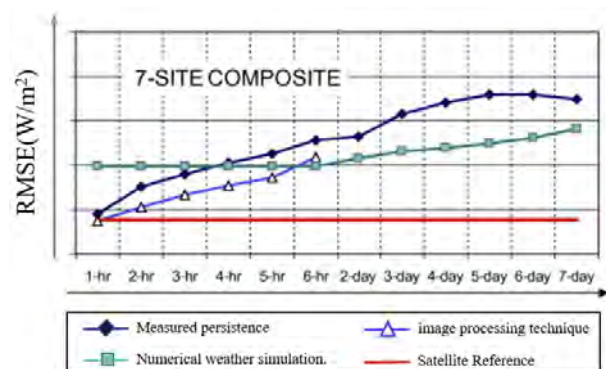


Fig. 1: Prediction accuracies of solar irradiance with different methods and their variations in forecasting period (Rerez et.al, 2010^[1])

METHODS

— Image processing

The image processing method for predicting future cloud images from the current ones is developed. The images are developed temporally for prediction of the images in spectrum space as explained in the previous section. Figure 2 shows a flow chart of transforming and developing of cloud images for prediction in this study.

First the successive cloud images are transformed with Fourier Transform to spectrum space. Next in the spectrum space, the spectrum images are developed temporally. We tried two ways for this time-development. One is a linear time-development, and the other is spectrum one. After the development, the time-developed spectrum images are return to the physical space with inverse Fourier Transform. In the spectrum space, cloud advections are corresponding to the

phase shifting of spectrum components and cloud developments are corresponds to amplitude changing of the components. From these relations, the travelling and developing of clouds can be predicted easily in the spectrum space.

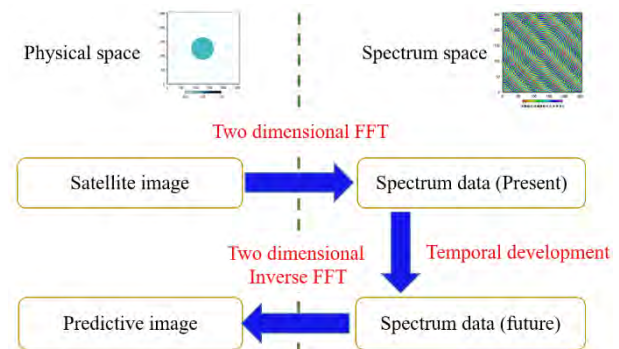


Fig. 2: Flow chart of cloud image prediction

Two dimensional Fast Fourier Transform (FFT) is used for transforming between the physical space and the spectrum one, because grid sizes in the physical space and interval of ground frequency in the spectrum space are constants. The linear regression or Maximum Entropy Method (MEM) is applied for the time-development processes in the spectrum space. When the linear regression is applied, the timeseries of amplitudes and phases of spectrum components are analysed with Least Square Method (LSM) and extrapolated for future prediction. In case when MEM is applied, the amplitudes and phases of spectrum components are extrapolated with MEM, just the same as the linear regression. The reason why MEM is employed for time development, not FFT, is that it can transform with high accuracy also with small number of data, and it also can evaluate spectrum components with arbitrary frequencies.

— Target images of clouds

The satellite images taken by HIMAWARI-8^[2] are used for analysis in this study. The satellite observes with 16 bands, from 0.47 to 13.28 μm in electric magnetic wavelength. In this study, the images in Band-3 are used. They are visible light images with 0.5 km in horizontal resolution and 2.5 minutes in time interval of images around Japan Islands.

RESULTS AND DISCUSSIONS

The successive satellite images taken by Himawari-8 for 2 hours, from 2 hours before the current with 2.5-minute interval, are used for prediction of future cloud patterns in this study. Figure 3 shows the resulted images in this study.

In Figure 3, cloud images taken by HIMAWARI-8 from 10:00 to 12:00 in 2019/02/02 with 0.5 km in horizontal resolution are used as input and are predicted with the linear regression models or MEM after 1 hour ahead from 12:00 to 13:00 in the same day. The cloud images on the upper row in the figure are observed ones, and the one at the lower row is the predicted cloud images. The labels [A] to [D] is timestamps; [A] and [B] are 10:00:00 and 10:57:30, respectively, and current times. [C] and [D] are 12:00:00 and 12:57:30, and in

prediction. The observation images in time [C] and [D] in the upper row in the figure are for reference of the prediction.

As shown in Figure 3, the advection and development of clouds are predicted by both LSM and MEM near the center of the images. On the other hand, the predicted images become blurred, and their borders become fuzzy in prediction.

Table 1 shows the statistical errors, correlation coefficients and RMSE, of the predicted images to the original satellite one. From this table, it is found that the prediction with the linear regression, LSM is higher accurate than the one with MEM, and the accuracy becomes lower as time-developing from [C] to [D]. This reason may be that each component in the spectrum space is developed in time individually, and the phases have shifted each other when the spectrum components are transformed inversely to the physical space. This prediction method still contains parts for development.

CONCLUSIONS

Predictions of solar irradiance and the PV outputs are effective for management of electric power grids that contains unstable generations from PV systems. In this study, the short-term prediction method of the solar irradiance for the

grid management. This method is an image processing of cloud patterns taken by a meteorological satellite and predict future cloud patterns by developing images temporally in the spectrum space. Advection and development of clouds are corresponding to phase shifting and increasing amplitude of spectrum components, respectively, and the future cloud patterns can be predicted in the spectrum space. The linear regression or MEM is applied for the time-development in the spectrum components of the images. The proposed method predicts the future cloud images, however the images are blurred. The low quality in the prediction may be caused in time-developing process.

REFERENCE

- [1] Rerez et.al, Validation of short and medium term operation solar radiation forecasts in the US, Solar Energy, vol. 84, issue 12, pp. 2161-2172, 2010
- [2] Japan Meteorological Agency: Satellite Imagery, <https://www.jma.go.jp/>, access 2021/07/30
- [3] R. Takada: Short-term prediction of cloud movements with meteorological satellite images processed in spectrum space, Bachelor Thesis, Gifu University, 2020 (in Japanese)

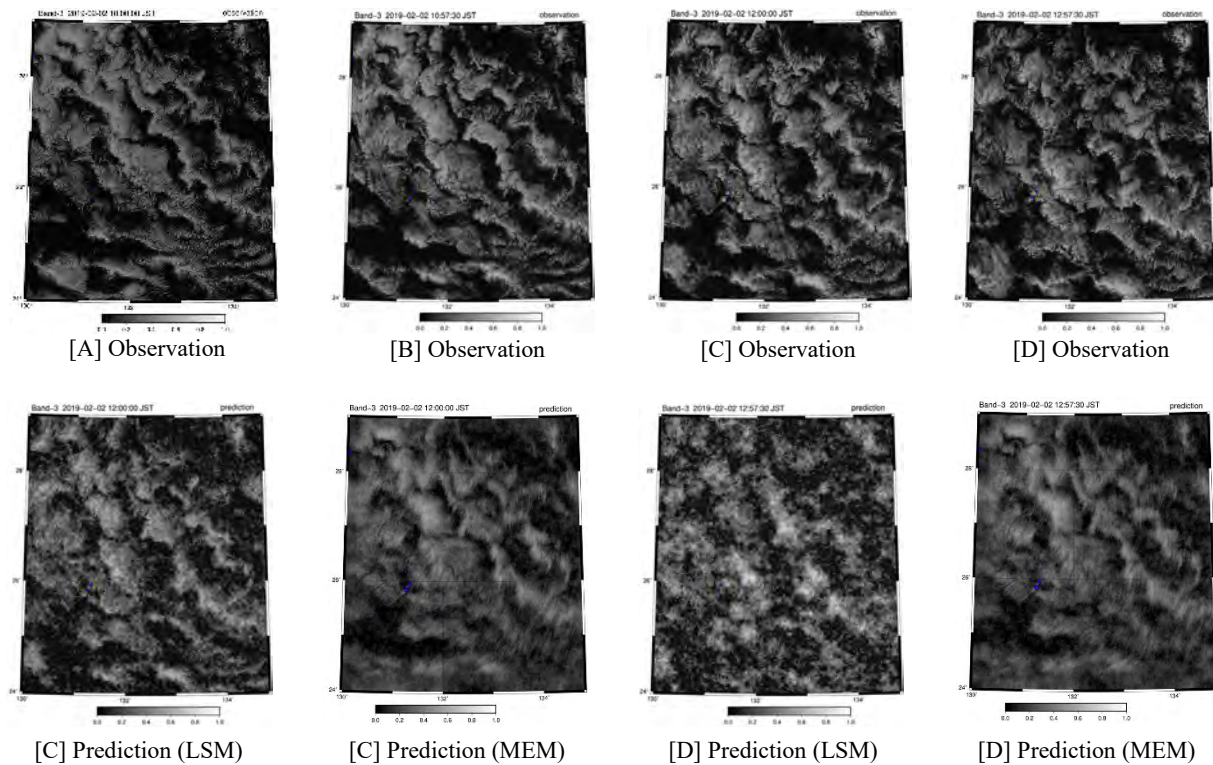


Fig. 3: Images observed with a meteorological satellite (images in upper row) and future cloud images (images in lower row) predicted with linear regression (LSM) or Maximum Entropy method (MEM). [A] to [D] indicate observation or prediction time; [A] 10:00:00, [B] 10:57:30, [C] 12:00:00, [D] 12:57:30

Table 1. Statistical error indices of predictions

	Prediction by LSM ([C] 12:00:00)	Prediction by MEM ([C] 12:00:00)	Prediction by LSM ([D] 12:57:30)	Prediction by MEM ([D] 12:57:30)
Correlation coefficient	0.699	0.324	0.322	0.179
RMSE	0.110	0.136	0.173	0.136

Application of Kalman filter to solar irradiance forecasting with a meteorological model in tropical region

Naoki Moriai¹, Daiki Harada¹ and Tomonao Kobayashi²

1. Graduate School of Natural Science and Technology, Gifu University

2. Faculty of Engineering, Gifu University

INTRODUCTION

Huge amount of photovoltaic (PV) systems are already installed in worldwide. In the tropical region, solar irradiance is usually high, and the region has advantage for PV generations. Because the PV output fluctuates by changing of weather and solar irradiance, PVs which are connected to electric grids cause of instability of power on the grids. As one of solutions of this problem, the weather and solar irradiance are forecasted with a numerical weather model and are utilized for appropriate grid management. For better grid management, the weather and solar irradiance with higher accuracy is required. However, the meteorological physical processes in the atmosphere in the tropical region is complicated and the accuracy of the weather and solar irradiance forecasting with the numerical model isn't high. Harada (2020) optimized physical parameters in a numerical weather model to improve the accuracy of predictions of solar radiation intensity in tropical regions. In his study, the correlation coefficient between observed and forecasted solar irradiances was improved. However, RMSE between the irradiances remained large. The forecasted irradiance is seemed to overestimate compare with the observed one, and it may be caused of the large RMSE. In this study, a postprocessing of the weather model is introduced and removed the bias from the solar irradiance forecasted with the model.

METHODOLOGY

In this study, the solar irradiance is forecasted with a numerical weather first, and the irradiance is adjusted with a postprocessing.

Numerical weather model, WRF

As a numerical weather model, WRF (The Weather Research and Forecasting) is used. WRF is a three-dimensional, fully compressible, non-hydrostatic numerical weather model developed by the National Center for Atmospheric Research, the National Centers for Environmental Prediction, and other organizations.

Kalman filter as a postprocessing

As a postprocessing of WRF simulation, Kalman filter is introduced to reduce the overestimation and adjust the forecasted solar irradiance. Kalman filter is employed widely in engineering field. Liu et al. (2014) also applied it to the solar irradiance forecasting. As following to their study, the mathematical model of the filter is set up. Here, a variable x in a system is consider. The development of x from the previous step can be indicated with the following equation.

The equation of state:

$$x_k = Ax_{k-1} + B\omega_k \quad (1)$$

Where x_k is the state quantity at step k , A and B are the transformation matrices, and ω_k is a noise (normal white noise with mean 0 and variance q_a) about the state quantity. If we assume that a part of the state quantity x_k is observed, the relation between the state quantity x_k and the observed value z_k can be shown as follows;

The equation of observation:

$$z_k = Hx_k + v_k \quad (2)$$

Where H is the transformation matrix and v_k is a noise associated with the observed values (normal white noise with mean 0 and variance R). Eqs. (1) and (2) are called the state-space representation equations. In this study, a linear system model for evaluation of the adjusted solar irradiance I_{WRF-KF} with Kalman filter from the forecasted one I_{WRF} with WRF is employed, and indicate it as follows;

$$I_{WRF-KF} = aI_{WRF} \quad (3)$$

Where a is a state variable of this model. From this formulation, A and B in Eq. (1) are unitary matrices in this study. In order to improve the accuracy, it is necessary to set a variable q_a for the noise of the state equation and the variable R for the noise of the observation equation. In this study, q_a and R are changed in the range of 10^{-10} to 10^{10} and 10 to 10^{21} , respectively, and the annual RMSE of the solar irradiances is calculated, and the optimal values for the variances are found.

Computational conditions

The resolution of the finest domain, Domain 3 is 2 km. The National Electronics and Computer Technology Center (NECTEC) of Thailand is located at the center of the domain, and the solar irradiance is observed at the center. Domain 1 (18 km resolution), Domain 2 (6 km resolution) and Domain 3 are nested each other for computation of weather. The computation period is from 2019/07/01 to 2020/09/30, but the first three months are not included in the output because they are the spin-up period of the state variable a in Kalman filter, and the output period is one year from 2019/10/01 to 2020/09/30. The analysis data and forecasted data until 72-hour ahead of NCEP operational Global Forecast System (GFS) 0.25-degree grids (horizontal resolution $0.25^\circ \times 0.25^\circ$, 1 hourly interval) is used as input data for initial and boundary values of WRF forecasting.

RESULTS AND DISCUSSIONS

The correlation coefficients and RMSEs of the forecasted solar irradiance I_{WRF} with WRF and the adjusted one I_{WRF-KF} with Kalman filter are summarized in Table 1. By applying Kalman filter as a postprocessing of WRF forecasting, the correlation coefficient remains the same, but the RMSE reduces about 52 W/m², and this result indicates that the accuracy of the computed solar irradiance is improved with Kalman filter.

Figure 1 shows time variation of the state variable a of Kalman filter. As a reference, result of monthly regression analysis of the forecasted and observed solar irradiances is also plotted on the figure. By referring of the linear system model of Kalman filter, Eq. (3), the following equation is introduced as a model of this analysis.

$$I_{OBS} = aI_{WRF} \quad (4)$$

Where I_{OBS} is the observed solar irradiance, and I_{WRF} is the forecasted one by WRF value, and a is the coefficient of the model. The trend of the state variable a in Kalman filter is similar to the one of the coefficient a of the regression analysis. This result explains that Kalman filter works properly. The state variable a of Kalman filter is updated every day, and it vibrates in short period as in the figure, however it doesn't show sudden changes. In dry season (November to March), the variable a is relatively high, but the value moves around 0.8

through a year. As explained before, the state variable a is updated every day, and it contributes to the improvement of the forecasting accuracy as indicated in Table 1.

Table 1: Annual correlation coefficients and RMSEs between observed and WRF forecasting

	Correlation Coefficient	RMSE (W/m ²)
Forecasted solar irradiance I_{WRF} with WRF	0.831	216.0
Adjusted solar irradiance I_{WRF-KF} with Kalman filter	0.831	163.9

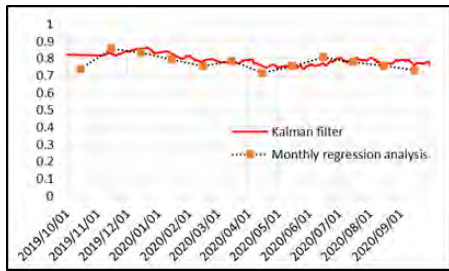


Fig.1: Timeseries of state variable a of Kalman filter and coefficients a of monthly regression analysis.

Figures 2 and 3 show daily solar irradiances in clear days and cloudy days, respectively. Their periods are from 2020/01/30 to 2020/02/01, and 2020/06/15 to 2020/06/17. In the figures, observed irradiance I_{OBS} , forecasted one I_{WRF} with WRF, and adjusted one I_{WRF-KF} with Kalman filter are plotted. In each figure, the forecasted irradiance I_{WRF} is overestimated compare with the observed one I_{OBS} . The adjusted irradiance I_{WRF-KF} is reduced from the forecasted one I_{WRF} by applying Kalman filter, and fits well with the observed one I_{OBS} . The adjusted irradiance I_{WRF-KF} represents the observed one I_{OBS} better in clear days as shown in Figure 2 than in cloudy days as in Figure 3. It is caused that the weather sometimes changes suddenly, e.g. squalls in the cloudy days in tropical region, Thailand, but WRF cannot simulate the sudden-change weather or cannot follow the changes well. This error isn't correct with Kalman filter presented in this study.

Figures 4 and 5 show the correlation maps between the observed and the forecasted irradiances, and between the observed and the adjusted ones, respectively. The lines with gradient 1 are plotted as a reference. Interval of the plotted data is 10 minutes, therefore the error seems large in these figures when the WRF cannot follow the sudden change of the weather as found in Figure 3. If the timeseries of solar irradiances are smoothed and the interval becomes longer, the error in the figures may be reduced. In the figures, the results of regression analysis are indicated with red lines. Its gradient is larger than

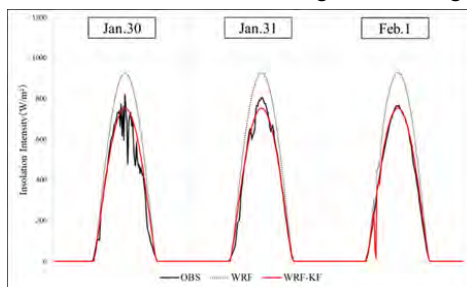


Fig.2: Timeseries of observed solar irradiance I_{OBS} , forecasted one I_{WRF} with WRF, and adjusted one I_{WRF-KF} with Kalman filter in successive three clear days.

1.0 in Figure 4, and it indicates that the forecasted irradiance with WRF, I_{WRF} is overestimated compared with the observed one I_{OBS} , the same as the explanations with Figures 3 and 4. On the other hand, the gradient of the red line is a little lower than 1.0, and it leads that Kalman filter adjusts the overestimate in WRF forecasting and evaluates appropriate irradiance.

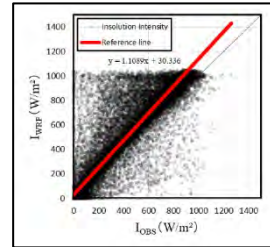


Fig.4: Correlation map between observed solar irradiance I_{OBS} and forecasted one I_{WRF} with WRF.

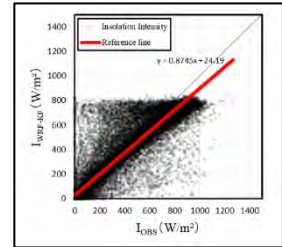


Fig.5: Correlation map between observed solar irradiance I_{OBS} and adjusted one I_{WRF-KF} with Kalman filter.

CONCLUSIONS

In this study, Kalman filter is employed as a postprocess of the numerical weather model WRF, and the forecasted solar irradiance with WRF is improved using it. The target is tropical area, Thailand. The WRF overestimates the solar irradiance, but the overestimation is removed by Kalman filter and appropriated one is evaluated. By applying Kalman filter, the correlation coefficient of the computed irradiance with WRF to the observed one remains the same, but its RMSE is reduced by about 52 W/m² and is improved. The state variable a of Kalman filter varies in time, but it doesn't show big changes. Its value is around 0.8 through a year. The WRF cannot represent sudden-change weather in tropical area, e.g. squall, or cannot follows the change well, and it causes of reducing forecasting accuracy. This error isn't corrected with Kalman filter presented in this study.

REFERENCES

- Harada, D: Optimisation of a weather forecasting model for the accurate calculation of solar radiation intensity in the tropics, Bachelor Thesis, Gifu University, 2020. (in Japanese)
- Skamarock, W. C., J.B. Klemp, J. Dudhia, D.O. Gill, D.M. Barker, W. Wang, and J.G. Powers: A description of the advanced research WRF version 3. Tech. Note TN-475+STR, 1-96. 2008.
- Liu, Y., S. Shimada, J. Yoshino, T. Kobayashi, K. Furuta, and Y. Miwa: Solar irradiance forecasting using the WRF model and Kalman filter, Grand Renewable Energy 4 p., 2014.
- National Centers for Environmental Prediction: NCEP Products Inventory – Global Products, <https://www.nco.ncep.noaa.gov/pmb/products/gfs/>, access 2021/07/23

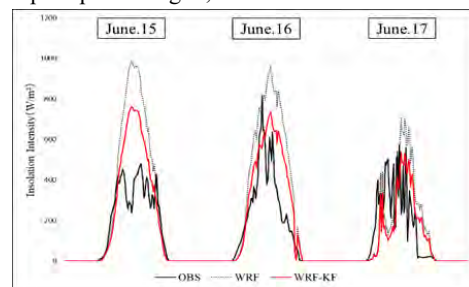


Fig.3: Timeseries of observed solar irradiance I_{OBS} , forecasted one I_{WRF} with WRF, and adjusted one I_{WRF-KF} with Kalman filter in successive three cloudy days.

Bacterial activity and EPS affect the performance of household wastewater treatment facility

Haoning Su¹, Miya Ogata³, Yuuki Okochi², Shinya Okumura², Yasushi Ishiguro³ and Fusheng Li³

1. Graduate School of Engineering, Gifu University, Japan

2. Kasugai Office, Aichi Prefectural Johkasou Association, Kasugai, Aichi, Japan

3. River Basin Research Center, Gifu University, Japan

INTRODUCTION

On-site wastewater treatment facilities were regarded as alternative technology of centralized wastewater treatment plants (WWTPs) for single households. The performance of this facility is greatly affected by activity of microbial communities which contributed to the oxidation of carbon and ammonia, reduction of nitrate. However, due to the limitation of volume and structure, it is difficult to achieve the continuous discharge and return of accumulated sludge compare with general WWTPs and no study is known to us investigating the microbial activity related with the performance of household wastewater treatment facility. In addition, the adhesion and aggregation properties of microbial cells are closely related to extracellular polymeric substances (EPS), which may have a close relationship with settleability of sludge and affect the final liquid-solid separation step. In this study, 15 units of household wastewater treatment facility were investigated to treat single household wastewater, and the sampling was conducted based on different periods after desludging operation reflects to different sludge retention time (SRT) among 22 to 586 days, as the sludge in this facility which have a much longer retention time than the sludge in WWTPs. Thus, specific objectives of this research were to: 1) evaluate the performance of this single household wastewater treatment facility and analyze the correlation of each water quality indexes by principal components analysis (PCA) and agglomerative hierarchical clustering (AHC); 2) identify relationships between treatment efficiencies and the microbial communities and EPS of accumulated sludge.

METHODS

(1) Treatment facilities and sample collection

This research was conducted in residential areas (Aichi prefecture, Japan). 15 typical household wastewater treatment facilities in these areas, using fluidized bed biofilm treatment method with the same structure, were selected to represent the different sludge retention time namely as short sludge retention time (S-SRT), middle sludge retention time (M-SRT) and long sludge retention time (L-SRT).

(2) Sample analysis

For water samples, transparency, turbidity, pH, biological oxygen demand (BOD) for particulate BOD (PBOD) and dissolved BOD (DBOD), chemical oxygen demand (COD_{Cr}) for particulate COD_{Cr} (PCOD) and dissolved COD_{Cr} (DCOD), total nitrogen (TN) for particulate N (PN) and dissolved N (DN) and total phosphorus (TP) for particulate P (PP) and dissolved P (DP) were measured. Dissolved organic carbon (DOC) (TOC-Vws, Shimadzu Co., Japan), and ultraviolet absorbance at 260 nm (UV260) and 390 nm (UV390) (UV-2600, SHIMADAZU, Japan) were measured for the samples after filtration through 0.2 µm membrane filters. For sludge samples, the activity of bacteria in sludge was analyzed based on dehydrogenase activity (DHA) (Zhou et al., 1996) and specific oxygen utilization rate (SOUR) (Mark C et al., 2016). Extracellular

polymeric substance (EPS) of sludge samples were extracted using the modified method described by Liang et al. (2010) and measured by the colorimetric methods (Basuvaraj et al., 2015).

(3) Statistical analysis

Measurement results in the series of water quality were used as the pooled data for analysis after standardization treatment of the obtained data for each index. Then, the principal component analysis (PCA) and agglomerative hierarchical clustering (AHC) were performed using the SPSS software (IBM SPSS Statistic 21.0, IBM Corp., Armonk, NY) for better understanding the interrelations of all measured water quality indexes (including SS, turbidity, BOD, COD, DOC, UV260, UV390, nitrogen and phosphorus).

RESULT AND DISCUSSION

(1) Water quality evaluation by PCA and AHC

The results of main physicochemical indexes of the effluent from 15 treatment facilities are shown in Fig 1.

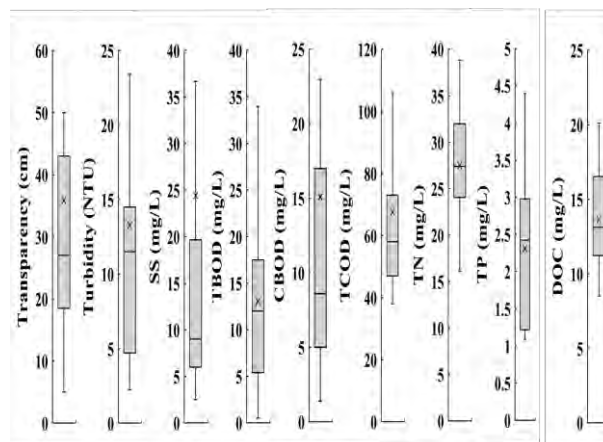


Fig. 1: Results of main physicochemical indexes of the effluent from 15 units during July 2020 – December 2020

Each treated water quality results scattered in a larger range, while the analyze with more specificity was conducted by PCA and AHC to clarify the correlation between each index and the factors that affect the treated water quality. Preliminary PCA results of component loadings together with previous study indicated that the treated water quality is affected by both suspended solids and dissolved organic matter, while results of component scores and cluster analysis showed that the facility of S-3 had a high score in the first principal component and formed one single cluster by itself, which was significantly different from the other 14 facilities. From these, we reanalyzed the data without outlier of S-3. There was no change in the overall trend that the 1st component was dominated by suspended solids while the 2nd component was dissolved organic matters. Reanalyzed PCA (component scores) and AHC results as shown in Fig. 2 (a) and Fig. 2 (b), remained 14

facilities were classified to be 3 groups named as Group 1, Group 2 and Group 3.

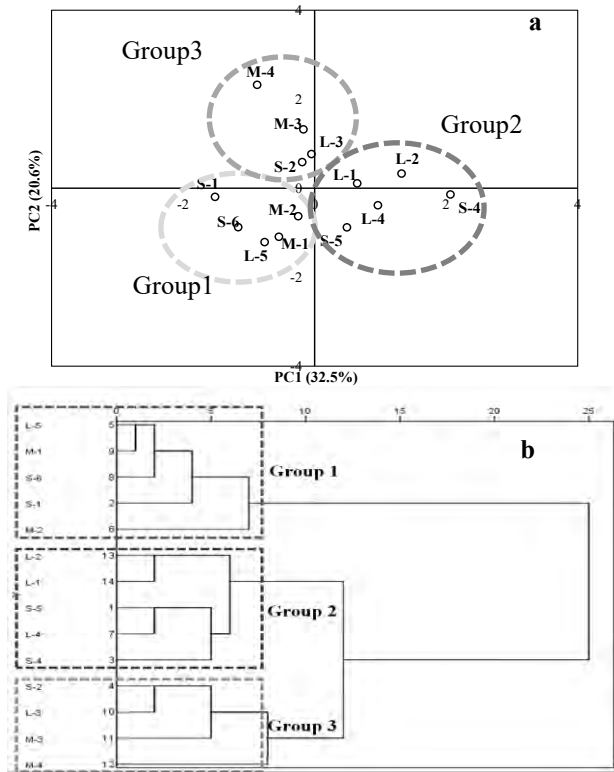


Fig. 2: Results of the statistical analysis using observed data for treated water (a: component scores of PCA; b: agglomerative hierarchical clustering)

(2) Treated water quality of each group

The comparison of the treated water quality of each group is shown in **Fig. 3**. The treated water quality of Group 1 tended to be better than other two groups, and the variability of the data was smaller. The treated water quality of Group 2 was not as good as that of Group 1, but the variability of the data was smaller than that of Group 3.

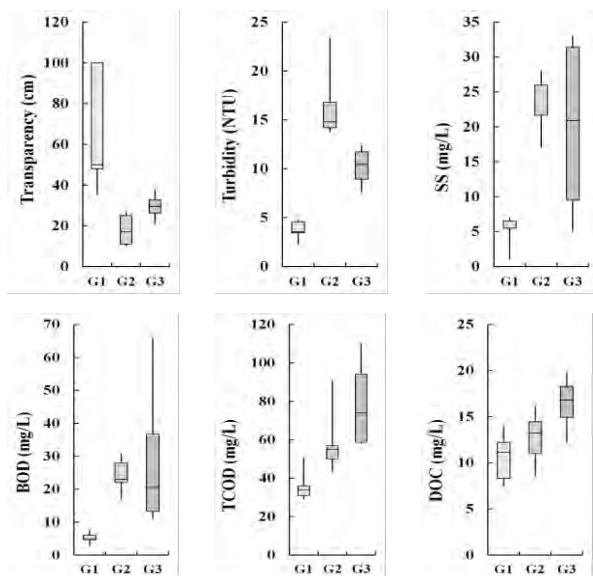


Fig. 3: Comparison of water quality of each group

(3) Characteristics of accumulated sludge based on bacterial activity and EPS

As shown in **Fig. 4 (a)** and **Fig. 4(b)**, the accumulated sludge of Group 1 had relatively higher bacterial activity which was characterized by dehydrogenase activity (a) and specific oxygen utilization rate (b), compare with the sludge of Group 2 and 3. Furthermore, as EPS quantified as loosely bound (LB-EPS) and tightly bound (TB-EPS) respectively, shown in **Fig. 4 (c)** and **Fig. 4 (d)**. Sludge of Group 1 had more content of TB-EPS with strong binding between the cells but less LB-EPS. On the contrary, sludge of Group 2 contains more LB-EPS than TB-EPS relatively.

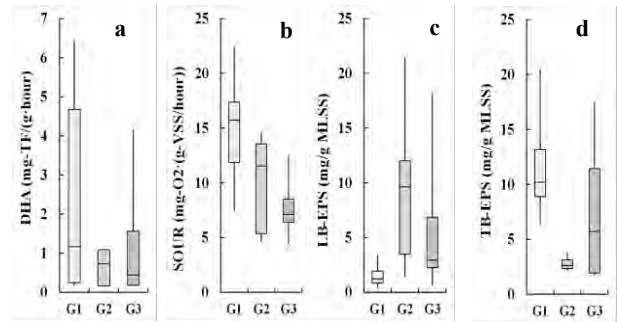


Fig. 4: Characteristics of accumulated sludge based on bacterial activity (a: dehydrogenase activity; b: specific oxygen utilization rate) and EPS (c: LB-EPS; b: TB-EPS)

Sludge contains more content of TB-EPS than LB-EPS and behaves as higher microbial activity as well. At the same time, the sludge volume index (SVI) of this kind of sludge (Group 1) showed lower values which means sludge particles are easily aggregated to be the settleable flocs. However, for the sludge of Group 2 and Group 3, lower microbial activity and more LB-EPS contents may affect the aggregation of sludge flocs and lead to the high concentration of suspended solids in the treated water.

The findings at this stage clarified the contribution of the activity of bacteria and different contents of EPS in accumulated sludge to the performance of household wastewater treatment facility. Higher microbial activity and more TB-EPS content in sludge may be beneficial to the treated water quality by promoting the biological degradation of dissolved organic matters and settleability of sludge.

REFERENCES

- Zhou, C., Yin, J., (1996) A method for measurement of ttc-dehydrogenase activity. Acta Scientiae Circumstantiae. CNKI:SUN:HJXX.0.1996-04-003
- Yoshiyama, K., Mellard, J. P., Litchman, E., and Klausmeier, C. A. (2009) Phytoplankton Competition for Nutrients and Light in a Stratified Water Column. American Naturalist 174:190-203.
- Mark C. M. van Loosdrecht;Per H. Nielsen;Carlos M.Lopez-Vazquez;Damir Brdjanovic.,2016.Experimental Methods in Wastewater Treatment. IWA PUBLISHING.3.5.3.2.
- Liang, Z.W., Li, W.H., Yang, S.Y., Du, P., 2010.Extraction and structural characteristics of extracellular polymeric substances (EPS), pellets in autotrophic nitrifying biofilm and activated sludge. Chemosphere 81,626–632.
- Basuvaraj, M., Fein, J., Liss, S.N., 2015. Protein and polysaccharide content of tightly and loosely bound extracellular polymeric substances and the development of a granular activated sludge floc. Water Res. 82, 104-17.

Steam gasification of woody biomass with renewable hydrogen

Sheng-Wen Xiao¹ and Kazuhiro Kumabe²,

1. Graduate School of Natural Science and Technology, Gifu University; BWEL

2. Faculty of Engineering, Gifu University

INTRODUCTION

In order to alleviate global warming, the development of sustainable energy has become the mainstream. However, when new power generation technologies such as wind power and solar power are connected to the power system, one of the problems arises. The resonance caused by the uncertainty of the wind power generation cycle will have a huge impact on the stability of the power system (Brouwer et al. 2014). Using hydrogen as an energy carrier for renewable energy technologies such as wind power can solve this problem (Basile and Iulianelli 2014).

On the other hand, the process of liquid fuel production via the steam gasification of woody biomass is developed (Kumabe, K. et al. 2014). In the steam gasification, CO₂ is produced due to the water-gas shift reaction ($\text{CO} + \text{H}_2\text{O} \rightleftharpoons \text{CO}_2 + \text{H}_2$). Now, the introduction of hydrogen, derived from renewable energy, into the steam gasification is tried to reduce the CO₂ emission.

In the study, first, the effect of the addition of hydrogen to the simulated syngas, produced from the steam gasification, on the product gas composition was examined. Next, the effect of the addition of hydrogen to the steam gasification on the product gas composition was investigated using fixed-bed reactors of both a semi-batch (gas flow type) and continuous reactor.

MATERIALS AND METHODS

In order to study the influence of the introduction of hydrogen on the gas phase reaction of the synthesis gas between 600 and 900°C, the simulated synthesis gas (CO: 25.00 vol%, CO₂: 7.97 vol%, H₂: 24.90 vol%, and N₂ base) was first used to carry out experiments with the hydrogen introduction (its concentration: 25, 35, 50, and 75 vol%) using the apparatus, as shown in Fig. 1.

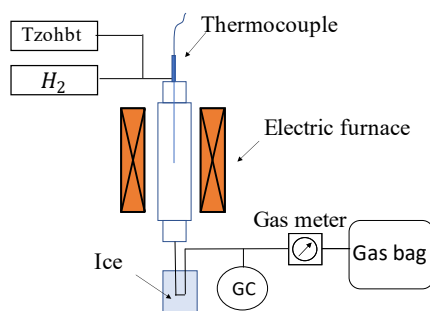


Fig. 1: Experimental apparatus for introducing hydrogen into simulated synthesis gas.

In the second stage, in order to study the reaction mechanism of the steam gasification of carbon in woody biomass and the

changes under the conditions of introducing hydrogen, carbon particles with a purity of 99.9% and a particle size of 20 microns

were used as raw materials in the steam gasification (700-900°C) using the apparatus shown in Fig. 2.

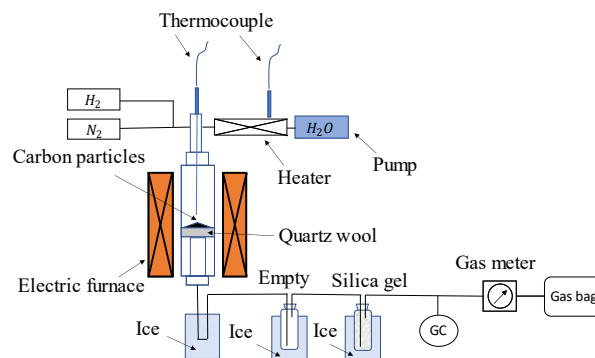


Fig. 2: Experimental apparatus of semi-batch fixed-bed reactor for carbon steam gasification.

The reaction conditions of carbon steam gasification without/with H₂ introduction using the semi-batch fixed-bed reactor are shown in Tables 1 and 2, respectively.

Table 1: Reaction conditions of carbon steam gasification without H₂ introduction using semi-batch fixed-bed reactor.

Temperature	700, 800, and 900°C
Gas pressure	1 atm
Mass of carbon particles	1 g
Flow rate of water(g)	62.22 mL/min
Flow rate of N ₂ (g)	100 mL/min
Time of reaction	60 min

Table 2: Reaction conditions of carbon steam gasification with H₂ introduction using semi-batch fixed-bed reactor.

Temperature	700, 800, and 900°C
Gas pressure	1 atm
Mass of carbon particles	1 g
Flow rate of water(g)	62.22 mL/min
Flow rate of N ₂ (g)	50 mL/min
Flow rate of H ₂ (g)	50 mL/min
Times of reaction	60 min

In the semi-batch fixed-bed reactor, the molar ratio of H₂O/C in the reaction is not steady. Considering the gas density around the carbon particles and the high diffusion of hydrogen that affect the kinetic of surface reaction (Li et al. 2012), it is decided to use the method of continuous feeding of carbon in order to steady the molar ratio of H₂O/C in the reaction, as shown in Fig. 3.

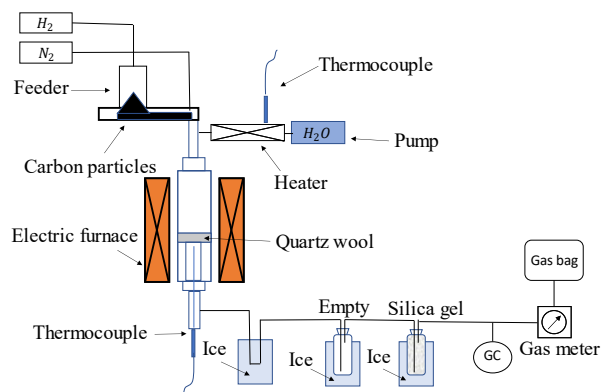


Fig. 3: Experimental apparatus of carbon continuous supply steam gasification.

RESULTS AND DISCUSSION

Based on the gas phase reaction, the experiment using simulated biomass gasification gas and introducing hydrogen under the condition of 600-900°C has obtained relatively clear results. The relationship of the increasing concentration of H₂ to the reduction ratio of CO₂, defined as the division of the initial CO₂ concentration (7.97 vol%) into the concentration in a product gas, is obtained, as shown in **Fig. 4**.

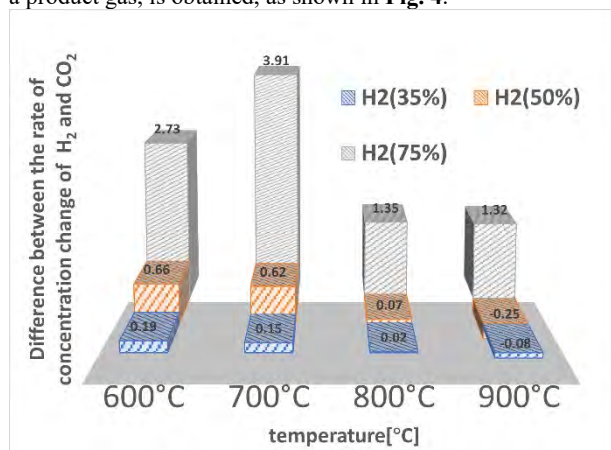


Fig. 4: Relationship of increasing concentration of H₂ to the reduction ratio of CO₂.

With the increase of hydrogen concentration, the production of CO₂ is obviously reduced, because in the water-gas shift reaction, hydrogen as a product will inhibit the progress of the reaction, reducing the CO₂ production.

Regarding the influence of temperature, between 600 and 700°C, the CO₂ reduction effect caused by the introduction of hydrogen is the most significant, and this is similar to any proportion of H₂ introduction.

In the semi-batch fixed-bed carbon steam gasification with the three sets of experiments at different temperatures, as shown in **Fig. 5**, the introduction of hydrogen significantly reduced the output of CO₂ due to the reaction rate of carbon.

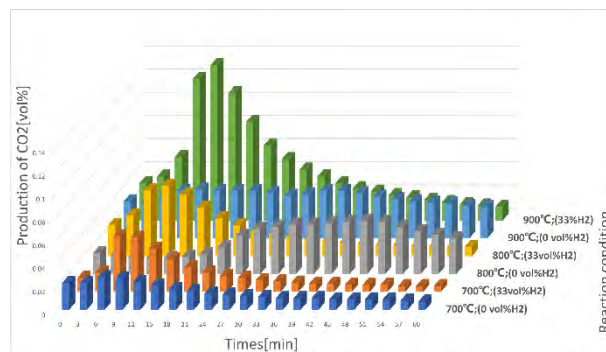


Fig. 5: Change in production of CO₂ with time for three sets of reaction condition in semi-batch fixed-bed carbon gasification.

It is currently in the carbon continuous feed gasification experiment, and the data of carbon continuous feed will be given in the future progress. And in the next stage, a continuous feed gasification experiment of woody biomass will be carried out.

CONCLUSIONS

Through experiments based on the gas phase reaction and the current preliminary simulation of the impact of the introduction of hydrogen on the carbon particles on the gasification process of woody biomass, it can be preliminarily understood that in the gas phase reaction, the introduction of hydrogen at the temperatures of 600-700°C is the most effective way to reduce CO₂ emissions. In the particle surface reaction stage, the introduction of hydrogen will print CO₂ production, while also inhibiting the carbon reaction. At 800°C, it has the most significant CO₂ suppression effect. At 900°C, while ensuring the suppression effect, the carbon reaction rate will also be greatly improved.

ACKNOWLEDGMENTS

REFERENCES

- Brouwer, A.S., Broek, V.D.M., Seebregts, A., and Faaij, A. (2014) Impacts of Large-scale Intermittent Renewable Energy Sources on Electricity Systems, and How These can be Modeled. *Renew. Sustain. Energy Rev.* 33:443-466.
- Basile, A. and Iulianelli, A. (2014) *Advances in Hydrogen Production, Storage and Distribution*. Woodhead Publishing.
- Li, Q., Xu, J., Gore, J. (2012) Multiphysics modeling of carbon gasification processes in a well-stirred reactor with detailed gas-phase chemistry. *Combustion and Flame* 159:1693-1707

Adsorbability of organic matter released from drinking water treatment sludge onto activated carbon

Sri Anggreini¹, Maulana Yusup Rosadi¹, Miya Ogata² and Fusheng Li²

1. Graduate School of Engineering, Gifu University, Gifu, 501-1193, Japan
2. River Basin Research Center, Gifu University, Gifu, 501-1193, Japan

INTRODUCTION

Organic matter (OM) in water is a complex mixture of organic compounds including humic substances, proteins, carbohydrates, lipids, and anthropogenic organic pollutants. OM causes several problems in the drinking water supply, including color and odor, the formation of carcinogenic disinfection by-products (DBPs), and promoting microbial growth in the water distribution system. Drinking water treatment produces residue known as drinking water treatment sludge (DWTS) which consists of flocs settled and detained in the sedimentation and filtration process, respectively. DWTS is gravity concentrated and the water is separated and recycled as raw water. OM in DWTS may affect the drinking water treatment process and finished water quality.

Activated carbon (AC) adsorption is considered as the most effective method to remove OM in water and its application is increasing. So far, many studies have been focused on the characteristics of OM released from DWTS based on instrumental analysis (Ahmad et al. 2016, Xu et al. 2017, Rosadi et al. 2020). However, the study based on the treatability by adsorption process is limited. Therefore, the objective of this study was to investigate the adsorbability of OM released from DWTS under different storage conditions. For this purpose, OM that released from DWTS under two different temperatures (20 and 40°C) and two oxygen conditions (with aeration and without aeration) was prepared and used for batch adsorption experiment. OM before and after adsorption was evaluated based on dissolved organic carbon (DOC), UV₂₆₀, and fluorescence excitation-emission matrix (EEM).

MATERIALS AND METHODS

Incubation experiment – The DWTS was collected from a drinking water treatment in Japan. This plant uses a rapid sand filtration system with a capacity of about 200,000 m³/day. The DWTS was transported to the laboratory and incubated under the condition with and without aeration at the temperatures of 20°C and 40°C. Five water samples were prepared, namely raw DWTS, without aeration 40°C (WOA-40), with aeration 40°C (WA-40), without aeration 20°C (WOA-20), and with aeration 20°C (WA-20). After 7 days incubation, centrifugation was conducted, and the supernatant was filtered through a 0.2 µm cellulose acetate membrane prior to being subjected to analysis.

Activated carbon – Filtrasorb-400 granular activated carbon (Calgon Co., USA) after crushing to powder below 45 µm was used in this study. The granular AC was washed with Milli-Q for 7 times and boiling for 1 hour before drying in an oven at 105°C. The granular AC was crushed and sieved with sizes below 45 µm, followed by washing with Milli-Q for removal of fine particles and drying in the oven at 105°C overnight.

Batch Adsorption experiment – Batch adsorption experiments were conducted according to the bottle-point method of variable AC doses in 500-ml flasks sealed with Teflon-lined rubber septa. To each flask, 100 ml of the water sample was added, followed by the addition of the adsorbent

with a designated dose within the range of 0-1.0 g/L. After 72 hours of shaking, the samples were filtered through a cellulose acetate membrane filter (0.2 µm) to remove AC. The concentration of OM was quantified as DOC (TOC 5000, Shimadzu Co.) and the UV₂₆₀ (Model UV-2600, Shimadzu Co.), respectively. The composition of OM was analyzed using a fluorescence spectrophotometer (RF-5300, Shimadzu Co.). The adsorption data were analyzed using the modified Freundlich isotherm model by Eq. (1).

$$q = K \left(\frac{C}{D_{AC}} \right)^{\frac{1}{n}} \quad (1)$$

where, q is equilibrium solid phase concentration, C is equilibrium liquid phase concentration, D_{AC} is activated carbon dose, and K and $1/n$ are the adsorption parameters reflecting the adsorption strength of adsorbate and its affinity with the adsorbent, respectively.

RESULTS AND DISCUSSION

Composition changes based on OM before and after adsorption – The fluorescence EEM results are shown in Fig. 1. Three peaks were detected such as P1 (protein-like), P2 (fulvic-like), and P3 (humic-like). The two corresponding apparent peaks of humic molecules (P2 and P3) gradually disappeared. However, the intensity of P1 could still be seen even the AC doses increasing to 1 g/L, suggesting protein-like substances were less adsorbable than humic ones. Gu et al. (1995) reported that OM fractions with larger MW (>3000 Da) have higher adsorption affinity and capacity compared with the smaller ones (<3000 Da). Similar phenomena were also observed during the adsorption of humic molecules (larger size) and protein-like substances (smaller size) onto AC.

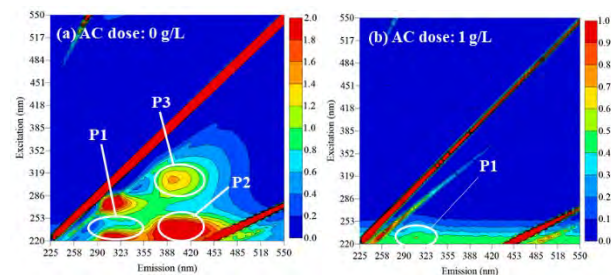


Fig. 1 Fluorescence EEM of OM at condition of without aeration of 40°C (WOA-40), (a) before and (b) after adsorption (DOC = 9.73 mg/L).

Adsorbability of OM based on the residual concentration profiles – The residual rate of UV₂₆₀ was much lower than DOC as shown in Fig. 2. DOC reflects all organic molecules (adsorbable and less or non-adsorbable) that present in DWTS, while UV₂₆₀ only reflects those possessing UV-absorbing features in DWTS. Therefore, AC was effective to remove UV adsorbing substances than non-UV adsorbing substances. Previous study also reported that AC was known to adsorb preferentially the UV₂₆₀ adsorbing substances, which yielded the great reduction of SUVA values. The residual rates based on the fluorescence EEM components are displayed in Fig. 3.

Table 1. Parameters of modified Freundlich isotherm based on different indices.

Indices	Parameters	Raw DWTS	WOA-40	WOA-20	WA-40	WA-20
DOC	$K_f(\text{mg/g})^{1-1/n}$	7.42	12.07	6.89	4.05	5.57
		(6.81-7.75) ^c	(11.37-12.86) ^d	(6.38-7.45) ^{bc}	(3.88-4.15) ^a	(3.75-6.19) ^{ab}
	$1/n$	0.67	0.54	0.67	0.78	0.73
		(0.65-0.71) ^a	(0.50-0.68) ^a	(0.63-0.81) ^a	(0.77-0.81) ^a	(0.48-0.84) ^a
	R^2	0.985	0.995	0.979	0.980	0.994
UV260	$K_f[\text{m}^{1/n-1}/(\text{g/L})^{1-1/n}]$	48.72	51.27	35.93	22.49	33.20
		(47.05-53.13) ^c	(50.71-54.59) ^c	(36.12-39.01) ^b	(21.41-24.93) ^a	(32.62-33.38) ^b
	$1/n$	0.36	0.46	0.58	0.55	0.46
		(0.34-0.41) ^a	(0.44-0.51) ^{ab}	(0.54-0.62) ^b	(0.53-0.62) ^b	(0.45-0.52) ^{ab}
	R^2	0.967	0.986	0.985	0.996	0.984
Protein-like (P1)	$K_f[\text{QSU}/(\text{g/L})]^{1-1/n}$	2.67	4.38	2.65	1.61	2.39
		(1.68-4.31) ^a	(3.85-6.54) ^a	(2.02-4.05) ^a	(1.09-2.84) ^a	(1.79-3.10) ^a
	$1/n$	0.67	0.57	0.68	0.69	0.70
		(0.50-0.73) ^a	(0.49-0.69) ^a	(0.57-0.79) ^a	(0.62-0.83) ^a	(0.56-0.71) ^a
	R^2	0.997	0.976	0.991	1.000	0.985
Fulvic-like (P2)	$K_f[\text{QSU}/(\text{g/L})]^{1-1/n}$	5.28	8.95	5.69	4.25	5.72
		(4.67-7.47) ^{ab}	(7.99-10.34) ^b	(5.20-7.22) ^{ab}	(3.97-5.10) ^a	(4.73-6.47) ^{ab}
	$1/n$	0.61	0.56	0.66	0.60	0.67
		(0.63-0.71) ^{ab}	(0.49-0.60) ^a	(0.56-0.72) ^{ab}	(0.56-0.69) ^b	(0.60-0.70) ^{ab}
	R^2	0.990	0.971	0.991	0.968	0.984
Humic-like (P3)	$K_f[\text{QSU}/(\text{g/L})]^{1-1/n}$	6.81	14.41	8.10	5.07	6.87
		(5.99-7.07) ^{ab}	(13.89-15.62) ^b	(6.82-10.77) ^{ab}	(4.69-6.25) ^a	(5.89-7.19) ^{ab}
	$1/n$	0.42	0.60	0.62	0.46	0.42
		(0.38-0.53) ^a	(0.35-0.68) ^b	(0.56-0.65) ^a	(0.37-0.51) ^{ab}	(0.34-0.45) ^{ab}
	R^2	0.986	0.994	1.000	0.993	0.999

Different letters (a,b,c,d) given behind the data shown the differences between the groups in the same row are statistically significant (Tukey's HSD test, $p < 0.05$). The letter 'ab' or 'bc' means the differences of the values with the letters of 'a' and 'b' or 'b' and 'c' are not statistically significant.

The residual rates of P3 were much lower than those of P2, followed by those of P1. The results demonstrated that humic-like was more preferably removed by AC than fulvic-like, followed by protein-like substances. The stronger adsorption of humic-like than fulvic-like and protein-like is probably due to the larger molar mass of humic-like molecules, resulting in a large number of reactive groups present per molecule. An important factor in the stronger adsorption strength of humic-like substances is the larger number of reactive ligands on humic-like molecules than fulvic-like molecules. A humic-like (13.2 kDa) molecule contains 32 carboxylic and 32 phenolic groups. However, fulvic-like (0.683 kDa) contains 4 carboxylic and 1 phenolic group (Weng et al. 2007).

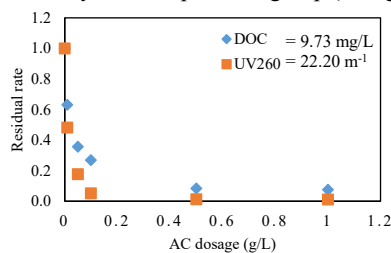


Fig. 2 Residual rates of OM vs. AC dosages (WOA-40).

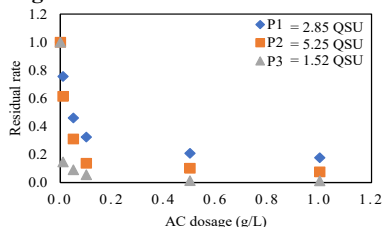


Fig. 3 Residual rates of fluorescence EEM components vs. AC dosages (WOA-40).

Adsorbability of OM based on the adsorption strength – The estimated parameters of modified Freundlich isotherm are summarized in **Table 1** and displayed in **Fig. 4**. The K values followed the order WOA-40 > raw DWTS > WOA-20 > WA-

20 > WA-40 for DOC-based, indicating OM released without aeration possessed higher adsorbability than with aeration conditions. For fluorescence EEM components at condition of WOA-40 as examples, the K value for P3 ($14.41 (\text{QSU}/(\text{g/L}))^{1-1/n}$) was generally higher than those for P2 ($8.95 (\text{QSU}/(\text{g/L}))^{1-1/n}$) and P1 ($4.38 (\text{QSU}/(\text{g/L}))^{1-1/n}$). This result is consistent with the residual rates of EEM components mentioned previously. It suggests that protein-like substances were less adsorbable than humic-like substances. The differences in molecular weight, functional group, and hydrophobic or hydrophilic feature of OM were probably the reason behind the differences in adsorbability of OM released from DWTS.

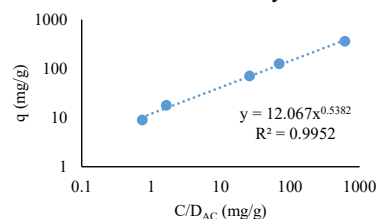


Fig. 4 Modified Freundlich isotherm for OM based on DOC (WOA-40).

CONCLUSIONS

The adsorbability of OM released from DWTS was investigated. The OM contains more constituting components with higher adsorbability and varied greatly in different temperature and oxygen conditions. Compositional analysis by fluorescence EEM indicated that humic-like and fulvic-like substances have higher adsorbability than protein-like substances.

REFERENCES

Weng, L., H. W., Riemsdijk, V., Hiemstra, T. (2007) Adsorption of humic acids onto goethite: Effects of molar mass, pH and ionic strength. *J. Colloid Interface Sci* 314:107-118.

Coexisting and competing algal species with moldy odor-causing blue algae in Nagara River

Wenqing Li¹, Haoning Su², Shoma Wakamiya³ and Fusheng Li⁴

1. Graduate School of Natural Science and Technology, Gifu University, Japan

2. Graduate School of Engineering, Gifu University, Japan

3. Faculty of Engineering, Gifu University, Japan

4. River Basin Research Center, Gifu University, Japan

INTRODUCTION

Odor and smell are important items that greatly affect the quality of tap water and are highly concerned by consumers and drinking water suppliers. As the major compounds causing moldy odor even at very low concentration levels, for instance, several ng/L, 2-methylisoborneol (2-MIB) and geosmin are mainly produced by *Cyanophyceae* (blue algae) and *actinomycetes* as their metabolic products. Understanding the coexisting and competing of these microorganisms with other algal and bacteria species in the tap water sources (rivers, lakes and reservoirs) is very important for better management of the sources and for controlling their growth and presence in water. In this study, analysis was conducted for the measurement results of eight families of algal species in the water intake of Nagara River and the coexisting and competing of the moldy odor-causing blue algae with other algal species were evaluated.

MATERIALS AND METHOD

The measurement results of algal species in the following eight families were analyzed: *Cyanophyceae*, *Flagellata*, *Chlorophyceae*, *Bacillariophyceae*, *Cryptophyceae*, *Chrysophyceae*, *Dinophyceae*, and *Euglenophyceae*. The results were obtained for water samples collected once a month from the water intake at the downstream of Nagara River over the past 20 years (1999-2019). Measurement was conducted through optical microscope observation. The analysis of the measurement results was conducted based on principal component analysis (PCA) and agglomerative hierarchical clustering (AHC) (IBM SPSS Statistic 21.0).

RESULTS and DISCUSSION

The monthly changes of the number concentration of the total algae (eight families) of at the Nagara River water intake for 20 years are shown in Fig. 1a. The mean number concentration showed distinct increase from May, reached its highest in June and then fluctuated with comparatively higher values till September. The mean number concentration remains stable at lower levels from December to April. Of the total eight observed algal families in the past 20 years, *Bacillariophyceae*, *Chlorophyceae* and *Flagellata* were found to be the dominating species, contributing greatly to the total algal species present in the river. In addition, it is clear from the box chart that, for all months in the period from April to October, the changes in the algal number were relatively large, indicating that the number concentration of algae fluctuated greatly in the past 20 years.

The monthly changes of the number concentration of *Cyanophyceae*, some species of which are well blamed for their significant contribution to the occurrence of moldy odor in most surface water sources, in the water intake of Nagara River in the past 20 years are shown in Fig. 1b. It can be seen

from the figure that the number concentration of *Cyanophyceae* was larger in the period from July to September, with the largest emerging in August, a trend clearly different from the trend of the total algae shown in Fig. 1a and the trends of the dominating three algal families observed in the river, *Bacillariophyceae*, *Chlorophyceae* and *Flagellata*. A relatively larger number changes over the past 20 years was also confirmed for the moldy odor-causing algal family in the month of its richest occurrence (i.e., in August).

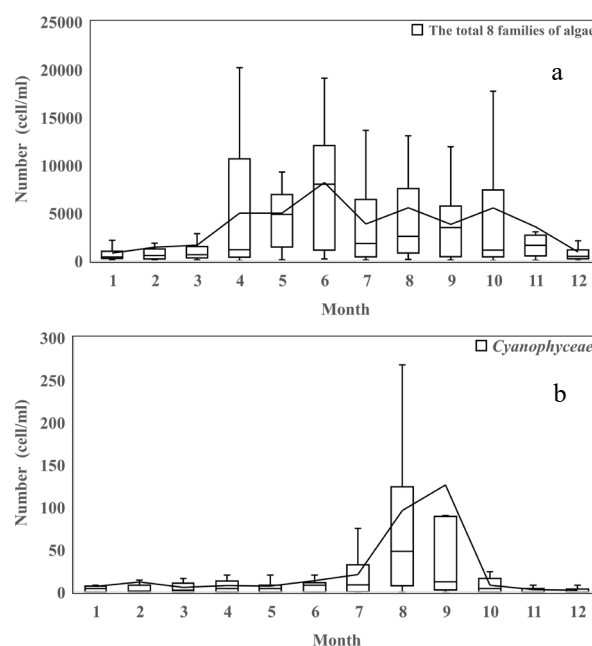


Fig. 1. The monthly changes of the number concentration of algae: (a) the total eight families of algae, (b) *Cyanophyceae*

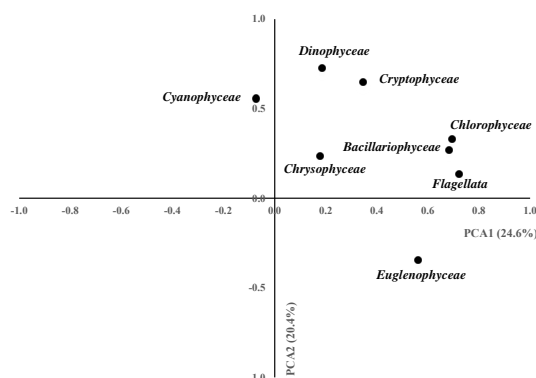


Fig. 2. Relations among eight algal families analyzed by principal component analysis

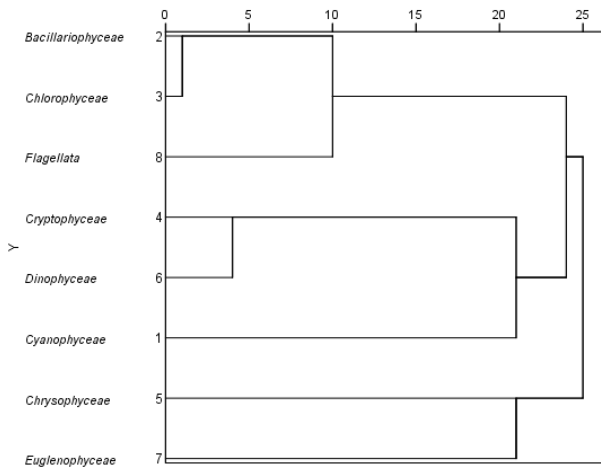


Fig. 3. Relations among eight algal families analyzed by agglomerative hierarchical clustering

To evaluate the coexisting and competing relations of the moldy odor-causing *Cyanophyceae* with other algal families in the water intake of Nagara River, principal component analysis and agglomerative hierarchical clustering were conducted by using the number concentration results of the eight algal families observed for the past 20 years. The result of principal component analysis is shown in Fig. 2, and that of the agglomerative hierarchical clustering is shown in Fig. 3.

As shown in Fig. 2, although *Cyanophyceae* was negatively correlated with other algae in the first principal component, its load rate in the first principal component was very small. In the second principal component, *Cyanophyceae* correlated negatively with *Euglenophyceae*; while it correlated positively with *Dinophyceae* and *Cryptophyceae*. The clustering result in Fig. 3 showed that *Cryptophyceae* and *Dinophyceae* were more strongly correlated, but the algal family of *Cyanophyceae* also fell in the group. It could be seen that *Cyanophyceae* was the family most distant from the family of *Euglenophyceae*. This is consistent with the result of the principal component analysis, thus revealing the likely coexisting relations of *Cyanophyceae* with *Dinophyceae* and *Cryptophyceae*, and the likely competing relation of *Cyanophyceae* with *Euglenophyceae*.

Since the family of *Cyanophyceae* is most abundant in August, to further investigate the coexistence and competition

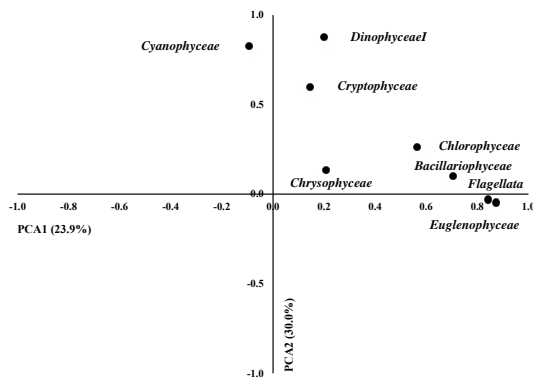


Fig. 4. Relations among eight algal families in August analyzed by principal component analysis

number concentrations in August of the past 20 years were compiled and analyzed by principal component analysis. The analysis result is shown in Fig. 4. *Cyanophyceae* and *Euglenophyceae* showed a strong negative correlation in both the first and second principal components. In addition, in the second principal component, the relation between *Cyanophytaaceae*, *Dinophyceae* and *Cryptophyceae* was also found more obvious. Agglomerative hierarchical clustering was also performed on the basis of data of August alone. As shown in Fig. 5, the group relation between *Cyanophyceae* and *Euglenophyceae* was still the furthest. *Cyanophytaaceae*, *Dinophyceae* and *Cryptophyceae* belonged to the same group, and *Cyanophyceae* and *Dinophyceae* were more closely related. The result showed that, in August, the coexisting relation between *Cyanophyceae* and *Dinophyceae* was more profound than the coexisting relation between *Cyanophyceae* and *Cryptophyceae*. With this analysis approach, *Cyanophyceae* and *Euglenophyceae* also revealed a competitive relation.

By conducting principal component analysis and agglomerative hierarchical clustering for the number concentration data of eight algal families in the past 20 years, we found that a coexisting relation of *Cyanophyceae* with *Dinophyceae* and *Cryptophyceae*, and a competing relation of *Cyanophyceae* with *Euglenophyceae* probably exist in the water of the source water intake located in the downstream of Nagara River. Further analysis will be conducted based on the dominating species extracted from all algal families. In addition, analysis on the likely interactions between algal species against the concentrations and composition of nutrients will be conducted along with the likely relations between algal species and bacteria.

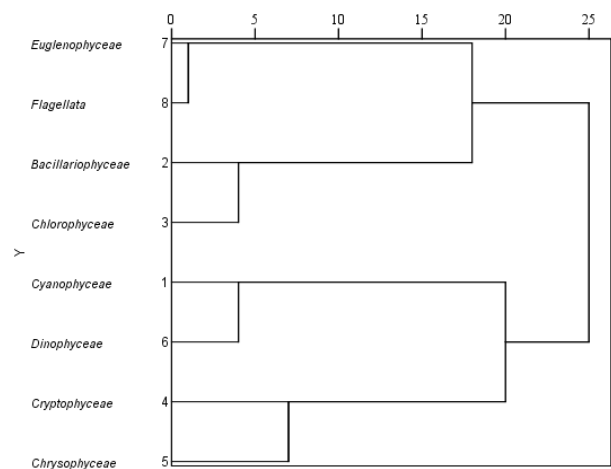


Fig. 5. Relationship among eight algal families in August analyzed by agglomerative hierarchical clustering

REFERENCES

- Guo, Q.Y., Zhang, X.H., Li, X., Chen, T.M., Yang, B.R., Ding, C., Wang, C.M., Pan, M., Ma, W.X., Yu, J.W., 2021. Variation and mitigation of musty, septic, chemical, grassy, fishy odors and corresponding odorants in a full-scale drinking water treatment plant with advanced treatments. *Chemosphere* 269, 128-691.

of *Cyanophyceae* with other algal species, the data of algal

Fate and effect of microplastic and heavy metal in agricultural soil added with biochar

Rahman Fariha¹, Shiamita Kasuma Dewi², Zaw Min Han³ and Wei Yongfen⁴

1. Graduate School of Natural Science and Technology, Gifu University, Japan

2. The United Graduate School of Agricultural Science, Gifu University, Japan

3. Graduate School of Engineering, Gifu University, Japan

4. River Basin Research Centre, Gifu University, Japan

INTRODUCTION

Globally, microplastics (MPs) pollution in the agroecosystem has increasingly become an environmental issue (Tunali et al., 2020). MPs are defined as plastics smaller than 5 mm in size and mainly originate from synthetic particles and environmental degradation. The extensive application of sludge, compost, and mulch films directly introduce MPs into agricultural fields (Zhang et al., 2020a). The negative biological effects of MPs are thought to be induced by two mechanisms first, small-sized MPs are accidentally ingested, causing direct damages to organisms (Chen et al., 2019). Secondly, MPs provide high specific surface area upon which, other environment pollutants may adsorb; thus, the MPs act as vectors transferring these contaminants such as organic compounds, heavy metals (Liu et al., 2019). Among the adsorbed toxic contaminants on MPs, heavy metals are toxic key contaminants of inorganic nature. Moreover, heavy metals pollution in soil environment and surface water has become another major challenge across the world. Over the past few decades, Cadmium (Cd) pollution has attracted worldwide attention. Excessive amounts of Cd can damage soil and aquatic ecosystems, affect organism growth and activity, and bring threat to downstream animals and human health. Biochar the carbon-rich material is recognized as a versatile reagent for contaminated land remediation owing to its high capacities to bind with heavy metals.

Although individual toxicity of MPs and Cd to organism and soil has been widely studied, limited knowledge is available on the interactions between cadmium and MPs, as well as potential impacts from their combinations. Moreover, some studies also have speculated that MPs presence could increase the bioavailability of other soil contaminants (Zhou et al., 2020b), but experimental analysis and concrete data have not been provided. Accordingly, it is worth and interesting to study whether MPs could increase the availability of Cd soil.

In the current study, experiment was conducted with earthworm co-exposure to MPs and Cd. The objective of this study was i) to determine the joint toxicity of MPs and Cd to the soil fertility and earthworms *Eisenia fetida* by evaluating the individual growth changes with biochar application.

MATERIALS AND METHODS

Soil, MPs, and earthworms Preparation:

The clean soil used in this study was topsoil (0-20 cm) collected from the university crop field area Gifu, Japan. After naturally air dried for 3 days, soils were sieved through a 2-mm mesh after removing stones and plant residues. Mulching sheet polythene used in this experiment as a microplastics with the particle size (≤ 5 mm) and the concentration was 3% and 10%. Artificially Cd-contaminated soil was obtained by spiking Cd (serving as Cd (NO₃)₂) in the clean soils. Briefly, Cd solution mixed with distilled water and sprayed into soils to obtain a final concentration of 5 mg kg⁻¹. Soils were then incubated at room temperature (25°C) for 30 days. Soils were then air-dried,

grounded to 2 mm sieves, and mixed with cow manure (0.50 g per earthworm) was added to soil surface per week (Xu et al., 2013). A deionized water was added to maintain the water holding capacity. The epigenic earthworm species *E. fetida* was chosen for this experiment due to its wide tolerance against environmental variables and survive metal contaminated area. Adult *E. fetida* with weight from 93 to 94 mg were purchased from a local earthworm culture farm. Before the incubation experiment worms were rinsed with deionized water and depurated with a hungry treatment. The body weight of individual was recorded before being transferred into experimental reactor. Rice husk biochar were brought from local market.

Experimental set up

The pretreated *E. fetida* were randomly transferred into reactor, each reactor containing 15 *E. fetida* and 400 g soil. 6 holes was made in the lid for ventilating. Eight experimental groups were set up: control group (without MPs and Cd); T₁, (Clean soil + BC); T₂= Cd only; T₃= (Cd+ BC); T₄ = (Cd+MPs3%); T₅= (Cd+MPs3%+BC); T₆ = (Cd+MPs10%); T₇ = (Cd+MPs10%+BC). Each treatment was prepared in triplicate. The reactor was placed in a dark room with a temperature of 25 °C ± 0.5 °C. The exposure experiment was carried out for 2 months; soils and *E. fetida* were collected at every 7 days after.

Earthworm growth parameters

Earthworms were gently taken out from each reactor by hand and washed with pure water for removing the adhering materials from their body every seven days. Earthworms were placed to a wet adsorption paper and then weighted on a live weight basis. The growth rate of the earthworms was calculated, Growth rate (%) = (Morg.₂-Morg.₁/Morg.₂)/ t

(where, Morg.₁ and Morg.₂ refer to initial body weight (mg) and final body weight (mg) of *E. fetida*, and t refers to the exposure days (Huerta Lwanga et al; 2017a).)

Soil parameters

The pH and electrical conductivity (EC) were measured by using the aqueous solution of pulverized dry sample with deionized water (w/v = 1/10) after shaken for 2 h (Cui et al., 2018). The organic matter content (loss on ignition) was measured by combusting the dried samples in a muffle furnace (Yamato, Japan) at 600 °C for 2 h. Total nitrogen and Total phosphorus was measured by using the molybdenum blue-absorption method with a spectrophotometer at the designated wavelength of 220nm and 880 nm respectively (Huang et al., 2012).

RESULTS AND DISCUSSION

Effects of contaminates on growth of *E. fetida*

Co-exposure to MPs + Cd and singly exposure to Cd both decreased growth rate compared to control (Fig. 1). T₂ and T₆ treatments (D₁₄ and D₂₁) was lower (P<0.05) than that in control. On the contrary, the growth rate slightly increased when applied biochar. T₁ shows significantly higher in D₁₄ and

D₂₁ compared to control. Addition of biochar increases the growth rate in all treatments (Fig.1). The degradation of MPs has just begun from 21st days, Fig.2. As indicated in previous studies, MPs have great potential to accumulate metal contaminants on their surfaces from the ambient environment due to strong hydrophobicity and higher specific surface area, and pollutants can easily be released inside of organisms after ingestion (Bakir et al., 2014). Thus, the Cd concentration in *E. fetida* and bio accessibility of Cd might have been enhanced by MPs, an explanation for the lower growth rate recorded in MPs + Cd group in this current study. The positive effect of biochar on *E. fetida* growth can be attributed to its soil-conditioning effects in terms of increasing soil water holding capacity, nutrients bioavailability, and microbial activities.

Effects of contaminates on soil property

The OM of all treatments were measured on D₇, D₁₄ and D₂₁. T₁ shows significantly higher in D₁₄ and D₂₁ compared to control. T₄ and T₆ had showed similar OM contents (lower than Biochar amendments). Addition of biochar increases the OM in all treatments (Fig.3). MPs has a linear hydrocarbon structure, large molecular size, lack of functional groups and high hydrophobicity, which make the synthetic polymer quite resistant to degradation under natural field conditions. As a result, the SOM of MPs treatment remained stable. On the other side, the use of biochar also increases the soil organic matter in soil in all treatments ($p < 0.05$). Due to its high carbon source helps to enhance soil organic matter in soil.

On the other hand, no differences (total nitrogen, TN) were observed in 7th day among the treatments. In 14th days, TN contents were significantly lower in T₂ and T₆ and highest TN were observed in T and T₂ treatments. In 21st day TN contents slightly increased in all treatments. Nitrogen (N) is essential to manage agricultural soil health and crop productivity. However, there are limited studies about the combine effects of MPs and Cd on the dynamics of soil nitrogen in agro-ecosystem. In Cd-contaminated soils, soil nitrogen is inhibited and usually block nitrogen supply for plants.

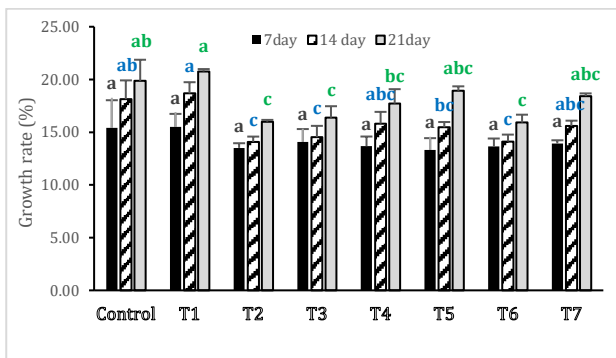


Fig.1 Growth status of earthworms under various treatments

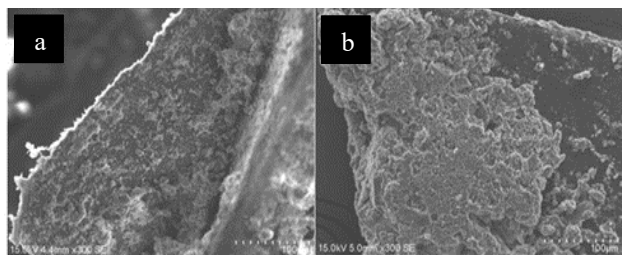


Fig.2 SEM image of MPs in soils of 7th days (a) and 21st days (b) after mixing

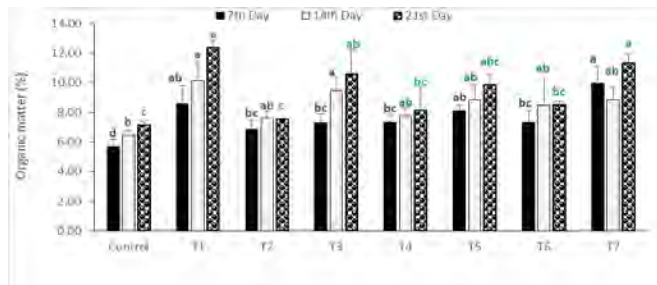


Fig.3 Organic matter content (%) of soils under various treatments

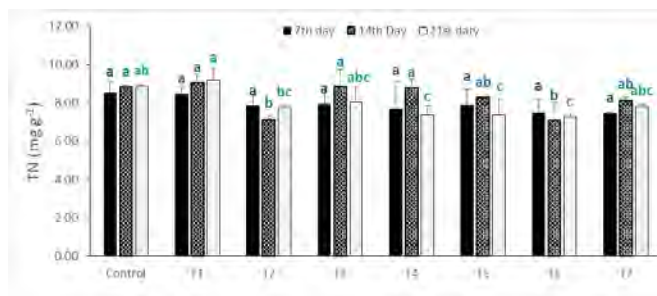


Fig.4 Total nitrogen content (mg g⁻¹) of soils under various treatments

REFERENCES

- Bakir, A., Rowland, S.J., Thompson, R.C., 2014. Enhanced desorption of persistent organic pollutants from microplastics under simulated physiological conditions. *Environ. Pollut.* 185, 16–23.
- Chen, Q.Q., Li, Y., Li, B.W., 2019. Is color a matter of concern during microplastic exposure to *Scenedesmus obliquus* and *Daphnia magna*? *J. Hazard. Mater.* 383, 121224.
- Cui, G., Li, F., Li, S., Bhat, S.A., Ishiguro, Y., Wei, Y., Yamada, T., Fu, X., Huang, K., 2018. Changes of quinolone resistance genes and their relations with microbial profiles during vermicomposting of municipal excess sludge. *Sci. Total Environ.* 644,494–502.
- Huang, K., Li, F., Li, J., Helard, D., Hirooka, K., 2012. Rapid Vermicomposting of Fresh Fruit and Vegetable Wastes Using Earthworm *Eisenia Foetida*. *J. Japan Soc. Civ. Eng. Ser. G (Environmental Res.* 68, III_113-III_120.
- Huerta Lwanga, E.H., Gertsen, H., Gooren, H., Peters, P., Salanki, T., van der Ploeg, M., Besseling, E., Koelmans, A.A., Geissen, V., 2017a. Microplastics in the Terrestrial Ecosystem: Implications for *Lumbricus terrestris* (Oligochaeta, Lumbricidae). *Environ. Sci. Technol.* 50, 2685–2691.
- Liu, P., Lu, K., Li, J., Wu, X., Qian, L., Wang, M., Gao, S., 2019. Effect of aging on adsorption behavior of polystyrene microplastics for pharmaceuticals: Adsorption mechanism and role of aging intermediates. *J. Hazard. Mater.* 384, 121193.
- Tunali, M., Uzoefuna, E.N., Tunali, M.M., Yenigun, O., 2020. Effect of microplastics and microplastic-metal combinations on growth and chlorophyll a concentration of *Chlorella vulgaris*. *Sci. Total Environ.* 743, 140479.
- temperate forested basin in northern Japan. *Hydrological Processes*, 15(10), 1817–1828.
- Xu, D., Li, C., Wen, Y., Liu, W., 2013. Antioxidant defense system responses and DNA damage of earthworms exposed to Perfluorooctane sulfonate (PFOS). *Environ. Pollut.* 174,121–127.
- Zhang, L., Xie, Y., Liu, J., Zhong, S., Qian, Y., Gao, P., 2020a. An overlooked entry pathway of microplastics into agricultural soils from application of sludge-based fertilizers. *Environ. Sci. Technol.*
- Zhou, Y., Liu, X., Wang, J., 2020b. Ecotoxicological effects of microplastics and cadmium on the earthworm *Eisenia foetida*. *J. Hazard. Mater.* 392, 122273.

MODIS-based estimation of carbon sequestration of different vegetation in Qilian Mountains, China

Zhou Jieli¹, Zhang Fuping² and Wei Yongfen³

1. Graduate school of Natural Science and Technology, Gifu University
2. Shaanxi Normal University, China
3. River Basin Research Center, Gifu University

INTRODUCTION

Vegetation can be thought of as a carbon sink and play an important role in climate change and global warming. Accurate estimation of vegetation carbon sequestration capacity can provide a scientific basis for formulating more scientific and reasonable carbon management measures.

Qilian Mountains have diverse vegetation and are an important ecological barrier in western China. At present, the estimation of carbon sequestration in the Qilian Mountains is mostly for single vegetation, and most of the studies are for small areas (F. Jin and Z. Zhang, 2005). In contrast, studies on the estimation of carbon sequestration for the entire Qilian Mountains and different vegetations are rarely reported. Therefore, in this study, by using satellite data based on net primary productivity (NPP) estimate model, the carbon sequestration of different vegetations in the Qilian Mountains in 2005 and 2015 was estimated, aiming to provide relevant departments with the research area's carbon sequestration in recent years and a scientific and intuitive reference for regional ecological protection.

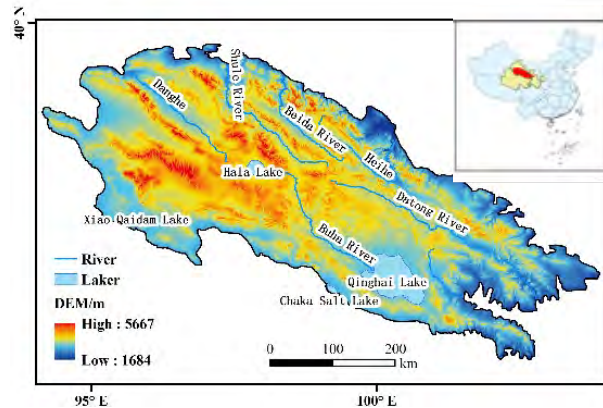


Fig.1 Study area

DATA AND METHODS

— Data

To estimate the carbon sequestration of different vegetations in 2005 and 2015, the following data were used:

- (1) Land use data: collected from the Resource and Environmental Science Data Center of the Chinese Academy of Sciences.
- (2) DEM data: collected from ASTGTM data of the Geospatial Data Cloud, with a spatial resolution of 30m.
- (3) MODIS-NDVI data set: collected from NASA's 16-day synthetic data, with a spatial resolution of 500m.
- (4) Evapotranspiration data: collected from NASA's 8-day synthetic data, with a spatial resolution of 500m.
- (5) Meteorological data: collected from the China Meteorological Science Data Sharing Network.

—Method

In this study, NPP was estimated based on the CASA model. The CASA model has the characteristics of high computational efficiency and a few input parameters, it is widely used in regional or global scale NPP estimation. And many studies have obtained satisfactory estimation results based on the CASA model. In this study, NPP was estimated based on the following equations ((1)-(10)):

$$NPP(x, t) = APAR(x, t) \times \varepsilon(x, t) \quad (1)$$

$$APAR(x, t) = SOL(x, t) \times FPAR(x, t) \times 0.5 \quad (2)$$

$$FPAR(x, t) = \alpha FPAR_{NDVI} + (1 - \alpha) FPAR_{SR} \quad (3)$$

$$FPAR_{NDVI}(x, t) = \frac{NDVI(x, t) - NDVI_{i, min}}{NDVI_{i, max} - NDVI_{i, min}} \times (FPAR_{max} - FPAR_{min}) + FPAR_{min} \quad (4)$$

$$FPAR_{SR}(x, t) = \frac{SR(x, t) - SR_{i, min}}{SR_{i, max} - SR_{i, min}} \times (FPAR_{max} - FPAR_{min}) + FPAR_{min} \quad (5)$$

$$SR(x, t) = \frac{1 + NDVI(x, t)}{1 - NDVI(x, t)} \quad (6)$$

$$\varepsilon(x, t) = T_{\varepsilon 1}(x, t) \times T_{\varepsilon 2}(x, t) \times W_{\varepsilon}(x, t) \times \varepsilon_{max} \quad (7)$$

$$T_{\varepsilon 1}(x, t) = 0.8 + 0.02 \times T_{opt}(x) - 0.0005 \times [T_{opt}(x)]^2 \quad (8)$$

$$T_{\varepsilon 2}(x, t) = 1.184 / \{1 + \exp[0.2 \times (T_{opt}(x) - 10 - T(x, t))]\} \times 1 / \{1 + \exp[0.3 \times (-T_{opt}(x) - 10 + T(x, t))]\} \quad (9)$$

$$W_{\varepsilon}(x, t) = 0.5 + 0.5 \times \frac{E(x, t)}{E_p(x, t)} \quad (10)$$

where,

APAR(x, t): the photosynthetically active radiation absorbed by pixel x in month t (gC/m²).

$\varepsilon(x, t)$: the actual light energy utilization rate (gC/MJ) of pixel x in month t.

SOL(x, t): the total solar radiation at pixel x in month t (gC/m²).
FPAR(x, t): the absorption ratio of the vegetation layer to the incident photosynthetically active radiation. The constant 0.5 in (1) represents the ratio of the effective solar radiation that can be used by vegetation to the total solar radiation.

FPAR_{min} and FPAR_{max}: 0.001 and 0.95, respectively.

SR_{i, max} and SR_{i, min}: the 95% and 5% inferior percentiles of NDVI of the i-th planting type, respectively. α is 0.5.

T _{$\varepsilon 1$} (x, t) and T _{$\varepsilon 2$} (x, t): the stress effects of low temperature and high temperature on light energy utilization.

W _{ε} (x, t): the water stress coefficient, reflecting the influence of water conditions.

ε_{max} : the maximum light energy utilization rate under the ideal conditions (gC/MJ).

T_{opt}(x): the optimum temperature for plant growth, which is defined as the monthly average temperature (°C) when the NDVI value reaches the highest in a certain area in a year.

E(x, t): the actual evapotranspiration of the area (mm).

E_p(x, t): the regional potential evapotranspiration (mm).

RESULTS AND DISCUSSION

— Land cover classification

According to the field investigation and existing materials, the land cover in the study area was classified into four categories: cultivated land, woodland, grassland, and others.

Table 1 Classification results

Land Cover	Land Area/ ($\times 10^4 \text{hm}^2$)		Land cover change (2005 - 2015)
	2005	2015	
Cultivated land	62.41	63.02	0.98
Woodland	165.04	165.3	0.16
Grassland	837.26	837.38	0.01
Others	878.79	877.76	-0.12

Table 1 shows that vegetations occupied more than half of the study area. Among the vegetations, grassland had the largest area, followed by woodland, cultivated land. From 2005 to 2015, the area of cultivated land increased the most, followed by woodland, grassland. The land for others (including water, construction land, and unused land) decreased.

—NPP estimation results

The estimated were average NPP and total NPP of the study area in 2005 and 2015, respectively, shown in Table 2 and Table 3.

Table 2 Average NPP estimated for different vegetation in the study area

Land Cover	2005	2015
	Average NPP ($\text{t} \cdot \text{hm}^{-2} \cdot \text{a}^{-1}$)	Average NPP ($\text{t} \cdot \text{hm}^{-2} \cdot \text{a}^{-1}$)
Cultivated land	5.03	5.63
Woodland	5.19	5.31
Grassland	3.82	4.37
Others	1.36	1.56

Table 3 Total NPP estimated for different vegetation in the study area

Land Cover	2005	2015
	Total NPP ($\times 10^4 \text{t/a}$)	Total NPP ($\times 10^4 \text{t/a}$)
Cultivated land	313.92	354.8
Woodland	856.56	877.74
Grassland	3198.33	3659.35
Others	1402.93	1604.92
Total	5771.74	6496.81

As shown in Table 2, the average NPP values of cultivated land and woodland are higher, than that of grassland and others. Table 3 shows that the total NPP of different vegetations has increased obviously from 2005 to 2015. Besides, grassland has the highest total NPP value due to its large area. Although the vegetation area only occupied about half of the study area, the vegetation NPP occupied about three-quarters of that in the study area.

—Estimation of carbon sequestration

According to the photosynthesis equation: $6\text{CO}_2 + 6\text{H}_2\text{O} \rightarrow \text{C}_6\text{H}_{12}\text{O}_6 + 6\text{O}_2$, to the production of 1kg organic matter can fix 1.63kg CO_2 . So, based on the NPP of vegetation,

the amount of carbon sequestered by vegetation was calculated and its distribution was shown in Fig. 2 and Fig. 3.

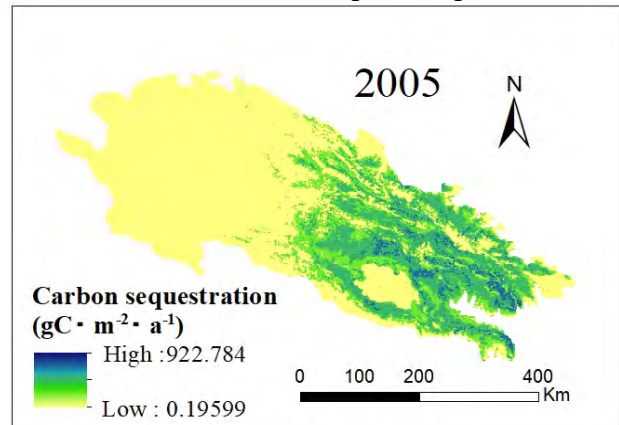


Fig. 2 Carbon sequestration distribution map in 2005

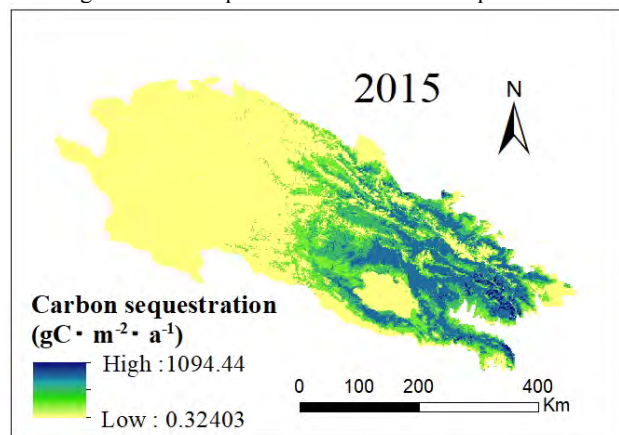


Fig. 3 Carbon sequestration distribution map in 2015

In terms of spatial distribution (Fig. 2 and Fig. 3), the carbon sequestration values in the eastern part of the study area are higher than that in the western part, which is consistent with the fact that the ecological system in the eastern part of the study area is better than that in the western part. As can be seen, compared to 2005, Carbon sequestration increased significantly in 2015. It can be inferred from this that the ecological conditions in the Qilian Mountains have been improving in recent years.

Many areas in the study area have not been developed and utilized due to soil quality and environmental factors, especially in the western part, and the amount of carbon sequestration in vegetation is small. Therefore, how to improve the unused land through technology and increase the vegetation coverage is a problem worthy of further exploration. Due to the large area of grassland, the contribution to carbon sequestration in the study area is great. Therefore, the study area must take further measures.

REFERENCES

- F. Jin, Z. Zhang. (2005) Value evaluation of forest ecosystem services of Qilian Mountain in Gansu province. Science of Soil and Water Conservation.
- National Bureau of Statistics. (2015) Gansu Statistical Yearbook. Beijing: China Statistics Press.

Association of bacterial community with heavy metals in soils of different coal mining areas

Yajie Wang¹, Zāw Min Han¹, Yongfen Wei² and Fusheng Li^{1,2}

1. Graduate School of Engineering, Gifu University

2. River Basin Research Center, Gifu University

INTRODUCTION

Coal as one of the main fossil fuel resources has played important role in the world in supporting energy supply and social activities. Heavy metals including chromium (Cr), cadmium (Cd), nickel (Ni), copper (Cu), zinc (Zn), arsenic (As), lead (Pb), and mercury (Hg) are ubiquitous in the coal. Exploitation of coal could result in soil pollution, even though the extent of pollution may differ with the condition of management and the exploitation technology. Heavy metals in soil can enrich through the food chain, and endanger human health and life, eventually. In soil, bacteria are the most abundant organism, which are sensitive to the content of heavy metals (Du et al., 2018). The bacterial richness, diversity and community structure are likely to differ significantly in the soil with different types and concentrations of heavy metals, so bacteria are possible to be better bio-indicators than other larger organisms. A better understanding on the effect of heavy metals on bacterial community is critical to optimize such monitoring methods and remediation schemes.

MATERIALS AND METHODS

six coal mines in Luliang, Shanxi Province of China with different annual output (M1: 0.6, M2: 1.2, M3: 1.5, M4: 1.8, M5:3.0 M6: 8.0×10^6 t) were selected as the research area. Surface soil (1-5cm) samples on three different sites (0, 1, and 3km away the mining area) of each coal mine were collected, and were labeled as A, B and C, respectively. The collected soil samples were frozen dried, sieved, and homogenized. The soil samples were then used for quantification of organic matter (OM), total nitrogen (TN), total phosphorus (TP), 7 heavy metal elements (Cr, Ni, Cu, Zn, As, Cd, and Pb), and bacterial community analysis based on genomic DNA. The genomic DNA was extracted using the DNA extraction kit (MOBIO, USA). The absolute abundance of DNA based on 16S rDNA was measured through quantitative real-time PCR (qPCR) following the procedures described in the literature (Li et al., 2021). The bacterial diversity and community structure were analyzed through high-throughput sequencing technology. The v4-variable region of the 16S rRNA gene was amplified by PCR with primers (515F-806R). The amplified genes were sequenced on the Illumina MiSeq platform. At 97% similarity level, the out representative sequences in the obtained high-quality sequences were taxonomically analyzed by RDP classifier Bayesian algorithm and compared with Silva database to obtain the community information at each classifiable level. The potential ecological risk index (RI) introduced by Hakanson (1980) is used to assess the degree of ecological risk caused by heavy metal concentrations in soil. The formulas are as follows:

$$RI = \sum_i^n E_i = \sum_i^n (T_i \times C_i)$$

$$C_i = C_D / C_R$$

Where n is the number of heavy metals, E_i is the single index of ecological risk factor of individual heavy metal, T_i is the heavy metal toxic response factor (Hakanson, 1980), C_i is the

single heavy metal pollution index, C_D is the measured heavy metal concentration, C_R is the geochemical background value. The calculated RI of heavy metals were used in the examination of relationships between heavy metals and bacterial community. The examination was conducted by Spearman correlation analysis, variance-partitioning analysis (VPA) and distance-based redundancy analysis (dbRDA).

RESULTS

The concentrations of the targeted heavy metals in soil of coal mines are summarized in **Table 1**. In this table, the analytical results of pH, EC, moisture, total phosphorus (TP), total nitrogen (TN) and organic matter (OM) are also included. The obtained results showed distinct variations in different soil samples.

The result of RI analysis of the heavy metals in soil of coal mines (will be provided in poster) showed that the overall potential ecological risk differs greatly in different samples, and fell in the range of 26.4-75.3, the highest value is of M3. The average ecological risk of individual heavy metal was of the order: Cd (28.2)> Ni (3.75)> As (3.26)> Cu (3.04)> Pb (2.96)> Cr (1.12)> Zn (0.49). The ecological risk for Cd account for 66% of the overall ecological risk, on average. The ecological risk for Cd fell in the range of 16.8-61.1, the highest value is also of M3. These results addressed that Cd was the key influence factor to cause the potential ecological risk in the soil of coal mines.

The richness of bacteria in soil of each coal mine are shown in **Fig. 1**. The richness of M1 is significantly higher than that of other coal mines, and the richness of M5 is the lowest. There are no significant differences between the richness of M5, M4 and M3. The correlation analysis (will be presented in poster) showed Zn, Cr, and Cd have inverse relationships with bacterial richness, indicating the effect of Zn, Cr and Cd on reducing the total bacteria in soil of coal mines.

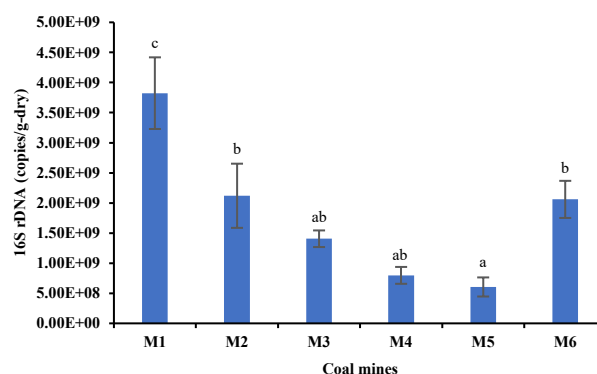


Fig.1: Total bacteria measured based on 16S rDNA in soil samples of the mines (M1-M6). The different letters indicate the difference is statistically significant ($p < 0.05$).

Alpha diversity indices varied between different soil samples. The variation of Shannon and Simpson was 7.37-10.16 and 0.956-0.997, respectively. The Chao 1 index and Ace

index ranged from 3637.9-4914.5 and 3693.5-5008.9, respectively. The correlation analysis (will be provided in poster) showed Zn has inverse relationships with Shannon index and Simpson index, suggesting the role of Zn in controlling the bacterial diversity in the soil of coal mines.

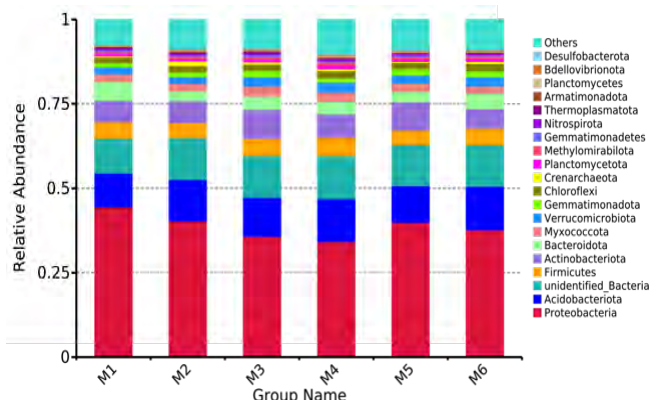


Fig. 2: Bacterial community for the top 20 dominant taxa at phylum level in the soil samples of the mines (M1-M6).

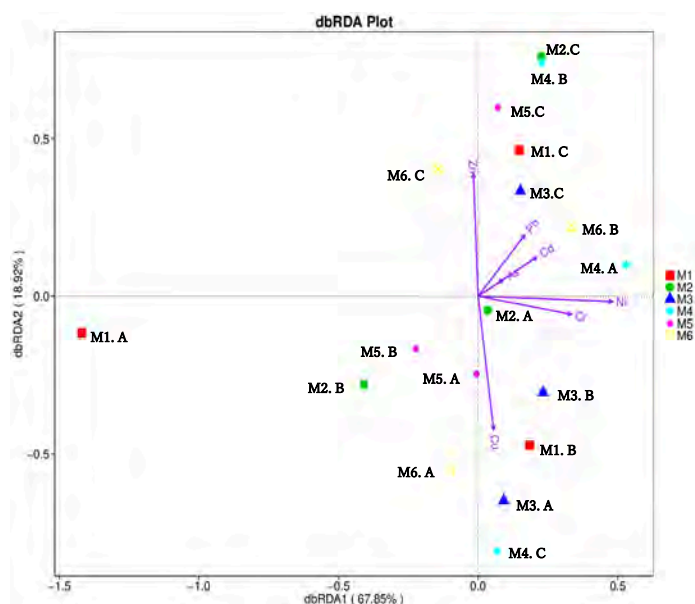


Fig. 3 Effect of heavy metals on bacterial community structure at phylum level. A, B and C represent the different sampling sites in each mine.

Table 1. Physiochemical properties and heavy metal content of soil samples of the mines (M1-M6).

*TN, TP and OM represent total nitrogen, total phosphorus and total organic matter in soil.

Coal mine		M1		M2		M3		M4		M5		M6	
Index	unit	range	mean	range	mean	range	mean	range	mean	range	mean	range	mean
pH	-	8.28-8.53	8.47	8.39-8.65	8.51	8.64-8.94	8.79	8.19-8.76	8.34	8.42-8.76	8.51	8.34-8.62	8.5
EC	mS/m	158-214	179	140-177	153	67-185	106	153-195	176	150-173	164	143-168	168
Moisture	%	22-27.4	24.3	23.6-25.5	24.6	22.5-25.1	23.8	23.2-26.4	25.5	21.8-24.6	23	21.2-29.5	23
OM	g/kg	15.4-17.7	16.8	15.1-17.9	16.3	18.4-21.5	20.2	16.9-20.1	19.1	17-19.2	17.9	18.3-20.5	19.1
TP	mg/kg	2.4-2.7	2.5	2.4-2.9	2.6	2.2-3.2	2.7	2.1-2.2	2.1	2.1-2.4	2.3	2.3-3.0	2.8
TN	mg/kg	520-620	537	503-528	514	516-613	558	498-587	532	532-632	585	519-620	562
Cr	mg/kg	29.8-33.8	31.7	21.2-36.2	27.5	36.1-47.9	38.4	35.6-37.8	36.6	38.8-43.9	41.9	22.2-31.9	29.7
Pb		14.7-15.8	15.3	10.1-16.4	12.6	15.6-22.8	18.3	15.4-16.3	15.8	14.6-17.4	16.3	10.3-15.0	14.2
Ni		16.9-21.2	20.0	14.7-20.9	17	15.2-21.0	20.0	20.5-26.1	23.7	19.0-23.7	21.8	22.2-31.9	18.6
Cu		12.1-14.0	13.2	12.8-14.3	13.6	13.8-18.2	14.8	13.2-14.6	13.8	12.8-16.6	15.1	9.2-12.7	12.1
Zn		28.8-43.7	35.1	27.4-33.5	29.8	35.4-59.5	44.9	33.8-34.9	34.2	36.1-40.8	38.9	19.8-53.7	35.5
Cd		0.08-0.10	0.09	0.07-0.10	0.08	0.09-0.20	0.13	0.09-0.10	0.09	0.09-0.10	0.09	0.06-0.10	0.09
As		3.32-3.75	3.44	2.15-5.06	2.97	2.04-4.95	3.23	3.36-4.63	4.14	4.54-5.39	5.12	2.30-3.38	3.02

In total, 86 bacterial phyla were identified from soil samples. The relative abundance of the top 20 phyla were chosen for the histogram analysis (Fig. 2). Proteobacteria, Acidobacteriota, Firmicutes, Actinobacteria, Bacteroidetes were dominating phyla, which accounted for 38.6%, 11.8%, 4.9%, 7.0% and 3.8%, respectively, on average. The relative abundance of each phylum in different soil samples were different.

The result of dbRDA of heavy metals and bacterial community structure at the phylum level was presented in Fig. 3. The analysis showed that Ni, Cu, Cr, and Zn signify a greater impact on bacterial community structure. dbRDA1 and dbRDA2 explained 67.85% and 18.92% of the total variation in the community structures, respectively. Ni ($r = 0.98$), Cr ($r = 0.96$), Cd ($r = 0.96$), and As ($r = 0.96$) were significantly correlated with dbRDA1, whereas Zn ($r = 0.96$) and Cu ($r = -0.93$) were significantly correlated with dbRDA2. The analysis of the combined effect of heavy metals on bacterial community structure (will be presented on poster) showed Ni and Cu had highest correlation with bacterial community structure, indicating the major roles of Ni and Cu in affecting community structure.

This study highlights the effects of heavy metals on the bacterial community in soil of coal mining areas. The changes of bacterial community are associated with Cd, and also closely associated with Zn, Cr, Ni and Cu. Different elements showed different effects on bacterial richness, diversity and community structure. Zn affects the bacterial richness, diversity and community structure. Cr and Cd mainly affect the bacterial richness. Ni and Cu show great effect on bacterial community structure.

REFERENCES

- Du, H., Harata, N., Li, F. (2018). Responses of riverbed sediment bacteria to heavy metals: Integrated evaluation based on bacterial density, activity and community structure under well-controlled sequencing batch incubation conditions. *Water Research*, 130: 115-126.
- Hakanson L. (1980). An ecological risk index for aquatic pollution control: a sedimentological approach. *Water Research*, 14(8): 975-1001
- Li, W., Su, H., Li, J., Bhat, S. A., Cui, G., Han, Z. M., ... Li, F. (2021). Distribution of extracellular and intracellular antibiotic resistance genes in sludge fractionated in terms of settleability. *Science of The Total Environment*, 760: 143317.

Changes of 16S rDNA and antibiotic resistance genes in the drinking water treatment process

Nadya Diva Sagita¹, Sutra Maysaroh¹, Maulana Yusup Rosadi¹ and Fusheng Li²

1. Graduate School of Engineering, Gifu University, Japan

2. River Basin Research Center, Gifu University, Japan

INTRODUCTION

The intensive use of antibiotics has resulted in the proliferation of antibiotic-resistant bacteria (ARB) and antibiotic resistance genes (ARGs), which have become emerging contaminants. It is estimated that antibiotic resistance will cause up to 10 million deaths annually by 2050 if no action is taken from now (O' Neil, 2014). Previous studies have detected ARGs pollution in aquatic environments such as surface water and groundwater (Wu et al., 2020). More seriously, various ARGs have been detected in the drinking water source and potable water (Su et al., 2018), posing a severe threat to human health. Therefore, it is crucial to understand ARGs' abundance in water sources and their removal in drinking water treatment plants (DWTPs).

Numerous studies have been conducted to investigate the reduction of ARGs in DWTPs. Su et al. reported that the sedimentation process could remove 55% of ARGs, and the sand filtration process achieved the removal value of 67% (Su et al., 2018). In contrast, chlorination resulted in the enrichment of ARGs (Xu et al., 2016). However, these studies only focused on the removal efficiencies of the water treatment units, and information regarding the relationship of water quality parameters with changes in the abundance of ARB and ARG is still unclear, requiring further investigation.

Accordingly, the main objective of this study was to investigate changes in the number of bacteria represented by the 16S rDNA and antibiotic resistance gene in the drinking water treatment process. The correlations between gene changes and other water quality parameters were also evaluated.

MATERIALS AND METHODS

Sample collection

All samples in this study were collected from August 2020 to December 2020 in two different DWTPs located in Aichi Prefecture, Japan. DWTP A has 76,500 m³/day, and DWTP B has 344,300 m³/day capacity. The treatment processes include coagulation-flocculation, sedimentation, filtration influent (intermediate-chlorination), rapid sand filtration, and purified water tank (after post-chlorination).

DNA extraction

Water samples (0.1–0.5 L) were filtered through 0.2-μm polytetrafluoroethylene membrane filters (Millipore, Ireland) using a vacuum filtration apparatus. The filters were then cut into small pieces, and DNA was extracted using the PowerSoil DNA Isolation Kit (Mobio, USA), following the manufacturer's protocol. All the extracted DNA samples were stored at -20°C until quantitative analysis.

ARGs quantification

Quantitative PCR (qPCR) was used to quantify the abundance of 16S rDNA, ARGs conferring resistance to sulfonamide and tetracycline antibiotics (*sulI* and *tetG*), and class 1 integron genes (*intI1*). The 16S rDNA was quantified as a measure of total bacterial load. *sulI* and *tetG* were chosen because they are the most common ARGs detected in surface water. The *intI1* gene was also quantified as an indicator of potential horizontal gene transfer for ARGs. The qPCR assays were conducted on a

Thermal Cycler Dice TP800 (Takara, Japan) using TB Green assays with a final volume of 25 μL. Each qPCR mixture contained 12.5 μL of TB Green Premix Ex Taq (Tli RNaseH Plus), 0.5 μL of each 10 μM primer, 9.5 μL of sterile Milli-Q water, and 2 μL of DNA template. DNA templates were included in triplicate, while negative controls (DNA-free water) and serial dilutions of standard plasmids were included in duplicate in each qPCR run. The standard curve of targeted genes was generated by 10-fold dilutions of the plasmid carrying the targeted gene. The copy number of each gene was calculated from the corresponding standard curve using the CT value of each gene in the qPCR runs.

RESULTS AND DISCUSSION

All of the targeted genes were detected in drinking water sources (Fig. 1). In the raw water of DWTP A and B, the concentration of 16S rDNA ranged from 10⁹ copies/L to 10¹⁰ copies/L. Meanwhile, the concentration of two classes of ARGs ranged from 10⁵ copies/L to 10⁷ copies/L. Overall, the processing unit obtained an ARGs removal of 99.74% in DWTP A and 98.02% in DWTP B. Both of the target ARGs were still detected in the purified water. The total concentrations of the target ARGs in the final effluent of DWTP A were 1.33×10³ copies/L, and 1.40×10⁴ copies/L for DWTP B. ARGs in purified water indicate that the existing technology in DWTP A and B cannot eliminate ARGs in drinking water.

According to the results shown in Table 1 and Table 2, intermediate-chlorination removed the most ARGs in DWTP A, followed by sedimentation and sand filtration. In contrast, the post-chlorination process removed no ARGs and increased the individual ARGs' abundance. In DWTP B, the intermediate-chlorination removed the most ARGs, followed by post-chlorination, sand filtration, and sedimentation.

Both DWTP A and DWTP B could remove ARGs by the sedimentation process. Su et al. (2018) reported a similar result on removing twenty-one ARGs, including sulfonamide and tetracycline resistance genes, where the sedimentation process effectively removed ARGs (55%) (Su et al., 2018). Since 16S rDNA had a strong positive correlation with ARGs in DWTP A (> 0.98), bacterial biomass was essential in ARG fate. According to the results shown in table 3, the decline of ARGs and *intI1* abundance might be linked to the removal of ARB-contained ARGs along with the deposition of suspended solids, indicated by the decrease of 16S rDNA. The aggregating function might explain the ARGs reduction efficiency. The added coagulant/flocculant would cause microorganisms and small suspended particles to form large granules (flocs) and lose their original stability. After that, the flocs would rapidly precipitate to the bottom of the sedimentation tank due to the gravity.

The total ARGs in DWTP A and DWTP B decreased significantly after the intermediate-chlorination process (p < 0.05). It can be seen from the Pearson correlation shown in Table 3 and Table 4 that the relationship between the targeted genes and the chlorine residue had strong negative correlations. The correlation suggests that the addition of chlorine impacted reducing the abundance of ARGs in the water. Inactivation of

ARGs mostly depends on the damage of DNA structure. Chlorine-based disinfection was added to the water in the chlorination process, and hypochlorous acid (HOCl), a powerful oxidant, was produced. Because of its electrical neutrality, HOCl can easily penetrate the cell wall and membrane of bacterial cells through passive diffusion. The reaction of HOCl with proteins and amino acids leads to protein fragmentation due to the cleavage of peptide bonds, which results in the irreversible aggregation of essential bacterial proteins and causes bacterial death, characterized by a reduction in the value of 16S rDNA. HOCl might also attack the DNA, leading to DNA breakage and impairment of DNA synthesis that caused the decline in the abundance of ARGs and *int11* (Nizer et al., 2020).

The abundance of all the targeted genes in DWTP A and DWTP B were decreased after the filtration process. The reduction could be due to quartz in the sand filter, which could filter and remove the suspended solids and waterborne pathogens from water. This result was consistent with the previous research that mentioned that the effect of sand filtration was superior in removing the absolute abundance of ARGs (67%) (Su et al., 2018).

All targeted ARGs in DWTP A gained an enrichment of 99% for total ARGs in the post-chlorination unit. The lower removal value of ARGs in post-chlorination indicates that ARBs' response to chlorine varies depending on concentration levels. Following Xu et al., a low chlorine dose (± 0.25 mg-Cl₂/L) would be more likely to damage the bacterial cells than inactivate the DNA.

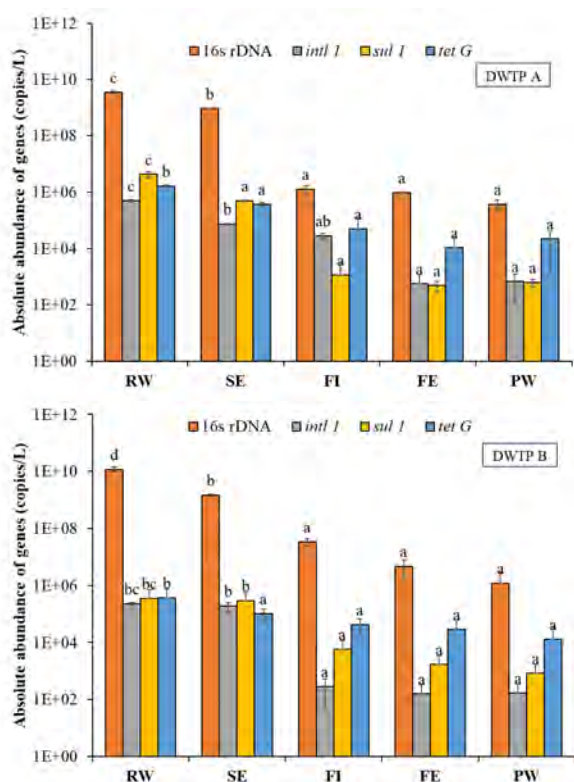


Fig. 1 Absolute abundances of targeted genes during treatment process. The different letters indicate the difference between two groups is significant based on the one-way ANOVA ($p < 0.05$). RW: raw water; SE: sedimentation effluent; FI: filtration influent (with Cl₂ addition); FE: filtration effluent; PW: purified water (after post-chlorination).

From various processes, chlorination was more effective in eliminating ARGs than coagulation, sedimentation, and sand filtration, judging from the process's removal rates for the targeted genes. The removal rates for the targeted genes showed that the intermediate-chlorination applied after sedimentation was more critical in eliminating ARGs than the post chlorination.

Table 1 The percent removals of targeted genes in the water treatment units of DWTP A (%).

	Sedimentation	Intermediate chlorination	Filtration	Post-chlorination
<i>sul1</i>	84.6	99.8	57.6	-25.8
<i>tetG</i>	87.8	86.4	78.1	-102.4
<i>int11</i>	90.1	61.5	98.0	-24.6
16S rDNA	78.5	99.9	23.3	61.8

Table 2 The percent removal values of targeted genes in the water treatment units of DWTP B (%).

	Sedimentation	Intermediate chlorination	Filtration	Post-chlorination
<i>sul1</i>	27.1	97.9	70.9	50.3
<i>tetG</i>	34.1	59.6	31.0	54.8
<i>int11</i>	26.3	99.9	43.8	-8.3
16S rDNA	49.4	97.7	86.4	74.1

Table 3 Correlation between targeted genes and water quality parameters in DWTP A.

	Turbidity	Suspended solid	Free chlorine
<i>sul1</i>	0.99	0.96	-0.89
<i>tetG</i>	0.99	0.98	-0.85
<i>int11</i>	0.99	0.97	-0.70
16S rDNA	0.98	0.98	-0.89

Table 4 Correlation between targeted genes and water quality parameters in DWTP B.

	Turbidity	Suspended solid	Free chlorine
<i>sul1</i>	0.73	0.76	-0.94
<i>tetG</i>	0.99	0.99	-0.82
<i>int11</i>	0.73	0.75	-0.95
16S rDNA	0.99	0.99	-0.94

REFERENCE

- Nizer, W. S. da C., Inkovskiy, V., & Overhage, J. (2020). Surviving reactive chlorine stress: Responses of gram-negative bacteria to hypochlorous acid. *Microorganisms*, 8(8), 1–27.
- O' Neil, J. (2014). Review on Antibiotic resistance. Antimicrobial Resistance : Tackling a crisis for the health and wealth of nations. *Health and Wealth Nations*, 1–16.
- Su, H. C., Liu, Y. S., Pan, C. G., Chen, J., He, L. Y., & Ying, G. G. (2018). Persistence of antibiotic resistance genes and bacterial community changes in drinking water treatment system: From drinking water source to tap water. *Science of the Total Environment*, 616–617, 453–461.
- Wu, D. L., Zhang, M., He, L. X., Zou, H. Y., Liu, Y. S., Li, B. B., Ying, G. G. (2020). Contamination profile of antibiotic resistance genes in ground water in comparison with surface water. *Science of the Total Environment*, 715.
- Xu, L., Ouyang, W., Qian, Y., Su, C., Su, J., & Chen, H. (2016). High-throughput profiling of antibiotic resistance genes in drinking water treatment plants and distribution systems. *Environmental Pollution*, 213, 119–126.

Changes of dissolved organic matter from source to treated water in drinking water treatment plant: Evaluation based on fluorescence excitation-emission matrix analysis

Maulana Yusup Rosadi¹, Nadya Diva Sagita¹, Sutra Maysaroh¹ and Li Fusheng²

1. Graduate School of Engineering, Gifu University

2. River Basin Research Center, Gifu University

INTRODUCTION

Dissolved organic matter (DOM) is a mixture of organic compounds with different physicochemical properties that can originate from microorganisms and/or terrestrially derived substances with large amounts of aromatic carbon and phenolic contents (i.e., humic substances), and can make up concerns related to the effectiveness of water treatment processes. Conventional monitoring techniques, such as specific ultra-violet absorbance at 254 nm, chemical oxygen demand, and dissolved organic carbon (DOC) has been widely used in many drinking water treatment plants to assess the removal efficiency of DOM during drinking water treatment (Li et al. 2020, Moyo et al. 2019). However, these parameters are not capable to reflect the composition of DOM that are complex and have a wide range of molecular structure, size distribution, hydrophobicity, and aromaticity (Li et al. 2020). Therefore, the sensitive analytical approaches are required to provide more detail on the reactivity and treatability of DOM.

Fluorescence excitation emission matrix (EEM) spectroscopy has been used for a rapid and highly sensitive analytical technique to determine the dynamics of DOM and can supply the information of DOM quality in various types of water. Since the fluorescence EEM analysis is more sensitive to UV-vis absorbance, it is important to examine the changes of DOM to ensure its reactivity and treatability throughout the drinking water treatment. This study aims to demonstrate the changes of DOM compositions in different physicochemical processes of drinking water treatment plant using fluorescence EEM analysis for assessing the drinking water quality.

MATERIALS AND METHODS

(1) Flowchart of drinking water treatment plant and sample collection

Water samples from a drinking water treatment plant were collected monthly from July 2020 to December 2020 in Aichi prefecture, Japan. Fig. 1. shows the flowchart of the drinking water treatment plant with a design capacity of 87,500 m³, and the samples were collected from the inlet and outlet of each unit process. The raw water of the plant originates from open reservoir. The plant uses polyaluminum chloride for coagulation with dose is around 25 mg/L. 10 mg/L of activated carbon is added in raw water. Sodium hypochlorite is injected in mid- and post-chlorination (0.5–1.2 mg/L).

(2) Sample Analysis

The collected water samples were filtered through 0.2-µm cellulose acetate membrane filter (Advantec, Japan). Filtered samples were analyzed for DOC using TOC-V_{wet} analyzer (Shimadzu, Japan). The fluorescence EEM was analyzed using RF-5300 spectrofluorometer (Shimadzu, Japan). The peak-picking method was used to describe the obtained fluorescence peaks. The fluorescence peaks can be classified into protein-like peaks: Peak 1 (tyrosine-like: Ex/Em: 220–237/305–320), Peak 2 (tryptophan-like: Ex/Em 215–237/340–

381) and Peak 4 (tryptophan-like: Ex/Em: 275–285/320–350) and humic-like peaks: Peak 3 (humic-like: Ex/Em: 320–360/420–460) and Peak 5 (humic-like: Ex/Em: 230–260/400–480) (Rodríguez-Vidal et al., 2021). The humification index (HIX) indicates the degree of DOM humification and was calculated as the area under the emission spectra of 435 to 480 nm divided by the sum of the emission spectra of 300 to 345 nm and 435 to 480 nm, at an excitation wavelength of 254 nm. The fluorescence index (FI) indicates microbial (FI > 1.9) or terrestrial source (FI < 1.4) of DOM and was calculated as the fluorescence intensity ratio of the emission wavelengths of 470 nm and 520 nm, at an excitation wavelength of 370 nm (Liden et al. 2017).

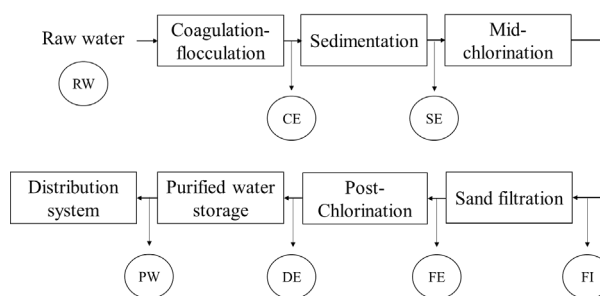


Fig. 1: Flowchart of the treatment process in the drinking water treatment plants. The circle icons represent the sampling points from each treatment unit. RW: raw water; CE: coagulation effluent; SE: sedimentation effluent; FI: filtration influent; FE: filtration effluent; DE: dechlorination effluent; PW: purified water.

RESULTS AND DISCUSSION

(1) DOM composition in different treatment units

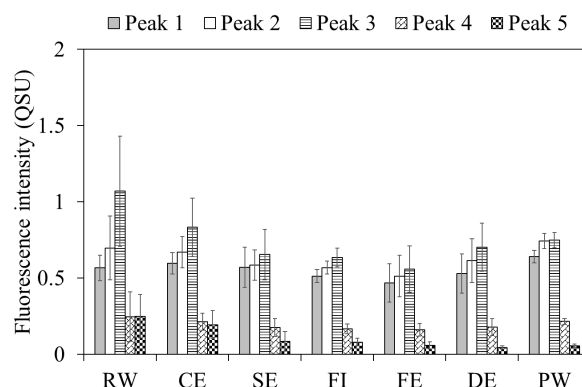


Fig. 2: Changes of DOM composition in different treatment units (n = 12).

Fig. 2 shows the changes of DOM composition throughout the treatment units. Raw water feeding the drinking water treatment contained high proportion of Peak 3 (56% of the total fluorescence intensity) that attributed to the presence of

terrestrially derived humic substances. The presence of tyrosine-like (Peak 1) and tryptophan-like (Peak 2 and 4) might be attribute to some biological activity associated with microbes and planktons (Rodríguez-Vidal et al., 2021). Coagulation, sedimentation, and sand filtration caused a decrease in fluorescence intensity, showing a better removal of humic-like substances than tyrosine-like and tryptophan-like substances. The increase and decrease of fluorescence intensity during post-chlorination indicates the desired primary reaction between chlorine and DOM fractions. The higher fluorescence intensity for PW can be explained by the increase of tryptophan-like Peak 2 and humic-like Peak 3 intensity due to the breakdown of aromatic structures in humic molecules into smaller compounds.

(2) Selective removal of DOM after coagulation and post-chlorination

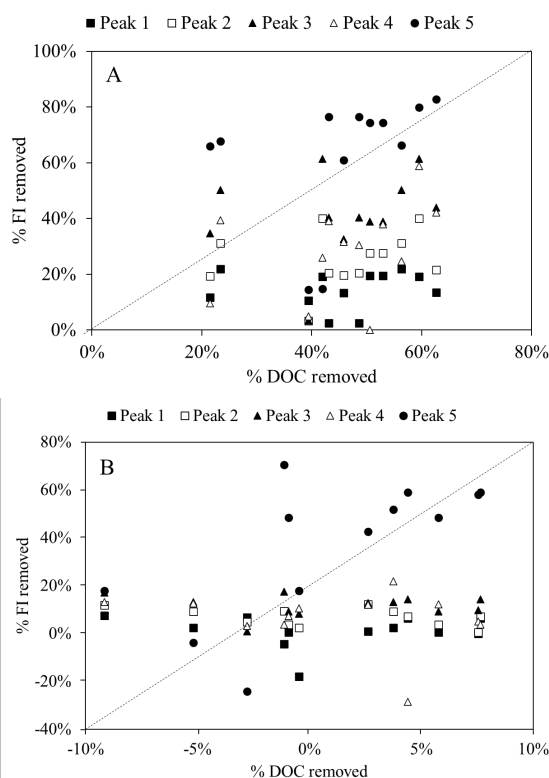


Fig. 3: Relationship between the removal of DOC and fluorescence intensity (FI) of DOM after (A) coagulation and (B) post-chlorination (n = 12).

Higher DOC concentration link to the high contribution of humic substances, preferentially removed by coagulation due to their high molecular weight (Moyo et al., 2019) (Fig. 3). In contrary, post-chlorination process was more effective to eliminate fluorescence DOM than DOC. Chlorination could increase DOC concentration by the hydrolysis of particulate organic matter and degradation of chlorine-killed bacteria, resulting in the negative removal value. As for the fluorescence DOM, Peak 5 was highly removed by chlorination than other components through the oxidation of unsaturated and conjugated groups (Yang et al., 2017), leading to the differential removal among the fluorescence DOM. The negative removal rate of fluorescence DOM suggests the plant are less effective in removing fluorescence DOM in the chlorination process. The raw water quality might influence

the composition and structure of fluorescence DOM and their changes throughout the treatment process.

(3) Changes of HIX and FI in RW and PW

Although, the removal of humic-like substances was higher by coagulation, sedimentation, and sand filtration process, the high HIX value in PW (Fig. 4) could be explained by the humification process that occur by the remaining humic-like substances and coincide with the decay of the residual chlorine. High FI in the PW indicates that most of terrestrially derived DOM was removed along the treatment. It is known that biopolymers and humic substances has a relatively high removal during the conventional treatment (Liden et al. 2017), thus explaining the increasing FI.

Fluorescence EEM analysis can rapidly and sensitively detect the fluorescence DOM during drinking water treatment process. Understanding the dynamics of fluorescence DOM is necessary to monitor and control the water quality since the DOC is strongly correlated to its fluorescent components. The findings can provide the important information that can be used to optimize the water treatment process to ensure the drinking water quality.

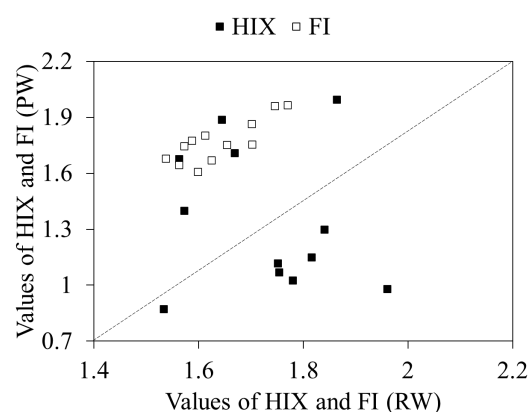


Fig. 4: Values of HIX and FI in RW (raw water) and PW (purified water) (n = 12).

REFERENCES



- Lidén, A., Keucken, A., and Persson, K.M. (2017) Uses of fluorescence excitation-emissions indices in predicting water treatment efficiency. *Journal of Water Process Engineering* 16:149–257.
- Moyo, W., Chaukura, N., Msagati, T.A.M., Mamba, B.B., Heijman, S.G.J., and Nkambule, T.T.I. (2019) The properties and removal efficiencies of natural organic matter fractions by South African drinking water treatment plants. *Journal of Environmental Chemical Engineering* 7(3):103101.
- Rodríguez-Vidal, F.J., García-Valverde, M., Ortega-Azabache, B., González-Martínez, A., and Bellido-Fernández, A. (2021) Using excitation-emission matrix fluorescence to evaluate the performance of water treatment plants for dissolved organic matter removal. *Spectrochimica Acta Part A* 249:119298.
- Yang, X., Zhou, Z., Raju, M.N., Cai, X. and Meng, F. (2017) Selective elimination of chromophoric and fluorescent dissolved organic matter in a full-scale municipal wastewater treatment plant. *Journal of Environmental Science* 57:150–161.


IC-GU12

Country	University/ Institution	Name/Title/Affiliation
Bangladesh	Bangladesh Agricultural University 	Md. Golam Rabbani Professor Department of Horticulture Liaison/Guest Professor
Bangladesh	University of Dhaka 	A. H. M. Nurun Nabi Professor Department of Horticulture Liaison/Guest Professor
China	Guangxi University 	Yu Wenjin Professor/Deputy Director Department of Science and Technology Liaison
		Yang Yanjuan Associate Professor Department of Science and Technology Guest Associate Professor
India	Assam University 	Piyush Pandey Professor Department of Microbiology Liaison/Guest Professor
India	Indian Institute of Technology Guwahati 	Lingaraj Sahoo Professor Department of Biosciences and Bioengineering Liaison/Guest Professor
Indonesia	Andalas University 	Khandra Fahmy Associate Professor Faculty of Agricultural Technology Liaison/Guest Associate Professor
Indonesia	Bandung Institute of Technology 	Eka Mulya Alamsyah Associate Professor School of Life Sciences and Technology Liaison/Guest Associate Professor
Indonesia	IPB University 	Irmanida Batubara Professor/Dean Biopharmaca Research Center Liaison/Guest Professor
Indonesia	Gadjah Mada University 	Siti Subandiyah Professor Department of Plant Protection Liaison/Guest Professor





Country	University/ Institution	Name/Title/Affiliation
Indonesia	University of Lampung 	Tusi Ahmad Lecturer Agricultural Engineering Department, Faculty of Agriculture Liaison
		Afandi Associate Professor Faculty of Agriculture, Department of Soil Science Guest Associate Professor
Indonesia	Sebelas Maret University 	Komariah Associate Professor Faculty of Agriculture Liaison/Guest Associate Professor
Laos	National University of Laos 	Somvilay Chanthalonnavong Faculty of Forestry Liaison
		Sithong Thongmanivong Associate Professor/Vice Dean Guest Associate Professor
Philippines	Mariano Marcos State University 	Marlowe Aquino Professor Graduate School and College of Agriculture Liaison/Guest Professor
Thailand	Chulalongkorn University 	Warinthorn Chavasiri Associate Professor Faculty of Science Liaison
		Ubonratana Siripatrawan Associate Professor Department of Food Technology, Faculty of Science Guest Associate Professor
Thailand	Kasetsart University 	Nantana Srisuk Associate Professor Department of Microbiology, Faculty of Science Liaison/Guest Associate Professor
Thailand	King Mongkut's University of Technology Thonburi 	Pongphen Jitareerat Associate Professor School of Bioresource and Technology Liaison
		Varit Srilaong Professor Dean of School of Bioresource and Technology Associate Dean/Guest Associate Professor










Country	University/ Institution	Name/Title/Affiliation
Vietnam Hanoi University of Science and Technology 		Nguyen Thi Minh Tu Associate Professor Forest Inventory and Planning Department, Silviculture Faculty Liaison
		Lien Ha Tran Associate Professor School of Biotechnology and Food Technology Guest Associate Professor
Vietnam Thuyloi University 		Pham Hong Nga Head International Cooperation Department Liaison
		Nguyen Canh Thai Associate Professor/Vice President Faculty of Civil Engineering Guest Associate Professor
JAPAN Gifu University 		Akio Ebihara Professor Faculty of Applied Biological Sciences Liaison (University of Dhaka)
		Emiko Yanase Professor International JD Program in Food Science and Technology, The United Graduate School of Agricultural Science Liaison (Indian Institute of Technology Guwahati)
		Isao Hirota Assistant Professor Faculty of Applied Biological Sciences Liaison (National University of Laos)
		Keigo Noda Associate Professor Faculty of Applied Biological Sciences Liaison (University of Lampung)
		Ken Hiramatsu Professor/Dean The United Graduate School of Agricultural Science CHAIRMAN of the 9th IC-GU12 Roundtable & Symposium 2021 Liaison (Mariano Marcos State University)
		Kohei Nakano Professor/Vice Dean The United Graduate School of Agricultural Science Liaison (Andalas University)

Country	University/ Institution	Name/Title/Affiliation
JAPAN Gifu University 		Masafumi Shimizu Associate Professor Faculty of Applied Biological Sciences Liaison (Guangxi University)
		Shinya Oba Professor Faculty of Applied Biological Sciences Liaison (Bangladesh Agricultural University)
		Takeo Onishi Associate Professor Faculty of Applied Biological Sciences Liaison (Sebelas Maret University)
		Tatsuro Nishiyama Associate Professor Faculty of Applied Biological Sciences Liaison (Thuyloi University)
		Tohru Mitsunaga Professor/Dean Graduate school of Natural Science and Technology · Faculty of Applied Biological Sciences Liaison (Hanoi University of Science and Technology, IPB University, Chulalongkorn University)
		Tomio Yabe Professor/Vice Dean The United Graduate School of Agricultural Science
JAPAN Shizuoka University 		Masaya Kato Professor/Vice Dean Graduate School of Integrated Science and Technology Liaison (King Mongkut's University of Technology Thonburi)
		Masayuki Yamashita Professor Graduate School of Integrated Science and Technology Liaison (Gadjah Mada University)
		Naoto Ogawa Professor Graduate School of Integrated Science and Technology Liaison (Assam University)

Country	University/ Institution	Name/Title/Affiliation
JAPAN Shizuoka University 		Shinji Tokuyama Associate Professor Graduate School of Integrated Science and Technology Liaison (Kasetsart University)
		Takashi Tanaka Associate Professor Graduate School of Integrated Science and Technology Liaison (Bandung Institute of Technology)

International Symposium


Country	University/ Institution	Name/Title/Affiliation
Indonesia Bung Hatta University 		Edwina Zainal Lecturer Faculty of Civil Engineering and Planning
Indonesia Sebelas Maret University 		Dwi Priyo Ariyanto Associate Professor Soil science Department, Faculty of Agriculture
		Komariah Associate Professor Dept. of Soil Science, Faculty of Agriculture
		Maria Theresia Sri Budiastuti Lecturer Department of Agrotechnology, Faculty of Agriculture
Indonesia University of Lampung 		Christine Wulandari Head Master Program of Forestry, Faculty of Agriculture
Indonesia Universitas Muhammadiyah Yogyakarta 		Zuhud Rozaki Head Department of Agribusiness, Faculty of Agriculture

Country	University/ Institution	Name/Title/Affiliation
JAPAN Forestry and Forest Products Research Institute 		HAN Qingmin Chief Plant Production Laboratory, Department of Plant Ecology
		Momi TSURUTA Department of Forest Molecular Genetics and Biotechnology
		So Hanaoka Chief of Breeding Laboratory Forest tree breeding in Hokkaido
JAPAN Gifu University 		Cahyo Wisnu Rubiyanto PhD student The United Graduate School of Agricultural Science
		Uemura Taketo MSc. student Graduate school of Natural Science and Technology
JAPAN Nagoya University 		Michiko Nakagawa Associate Professor Graduate School of Bioagricultural Science
JAPAN Shizuoka University 		Atsuhiko Iio Associate Professor Graduate School of Integrated Science and Technology
Thailand Chulalongkorn University 		Sasitorn Pongparn Associate Professor Department of Botany, Faculty of Science
Thailand Maejo University 		Sutheera Hermhuk Lecturer Faculty of Agriculture Production
Thailand Silpakorn University 		Suthathip Umnouysin Lecturer Department of Biology, Faculty of Science
Thailand Wildlife & Plant Conservation 		Wongsatorn Phumphuang Forestry Technical Officer Practitioner Level. Department of National Parks
Vietnam Vietnam National University of Forestry 		NGUYEN TRONG MINH Lecturer Forest Inventory and Planning Department, Silviculture Faculty


Board members of Symposium

JAPAN Gifu University 	Shogo Kato Associate Professor Faculty of Applied Biological Sciences
	Toshiyuki Ohtsuka Professor River Basin Research Center Head Organizer of the Symposium 2021
	Yuzuru Mukai Professor Faculty of Applied Biological Sciences

Executive Committee of Poster Session

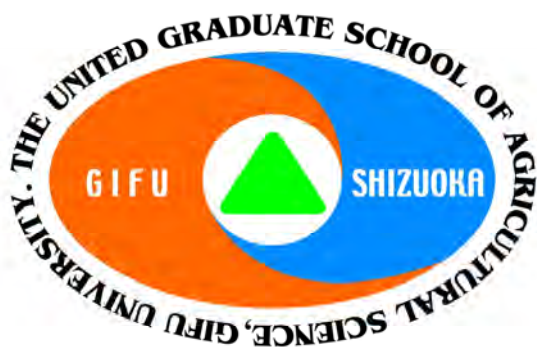
JAPAN Gifu University 	Kohei Nakano Professor/Vice Dean The United Graduate School of Agricultural Science
	Yasushi Ishiguro Assistant Professor River Basin Research Center

Secretariat Division

JAPAN Gifu University 	Kouichirou Aoki Section Head The United Graduate School of Agricultural Science gjab00024@jim.gifu-u.ac.jp
	Yoko Takahashi Leader The United Graduate School of Agricultural Science gjab00025@jim.gifu-u.ac.jp
	Shigeno Kurimoto Secretary The United Graduate School of Agricultural Science gjab00046@jim.gifu-u.ac.jp
	Postal address: 1-1 Yanagido, Gifu 501-1193, JAPAN Phone: +81-58-293-2984 Fax: +81-58-293-2992

The United Graduate School of Agricultural Science, Gifu University
1-1 Yanagido, Gifu 501-1193, Japan
Tel: +81-58-293-2984 (or, 2985)
E-mail: renno@gifu-u.ac.jp
Home Page: <http://www.ugsas.gifu-u.ac.jp/eng/>

Promotion Office of Gifu University Rearing Program
for Basin Water Environmental Leaders, Gifu University
1-1 Yanagido, Gifu 501-1193, Japan
Tel: +81-58-293-2085
E-mail: bwel@green.gifu-u.ac.jp
Home Page: <https://www.green.gifu-u.ac.jp/BWEL/eng/index.html>



ISBN978-4-909365-07-1